INFORMATION TO USERS

This was produced from a copy of a document sent to us for microfilming. While the most advanced technological means to photograph and reproduce this document have been used, the quality is heavily dependent upon the quality of the material submitted.

The following explanation of techniques is provided to help you understand markings or notations which may appear on this reproduction.

1. The sign or "target" for pages apparently lacking from the document photographed is "Missing Page(s)". If it was possible to obtain the missing page(s) or section, they are spliced into the film along with adjacent pages. This may have necessitated cutting through an image and duplicating adjacent pages to assure you of complete continuity.

2. When an image on the film is obliterated with a round black mark it is an indication that the film inspector noticed either blurred copy because of movement during exposure, or duplicate copy. Unless we meant to delete copyrighted materials that should not have been filmed, you will find a good image of the page in the adjacent frame.

3. When a map, drawing or chart, etc., is part of the material being photographed the photographer has followed a definite method in "sectioning" the material. It is customary to begin filming at the upper left hand corner of a large sheet and to continue from left to right in equal sections with small overlaps. If necessary, sectioning is continued again—beginning below the first row and continuing on until complete.

4. For any illustrations that cannot be reproduced satisfactorily by xerography, photographic prints can be purchased at additional cost and tipped into your xerographic copy. Requests can be made to our Dissertations Customer Services Department.

5. Some pages in any document may have indistinct print. In all cases we have filmed the best available copy.

University
Microfilms
International

300 N. ZEEB ROAD, ANN ARBOR, MI 48106
18 BEDFORD ROW, LONDON WC1R 4EJ, ENGLAND

UCCI, DONALD RICHARD

AN ACQUISITION AID FOR A PHASE LOCKED LOOP

City University of New York PH.D. 1979

PLEASE NOTE:

In all cases this material has been filmed in the best possible way from the available copy. Problems encountered with this document have been identified here with a check mark ✓.

1. Glossy photographs _____
2. Colored illustrations _____
3. Photographs with dark background ✓
4. Illustrations are poor copy _____
5. Print shows through as there is text on both sides of page _____
6. Indistinct, broken or small print on several pages _____ throughout _____
7. Tightly bound copy with print lost in spine _____
8. Computer printout pages with indistinct print _____
9. Page(s) _____ lacking when material received, and not available from school or author _____
10. Page(s) _____ seem to be missing in numbering only as text follows _____
11. Poor carbon copy _____
12. Not original copy, several pages with blurred type _____
13. Appendix pages are poor copy _____
14. Original copy with light type _____
15. Curling and wrinkled pages _____
16. Other _____

University Microfilms International

300 N. ZEEB RD., ANN ARBOR, MI 48106 (313) 761-4700

AN ACQUISITION AID FOR A PHASE LOCKED LOOP

by

Donald R. Ucci

A dissertation submitted to the Graduate
Faculty in Engineering in partial fulfillment
of the requirements for the degree of
Doctor of Philosophy, The City University of New York.

1979

This manuscript has been read and accepted for the Graduate Facutly in Engineering in satisfaction of the dissertation requirement for the degree of Doctor of Philosophy

7/19/79
Date

Chairman of Examining Committee

7-19-79
Date

Executive Officer

Prof. D. L. Schilling (mentor)

Prof. G. Eichmann

Dr. J. Garodnick

Prof. H. Taub

Dean F. Thau

ABSTRACT

A method for acquisition of a Phase Lock Loop (PLL) receiver is presented. A structure designed for this purpose is described. The method uses an iterative technique to estimate the frequency of an unknown Doppler shifted unmodulated carrier signal imbedded in noise. The acquisition process can be achieved even if the system is below threshold. The acquisition times for a given probability of error are presented for two modes of operation - one which provides a reduced acquisition time but requires more hardware complexity, and another which produces slightly less reduced acquisition times but a simpler hardware design. Results for a hardware implementation are presented.

To my wife and my parents

"Theory without application is like the smile of the Chesire cat; application without theory is blind man's bluff."

(Quote from R. Bellman, IEEE Transactions on Automatic Control, April, 1973.)

ACKNOWLEDGEMENT

The author wishes to express his sincere gratitude to his mentor, Professor Donald L. Schilling for his expert counsel and continued encouragement that he afforded me throughout this research.

The author also wishes to thank the members of his Doctoral Committee: Professors George Eichmann, Herbert Taub and Frederick Thau for the time and effort each has spent on the reading and criticism of this dissertation. He especially wishes to thank Dr. Joseph Garodnick for his zealous and incisive reading of the first draft, and his keen insight and determined concern in this work.

Thanks are also due to Drs. Chaim Ziegler and Tuvia Apelewicz whose efforts put the author on the "write" track.

In addition, the author wishes to thank all his colleagues in room T502F for their encouragement and concern throughout this work, particularly Mr. Jim Cartwright and Mr. Vaman Rao Dhadesugoor for their invaluable aid in the construction and testing of the hardware system.

The excellent typing of this dissertation was performed by Ms. Maie Croner and Ms. Louise Dennis of New York University.

Finally, the author greatly appreciates the patience of his parents, Gaetano and Rose, and his wife Frances. Their love, encouragement and fortitude helped to ease many difficult periods that arose during the course of this research.

The research contained in this dissertation was partly supported by the Department of the Air Force under Grant AFSOR 77-3217.

TABLE OF CONTENTS

LIST OF TABLES

LIST OF ILLUSTRATIONS

Chapter 1

INTRODUCTION

1.1 Phase Lock Loops in Communication Systems

Phase lock loop systems manifest themselves in a broad range of applications such as telecommunications (satellite) systems, navigational and control systems analog and digital data links, and FM systems. In addition we find the phase lock principle in frequency synthesis, electric power generation, and biophysics. In recent years there has been a significant increase in the use of Phase Lock Loops (PLLs). This is evident from from the large volume of papers in the literature which are concerned with the application and behavior of phase lock loops. An extensive bibliography is given in [12] for work prior to 1975.

This trend is due in part to the new methods of fabrication of integrated circuits. Many types of PLLs are now available in "chip" form and so new and existing systems, whether analog or digital, can be designed and modified economically and efficiently.

Another reason for this tendency is due to the inherent nature of communication problems and the solution afforded by a phase lock loop structure. Most communication systems need to first establish a reference point in order to operate

properly. A phase lock loop can provide this reference point and maintain it while the system is processing information. Without this reference the output of the communication link would be meaningless. The phase lock loop system can perform this task under a variety of circumstances and may be used in either analog or digital systems. This aspect of operation is called carrier tracking in analog systems and bit synchronization in digital systems. In either case the effect of the phase lock loop mechanization is to synchronize a local reference source with an incoming message or information bearing signal. Such a system is said to be a coherent communication system [27].

Another use for a phase lock loop is that of a frequency demodulator. In essence the loop fulfills the same function as an FM discriminator except that, when operating in a highly noisy environment it performs better than the discriminator [22].

In certain types of communication systems the input carrier signal is not transmitted, that is it is suppressed. This causes problems if one wishes to use a phase lock loop to establish a reference for coherent detection. However, a related structure called the Costas Loop [7], which uses the phase lock principle, can extract a reference signal from this type of transmission. There exist other kinds of loops in this class which can also perform this function. Some examples are the Squaring loop, the N^{th} order loop, the

decision aided loop, the delay locked loop, etc. One such system which finds a need for this application is called "Spread Spectrum Systems" [8] and is used for "hiding" signals in noise, that is, to make them appear as noise and thus not be detected by unwanted observers.

In all of the above applications it is assumed that the phase lock system is operating in the synchronous or locked mode. This mode has been investigated and written about extensively in the literature since, for this mode, many approximations can be made to simplify the analysis. The locked mode has associated with it specific problems such as the steady state phase error probability density function, the mean time for cycle slipping when locked or loss of lock, the location of the threshold, etc. Since most practical systems have noise associated with them, these attributes are generally characterized statistically. Nevertheless, a great deal of analysis has been devoted to the noiseless system in order to determine certain important properties and gain insight of the phase lock principle.

However, there is one other mode of operation of a PLL to be considered, that is, the asynchronous or unlocked mode. This mode which is not as well documented but is coming more so into the forefront of communications is far more complex to analyze. The nonlinearities of the system in this mode when further compounded by the addition of noise produce a system which is governed by a nonlinear stochastic

relationship.

A phase locked loop system is said to be in the frequency locked mode when the frequency error between the input signal and local oscillator is negligible. When the two signals are of identical frequency and their phase difference is exactly $\pi/2$ radians then they are said to be in phase lock [28]. If the loop is not in the lock states it is then in the asynchronous, or acquisition, mode. Prior to performing any of the aforementioned functions the loop must acquire lock.

The acquisition mode also has measures which characterize its operation. As before they are generally statistical in nature although some are derived through a deterministic basis. Some of these are the maximum frequency acquisition range, also called the pull in or capture range, the signal acquisition (or pull-in) time which is the time to reach steady state, and the probability of false lock as well as other properties. (For an extensive list of phase lock loop jargon see [10] or [14].)

Here we digress a moment to discuss the term "false lock." False lock is a condition which occurs in a PLL system if other signals are present in the input bandwidth. If the input signal is frequency modulated, for example it may be a Frequency Shift Keyed (FSK) signal, sidebands which are within the acquisition bandwidth are generated. The loop may lock onto one of these "false carriers" instead

of the real signal. Lindsey denotes false lock as any condition in which the system synchronizes to a frequency other than the input signal frequency [15].

A related problem which crosses the boundary between the two modes is the ability of a system to distinguish loss of lock from noise. An even more fundamental problem for a phase lock system operating in the acquisition mode is to sense a frequency and phase difference and to separate this condition from noise variations.

We now present a discussion of the basic phase lock structure. A simplified diagram is shown in Fig. 1.1.1. A more general structure is given in [14]. The basic components of a phase lock loop are the Phase Detector (PD) or Phase Comparator (PC), a loop filter with associated transfer function H(s), and a Voltage Controlled Oscillator (VCO). The signal a(t) as shown in Fig. 1.1.1 is an acquisition aid and is usually omitted in the synchronous mode. This dissertation is concerned with the generation and effect of this signal.

The PD is essentially a multiplier-low pass filter combination which passes only the baseband difference frequency signal, that is the difference signal between the input signal and VCO signal frequencies. Much work has been done investigating the effects of different PD on the PLL performance. In general, all higher order harmonics generated by the multiplication process and referred to as double frequency terms are omitted from the analysis. The loop filter

is a smoothing circuit which determines the order of the loop. The order of the PLL is equal to one plus the number of poles in the loop filter. Thus if there is one pole in H(s) the loop is said to be of second order. The output of H(s) is generally the output of the loop although other choices are available. The VCO input signal attempts to move the VCO instantaneous frequency towards the incoming signal frequency. This is the means by which the PLL mechanization is accomplished.

When the phase error at the output of the PD is small the loop can be linearized (the close tracking mode) and becomes similar to a linear control system. Thus a PLL can be called a synchronous control system. The general nonlinear differential equation governing the phase lock loop is often written in mixed notation, that is, in terms of time derivatives and Laplace Transforms. The variable in this equation is usually the phase error. The reason for this is that the filter is more easily described in the frequency domain and the equation of operation in the time domain. Also by specifying the filter as H(s) a general equation is found after which investigations for a particular H(s) are performed.

1.2. Statement of the Problem

This dissertation is concerned with the aspect of signal acquisition time, in particular signal acquisition through the use of an acquisition aid. We assume that the phase lock loop structure may initially be operating either above

or below threshold and that, due to its narrow bandwidth it cannot lock to the incoming signal by its own means. Thus an acquisition aid is needed. Also once lock is acquired we assume the acquisition aid is removed but the system remains in lock.

The transmitted carrier signal at frequency ω_c (radians/sec) is assumed to be unmodulated throughout the acquisition process; however, the received input frequency may be different due to the transmitter oscillator instabilities (even in crystal oscillators) and Doppler frequency shift due to atmospheric disturbances. We shall group the total of all these variations into one and refer to it as the Doppler shift, Ω_D (radians/sec). In all cases we assume that the Doppler shift is varying slowly throughout the acquisition time period, T_{ACQ}. It may therefore be considered constant for the acquisition process. The methods we develop are dependent on the Signal-to-Noise Ratio (SNR) or the Signal-to-Noise Density Ratio (SNDR). We will always assume that one of these values is known a-priori or that a good estimate may be obtained prior to initiating the acquisition scheme. With these considerations in mind we derive the estimate of the Doppler shift from the input signal and noise.

1.3 Summary of Prior Work

At this point we will perform a qualitative review of the present techniques used as an acquisition and in a sychronous control system.

One of the more established methods and still used extensively is the swept frequency method mentioned earlier. This technique was investigated experimentally by Frazier and Page [9] who obtained an empirical formula that predicts the maximum sweep rate for an "acquisition probability" of 90% in the presence of noise. They have derived formulae for the two distinct cases -- one for which there is IF limiting and one for no IF limiting. For large SNR the sweep rate is approximately the square of the loop's natural frequency, ω_n (for a definition of natural frequency of a PLL refer to [10,14 or 26]. Since the results are empirical a safety margin is advisable. If the sweep rate is chosen $\leq 0.386\omega_n^2$ the technique assures 100% lock in the absence of noise. Richman [19] has examined the use of a quadricorrelator as a frequency difference detector. The use of such a device has shown that there is a definite reduction in time for acquisition and a significant increase in pull in range. Williamson [30] has recently examined the use of non-linear loop filters in the PLL structure and found improved acquisition performance for initially large detuning in the absence of noise. A guide to three types of frequency searching strategies is given in [6]. Viterbi [26] has also examined acquisition aids. We discuss this in Sec-

tion 3.5.

Acquisition aids for Costas loop type configurations have also been investigated. A device which uses a differentiator and/or integrator in either arm of a Costas loop which increases the acquisition properties and also helps prevent sideband lock [4]. This device is similar to the device we use since it performs a discrimination of the input waveform. However, the signal derived as such is continuously fed to the VCO and is not injected into the system. Cahn [5] designed an acquisition aid by making a composite Automatic Frequency Control Costas (AFC/Costas) loop which extracted, from the input signal, a control signal which was proportional to the frequency error.

1.4 Summary of Results Obtained

In this section we present a brief description of the contents of this dissertation and we qualitatively summarize the results obtained.

In Chapter 2 we begin with the basic structure for the injection locking technique we have chosen. We discuss the system design and the method of estimating the frequency offset. We also present briefly the technique to be employed, that is the iterative procedure that will be used to determine the parameters needed for the acquisition process. In all cases we assume that the SNR is known or a good estimate is obtainable. We discuss the components comprising the acquisition time namely, the integration and processing time.

The tradeoff between the processing time and system resolution is examined. We discuss the effect of noise and identify the two noise processes with which we are concerned -- the Gaussian channel noise and the Poisson spike or impulse noise. We state our independence assumption regarding these two processes.

Chapter 3 examines more deeply the relationships established in the previous Chapter. We discuss the discriminator operation and the spike noise phenomenon at its output and the effect of the integrator on this output. From this we develop the equations for the frequency estimate and its statistical characteristics are examined. The theoretical calibration curves are found for various values of operating SNR. In determining the variance of the estimate a worst case analysis is always chosen. We discuss the general equation for the system which we use to reduce the acquisition time. However since this equation is difficult to solve for all regions we examine it in two regions of operation -- the low SNR or spike region and the high SNR or Gaussian region. From these considerations we develop the equations for determining the parameters to be used to reduce the acquisition time for an unaided loop (in the low SNR region if the loop is unaided it may never lock). We present the results of the technique we call, for want of a better name, the quasi-optimal approach for which we wish to minimize the overall acquisition time; here we become cognizant of the moving threshold problem. Also presented are the results for a

Constant-Bandwidth Reduction (CBR) method. Here we find we can trade off hardware complexity for acquisition time. We also present a comparison of other technqiues.

The hardware simulation and results are discussed in Chapter 4. We begin with the system implementation including the use of a special purpose microprocessor built by Dr. Tuvia Apelewicz. This device is used to perform the integration and sample-and-hold function. The results of the experiment are then presented. We find, generally a close agreement between the theory and the empirical tests.

Finally in Chapter 5 we present our conclusions regarding the research comprising this dissertation. We also present a series of questions and some new problems that arise as a result of this thesis and which merit investigation.

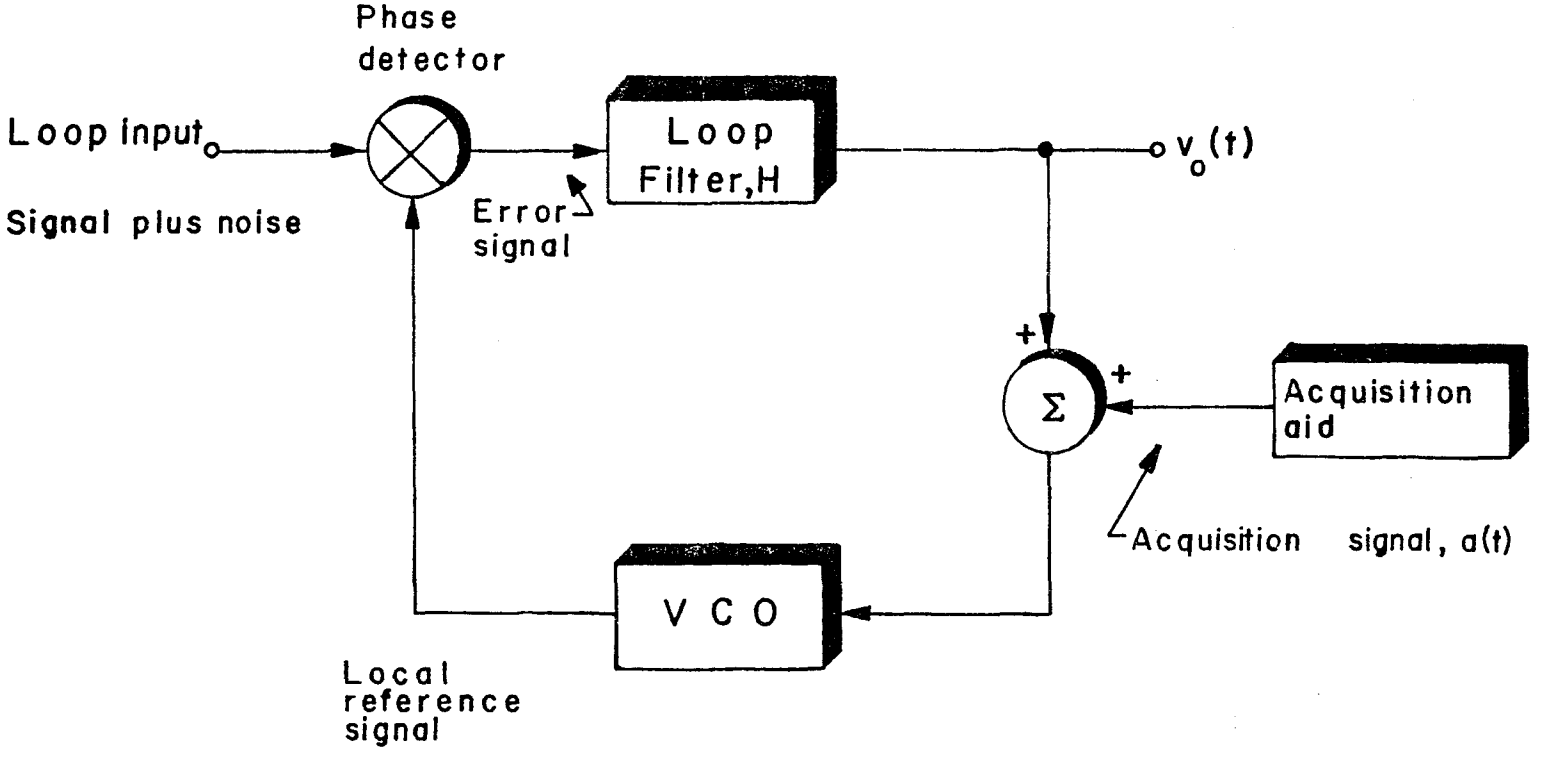

Figure 1.1.1 A Basic PhaseLock Loop

Chapter 2

SYSTEM DESCRIPTION

In this chapter the Phase Lock Loop (PLL) structure for the acquisition problem is defined. The problems encountered in using such a configuration are posed and the system's anomalies are explored.

A PLL can be used for many purposes, for example, an FM demodulator, a carrier tracker, a bit synchronizer and many more. However, before it can perform a useful function, the loop must be able to acquire lock, or simply acquire. That is, it must be able to synchronize a local oscillator with the frequency and in some instances phase of an incoming signal. A PLL is said to have acquired frequency (phase) lock when the difference between the input frequency (phase) and the local oscillator frequency (phase) is negligible.

Under certain conditions a PLL can acquire lock by itself without an acquisition aid. These conditions are high Signal-to-Noise-Ratio (SNR), for example, a SNR $\geq$ 20dB, and small frequency detuning by which we mean initial frequency offset between the input and local oscillator signals. The initial detuning should be small when compared to a parameter called the loop bandwidth, B_L. When this is the case the input signal is said to be in the pull-in or lock range of the PLL and as such the system will acquire. An important parameter here is the acquisition time, T_{ACQ}. The acquisition time depends upon many parameters of the system and is in

general difficult to compute except in the simplest cases without the presence of noise. When noise is present a statistical analysis must be performed [14,26].

However, since most loops used in applications mentioned above are narrowband devices, the initial detuning is large compared to B_L. Thus, the signal is out of the lock range of the PLL. Furthermore, if the loop bandwidth is increased to accommodate this detuning then the SNR is decreased (assuming there is noise present) which discourages the locking process. For these conditions, i.e., low SNR and large initial detuning, an acquisition aid is needed.

In this thesis we are concerned with establishing an acquisition aid for a phase locked loop. The method used for the acquisition is an iterative technique which moves a local frequency source, for example a Voltage Controlled Oscillator (VCO), closer to an input carrier signal whose frequency is known only to lie in a particular frequency band. It is assumed that the carrier is unmodulated throughout the acquisition mode.

During a particular iteration this uncertainty band is denoted by B_K, where the subscript K denotes the iteration number. The corresponding time for the K-th iteration is denoted by T'_K. If a total of N iterations are needed then

the acquisition time for the aided process is the sum of all iteration times, $T'_0, T'_1, \cdots, T'_{N-1}$.

Initially the unknown bandwidth is B_o Hertz (Hz). Although this bandwidth may be small compared to the carrier frequency it is assumed to be wide enough so that an ordinary PLL would be operating below its threshold region if the loop bandwidth were increased to accommodate B_o. However, by using the iterative technique acquisition can be accomplished. The procedure is designed such that each iteration narrows the uncertainty bandwidth from B_o to a smaller value. In this way an initially low SNR due to the large initial bandwidth can be increased after each iteration because the IF bandwidth is narrowed. When the uncertainty is small enough compared to the final, desired loop bandwidth, B_F, a narrow tracking loop of bandwidth B_F can be switched in to complete the locking procedure. This is usually done when the SNR is high, for example, 20dB and so the system is above threshold. The criteria for this procedure is to minimize the total acquisition time for a certain probability of acquisition.

The system uses a Frequency Modulation Discriminator (FMD) in the loop structure. This makes the loop appear to be an FM demodulator using Feed Back (FMFB). The difference here, however, is that in the FMFB, the frequency difference is such that the loop is always in a locked state and also

that the discriminator output is applied continuously to the VCO through a low pass filter. In our case the loop is not locked and the output of the FMD, after processing by an integrator, is applied to the VCO only at certain discrete times. Thus we have an injection locked system.

The number of iterations needed, as well as the iteration times and bandwidths are parameter dependent. The method for choosing the number of iterations and the iteration times and bandwidths will be explored. Also we make the important note that although the FMD will be operating below the threshold. it can be calibrated whereas an ordinary PLL cannot for reasons discussed above.

2.1 The Basic Acquisition Structure.

The block diagram of the basic acquisition aided Phase Lock Loop structure is shown in Fig. 2.1.1. Note that with the switch S in position 1, the loop is in the acquisition mode and with S in position 2, the loop enters a tracking mode. (Position 2 defines the basic or ordinary PLL.) This thesis is concerned with the behavior of the PLL in the acquisition mode. This is the first task of the loop. When the acquisition process has been completed (at a time T_{ACQ}), the loop automatically switches to the tracking mode. The acquisition process is an iterative one in which the number of iterations depends upon the system parameters as will be discussed below.

The received signal, $r(t)$, consists of a carrier signal, $s(t)$, and a noise term $n_w(t)$. The carrier signal is

$$s(t) = A \sin[\omega_c+\Omega_D)t + \phi] \qquad (2.1.1)$$

where A is the signal amplitude, ω_c is the known nominal radian carrier frequency, ϕ is some unknown random phase uniformly distributed in the interval $[-\pi,\pi]$ and Ω_D is the unknown Doppler frequency shift due to atmospheric or dynamic conditions, system instabilities (for example, oscillator or component drift, which is usually slow compared to the acquisition time), or other causes.

We assume that Ω_D is uniformly distributed in the interval $-\Omega_{max} \leq \Omega_D \leq \Omega_{max}$, and that Ω_{max} is known <u>a priori</u> from channel characteristics, system parameters or some other means. It is this Doppler shift which we wish to estimate with our acquisition technique. The noise $n_w(t)$ is derived from stationary, white, Gaussian channel noise of two sided power spectral density (p.s.d.) $\eta_o/2$ Watts/Hz as follows. Since in a practical system we would not allow noise frequencies outside the signal range to enter the receiver, we can assume that $r(t)$ is filtered by a symmetric Wideband Band Pass Filter (WBPF) centered at ω_c and extending in frequency, with a flat passband, such that only frequencies below $2\omega_c$ may be passed (that is the passband is d.c. to $2\omega_c$ rad/sec). The power

spectral density of $n_w(t)$ is assumed negligible for $|\omega| \geq 2\omega_c$. Thus we have defined the narrowband stationary noise process $n_w(t)$ [29].

The Phase Comparator (PC) multiplies $r(t)$ by the voltage controlled oscillator signal

$$v_c(t) = 2 \cos(\omega_v t+\phi_v) \tag{2.1.2}$$

in which ω_v is the VCO nominal frequency and ϕ_v is the VCO phase. The output of the PC is $d(t) = r(t)v_c(t)$, that is,

$$\begin{aligned} d(t) &= 2A \sin[(\omega_c+\Omega_D)t + \phi]\cos(\omega_v t+\phi_v) \\ &\quad + 2n_w(t)\cos(\omega_v t+\phi_v). \end{aligned} \tag{2.1.3a}$$

Using the identity $2 \sin x \cos y = \sin(x+y) + \sin(x-y)$ we can write $d(t)$ as

$$\begin{aligned} d(t) &= A \sin[(\omega_c+\Omega_D-\omega_v)t + \psi] \\ &\quad + A \sin[(\omega_c+\Omega_D+\omega_v)t + \psi'] + n_1(t) \end{aligned} \tag{2.1.3b}$$

where $\psi = \phi - \phi_v$, $\psi' = \phi + \phi_v$ and $n_1(t) = 2n_w(t)\cos(\omega_v t+\phi_v)$. Due to the characteristics of $n_w(t)$ mentioned before we may rewrite $n_w(t)$ in quadrature form [26] as

$$n_w(t) = x'(t)\cos \omega_c t - y'(t)\sin \omega_c t \qquad (2.1.4)$$

where $x'(t)$ and $y'(t)$ are independent, zero mean, Gaussian processes, with identical power spectral densities. These densities are similar to that of $n_w(t)$ but shifted down in frequency so that they are centered about zero frequency. Thus, if $G_{n_w}(f) = \eta_o/2$ for $|\omega| < 2\omega_c$, $G_{x'}(f) = G_{y'}(f) = \eta_o$ for $|\omega| < \omega_c$ where $G(f)$ represents the power spectral density. Using the above identity for $2 \sin x \cos y$ and the identity $2 \cos x \cos y = \cos(x+y) + \cos(x-y)$ we can now write $n_1(t)$ as

$$\begin{aligned} n_1(t) = {} & x'(t)\{\cos[(\omega_c+\omega_v)t+\phi_v] + \cos[(\omega_c-\omega_v)t-\phi_v]\} \\ & - y'(t)\{\sin[(\omega_c+\omega_v)t+\phi_v] + \sin[(\omega_c-\omega_v)t-\phi_v]\} \end{aligned} \qquad (2.1.5)$$

Examining Eqs. (2.1.3b) and (2.1.5) we find terms of $d(t)$ at the difference frequency $\omega_\Delta = \omega_c - \omega_v$ and the sum frequency $\omega_\Sigma = \omega_c + \omega_v$. We now observe that the spectrum of the signal at the difference frequency is narrow when compared to the sum frequency term. The spectrums of $x'(t)$ and $y'(t)$ are negligible for $|\omega| > \omega_c$. Since ω_c and ω_v are close in magnitude and the frequency range of the loop components is much less than ω_c or ω_v all terms centered about the sum frequency may be neglected. Furthermore, we now pass $d(t)$ through a

Variable Bandpass Filter (VBPF) centered at $f = f_c$ and bandwidth $B_K << f_c$ as shown in Fig. 2.1.2. This produces a bandpass noise process with power spectral density $\eta_o/2$. Rewriting this noise as the sum of two low pass zero mean Gaussian noise processes $x(t)$ and $y(t)$ centered at $f_I = f_c - f_v + f_D$ we have

$$n_1' = x(t)\cos(\omega_I t) + y(t)\sin(\omega_I t) \tag{2.1.6a}$$

The p.s.d. of $x(t)$ and $y(t)$ is given by $G_x(f) = G_y(f)$ as

$$G_x(f) = \begin{cases} \eta_o & 0 \leq f \leq B_K/2 - f_D \\ \eta_o/2 & B_K/2 - f_D < f \leq B_K/2 + f_D \\ 0 & \text{elsewhere} \end{cases} \tag{2.1.6b}$$

(This will be illustrated in the next chapter.)
The input to the FMD can be written now as

$$e(t) = A\sin(\omega_I t+\psi) + x(t)\cos(\omega_I t) + y(t)\sin(\omega_I t) \tag{2.1.7}$$

This signal is processed by the FMD, which is assumed to be of the differentiating type, producing a d.c. voltage, $V(t)$, proportional to the instantaneous frequency of the input signal. Since we assume no modulation is present during the acquisition process, this voltage is essentially constant

varying only due to the noise (the Doppler drift is assumed to be varying very slowly compared to the acquisition time). Depending upon the signal to noise ratio the d.c. output of the FMD will vary not only due to the Gaussian noise but also due to spike noise. That is, if the discriminator is operating at or below threshold, spikes will be introduced into the output. However, the effect of these spikes can be accounted for [23] and so the discriminator output can still be calibrated. Herein lies a crucial point in this technique. A phase lock loop operating below threshold cannot be calibrated due to the nonlinear nature of its operation.

The reason for this is as follows. The means by which a PLL achieves acquisition is through repeated reductions of the phase error by 2π radians. This is of course assuming that the PLL can lock initially. These reductions of 2π in the phase error are called cycle slips, since at this time the local oscillator is not in synchronization with the incoming signal. This is true whether or not there is noise present. For the no noise case this behavior is best illustrated by a phase plane plot in which the frequency error $\dot{\phi}(t)$ is plotted versus the phase error $\phi(t)$; thus time is implicit in the diagram. A typical phase plane plot is shown in Fig. 2.1.3 for a second order PLL. Since $\phi(t)$ is periodic with period 2π it is only necessary to plot the function $\dot{\phi}(t)$ for

$\phi(t)$ in the interval $(-\pi,\pi)$. The plot is best and most easily made using an analog computer.

We note from the plot that for large $\dot{\phi}(t)$ the trajectories, that is variation of $\dot{\phi}(t)$ with $\phi(t)$, are almost sinusoidal decaying slightly for $\phi(t) = -\pi$ to $\phi(t) = \pi$ when $\dot{\phi}(t)$ is positive. The opposite is true for $|\dot{\phi}(t)|$ large and negative. The rate of decay increases, and so does the total decay, as $|\dot{\phi}(t)|$ decreases in each strip of width 2π. This process continues until the point where $\dot{\phi}(t)$ lies below the line A - A (or above A' - A') in Fig. 2.1.3. At this point, the PLL stops skipping cycles and will eventually achieve lock. For example, if the process starts at point B, the system will skip three complete cycles before reaching line A - A and finally achieving lock.

This occurs even without noise and is due to, among other things, the initial detuning, or frequency offset, of the system. When noise is present the system will jitter along its trajectory. If the noise is sufficiently large, then, while the loop is trying to achieve lock, it might be pushed to a higher trajectory, an integer multiple of 2π radians away from the equilibrium point. This of course will increase acquisition time. Another possibility is that frequency lock has been achieved; however, a noise spike may push the system out of lock. Such a condition is called loss

of lock and is not a rare event in a low SNR system. An extensive coverage of these topics, as well as frequency of cycle slipping, mean time of cycle slipping, and loss of lock, etc., can be found in [14, 26].

Thus, although in its tracking mode, a PLL can produce threshold extension over the FMD, in an acquisition mode, the discriminator has the advantage that the spike noise phenomenon can be used to obtain a more accurate estimate of the input frequency.

Since the output of the FMD is proportional to the instantaneous frequency, ω_I, of its input signal, if we subtract a d.c. voltage proportional to ω_Δ, the result is a voltage proportional to Ω_D, the parameter we are trying to estimate.

The estimate voltage, p(t), is then smoothed by a dc detecting circuit which is modeled as an integrator. The integration time for the K-th iteration, T_K, is yet to be determined by system considerations as will be described in a later chapter. The output of the integrator, y(t) is sampled and held at time $t = T_K$. We note here that the Sample and Hold (S/H) unit is assumed ideal, that is, it will hold this voltage indefinitely or until it is changed by external circuitry. In essence this means that there is no leak. Since all analog S/H exhibit leak, a practical solution would be to use some appropriate digital circuitry.

This voltage, $y(T_K)$, updates the VCO instantaneous frequency. At a time T_K^+, an infinitesimally small time after the integration-sampling period the output of the integrator is decoupled from the (S/H) unit. Thus, the VCO stays at its new frequency until the next sampling update at $t = T_{K+1}$. Also, at $t = T_K^+$ the VBPF bandwidth is changed to its new bandwidth, B_{K+1}. (The center frequency remains the same.) The choice of the bandwidths and integration times are the topic of this thesis.

2.2 System Design Considerations.

We now consider the error signal $e(t)$. This signal is the input to the FMD. Let us suppose that the noise is zero, that is, $x(t) \equiv 0$ and $y(t) \equiv 0$. Then the signal portion of $e(t)$ is $e_s(t)$ where

$$e_s(t) = A \sin[\omega_I t + \psi]. \tag{2.2.1}$$

Let ω_a be the difference frequency between the transmitter's actual frequency, ω_c, and the VCO nominal frequency ω_v, that is, $\omega_a = \omega_c - \omega_v$. Then we can rewrite eq. (2.2.1) as

$$e_s(t) = A \sin[(\omega_a+\Omega_D)t + \psi]. \tag{2.2.2}$$

If we let $\omega_a = 0$, that is, we set the VCO operating frequency equation to the carrier frequency, then the frequency of

$e_s(t)$ is Ω_D. This also means that the bandpass filter characteristic of Fig. 2.1.2 is centered around $f = f_a = 0$. Now we note that Ω_D can be either positive or negative in the frequency range $|\Omega_D| \leq \Omega_{max}$. Thus, $e_s(t)$ is either

$$e_s(t) = A \sin[\Omega_D t + \psi], \quad \Omega_D \geq 0 \tag{2.2.3a}$$

or

$$e_s(t) = -A \sin[\Omega_D t + \psi] = A \sin[\Omega_D t + \psi + 180°]. \tag{2.2.3b}$$

When this signal is processed by the FMD a d.c. signal which is proportional to the frequency but not the phase results at the discriminator output. Since we know the magnitude of Ω_D but not its sign there is an ambiguity factor present in this case. Obviously this is an important factor to know because by making the wrong choice (a positive frequency shift when Ω_D is negative or a negative shift when Ω_D is positive) the system will move the VCO in the opposite direction. This will increase the frequency error and never allow acquisition to occur.

To avoid this problem, we must offset the VCO center frequency from the input transmitter frequency thus shifting the bandpass filter characteristic above d.c. From Fig. 2.1.2, the first possible choice is $f_a = \omega_a/2\pi = f_{max} = \Omega_{max}/2\pi$. This results in a bandpass characteristic as shown in Fig. 2.2.1.

Thus any ambiguity in the Doppler frequency offset is resolved since a frequency of d.c. corresponds to a Doppler shift of $-f_{max}$ whereas a frequency of $2f_{max}$ corresponds to a Doppler shift of f_{max}. So the bandwidth of the filter must be $2f_{max}$ initially. (Notice, when $f_a = 0$, the bandwidth was only f_{max}.)

However, one notices that for any $f_a > f_{max}$ the constraint on the bandwidth of the variable bandpass filter is satisfied. To choose f_a properly we consider another aspect of the system operation. Since an FM discriminator is used to detect the frequency difference it will require several cycles of the input signal frequency (i.e., the frequency of $e(t)$) to develop a proper output level. This is true whether we use a zero crossing detector FMD, or the differentiating envelope detection type FMD. If we allow the lowest frequency of $e(t)$ to be near d.c. the discriminator will require an inordinately long time to produce an output voltage. Since our main objective is to minimize the acquisition time f_a should be made larger than f_{max} so that the FMD response time is shortened. However, if f_a is made much larger than f_{max} then small variations about f_a, such as the Doppler shift $f_D = \Omega_D/2\pi$ will produce only small changes in d.c. voltage. This will cause the system to lose resolution. So a compromise must be made for f_a such that the response time of the FMD is small but the resolution obtained is good.

We will choose $f_a = mf_{max}$ where m is some number greater than unity. For example, suppose we choose $m = 2$. If $f_{max} = 1kHz$, then B_o, the initial value of the bandwidth of the VBPF, is 2kHz. Since a filter requires a transient or rise time approximately equal to the inverse of its bandwidth, the VBPF would need a settling time of $T_r = 1/(2 \times 10^3) = .5ms$. The lowest frequency at the discriminator input, for $m = 2$, is $f_L = 1kHz$. Thus the FMD may need $T_F = (2/f_L)$ seconds to settle or $T_F = 2ms$. Thus the total processing time is $T_{PK} = T_R + T_F = 2.5ms$. If $f_{max} = 10kHz$ then $T_r = 0.050ms$, and $T_F = 0.20ms$, so that $T_{PK} = 250\mu s$. If $f_{max} = 10kHz$ and $m = 10$ we have $T_r = .05ms$, $T_F = .021ms$ so $T_{PK} = .071ms$. Thus we can gain in processing time T_{PK} by making a gain in T_F. The BPF characteristic for this case is shown in Fig. 2.2.2.

Now if $f_c = 1mHz$ and $f_{max} = 10kHz$ we can choose $m = 2$ so that $f_a = 20kHz$ Then $f_v = 980kHz$ Suppose we can operate the FMD on decade ranges of 500Hz, that is the lowest scale is 0 - 500Hz, the next scale is 0 - 5kHz, etc. To satisfy the bandwidth requirement for the above case, we need to use the 50kHz scale ($10kHz \leq f_I \leq 30kHz$). If the resolution of the FMD is 0.01% of full scale we can resolve the frequency to within 5Hz. However, if we choose $m = 10$, then $f_a = 100kHz$ and $f_v = 900kHz$. To use FMD we must now operate on the higher scale, 500kHz ($90kHz \leq f_I \leq 110kHz$) and can now only resolve the the frequency to within 50Hz. This may be too little depending upon B_F. So although we would gain processing time, we lose resolution.

The purpose of the structure we have described is to minimize the total acquisition time. We must now define the acquisition time. The total acquisition time is the time for the system to reduce its uncertainty bandwidth from B_o to B_F where B_o is the initial uncertainty Doppler region and B_F is the final loop bandwidth. Since the technique we describe is an iterative one and since each iteration is independent of the previous one, the total acquisition time, T_{ACQ}, is the sum of each of the individual iteration times, T_K'. The time T_K' depends upon the processing time T_{PK} and the integration time T_K. The processing time will be defined as

$$T_{PK} = C/B_K \tag{2.2.4a}$$

where C is a constant. The reason for this is, as discussed briefly above, a filter's response time is inversely proportional to its bandwidth. Since we must allow the VBPF, discriminator, and VCO to reach steady state, T_{PK} is chosen as in Eq. (2.2.4a). The integration time is T_K which will be determined in the next chapter. If we assume we need M iterations, that is, $K = 0,1,2,\cdots,M-1$ we have

$$T_{ACQ} = \sum_{K=0}^{M-1} T_{PK} + T_K = \sum_{K=0}^{M-1} T_K' \tag{2.2.4b}$$

2.3. Effects of Noise.

2.3.1. Spike Noise Phenomenon .

Thus far we have considered some system design problems without the presence of noise. However, we have discussed threshold in FM discriminators and PLLs, a condition which is brought about by noise phenomena. Thus a discussion of noise is needed before we proceed.

In any practical communications system, the problem of noise is always present. When the SNR in an FM system is high (SNR $\geq$ 15dB) the noise at the output of the FM discriminator is predominantly thermal noise with a Gaussian probability density. This is illustrated in Fig. 2.3.1a, and is referred to as "smooth" noise or Gaussian noise. However, when the SNR at the discriminator input is made smaller the output noise waveform changes character. Superimposed on the Gaussian noise is a pulse type noise called "spike" or "click" noise. This terminology occurs because the output waveform, if viewed on an oscilloscope appears as Gaussian noise with spikes. This is shown in Fig. 2.3.1b. If one listens to this discriminator output, a clicking sound would be heard. When these spikes are present, the system's output SNR diminishes in a nonlinear fashion. This nonlinearity signifies the threshold phenomenon. The mechanism by which a spike can occur can be explained heuristically as follows [18, 24]. Consider the noise $n(t)$ in quadrature form as in Eq. (2.1.4). Consider also a coordinating

system rotating clockwise with angular frequency ω_c. In this coordinate system a carrier signal with no offset varying with frequency ω_c is stationary. Let the carrier be $v_c(t) = A_c \cos \omega_c t$. Thus, using a phasor representation for this signal and the quadrature noise we see that the $n_c(t)$ noise term is in phase with the carrier and lies in the horizontal direction while the $n_s(t)$ term is in quadrature with this combined signal. This is shown in Fig. 2.3.2a.

If the signal to noise ratio is large then the resultant noise phasor $r(t)$ will vary randomly about the point O' in Fig. 2.3.2 without making many large excursions. This is due to the fact that $r(t)$ is Gaussian and the probability that $|r(t)| >> A$ is small when the signal power is large compared to the noise power. Thus as $\phi(t)$ changes, $\theta(t)$ remains relatively small, as shown in Fig. 2.3.2b. However, as the SNR decreases it becomes more likely that $|r(t)| \geq A$. When this occurs, a possibility exists that the noise may rotate the resultant phasor $R(t)$, by 2π radians about the origin as illustrated in Fig. 2.3.2c. This path is the spike producing path. To see this we observe the phase $\theta(t)$ as a function of time during this path. Just prior to the spike occurrence the phase $\theta(t)$ is jittering randomly with small excursions about θ equal zero. During the spike path time, the phase of $\theta(t)$ changes rapidly by 2π radians after which time the phase $\theta(t)$ again jitters randomly with small excursions about $\theta = 2\pi$. This is illustrated in Fig. 2.3.3. If we

observe $d\theta/dt = \dot{\theta}(t)$ which is the instantaneous frequency of the signal and also the output of the discriminator then we notice that during the time interval $[t_1,t_2]$, as $\theta(t)$ changes by 2π, $\dot{\theta}(t)$ exhibits a spike. If we model this spike as an impulse then we see it has a strength equal to 2π because $\theta(t)$ changes by 2π and $\theta(t)$ is the integral of $\dot{\theta}(t)$. Thus we have the phenomenon of spike noise. The noise power of spikes contributed to the output of a system which uses an FMD and baseband (low pass filter) can be shown to be significant [24]. Since a lowpass filter is similar to an integrator the spike noise power will appear at the output of the acquisition aided loop proposed above.

An estimate of the time duration of the spikes when no offset is present can be found by considering the spectrum of the noise. Since a spike is a pulse like phenomenon, it consists of spectral components up to some frequency f_{spike}. Thus its time duration is of the order of $1/f_{spike}$. The spike bandwidth for zero offset is $B/2$ thus the spike duration is $2/B$ where B is the IF bandwidth. In our case $B = 2f_{max}$. If, however, the carrier is offset for example at the lower end of the spectrum, then the noise spectrum has component frequencies most of which are higher than the offset carrier extending over a bandwidth B. Thus spikes for this case will be narrower than the ones for the case of no offset and will have larger amplitudes since the area of each spike

is fixed at 2π radians. Also because of the higher relative frequencies with respect to the offset carrier the rate of occurrence of spikes will increase. The polarity of these spikes will be positive if we are at the lower end of the band. A similar situation occurs at the higher end.

Since the noise power of these spikes at the output of our system can be large, they will significantly effect our results and as such are accounted for in the ensuing analysis.

2.3.2. Effect of Spikes on System Performance.

The effect of the spikes on the output of the discriminator can now be accounted for if we consider the spikes as described above. Let us suppose that we observe the discriminator output for a particular value of offset Doppler frequency. In particular, consider that f_D is such that the resulting carrier frequency f is $f = f_c + f_D < f_c$, that is, $-f_{max} \leq f_D < 0$. Then the output of the discriminator when operating below threshold would consist of a d.c. voltage proportional to the input frequency f, smooth noise due to the Gaussian noise and spike noise due to the low SNR operating point. This signal is shown in Fig. 2.3.4a. Notice that there are many more positive spikes shown than negative ones. This is due to the assumed negative offset. Also note that the spikes are of approximately the same duration. This should be the case because the carrier is unmodulated. However, there will always

be some variation in the pulse widths and amplitudes due to the random nature of the signal. In any event the area under each spike is 2π radians and has the same sign as the spike.

At this point we make the following conjecture. We state that the spike noise and the Gaussian noise are independent or uncorrelated. This is due to the fact that when the Gaussian noise is large it manifests itself as a spike and thus is accounted for in the spike process.

Figure 2.3.4b depicts the output at the integrator. This waveform has step-like changes due to the integration of the spikes. If we sample this waveform at some time $t = T_K$, and scale the result properly, (by the integration period T_K, that is, we integrate from $t = 0$ to $t = T_K$) we expect the output to represent the d.c. level of the input. Of course, this is a random variable since $z(t)$ is a random process. However, if T_K is sufficiently long we obtain a good estimate of the d.c. value. Thus we can calibrate the FMD (in terms of a voltage or frequency output versus offset frequency input) even though it is operating below threshold since the average number of spikes per second is known [23]. We note that calibration depends upon the input signal-to-noise ratio. That is, the increase in the number of spikes is related to the SNR. Therefore, it is important that we know the SNR or the Signal-to-Noise Density Ratio (SNDR) a priori.

In many cases this can be done. If it is not, it must be estimated. (The topic of estimation of the SNR and effect of an incorrect estimate is left for future study.)

Figure 2.3.4 also allows another observation to be made. We see that, for an offset frequency, the discriminator output will have an increase of positive or negative spikes depending upon the sign of the offset. (We note that d.c. contributed by the spikes increases in a manner which opposes the offset.) Since each spike is independent we cannot assume a pattern of pulses exists. For example, suppose there are twice as many positive spikes as negative spikes. We cannot state that in every triplet of spikes there will be two positive spikes and one negative spike. In fact, many positive spikes may arrive before the first negative spike is generated. In this case, as can be seen from Fig. 2.3.4b, the integrator output continuously increases. If the integrator output is connected directly to the VCO by-passing the sample and hold circuit, the accumulated voltage might become too large and so drive the VCO very far from the input signal frequency. This may not allow acquisition to occur using the above described technique. However, using the sample and hold, and providing that the integration time is long enough, we include negative spikes at the integrator input. In this manner we do not apply a larger than needed bias voltage to the VCO, but instead an averaged value which is a better representation of the input signal frequency.

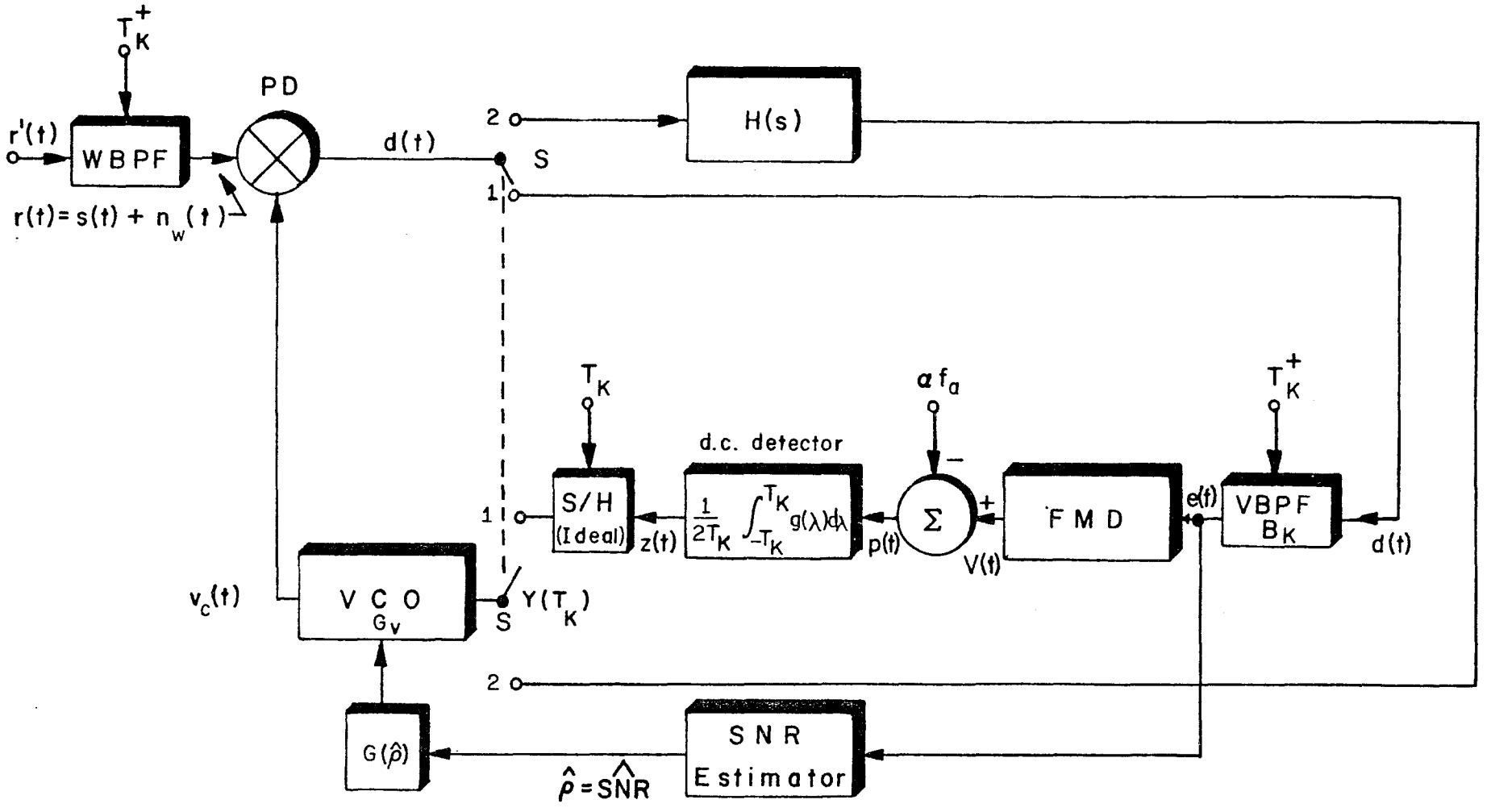

Figure 2.1.1 Acquisition-aided Phase Locked Loop Structure

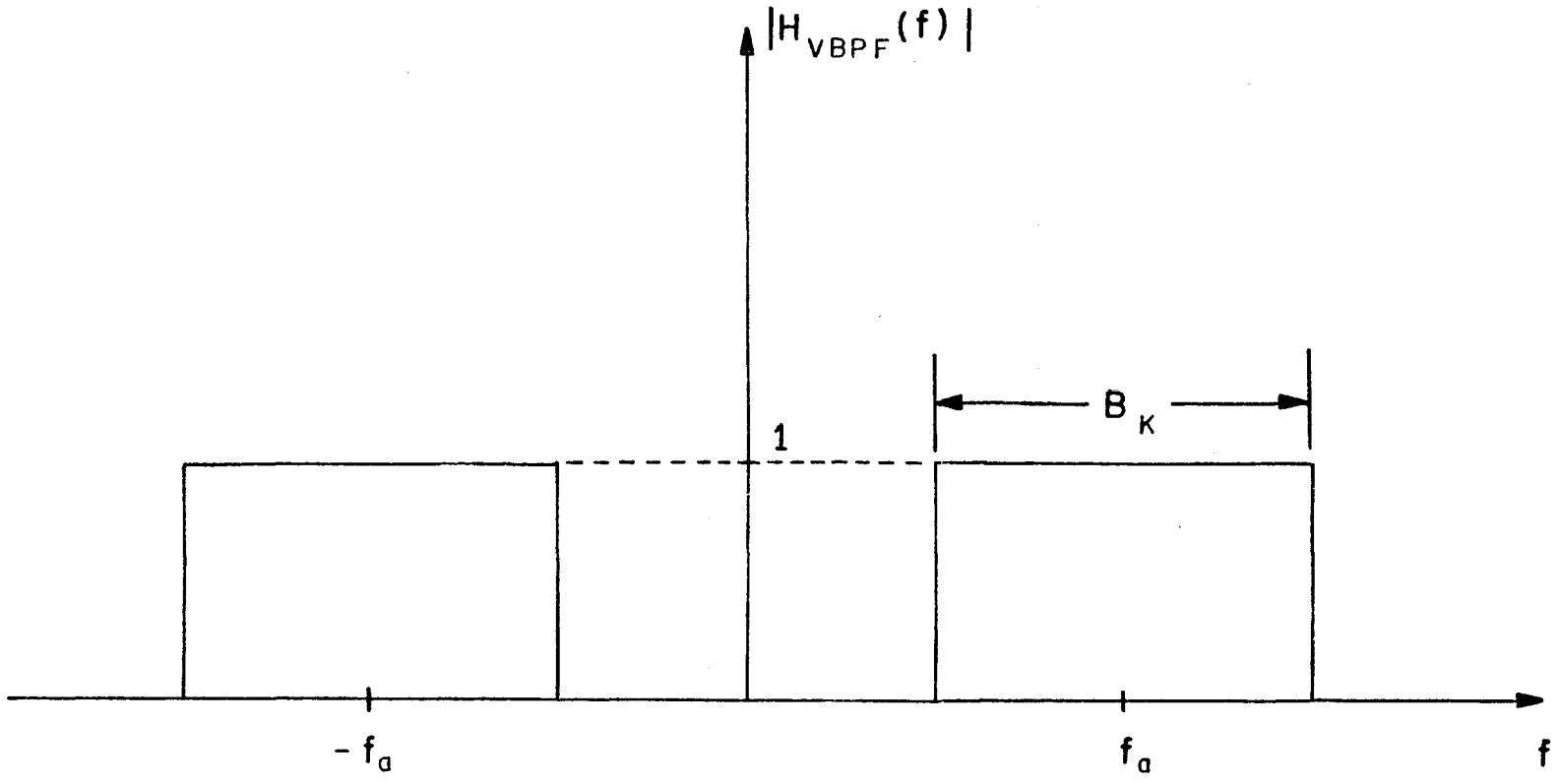

Figure 2.1.2 A Variable Bandpass Filter Characteristic

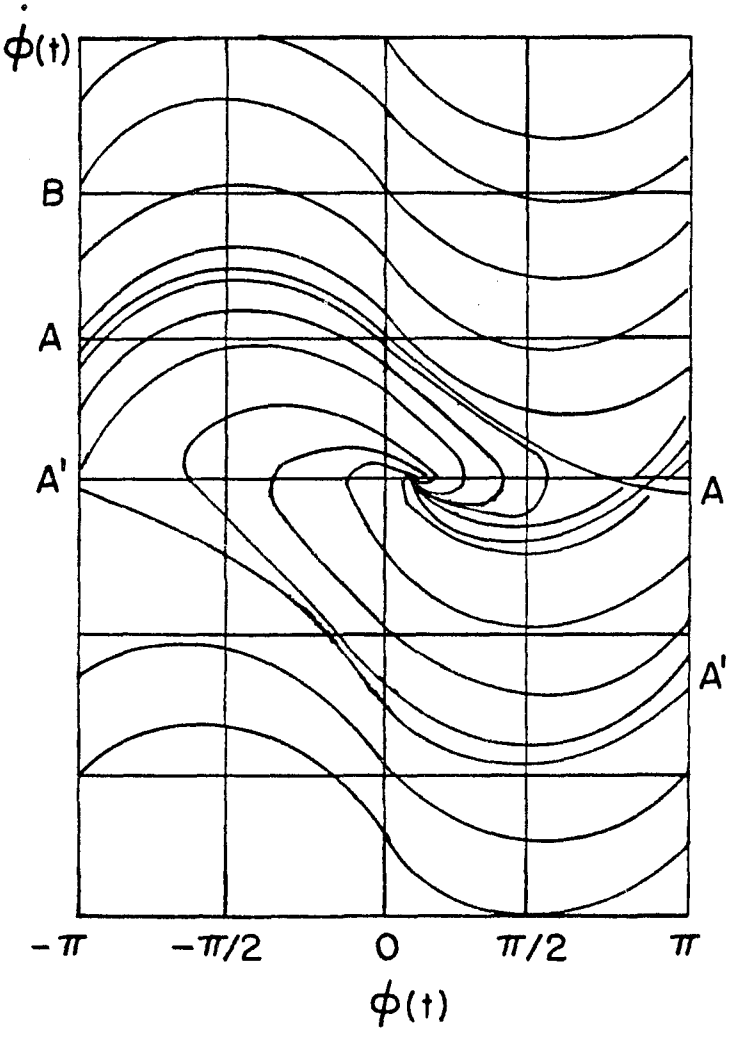

Figure 2.1.3 Phase Plane Trajectories for Second-Order Loop with Imperfect Integrator (From [26])

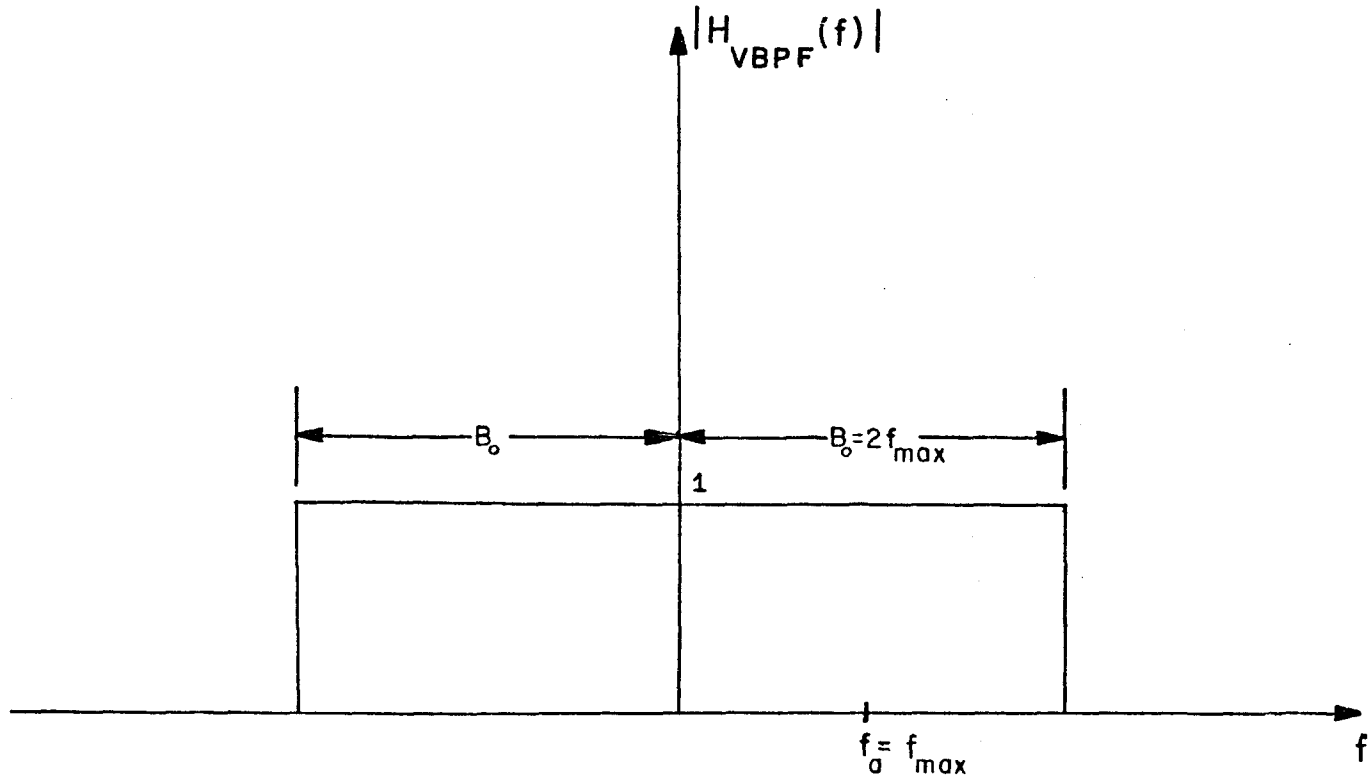

Figure 2.2.1 A Preliminary BPF Characteristic

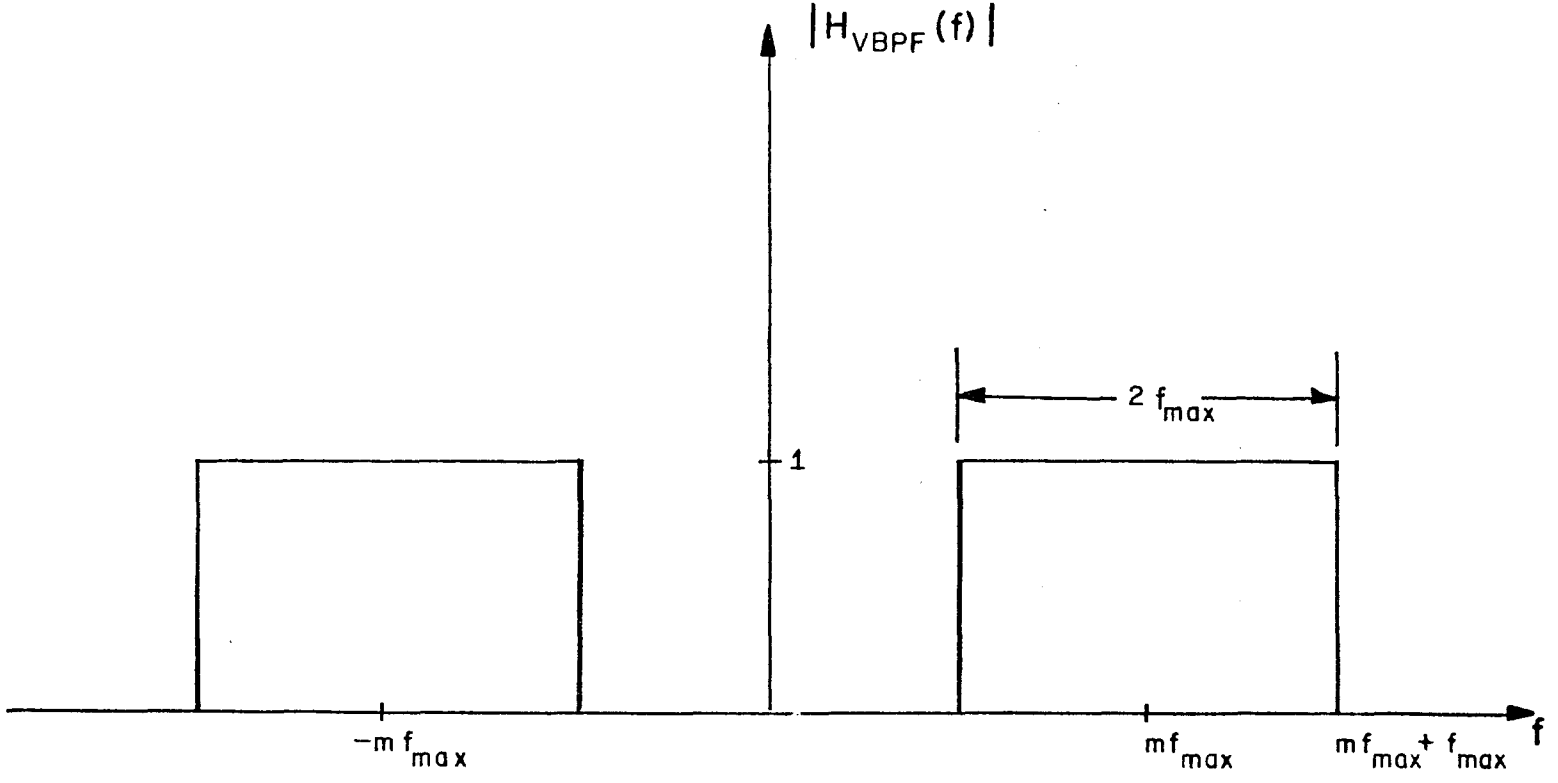

Figure 2.2.2 A Possible VBPF Characteristic

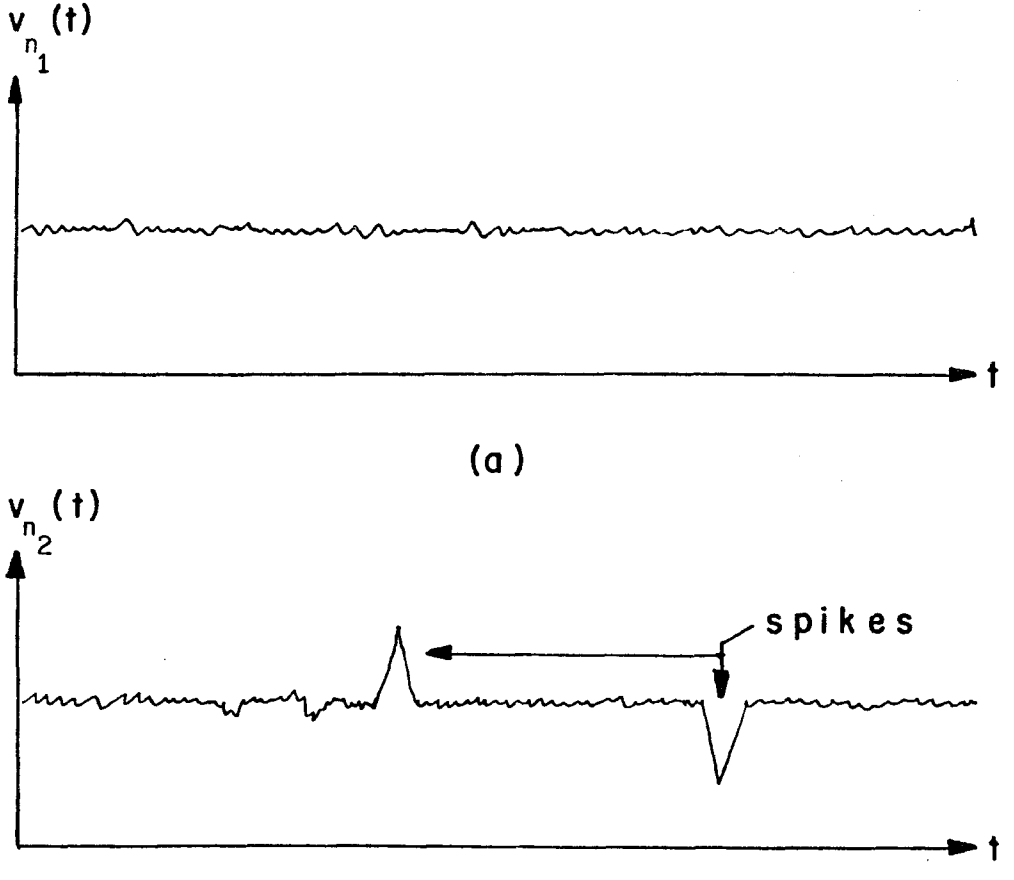

Figure 2.3.1 Discriminator Output Noise (a) Gaussian Noise

(b) Gaussian plus Spike Noise

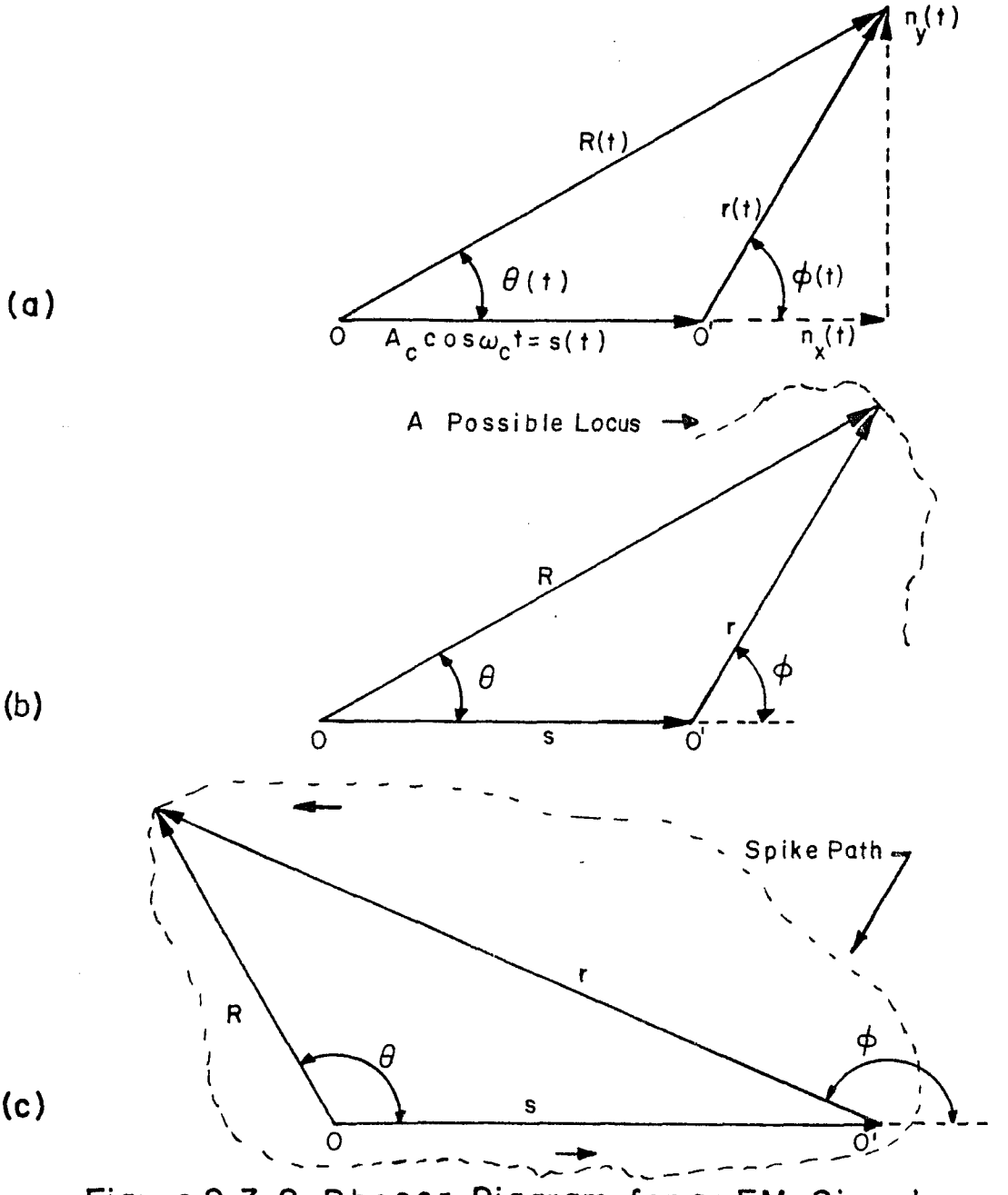

Figure 2.3.2 Phasor Diagram for an FM Signal

(a)Phasor Representation of Signal plus Noise

(b)Typical Locus for the Resultant, R(t)

(c)Locus Producing a Spike

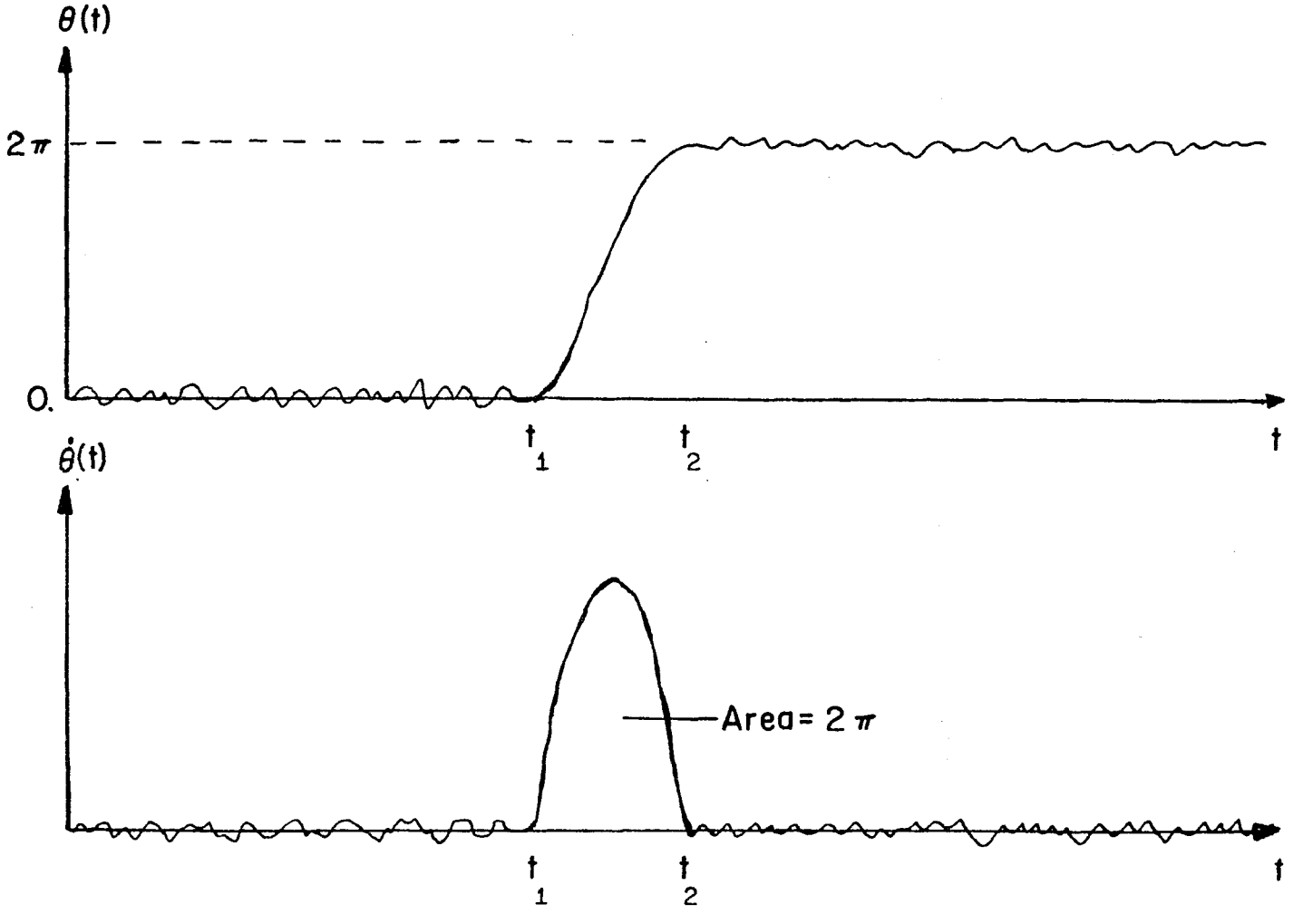

Figure 2.3.3 Illustrating the Spike Phenomenon(a) $\theta(t)$ vs.t (b) $\dot{\theta}(t)$ vs. t

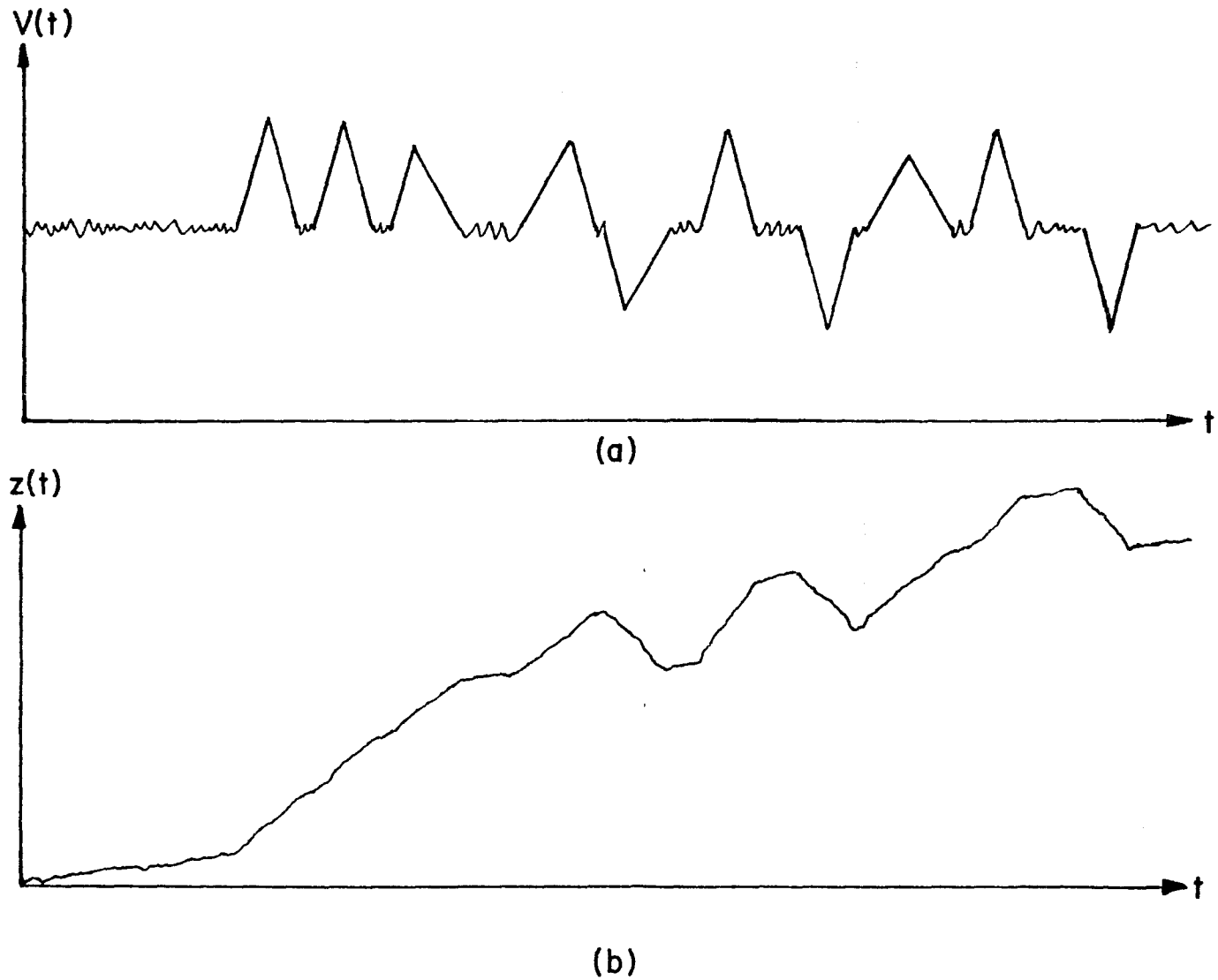

Figure 2.3.4 Possible System Output (a) at the Discriminator (b) at the Integrator

Chapter 3

ANALYSIS AND THEORETICAL RESULTS

We have shown in the previous chapter the structure of the acquisition loop and the parameters affecting the operation. In this Chapter we derive conditions for determining the sampling and integration times, the bandwidths and the number of iterations needed for the system to acquire lock. The analysis is divided into two regions. The first region is the high carrier signal-to-noise ratio case in which the smooth noise predominates. In this region we assume the occurrence of impulse or spike noise is rare and thus the noise power of the Gaussian noise overrides the inband spike noise power.

In the second region the spike noise is the predominant factor and the Gaussian noise is small. However, during the acquisition process the signal-to-noise ratio increases because the bandpass filter bandwidth is narrowed after each iteration. As this occurs the system changes its operating state and eventually reaches the high signal-to-noise region. So for this case we operate in two regions as opposed to the first case described above.

Since there is no reason to allow more noise to enter into the system than is necessary, another variable bandpass filter

is placed before the phase comparator. The only difference between this filter and the one inside the loop is that the center frequency of this external filter is at the carrier frequency f_c. The bandwidth of this filter will be changed in the same manner as that of the internal filter.

We will examine two approaches to the acquisition problem for both high and low SNR. One approach will be to reduce the bandwidth on each iteration by a fixed amount. This allows predetermined filters to be used each time and therefore the number of iterations to be performed and the integration times needed must be found. In the other approach a quasi-optimal technique will be used to find the "best" set of values of bandwidths and sampling times to be used.

3.1. Discriminator Operation.

Consider the inner loop configuration of Fig. 2.1.1 as modified in Fig. 3.1.1. Here we have distributed the gain of the VCO, $G_{VCO}(S_i/\eta B_K)$ in three stages: First, a constant value, G_V in volts per volt, at the output of the integrator; next a variable gain $g(S_i/\eta B_K)$ in volts per volt, which is dependent upon the signal-to-noise ratio parameter; finally, a unity gain, $G_V' = 1$ radian/sec/volt incorporated in the VCO itself. Thus $G_{VCO} = G_V' G_V g(S_i/\eta B)$. This need not be done in practice exactly in this manner, however, here it allows for an easier understanding of the ensuing analysis.

To determine the d.c. voltage at the discriminator output, V(t), we proceed as follows. The input signal without noise is

$e_s(t)$ as given by Eq. (2.2.2) and repeated below

$$e_s(t) = A \sin[(\omega_a+\Omega_D)t + \psi] \tag{3.1.1}$$

where Ω_D is the Doppler shift as explained in Chapter 2. Let us model the frequency discriminator as a limiter-differentiator-envelope detector configuration. Then the signal portion output of the differentiator, $e_s'(t)$ (not shown in Fig. 3.1.1), is

$$e_s'(t) = \alpha_1 A_L(\omega_a+\Omega_D)\cos[(\omega_a+\Omega_D)t + \psi]. \tag{3.1.2}$$

where α_1 is a constant associated with the differentiation process and A_L is the limiter amplitude. The limiter is necessary to remove any amplitude variations to the discriminator. The amplitude changes can be viewed as amplitude modulation which, under certain operating conditions, can degrade the system performance. The envelope detector output produces an output voltage proportional to the envelope of $e_s'(t)$. Thus the signal portion output of the FMD is $V_s(t)$ and is given by

$$V_s(t) = \alpha(\omega_a+\Omega_D) = 2\pi\alpha(f_a+f_D) \tag{3.1.3}$$

where $\alpha = \alpha_1 A_L$ and is the discriminator constant in volts/

radian/sec. From Eq. (3.1.3) we see that if there were no noise the output $V_s(t)$ would be proportional to the Doppler offset.

Let us now consider the noise as it is processed by the discriminator. We denote by $e_n(t)$ the noise component of the signal $e(t)$ at the output of the variable bandpass filter. The input to the FMD is $e(t) = e_s(t) + e_n(t)$ or

$$e(t) = A \sin(2\pi(f_a+f_D)t + \psi) + e_n(t). \qquad (3.1.4)$$

The noise component $e_n(t)$ contains two independent terms as discussed in the previous chapter - $e_{n_g}(t)$, the Gaussian noise process and $e_{n_s}(t)$ the spike noise process. We shall consider each noise process separately. We wish to have the discriminator determine the frequency of the signal portion of $e(t)$. Thus without loss of generality we will assume $\psi \equiv 0$ since it can be included in the noise term. $e_{n_g}(t)$ is a random process with a bandlimited power spectral density of $\eta/2$ watts/Hz. We can rewrite $e_{n_g}(t)$ as a sum of low pass noise process $n_x(t)$ and $n_y(t)$ as follows:

$$e_{n_g}(t) = n_x(t)\cos(2\pi f_I t) + n_y(t)\sin(2\pi f_I t) \qquad (3.1.5)$$

where $f_I = f_a + f_D$. We must now determine the power spectral

densities of the lowpass processes $n_x(t)$ and $n_y(t)$. It can be shown that [25] $G_{n_x}(f) = G_{n_y}(f)$ and

$$G_{n_y}(f) = G_{n_x}(f) = G_n(f-f_I) + G_n(f+f_I) \tag{3.1.6a}$$

where G_{n_x} G_{n_y} and G_n are the p.s.d. of $n_x(t)$, $n_y(t)$ and $e_{n_g}(t)$, respectively. Consider the power spectral density of $e_{n_g}(t)$ as indicated in Fig. 3.1.2. We note that the bandpass process is centered at frequency f_a and that f_I is the instantaneous carrier frequency. We have, in addition, illustrated two cases: one for which the Doppler frequency is below f_a (Case a) and one for which the Doppler frequency is above f_a (Case b). To determine $G_{n_x}(f)$ and $G_{n_y}(f)$ we perform Eq. (3.1.6a) and find [33]

$$G_{n_x}(f) = G_{n_y}(f) = \begin{cases} \eta & 0 < |f| \leq f_{max} - \Delta f \\ \eta/2 & f_{max} - \Delta f < f \leq f_{max} + \Delta f \end{cases} \tag{3.1.6b}$$

where Δf is the magnitude of the offset frequency f_D. This is illustrated in Fig. 3.1.3. Note that in either case the spectral density is the same.

For a conventional discriminator the determination of the output p.s.d. for the high SNR case is straightforward since the IF center frequency is $f_{IF} = f_a$, that is the carrier

frequency. However, in our case, the carrier frequency is a random variable and so we must use $f_{IF} = f_I$. This poses no problem as the ensuing analysis shows.

Using Eqs. (3.1.4) and (3.1.5) we can write

$$e_{n_g}(t) = [A + n_y(t)]\sin(2\pi f_I t) + n_x(t)\cos(2\pi f_I t) \qquad (3.1.7)$$

Alternately we can write Eq. (3.1.7) in a phasor representation as

$$e_{n_g}(t) = a(t)\sin(2\pi f_I t + \theta(t)) \qquad (3.1.8a)$$

where

$$a(t) = \sqrt{[A + n_y(t)]^2 + [n_x(t)]^2} \qquad (3.1.8b)$$

and

$$\theta(t) = \tan^{-1}\frac{n_x(t)}{A + n_y(t)} \qquad (3.1.8c)$$

To see this we expand $e(t)$ using the trigonometric identity for the sine of the sum of two angles

$$e_{n_g}(t) = a(t)[\cos\theta(t)\sin 2\pi f_I t + \sin\theta(t)\cos 2\pi f_I t] \qquad (3.1.9a)$$

But

$$\cos\theta(t) = [A + n_y(t)]/a(t) \qquad (3.1.9b)$$

and

$$\sin \theta(t) = n_x(t)/a(t) \tag{3.1.9c}$$

Substituting Eq. (3.1.9b) and (3.1.9c) in Eq. (3.1.9a) produces Eq. (3.1.7).

The frequency discriminator now processes $e_{n_g}(t)$ as given in Eq. (3.1.8a). As before the amplitude variations in $a(t)$ are removed by the limiter. Thus the output of the differentiator envelope detector is

$$V(t) = 2\pi\alpha f_I + \alpha \frac{d}{dt} \theta(t). \tag{3.1.10}$$

In the high signal-to-noise ratio case the Gaussian noise predominates. If we invoke this case we see that $A >> n_y(t)$ and $A >> n_x(t)$ except for rare instances. Thus $\theta(t)$ is small so that $\tan \theta(t) \approx \theta(t)$ and so we have

$$\theta(t) \approx \frac{n_x(t)}{A + n_y(t)} \approx \frac{n_x(t)}{A} \tag{3.1.11}$$

Here $\theta(t)$ represents the variation due to the (Gaussian) noise. Therefore the term $\alpha d\theta(t)/dt$ represents the output noise process $n_p(t)$.

$$n_p(t) = (\alpha/A) dn_x(t)/dt \tag{3.1.12}$$

Since $n_x(t)$ is a Gaussian process and differentiation is a linear operation, we have that $n_p(t)$ is also a Gaussian process.

We now determine the power spectral density of $n_p(t)$. In the frequency domain the time derivative, $d(\cdot)dt$, appears as a filter with transfer function $H_d(j\omega) = j\omega$. The function $(\alpha/A)d(\cdot)/dt$ is then modeled as a filter $H(j\omega) = j\omega/A$.

Since differentiation is a linear process we find the power spectral density, $G_{n_p}(f)$, of $n_p(t)$ as $G_{n_p}(f) = |H(j2\pi f)|^2 G_{n_c}(f)$ or

$$G_{n_p}(f) = (2\pi\alpha/A)^2 f^2 G_{n_x}(f) \tag{3.1.13a}$$

or

$$G_{n_p}(f) = \begin{cases} \frac{4\pi^2\alpha^2}{A^2} f^2\eta & 0 \leq f \leq f_{max} - \Delta f \\ \frac{4\pi^2\alpha^2}{A^2} f^2\eta/2 & f_{max} - \Delta f < f \leq f_{max} + \Delta f \end{cases} \tag{3.1.13b}$$

The density is plotted in Fig. 3.1.4. We shall use this information later to determine the inband noise power at the integrator output.

We now consider the spike noise phenomena. Even in the high signal-to-noise ratio case, occasionally some spikes

will be introduced into the system. For the no modulation case (in our instance $\Delta f = 0$) the number of positive spikes/sec, N_+, and negative spikes/sec, N_-, are equal and given by [ ]

$$N_+ = N_- = (B/4\sqrt{3})\,\mathrm{erfc}\,\sqrt{S_i/\eta B} \tag{3.1.14}$$

where $B = 2f_{max}$ is the IF bandwidth, η is the p.s.d., $S_i = A^2/2$ is the carrier power, and erfc is the complimentary error function defined as

$$\mathrm{erfc}(x) = \frac{2}{\sqrt{\pi}} \int_x^\infty e^{-y^2}\,dy \tag{3.1.15}$$

The total number of spikes per second for a carrier at the IF center frequency is $N_c = N_- + N_+ = 2N_- = 2N_+$.

When modulation is present the number of spikes per second increases as was stated in Chapter 2, Section 2.3.1. The increase in the number of spikes per second is [ ].

$$\delta N = |\Delta f| e^{-S_i/N_i} \tag{3.1.16}$$

In Eq. (3.1.16) Δf is the frequency offset from the center frequency of the bandpass filter and $N_i = \eta B$, the input noise power. Thus the total number of spikes per second is

$$N_T = N_c + \delta N \tag{3.1.17}$$

If $\Delta f = 0$, $\delta N = 0$, and we have that the number of positive and negative spikes is equal as we saw before in Chapter 2. We also noted there the polarity of these additional spikes at the discriminator output always opposes the polarity of the output signal produced by the offset Δf. This is illustrated in Fig. 3.1.5 for a sinusoidally modulated carrier.

The total area of these spikes is 2π radians. Thus if we observe the discriminator output in the presence of noise we see the waveform of Fig. 2.3.4. We wish to determine the d.c. value of this waveform. We see it consists of three parts: (a) the signal given by Eq. (3.1.3), (b) Gaussian noise, and (c) spike noise. Since the Gaussian noise is channel noise we assume it to be zero mean, that is, its average value is zero. Thus the Gaussian noise adds no d.c. to the output signal.

On the other hand, the spike noise does introduce a d.c. value into the output waveform. The amount of d.c. offset can be determined by realizing that for a given offset frequency more spikes will be produced in one direction than the other. If we consider the spikes as a pulse waveform then the amount of d.c. each spike introduces is

$$N_{DC} = 2\pi\alpha \tag{3.1.18}$$

where again α is the discriminator constant. The total d.c. introduced by all the spikes is

$$N_S = 2\pi\alpha\delta N \tag{3.1.19a}$$

This is due to the fact that the number of positive and negative spikes generated with no offset is equal. Thus the net d.c. offset is determined only by δN. Using Eq. (3.1.16) we find

$$N_S = 2\pi\alpha|f_D|e^{-S_i/N_i} \tag{3.1.19b}$$

Since $2\pi|f_D| = |2\pi f_D| = |\Omega_D|$ we have

$$N_S = |\Omega_D|e^{-S_i/N_i} . \tag{3.1.20}$$

The above is necessarily true only if we view the waveform over the doubly infinite time interval $t = [-\infty,\infty]$. Obviously this is too long a time to wait to produce a meaningful result. However, if one observes the output of the discriminator for a time which is substantially longer than the time between spikes, then on the average, Eq. (3.1.20) will be true. This basic assumption is made throughout the ensuing discussion.

3.2. Determination of the Calibration Curves

Consider again the output of the discriminator which may be written as

$$V(t) = \alpha(\omega_a+\Omega_D) + n_p(t) + n_p(t) \tag{3.2.1}$$

where $n_p(t)$ is zero mean Gaussian noise and $n_s(t)$ is the spike noise. From this voltage we subtract an amount of d.c. equal to $\alpha\omega_a$ and obtain

$$p(t) = \alpha\Omega_D + n_p(t) + n_s(t) \tag{3.2.2}$$

This signal, illustrated in Fig. 2.3.4a, is the input to the integrator shown in Fig. 3.1.1. $p(t)$ is a random process consisting of two noise processes. These noise processes are assumed independent and stationary. The stationarity can be realized if we allow the filter discriminator configuration time to reach steady state. By allowing a specified processing time $T_P = C/B_{IF}$, the steady state condition is attained. Independence of the Gaussian and spike noise as well as the independence of the spikes among themselves is assumed but can be borne out experimentally [20].

We now consider the integrator structure. We model the integrator as an averaging filter governed by

$$q(T_K) = \frac{1}{2T_K} \int_{-T_K}^{T_K} x(\beta)\,d\beta \tag{3.2.3}$$

where q is the filter output, T_K is the integration time constant, x is the input and β is a dummy variable of integration. If $x(t)$ is a constant, e.g., X, such as a d.c. voltage and if we perform the above integration subsequently sampling q at time T_K, the output will be the constant d.c. value x. In our system this would be representative of the frequency offset $\Delta f = \pm f_D$. Thus this form of d.c. detectors is appicable to our situation.

If $x(t) = p(t)$ then a possible output, $z(t) = q(t)$, is shown in Fig. 2.3.4b. With $p(t)$ as given by Eq. (3.2.2) we have

$$z(T_K) = 2\pi\alpha f_D + n_g(T_K) + n_{sp}(T_K) \tag{3.2.4}$$

Here $n_g(t)$, the Gaussian noise, is defined as

$$n_g(T_K) = \frac{1}{2T_K} \int_{-T_K}^{T_K} n_p(\lambda)\,d\lambda \tag{3.2.5a}$$

while $n_{sp}(T_K)$, the spike noise, is given by

$$n_{sp}(T_K) = \frac{1}{2T_K} \int_{-T_K}^{T_K} n_u(\lambda)\,d\lambda \tag{3.2.5b}$$

Since $n_p(t)$ is a zero mean Gaussian process, $n_g(T_K)$ is a zero mean Gaussian random variable.

Considering $n_{sp}(T_K)$ we see that it is derived from the spike noise term. If the integration time T_K is large

compared to the average time between spikes, T_{sp}, then by the central limit theorem $n_{sp}(t)$ can also be considered Gaussian [32]. The average time between spikes is inversely proportional to the number of spikes per second, N_T. N_T consists of two terms as can be seen from Eq. (3.1.17). The minimum number of spikes/second occurs for $\Delta f = 0$ and is $N_{min} = N_c$. The maximum number of spikes per second is $N_{max} = N_c + |\delta N|_{max}$ where $|\delta N|_{max}$ is found from Eq. (3.1.16) with $\Delta f = f_{max}$. For the central limit theorem to hold we need many spikes per second at the input to the integrator. We cannot guarantee that Δf will equal f_{max}. Therefore we will assume that N_c is sufficient for the central limit theorem to hold in all cases.

Although $n_{sp}(t)$ is Gaussian it is not zero mean since we have shown that the spikes introduce d.c. into the integrator output for $\Delta f \neq 0$. We can approximate the d.c. value by Eq. (3.1.20) and define a new zero mean process, $n'_{sp}(t)$ as

$$n'_{sp}(t) = n_{sp}(t) - \overline{n_{sp}}(t) \tag{3.2.6}$$

where the bar (—) denotes the expected value of (•). With $\overline{n_{sp}} = \alpha\Omega_D e^{-S_i/\eta B}$ we rewrite Eq. (3.2.4) as

$$z(t) = \alpha\Omega \left(1-e^{-\quad/\eta B}\right) + n_g(t) + n'_{sp}(t) \tag{3.2.7}$$

The reason for the term $-\alpha\Omega_D e^{-S_i/\eta B}$ is that, whether Ω_D is positive or negative it always tends to reduce the d.c. producing it, that is, the frequency offset Ω_D.

The reason for this is as follows. Let us consider the phasor diagram of Fig. 2.3.2 . For a carrier frequency at the center of the band there is an equal number of noise frequencies above and below this carrier. Therefore we expect an equal number of positive and negative spikes. If we consider a counter-clockwise (ccw) rotation as positive then such a rotation produces a positive spike. So the noise components at frequencies greater than the carrier produce positive spikes. A similar argument shows that negative spikes are produced by noise components below the carrier. Now consider a positive offset such that the true carrier frequency lies above the center of the band. Due to this offset more noise frequencies lie below the carrier than above it. From the arguments presented above this means more negative spikes will be produced. Thus a positive offset produced negative spikes which reduces the d.c. value at the discriminator output. A similar argument can be made for an offset which produces a carrier whose frequency is below the center of the band.

The input to the sample and hold unit is $y_1(t) = G_V z(t)$ so that

$$y_1(t) = G_V \alpha\Omega_D \left(1-e^{-S_i/\eta B}\right) + G_V n_g(t) + G_V n'_s(t) \qquad (3.2.8)$$

Without a loss in generality we define the gain $G_V\alpha$ as

$$G_V\alpha \equiv 1. \tag{3.2.9}$$

Then from Eqs. (3.2.8) and (3.2.10) we have

$$y_1(t) = \Omega_D\left(1-e^{-S_i/\eta B}\right) + G_V n_g(t) + G_V n_s'(t) \tag{3.2.10}$$

The expected value of $y_1(t)$, that is $E[y_1(t)] = \overline{y_1(t)}$ is

$$y_1(t) = \Omega_D\left(1-e^{-S_i/\eta B}\right) \tag{3.2.11}$$

which would be the value we would obtain if T_K were infinite. This means that the d.c. value of y_1 is directly related to Ω_D. Equation (3.2.11) forms the basis of our calibration curve. These curves are important for, once $S_i/\eta B$ is known, then the frequency offset can be computed for the value $\overline{y_1}$.

These calibration curves are essential for proper system functioning because they define the possible operating points. They also provide us with information needed for proper gain setting as will be seen shortly.

A set of calibration curves is plotted in Fig. 3.2.1 and a tabulation of the slope $\zeta = \left(1-e^{-S_i/N_i}\right)$ is made in Table 3.2.1. The ordinate is normalized to the variable $y_n = \overline{y_1}/\Omega_{max}$ and the abscissa to the variable $\nu = \Omega_D/\Omega_{max}$.

Both y_n and ν are continuous and lie in the closed interval [-1,1]. A few points should be made regarding these curves. First we note they all pass through the origin which means that for a zero offset frequency we expect zero d.c. output. In a practical arrangement this allows the system quiescent point to be set. Each curve is linear with respect to the frequency offset and the slope of each curve depends on the signal-to-noise ratio through the parameter ζ. The curves are bounded by two extremes: The infinite signal-to-noise ratio curve is the upper bound (slope $\zeta = 1$) and the infinite noise-to-signal ratio curve is the lower bound (slope $\zeta = 0$). As one would expect, in the latter case no amount of processing will yield a useful estimate of the frequency offset f_D. Also, one notices that for high SNR, e.g., SNR $\geq$ 10dB, the curves are extremely crowded, almost to the point of coalescing. This intimates that for high SNR the system is for all intents and purposes operating on one curve. This point will be raised later in determining the scheme for minimizing the acquisition time.

In Fig. 3.2.2 we have plotted the calibration curves for two particular values of SNR. The curve labeled 1 is for the no noise case, SNR = ∞. Curve 2 is for SNR = β, $|\beta| < \infty$, an intermediate value. Now suppose that the actual offset frequency is $\Omega_D = \Omega_{D_1}$ corresponding to $\nu = \nu_{D_1}$. Then, depending upon which curve the system is operating, we obtain an estimate for y_n, either y_{n_1} or y_{n_2}, as indicated. Since curve 1 is

the no noise case, obviously y_{n_1} is the "correct" d.c. value. Therefore, curve 2 and all other curves for which the SNR is not infinite must be mapped onto curve 1. We can do this by letting

$$g = 1/[1-\exp(-S_i/N_i)] \triangleq 1/\zeta \tag{3.2.13}$$

Thus the overall VCO gain is $G_{VCO} = G_V' G_V g$ or

$$G_{VCO} = G_V/[1-\exp(-S_i/N_i)] \tag{3.2.14}$$

If the gain of the S/H circuit is unity, then the output of the S/H is

$$y_2(T_K) \triangleq y_1(t)\big|_{t = T_K} \tag{3.2.15a}$$

Also

$$y(T_K) = g y_2(T_K) = y_2(T_K)/[1-\exp(-S_i/N_i)] \tag{3.2.15b}$$

Let us define the VCO instantaneous frequency, ω_q, as

$$\omega_q = \omega_V + \hat{\Omega}_D \tag{3.2.16}$$

where $\hat{\Omega}_D$ is the VCO estimated offset frequency. Since $G_V' = 1$,

$$\hat{\Omega}_D = y(T_K) \tag{3.2.17}$$

From Eqs. (3.2.10),(3.2.15) and (3.2.17) we have

$$\hat{\Omega}_D = \Omega_D + n_{g_1}(T_K) + n_{s_2}(T_K) \tag{3.2.18}$$

where $n_{g_1}(T_K) = G_V n_g(T_K)/[1-\exp(S_i/N_i)]$ and $n_{s_2}(T_K) = G_V n'_{sp}(T_K)/[1-\exp(S_i/N_i)]$. Since $n_{g_1}(T_K)$ and $n_{s_2}(T_K)$ are Gaussian random variables so is $\hat{\Omega}_D$.

If the noise is zero, we see from Eq. (3.2.18) that $\hat{\Omega}_D = \Omega_D$ and we have a perfect estimate. However, there is noise present and so further considerations must be made. We have tacitly assumed here that we integrated for a time, T_K, long enough to extract the true d.c. value of the signal y. This is not so since T_K would be infinite. In fact, we have used only the first moment, that is, the mean of y thus far. In the next section we use the second central moment to determine the system parameters.

3.3. Determination of the System Parameters.

To determine the effect of the noise on the estimate of Ω_D, we consider the following. From Eq. (3.2.18) we see that $\hat{\Omega}_D$ is a Gaussian random variable with mean Ω_D and variance $\sigma^2_{\hat{\Omega}_D}$ in $(\text{radian/sec})^2$ which due to the assumed independence

of n_{g_1} and n_{s_2} is given by

$$\sigma^2_{\hat{\Omega}_D} = \sigma^2_{n_{g_1}} + \sigma^2_{n_{s_2}} \tag{3.3.1}$$

where $\sigma^2_{n_{g_1}}$ and $\sigma^2_{n_{s_2}}$ are the variances of n_{g_1} and n_{s_1} respectively. The probability density, $p_{\hat{\Omega}_D}(\hat{\Omega}_D)$, of $\hat{\Omega}_D$ appears as in Fig. 3.3.1. Considering the shape of $p_{\hat{\Omega}_D}(\hat{\Omega}_D)$ we see that our estimate lies in an interval $I_u = (\Omega_D \pm \ell\sigma_{\hat{\Omega}_D})$, where ℓ is a number greater than zero, and $\sigma_{\hat{\Omega}_D}$ is the standard deviation of $\hat{\Omega}_D$ with a probability $P_{\hat{\Omega}_D}$; that is,

$$\Pr(|\hat{\Omega}_D - \Omega_D| \leq \ell\sigma_{\hat{\Omega}_D}) = P_{\hat{\Omega}_D} \tag{3.3.2}$$

This means that the estimate for Ω_D now lies in a new bandwidth $W = 2\ell\sigma_{\hat{\Omega}_D}$, with probability $P_{\hat{\Omega}_D}$.

Another way to visualize this is shown in Fig. 3.3.2 which is in essence an inversion of Fig. 3.2.2. In this case let us assume $g(S_i/N_i) = 1$ for all S_i/N_i. Then the normalized estimate $\hat{\Omega}_D/\Omega_{max}$ when plotted for values of normalized output voltage, $y_2/(y_2)_{max}$, appears as in Fig. 3.3.2. $y_2/(y_2)_{max}$ us a Gaussian random variable as indicated in Eq. (3.2.15).

Thus for a particular measured value $y_2'/(y_2)_{max}$, there is a Gaussian distribution about this point. For different values of SNR, we see different values of the frequency estimate μ_1 and μ_2. (This is expected since we have assume $g = 1$). But also we see different uncertainty regions for each operating point. For curves β and α we see that $2\sigma_\beta > 2\sigma_\alpha$. Thus with each operating curve we have a different uncertainty region. This variation with SNR is reflected in the noise terms of Eq. (3.2.18) by the factor $1/[1-\exp(-S_i/N_i)]$. This factor appears, as will be shown shortly, in the variances $\sigma^2_{n_{g_1}}$ and $\sigma^2_{n_{s_2}}$

If the new bandwidth W is less than the previous unknown bandwidth then we have achieved a gain over our previous operating point. For example, originally our unknown bandwidth was $2\Omega_{max}$. If W is less than $2\Omega_{max}$ we have narrowed our uncertainty bandwidth. It will be shown that W is inversely related to the integration time T_K. Thus, the longer we integrate the smaller our uncertainty bandwidth becomes. We must note, however, that we can make an error. By choosing a finite value for ℓ in Eq. (3.3.2) we allow for the possibility of the estimate falling outside our new bandwidth. However, since $\hat{\Omega}_D$ is Gaussian, by choosing $\ell \geq 3$ the probability of error drops quickly. For 3 standard deviations the probability of error, p, after one iteration is less than 2.6×10^{-3}. In Appendix 1 it is shown that the probability of error for n iterations is, from Eq. (A1-6), $P_n = 1 - (1-p)^n$.

In the event that an error is made we will need some form of indicator, that is, a lock indicator. Since often data is transmitted once lock is achieved the detection of data can be used as a lock indicator. Or another possible choice is a threshold detector. If lock is achieved the voltage at the output of the BPF should be considerable. If only noise is present it will be small. For a typical lock indicator and a discussion see [11].

So herein lies our method. We begin with an initial uncertainty bandwidth $W_o = 2\Omega_{max}$. After a processing time T_{P_o}, we integrate for a time T_o and then we sample the output, y_1. After an appropriate scaling by g we move the VCO a certain amount, $gy_1(T_o)$. An infinitesimal time afterward, T_o^+, we change the bandwidth of the VBPF to W_1 and continue the process with a new processing time T_{P_1} and integration time T_1. This iterative technique is maintained until the bandwidth is reduced so that a tracking loop will be able to lock automatically since, at this point, it will be operating above threshold. This method assumes that the SNR is known or a good estimate is available. For proper operation this must be known a priori. Also, a mechanism for switching the bandwidths and establishing the new processing and integration times is assumed available. A pre-programmed microprocessor with a Read Only Memory (ROM) could be used for this purpose. Also we mention that as the bandwidths change the SNR increases.

As such the variance of $\hat{\Omega}_D$ decreases and we achieve an even better estimate since we are moving the operating point to the high SNR region.

In the ensuing analysis we have chosen to make the new bandwidth, B_{K+1} in Hz equal to $\gamma\sigma_{\hat{f}_D}$, that is,

$$B_{K+1} = \gamma\sigma_{\hat{f}_D} \tag{3.3.3a}$$

$$\gamma = 2\ell \tag{3.3.3b}$$

$$\sigma_{\hat{f}_D} = \sigma_{\hat{\Omega}_D}/2\pi \tag{3.3.3c}$$

In the next subsections we consider the two regions: high SNR and low SNR and determine the parameters for estimation procedure.

3.3.1. High Signal-to-Noise Ratio Region.

First we consider the system operating in the high SNR region which we set to be $S_i/\eta B_o = S_i/(2\eta f_{max}) \geq 10$db. In light of this fact we state that the number of spikes/second is small and thus the spike noise does not contribute appreciable noise power to the integrator output. As an example suppose we choose $B_o = 200$kHz, $S_i/\eta B_o = 10$dB and assume $\Delta f = f_{max} = 100$kHz. Then using Eqs. (3.1.14), (3.1.16) and (3.1.17) we find $N_T = (10^5/\sqrt{3})\text{erfc}\ \sqrt{10} + 10^5 e^{-10} \simeq 5$ spikes/sec. This is minimal when compared to the number of spikes per second

for the same bandwidth and Δf as above but for $S_i/\eta B_o = 0dB$. In this case $N_T = 45 \times 10^3$ spikes/sec. For this reason we will neglect $n_{sp}(t)$ in Eq. (3.2.4) and accordingly $n_s'(t)$ in Eq. (3.2.9b). The d.c. term in Eq. (3.2.9b) contributed by the spikes will also be in general negligible (for example, $e^{-10} \times 4.4 \times 10^{-5} << 1$) however, we shall retain it in the ensuing analysis.

Consider now Eq. (3.2.18) when $n_{s_2}(T_K)$ is negligible. We have then that

$$\hat{\Omega}_D\Big|_{\text{High SNR}} = \hat{\Omega}_{DH} = \Omega_D + n_{g_1}(T_K) \tag{3.3.4}$$

where $\hat{\Omega}_{DH}$ designates the estimate in the high SNR region. To determine the new uncertainty bandwidth we must find the variance of $\hat{\Omega}_{DH}$. From Eq. (3.3.4) we see that $\sigma^2_{\hat{\Omega}_{DH}} = {}^{2}_{n_{g_1}}$. Therefore we must determine the variance of the noise $n_{g_1}(T_K)$.

To do this we first examine Eq. (3.2.5a). It is known that for a filter defined as in Eq. (3.2.3), the mean of q, that is, $\bar{q}$ and the variance σ_q^2, is given by [16]

$$\bar{q} = \bar{x} \tag{3.3.5a}$$

$$\sigma_q^2 = \frac{1}{2T_K}\int_{-2T_K}^{2T_K}\left(1 - \frac{(\tau)}{2T_K}\right)C_x(\tau)d \tag{3.3.5b}$$

where $C_x(\tau)$ is the covariance function of the input process x.

In our case $q(t) = z(t)$ and $x(t) = n_p(t)$. Since $\overline{n_p(t)} = 0$, $C_{n_p}(\tau) = R_{n_p}(\tau)$ the correlation function. To find $R_{n_p}(\tau)$ we must perform the inverse Fourier transform of $G_{n_p}(f)$ as given by Eq. (3.1.13b). Next, to find σ_z^2 we must substitute $R_{n_p}(\tau) = C_{n_p}(\tau)$ into Eq. (3.3.5) and evaluate the integral. This is a tedious process. An alternative method is used in Appendix 2. The result is from Eq. (A2.14)

$$\sigma_z^2(T_K, B_K, S_i/\eta, \Delta f) = \frac{\alpha^2}{\frac{4S_i}{\eta B_K}} \frac{1}{T_K^2} \left[1 - \frac{\sin 2\pi B_K T_K}{2\pi B_K T_K} \cos 4\pi \Delta f\, T_K\right] \quad (3.3.6)$$

Examining Eq. (3.3.6) we see that σ_z^2 is a function of the IF bandwidth B_K, the integration-sampling time, T_K, the signal-to-noise power spectral density ratio, SNRD = S_i/η, and offset frequency $\Delta f = f_D$. The dependence of σ_z^2 on Δf must now be examined. From Fig. 3.1.4 we note that there are two extreme cases for $G_{n_p}(f)$. The first is for $\Delta f = 0$ in which case the p.s.d. wholly contained in the interval $|f| \leq f_{max}$. This is illustrated in Fig. 3.3.3a along with $G_{n_c}(f)\big|_{\Delta f = 0}$. The other extreme occurs for $\Delta f = f_{max}$, and is indicated in Fig. 3.3.3b along with $G_{n_c}(f)\big|_{\Delta f = f_{max}}$. All other values for Δf result in a p.s.d. as shown in Fig. 3.1.4. We see from Fig. 3.3.3a that for $\Delta f = 0$ the height of the p.s.d. is H_1 where H_1 is proportional to ηf_{max}^2. From Fig. 3.3.3b it is evident that the height of $G_{n_p}(f)$ for $f = f_{max}$ is

$H_1/2$. It is also obvious from Fig.3.3.3 that the total noise is greater for $\Delta f = f_{max}$ than for $\Delta f = 0$. However, the total noise for $|f| \leq f_{max}$ is higher for the case when $\Delta f = 0$. In fact, for $\Delta f \neq 0$, the total noise in the region $|f| \leq f_{max}$ is always smaller than for $\Delta f = 0$. Since the estimate is known to be in the region $|f| \leq f_{max}$, the total inband noise power is maximum when $\Delta f = 0$. This realization tells us that a low pass of bandwidth $B_{LPF} = f_{max}$ should be placed at the discriminator output so that unwanted, irrelevant noise does not enter the integrator. However, since an integrator is like a low pass filter, if the bandwidth of the integrator is sufficiently small the lowpass filter is not needed. The integrator bandwidth depends upon the integration time which is as yet undetermined. Thus, if a LPF is not included, then for each particular integration time this aspect must be verified. We will assume a LPF is included in the ensuing analysis.

By choosing $\Delta f = 0$ we have found the worst case variance for σ_z^2 that is from Eq. (3.3.6).

$$\sigma^2_{\hat{\Omega}_{DH^W}} = \frac{\alpha^2}{4(S_i/\eta B_K)} \frac{1}{T_K^2} \left[1 - \frac{\sin 2\pi B_K T_K}{2\pi B_K T_K}\right] \tag{3.3.7}$$

where $\sigma^2_{\hat{\Omega}_{DH^W}}$ is in $(\text{radian/sec})^2$. Since

$$n_{g_1} = \frac{G_V}{\left(1-e^{-S_i/\eta B_K}\right)} n_g \tag{3.3.8a}$$

we find that, in the worst case

$$\sigma^2_{n_{g_1}} = \frac{G_V^2}{\left(1-e^{-S_i/\eta B_K}\right)^2} \sigma^2_{\hat{\Omega}_{DH}{}^w} \tag{3.3.8b}$$

With $G_V\alpha = 1$, then from Eqs. (3.3.7) and (3.3.8b) we obtain

$$\sigma^2_{n_{g_1}} = \frac{1}{4(S_i/\eta B_K)} \frac{1}{T_K^2} \left[1 - \frac{\sin 2\pi B_K T_K}{2\pi B_K T_K}\right] \Big/ \left(1-e^{-S_i/\eta B_K}\right)^2 \tag{3.3.9}$$

where $\sigma^2_{n_{g_1}}$ is in $(\text{rad/sec})^2$ also. For the worst case variance in Hz^2 we divide $\sigma^2_{n_{g_1}}$ by $(2\pi)^2$ and obtain $\sigma^2_{\hat{f}_H}$ where

$$\sigma^2_{\hat{f}_H} = \left[\frac{1}{16\pi^2(S_i/\eta B_K)}\right] \frac{1}{T_K^2} \left[1 - \frac{\sin 2\pi B_K T_K}{2\pi B_K T_K}\right] \Big/ \left(1-e^{-S_i/\eta B_K}\right)^2 \tag{3.3.10}$$

Using Eqs. (3.3.3a) and (3.3.10) we see that our worst case bandwidth for the next iteration is given by

$$B_{K+1} = \gamma\sigma_{\hat{f}_H} = \frac{(\gamma/2)B_K}{\sqrt{\rho_K}} \frac{\sqrt{1-Sa(\xi_K)}}{\xi_K} \frac{1}{1-e^{-\rho_K}} \tag{3.3.11a}$$

where we have introduced for simplification the notation

$$\rho_K \triangleq S_i/\eta B_K \tag{3.3.11b}$$

$$\xi_K \triangleq 2\pi B_K T_K \tag{3.3.11c}$$

and $Sa(x) = (\sin x)/x$, the sampling function. Equation (3.3.11) is the defining relationship for the system in the high SNR case. We see from this equation that the new bandwidth is inversely proportional to the integration time. The longer the integrator is operational the narrower the uncertainty in the bandwidth becomes.

From Eq. (2.2.4), which is repeated here

$$T_{PK} = C/B_K \tag{3.3.12a}$$

$$T_{ACQ} = \sum_{K=1}^{N=1} T_{PK} + T_K \tag{3.3.12b}$$

and Eq. (3.3.11) we see that T_{ACQ} is a nonlinear discrete function of N, T_K, B_K and ρ_K. However, if the set of bandwidths is defined then we can use Eq. (3.3.11) to find the corresponding set of integration times and thus calculate T_{ACQ} from Eq. (3.3.12). Of course this method assumes N known. The best N, N^*, is not known <u>a priori</u>. We will see later that it is not an easy matter to find the best N. However, we will assume N is chosen <u>a priori</u> and then determine T_{ACQ}.

We now wish to use Eq. (3.3.11) to find the integration times. Let us first assume that we choose a fixed set of intermediate bandwidths, $\{B_K\} = \{B_o, B_1, \cdots, B_{N-2}, B_{N-1} = B_F\}$ where the initial bandwidths are parameters of the system known a priori. We must choose $N - 2$ bandwidths $\{B_1, B_2, \cdots, B_{N-2}\}$. Furthermore, let us first assume we choose them arbitrarily except for the constraint that $B_{K+1} < B_K < B_{K-1}$, that is, the bandwidths decrease with increasing iteration number. We will see later that the bandwidths depend on S_i/η. Using this set of values in Eq. (3.3.11) we find the appropriate $\{T_K\}$ and thus T_{ACQ}. To do this we proceed as follows.

If we examine Eq. (3.3.11a) we see we can separate it into two functions, one dependent upon ξ_K and the other on ρ_K. In particular we can write

$$r_K = g(\xi_K)h(\rho_K) \tag{3.3.13a}$$

where

$$g_K \triangleq g(\xi_K) \triangleq \frac{1}{\xi_K}\sqrt{\left(1 - \frac{\sin \xi_K}{\xi_K}\right)}\,, \tag{3.3.13b}$$

$$h_K \triangleq h(\rho_K) \triangleq \frac{\gamma/2}{\sqrt{\rho_K}}\,\frac{1}{1-e^{-\rho_K}} \tag{3.3.13c}$$

and

$$r_K \triangleq B_{K+1}/B_K \tag{3.3.13d}$$

Here r_K is the ratio of the new bandwidth to the old bandwidth and to be useful it must lie in the region $0 < r_K < 1$. Thus for our constant bandwidth reduction approach we can choose a set of r_K's and solve Eq. (3.3.13) for T_K by numerical methods. However, we must be careful. We find in certain cases that an arbitrary choice of r_K's, and therefore B_K's, does not always yield a solution. To see this we examine Eq. (3.3.13) more closely.

First consider Eq. (3.3.13b). Since g_K is a function of a single variable we can plot g_K versus ξ_K as in Fig. 3.3.4. The asymptote $y = 1/\xi_K$ is also shown. We see that this function is a monotonically decreasing function. Its maximum value occurs at the origin and is $g_K\big|_{max} = \lim_{\xi_K \to o} g_K(\xi_K) = 1/\sqrt{6} \simeq .408$. This limit is most easily obtained by expanding $Sa(\xi_K)$ in a power series, then bringing the $(1/\xi_K)$ in Eq. (3.3.13b) inside the square root and dividing.

We note here that for ξ_K to approach zero either B_K or T_K must approach zero. However, a zero bandwidth system has no meaning thus it must be the integration time which approaches zero. This in turn states that we do not integrate but merely sample the discriminator output at the end of the processing interval $t = T_{PK}$. Since the discriminator output noise process has finite variance we obtain a finite value for the new bandwidth $B_{K+1} = B_K h(\rho_K)/\sqrt{6}$.

The function h_K also varies inversely as ρ_K and is maximum for $\rho_K = 0$ ($h_K(0) = \infty$). Thus, h_K is also a monotonically decreasing function. This is shown in Fig. 3.3.5. For $\rho_K \geq 10$, $1 - e^{-\rho_K} \approx 1$. Therefore $h_K \approx (\gamma/2)/\sqrt{\rho_K}$. Since in the high SNR case $\rho_K \geq 10$, $h_K|_{max} \approx (\gamma/2)/\sqrt{10}$ and so r_K has a maximum value given by

$$r_K|_{max} = g_K|_{max} h_K|_{max} = \frac{1}{\sqrt{6}} \frac{\gamma/2}{\sqrt{10}} \quad . \tag{3.3.14}$$

For $\gamma = 6$, $r_K|_{max} \approx 3/8$ which yields a gain in SNR of 4.26dB. To try to reduce the bandwidth to one-fourth its previous value, and so gain 6dB in SNR, is futile. No solution exists for this case.

Rather than arbitrarily choosing the new bandwidths, $B_1, B_2, \cdots, B_{N-2}$, and so the ratios $r_o = B_o/B_1$, $r_1 = B_1/B_2$, $\cdots, r_{N-2} = B_{N-2}/B_{N-1}$, we now proceed to find a quasi-optimum set of values for the B_K's. The B_K's should be optimum in the sense that they minimize the acquisition time, T_{ACQ}.

To find the best set of B_K's we establish a cost criterion, J, and minimize it with respect to the set of B_K's. Our cost criterion is

$$J = \sum_{K=K_o=o}^{K_f=N-1} T(B_K, B_{K+1}) \tag{3.3.15}$$

subject to the conditions that B_o and B_{N-1} are specified

and the inequality constraint that $B_{K+1} < B_K$. Note this is a strict inequality for if we include the equality sign we have in essence not changed the state. This gains us nothing in terms of minimizing J. (This condition is the same as that obtained from Eq. (3.3.13d) with $0 < r_K < 1$.)

Equation (3.3.15) can be minimized by using the discrete Euler-Lagrange Equation [21]

$$\frac{\partial T(B_K, B_{K+1})}{\partial B_K} + \frac{\partial T(B_{K-1}, B_K)}{\partial B_K} = 0 \tag{3.3.16}$$

However, Eq. (3.3.15) poses an additional problem in that the solution for its minimization can only be found for $K = K_f$, and therefore N, fixed. Thus our only recourse is to set a value for N and minimize J for each of these cases. We then choose as our best value for the acquisition, T^*_{ACQ}, the minimum over this set, that is,

$$T^*_{ACQ} = \min_N \{T_{ACQ}\} \tag{3.3.17}$$

This may seem like an arduous task since N is unspecified. However, since we do not want to perform many iterations because the probability of error increases we can set a maximum value on K_f, for example, $K_f = 10$. For this value and for $p = 1.3 \times 10^{-3}$, $1 - p = .9987$, and $(1-p)^{10} = .987$. Thus, the probability of error after 10 iterations is $P_{10} = 1 - .987 = .013$.

($P_2 = .0026$, $P_3 = .0039$). This is about the level of error we wish to tolerate. To decrease it we would have to increase the number of standard deviations for each iteration to some number greater than 3. This would reduce p but also increase T_K. Thus a tradeoff exists.

Another point is to be made here. If the minimization process produces a set of B_K's such that $B_{K+1} > B_K$ for a particular N, we disregard this case. The reason we can do so is this. Although mathematically these B_K's may produce a smaller J for a particular N, from a practical point it means we are widening our bandwidth to allow more noise in than previously. This is something a communications system should not do. At most we should leave the situation as before, that is set $B_{K+1} = B_K$. But by doing this we haven't changed the system state and so we have the same conditions as before. A minimization at this point produces the same result, that is, $B_{K+1} > B_K$. Thus we exclude this "solution" from our set.

When we apply Eq. (3.3.16) to Eq. (3.3.12) we encounter unwieldy mathematics. We found the difficulty was with the function $g(\xi_K)$. So we conclude that a simplifcation of this function might be helpful. Functions of various forms were tried but the most successful one was the simplest. We chose the approximating function, $g_a(\xi_K) = g$ as

$$g_a(\xi_K) = \frac{\alpha_o}{1+\beta_o \xi_K} \tag{3.3.18}$$

where α_o and β_o are constants. Since $g(0) = 1/\sqrt{6}$ we see $\alpha_o = 1/\sqrt{6}$. β_o was chosen to match the value of g_K at $\xi_K = 8.0$. Using this value we found $\beta_o = .311$. The result is shown in Fig. 3.3.6). Although the fit is not the best in the mean square error sense, we find that the results obtained using this approximation are quite good.

Substituting the above approximation in Eq. (3.3.13) and using Eq. (3.3.17b) we find that

$$T_K \approx \frac{1}{2\pi\beta_o}\left[\frac{(\gamma/2)}{\sqrt{\rho_K}}\,\frac{\alpha_o}{1-e^{-\rho_K}}\,\frac{1}{B_{K+1}} - \frac{1}{B_K}\right] \tag{3.3.19}$$

We now use Eqs. (3.3.19) and (3.3.12a) in Eq. (3.3.15) and perform the operations indicated by Eq. (3.3.16). After simplifying the result we find, due to the above approximation, the quasi-optimal solution for the K-th bandwidth, B_K^*, is

$$B_K^* = \left\{\frac{\left[\frac{\sqrt{B_{K-1}}}{1-e^{-\rho_{K-1}}} + \frac{a}{b}\right](1-e^{-\rho_K})B_{K+1}}{\left[\frac{1}{2} + \frac{\rho_k e^{-\rho_K}}{1-e^{-\rho_K}}\right]}\right\}^{2/3} \tag{3.3.20a}$$

where

$$a = c - 1/(2\pi\beta) \tag{3.3.20b}$$

$$b = b'(\gamma/2)/\sqrt{S_i/\eta} \tag{3.3.20c}$$

and

$$b' = \alpha/2\pi\beta \qquad (3.3.20d)$$

The above equation can be solved iteratively for a given initial guess, $(\underline{B}_K)_I$ where $(\underline{B}_K)_I$ is an N vector of initial values. For our purposes we chose a value of C = 3. That is, $T_{PK} = 3/B_K$ for all iterations, K = 0,1,...,N-1. This seems to be a sufficiently long enough settling time to wait. With this value of C, we found that the convergence of Eq. (3.3.20a) was fast. Of course, N is chosen as well as B_o and B_{N-1}. These values are then used in Eqs. (3.3.19) and (3.3.12a) to find T_K^* and T_{PK}^*, the quasi-optimal integration and processing times respectively. These are then used in Eq. (3.3.12b) to find T_{ACQ}^*, the quasi-optimal acquisition time. By perturbing the solution vector $\underline{B}_K^*$ about the solution and then evaluating T_{ACQ}, we find, in most cases, that B_K^* produces the minimum T_{ACQ} for any given N and S_i/η. Furthermore, we find that, since the system is above threshold to begin with, one integration is sufficient. Thus the minimum occurs as an interior point for all values of B_o, B_{N-1}, and S_i/η. In addition we find that the integration time for high SNR is substantially less than the processing time T_{PK}. So we conclude that at most a few iterations suffice in all cases.

3.3.2. Low Signal-to-Noise Ratio Region.

We now examine the system operation when the SNR is below threshold. In this region the inband noise power contributed by the spikes is substantial, that is, $n_{s_2}(T_K)$ in Eq. (3.2.18) is not negligible. We therefore must determine the noise variance of the spike process as it relates to the integrator output.

Let us assume that the spikes appearing at the discriminator output are perfect impulses. Since the longest spike is of the order of $T_\Delta = 2/B$ seconds duration, if the time constant of the filter, i.e., integrator, is large compared to T_Δ, the spikes appear as impulses.

We first define the Poisson Impulse Process (PIP), $p_i(t)$ such that

$$p_i(t) = \sum_{\ell} \delta_D(t-\tau_\ell) \tag{3.3.21}$$

where δ_D is the Dirac Delta or impulse function defined by

$$\delta_D(t) = \begin{cases} \infty, & t = 0 \\ 0, & \text{elsewhere} \end{cases} \tag{3.3.22a}$$

and

$$\int_{-\infty}^{\infty} \delta_D(\lambda)\,d\lambda = 1 \tag{3.3.22b}$$

The τ_ℓ are independent, identically distributed random variables (i.i.d.r.v.) with a distribution function $P_m(t)$ defined as

$$P_m(t) = e^{-\lambda t}(\lambda t)^m/m! \tag{3.3.23}$$

where $P_m(t)$ is the probability that m impulses arrive in the time interval $[o,t]$. λ is the mean arrival rate in impulses per second. We assume λ is constant. For a constant λ, $p_i(t)$ is a stationary Poisson distributed process with parameter λt. Furthermore, it can be shown [17] that

$$E[p_i(t)] = \lambda \tag{3.3.24}$$

and

$$R_p(\alpha) = E[p_i(t)\,p_i(t+\alpha)] = \lambda^2 + \delta_D(\alpha) \tag{3.3.25}$$

Now let us consider a process $q_\ell(t)$ where

$$q_\ell(t) \triangleq \sum_\ell a_\ell \delta_D(t-\tau_\ell) \tag{3.3.26}$$

where the coefficient, a_ℓ, represents the strength of the impulse occurring at time τ_ℓ. The a_ℓ are i.i.d.r.v., independent of τ_ℓ, and have mean

$$E(a_\ell) = \bar{A} \tag{3.3.27a}$$

and second moment

$$E(a_\ell^2) = \overline{A^2} \tag{3.3.27b}$$

for all ℓ. We show in Appendix 3 that, with $q_\ell(t)$ defined as above, we have from Eqs. (A3.4) and (A3.9) that

$$E(q_\ell) = \bar{A}\lambda \tag{3.3.28a}$$

and

$$R_q(\tau) = E[q_\ell(t_1)q_\ell(t_2 = t_1+\tau)] = \lambda\overline{A^2}\delta_D(\tau) + \lambda\bar{A}^2 \tag{3.3.28b}$$

so that

$$C_q(\tau) = \overline{A^2}\lambda\delta_D(\tau) \tag{3.3.28c}$$

We must now determine $\bar{A}$ and $\overline{A^2}$. To do this we reconsider the process $q_\ell(t)$. Since $q_\ell(t)$ represents the spike noise at the discriminator output, that is, $q_\ell(t) = n_s(t)$, the a_ℓ must be $\pm 2\pi\alpha$. We now must determine the distribution of the a_ℓ. Let us first let

$$b_\ell = a_\ell/2\pi\alpha \tag{3.3.29}$$

Thus $b_\ell = \pm 1$. With N_+ and N_- as the number of positive and negative spikes with no modulation respectively and δN the

increase in the number of spikes we find

$$P_{b_\ell/\Omega_D} = \left[\frac{N_+ + \delta N U(-\Omega_D)}{N_T}\right] \delta_D(b_\ell - 1) + \left[\frac{N_- + \delta N U(\Omega_D)}{N_T}\right] \delta_D(b_\ell + 1) \tag{3.3.30}$$

where P_{b_ℓ/Ω_D} is the conditional density of the b_ℓ given $\Delta\omega = \Omega_D$. N_T is the average number of spikes/second given by

$$N_T = N_+ + N_- + \delta N \tag{3.3.31}$$

and $U(x)$ is the unit step function defined as

$$U(x) = \begin{cases} 1 & x > 0 \\ 0 & x \leq 0 \end{cases} \tag{3.3.32}$$

From Eq. (3.3.30) we see that

$$E(b_\ell/\Omega_D) = \frac{1}{N_T}\left\{ N_+ - N_- + \delta N[U(-\Omega_D) - U(+\Omega_D)] \right\} \tag{3.3.33}$$

Since $N_+ = N_-$, and $U(-x) - U(x) = -\mathrm{sgn}(x) = \mathrm{sgn}(-x)$ we have

$$E(b_\ell/\Omega_D) = -\frac{\delta N}{N_T}\,\mathrm{sgn}(\Omega_D) \tag{3.3.34}$$

Now $\delta N = |\Omega_D/2\pi| e^{-S_i/\eta B_K}$ so $E(b_i/\Omega_D)$ is

$$E(b_\ell/\Omega_D) = (-|\Omega_D|/2\pi N) e^{-S_i/\eta B_K}\,\mathrm{sgn}(\Omega_D) \tag{3.3.35a}$$

which is of the form $c(-|x|\text{sgn } x)$ where c is a constant. However, $-|x|\text{sgn } x = |x|\text{sgn}(-x) = -x$. Thus we have

$$E(b_\ell|\Omega_D) = -\frac{\Omega_D}{2\pi N_T} e^{-S_i/\eta B_K} \tag{3.3.35b}$$

Since $a_\ell = 2\pi\alpha b_\ell$ we have

$$E(a_i|\Omega_D) = -\frac{\alpha\Omega_D}{N_T} e^{-S_i/\eta B} \tag{3.3.36}$$

Finally, since $N_T = \lambda$ and $E(q_\ell) = \bar{A}\lambda$ we have

$$E(q_\ell) = -\alpha\Omega_D e^{-S_i/\eta B_K} \tag{3.3.37}$$

This agrees with our intuitive concept of the d.c. value of the spikes.

Now we must find $\overline{A^2}$. Since $a_\ell = 2\pi\alpha b_\ell$, $\overline{A^2} = (2\pi\alpha)^2 E(b_\ell^2)$ we find

$$E(b_{\ell|\Omega_D}^2) = (+1)^2 P(b_{\ell|\Omega_D} = +1) + (-1)^2 P(b_{\ell|\Omega_D} = -1) =$$

$$= P(b_{\ell|n_p} = +1) + P(b_{\ell|n_p} = -1) = 1 \tag{3.3.38a}$$

and

$$\overline{A^2}_{|\Omega_D} = (2\pi\alpha)^2 \tag{3.3.38b}$$

Thus we have found the conditional variance of the a_ℓ's given Ω_D. So, from Eq. (3.3.28c) we find

$$C_q(\tau) = (2\pi\alpha)^2 \lambda \delta_D(\tau) \tag{3.3.39}$$

Note that this is a conditional covariance based on knowing Ω_D. This is similar to the p.s.d. we found in the high SNR case which was a function of $\Delta f = f_D$. We expect this since the offset frequency influences the number of spikes per second. Thus, that term was also a conditional variance. We eliminated the dependence in that case by choosing $\Delta f = 0$ for worst case noise. In this case we will make a similar although different assumption as will be seen shortly.

This impulsive noise process is now passed through the integrator. It can be shown that for filtered impulse noise if the correlation times of the spikes are less than the time constants of the filter by an order of magnitude or more then, by the central limit theorem, the output process is approximately Gaussian [31]. Thus for the spike noise case we find that the output process of the integrator is Gaussian. The process $q_\ell(t)$ described above is just $n_s(t)$ as in Eq. (3.2.1). The output of the integrator is $n_{sp}(T_K)$ as in Eq. (3.2.5b) with mean

$$\overline{n_{sp}} = -\Omega_D e^{-S_i/\eta B_K} \tag{3.3.40}$$

With $n'_{sp} = n_{sp} - \overline{n_{sp}}$, we now need the variance of n'_{sp}. Since by design n'_{sp} is zero mean, $\overline{n'^2_{sp}}$ is the variance of n'_{sp}. Denoting this variance as $\sigma^2_{n_{sp}}$ we have

$$\sigma^2_{n'_{sp}} = \left(\frac{1}{2T_K}\right)^2 \int_{-T_K}^{T_K} \int_{-T_K}^{T_K} E[n_s(t_1) n_s(t_2=t_1+\tau) dt_1 dt_2] - \overline{n^2_{sp}} \tag{3.3.41a}$$

or

$$\sigma^2_{n'_{sp}} = \left(\frac{1}{2T_K}\right)^2 \int_{-T_K}^{T_K} \int_{-T_K}^{T_K} C_q(t_1-t_2) dt_1 dt_2 \tag{3.3.41b}$$

where $C_q(\tau)$ is given by Eq. (3.3.39). Upon substitution of Eq. (3.3.39) in Eq. (3.3.41b) and subsequently performing the integration we obtain

$$\sigma^2_{n'_{sp}} = 4\pi^2\alpha^2\lambda/(2T_K) \tag{3.3.42a}$$

Using $\lambda = N_T$ we find

$$\sigma^2_{n'_{sp}} = \frac{1}{2T_K} (2\pi\alpha)^2 \left[\frac{B_K}{2\sqrt{3}} \operatorname{erfc} \sqrt{S_i/\eta B_K} + \frac{|\Omega_D|}{2\pi} e^{-S_i/\eta B_K}\right] \tag{3.3.42b}$$

We now examine Eq. (3.3.42b) in order to determine the worst case value for $\sigma^2_{n'_{sp}}$. Here we must be careful because there are two possibilities which can lead to different worst cases. The first is for $\Omega_D = 0$. In this respect $\sigma^2_{n'_{sp}}$ is

minimum. For certain cases then, under this assumption, λ may be too small for the Gaussian assumption to hold. We will now assume this is not true and that even for small Ω_D, there will be enough spikes for the Gaussian assumption to hold.

The other possibility is that $\Omega_D = \Omega_{max}$ and so $\sigma^2_{n'_{sp}}$ is maximum. This will increase the variance and so the acquisition time. We note here the important point that the spike noise variance varies inversely as T_K and not as T_K^2 as in the Gaussian noise only case (high SNR). Thus we expect our limiting factor to be the spike noise as mentioned earlier. Denoting this worst case variance by σ^2_{sp} we have

$$\sigma^2_{sp} = \frac{(2\pi\alpha)^2}{2T_K} \frac{B_K}{2} \left[\frac{\text{erfc}}{\sqrt{3}} \sqrt{S_i/\eta B_K} + e^{-S_i/\eta B_K} \right] \tag{3.3.43}$$

where we have used the fact that $f_{max} = B_K/2$ for any iteration. σ^2_{sp} is in $(\text{rad/sec})^2$. Thus, to find the variance in Hz^2 we divide Eq. (3.3.43) by $4\pi^2$ to obtain

$$\sigma^2_s = \frac{\sigma^2_{sp}}{4\pi^2} = \alpha^2 \frac{B_K}{4T_K} \left[\frac{\text{erfc}}{\sqrt{3}} \sqrt{S_i/\eta B_K} + e^{-S_i/\eta B_K} \right] \tag{3.3.44}$$

Since $n_{s_2}(T_K) = G_V n'_{sp}(T_K)/(1-e^{(S_i/N_i)}$,

$$\sigma^2_{n_{s_2}} = \frac{G_V^2}{\left(1-e^{-S_i N_i}\right)^2} \sigma^2_s \tag{3.3.45}$$

and since $G_V\alpha \equiv 1$ we have

$$\sigma^2_{n_{s_2}} = \frac{B_K}{4T_K} \frac{1}{\left(1-e^{-S_i/\eta B_K}\right)^2} \left[\frac{\text{erfc}\sqrt{S_i/\eta B_K}}{\sqrt{3}} + \exp(-S_i/\eta B_K)\right] \quad (3.3.46)$$

Since the noise processes n_{g_1} and n_{s_2} are independent, the overall worst case variance for the low SNR case is the sum of the two worst case variances, that is,

$$\sigma^2_{\hat{f}_D} = \left(\frac{1}{2\pi}\right)^2 \frac{1}{\left(1-e^{-\rho_K}\right)^2} \left[\frac{\eta B_K}{4S_i} \frac{1}{T_K^2} \left(1 - \frac{\sin \xi_K}{\xi_K}\right) + \frac{(2\pi)^2}{4T_K} B_K \left(\frac{\text{erfc}\sqrt{\rho_K}}{\sqrt{3}} + \exp(-\rho_K)\right)\right] \quad (3.3.47)$$

where $\sigma^2_{\hat{f}_D}$ is in Hz^2. By examining a few instances of the above we find that the spike noise term predominates for SNR < 10dB, while for a larger SNR the Gaussian term is the most influential. Therefore, when the SNR, ρ, is well below +10dB we need only contend with Eq. (3.3.46). Now using Eq. (3.3.47) along with

$$B_{K+1} = \gamma\sigma_{n_{s_2}} \quad (3.3.48)$$

and solving for T_K we obtain,

$$T_K = \frac{\gamma^2 B_K}{4(B_{K+1})^2}\left[\frac{\operatorname{erfc}\sqrt{\rho_K}}{\sqrt{3}} + \exp(-\rho_K)\right] \Big/ \left(1-e^{-\rho_K}\right)^2 \qquad (3.3.49)$$

Using Eq. (3.3.49) in the performance index of Eq. (3.3.12b) and performing Eq. (3.3.16) we find

$$B_K = (1-\exp(-\rho_K))B_{K+1}$$

$$\left\{ \frac{\left[\frac{12}{\gamma^2} + \frac{2B_{K-1}[(1/\sqrt{3})\operatorname{erfc}\sqrt{\rho_{K-1}} + \exp(-\rho_{K-1})]}{B_K(1-\exp(-\rho_{K-1}))^2}\right]}{\left[\left[\frac{\operatorname{erfc}\sqrt{\rho_K}}{\sqrt{3}} + e^{-\rho_K}\right]\left(1 + \frac{2\rho_K e^{-\rho_K}}{1-e^{-\rho_K}}\right) + \rho_K e^{-\rho_K}\left(1 + \frac{1}{\sqrt{3\pi\rho_K}}\right)\right]} \right\}^{1/2} \qquad (3.3.50)$$

Eq. (3.3.50) is a quasi-optimal relation for the set of B_K's for the low SNR case as was Eq. (3.3.20a) for the high SNR case. We find though that Eq. (3.3.50) does not converge for $N > 2$ as did Eq. (3.3.20a). Alternative forms also proved futile.

However, since this region provides only a $1/T_K$ variation, whereas the high SNR case provides a $1/T_K^2$ variation in noise power, it is beneficial traverse from the low SNR case to the high SNR case as quickly as possible. We decide to use a maximum of two iterations for this purpose, that is, $N = 1$

or $N = 2$. With this constraint imposed we can now use numerical methods to solve Eq. (3.3.50) for B_1 and then use Eq. (3.3.49) to find the integration times. We then will choose N so that the time to reach a SNR of 10dB is minimized. Once we have chosen N and narrowed the bandwidth to either B_1 for $N = 1$, or B_2 for $N = 2$, we use the high SNR case to find the total acquisition time. Also, we do not want a large N because the probability of error will increase. To maintain the same $P(\varepsilon)$ for larger N, the T_K's will have to increase since γ will have to increase. Thus the acquisition time will become larger.

The above procedure is well defined assuming that we have no ambiguity as to the operating region. However, we find that since for some values of ρ, the spike noise is greater than the Gaussian noise and for other values of ρ the opposite is true we expect at some point they will be on the same order of magnitude. This is so because in the region of interest the variance of the estimate $\hat{f}_D$ is a well behaved function of ρ and T_K. We find an ambiguity arises for $4 < \rho < 10$dB. In this region we must use Eq. (3.3.47) for the variance of the estimate. Use of this equation for minimizing T_{ACQ} is, however, difficult. In fact, this is precisely the reason we chose to use the approximating techniques described above.

After examination of some of the computer solutions in both the high and low SNR regions without regard to the above consideration leads to an interesting development. For ρ in the region described above we find that one iteration gives good results as to the minimal acquisition time. One intuitively feels that for $4 < \rho < 10\text{dB}$ only one integration is necessary for reaching the high SNR region. We find that the integration time is on the order of the processing time so that certainly we would not need more than one integration. In essence, more than one iteration is detrimental since the processing time increases T_{ACQ} more than the integration time. If we then use Eq. (3.3.47) to solve for the integration time, T_K, we then have resolved the ambiguity.

To do this we use Eqs. (3.3.3a) and (3.3.47) to solve for T_K. Since we intend to use only one iteration B_{K+1} is known and so the only unknown is T_K. We can solve for T_K as follows.

$$T_K = \left[\frac{(\gamma|2)}{2\pi B_{K+1}}\,\frac{1}{\zeta_K}\right]\cdot\left\{\left[\left(1-\frac{\sin(\xi_K)}{\xi_K}\right)\Big/\rho_K\right] + (2\pi\xi_K)\left[e^{-\rho_K}+\frac{\operatorname{erfc}\sqrt{\rho_K}}{\sqrt{3}}\right]\right\}^{1/2} \tag{3.3.51}$$

This is a "nonlinear" quadratic equation and can be solved iteratively by numerical techniques. In fact, Eq. (3.3.51) is

valid in all regions and, if B_{K+1} is known, it will produce a more accurate value of T_K.

Thus our technique is completely specified and we can now evaluate the performance of the system.

3.4. Results.

In this section we examine some particular cases for the acquisition problem. The results are shown in the accompanying figures and tables. The acquisition times are determined from the solutions to Eqs. (3.3.15), (3.3.19), (3.3.49), and (3.3.51). For each case we first determine the appropriate operating region of the system. To do this we proceed as follows. We assume operation in one region and use the appropriate relationship to calculate the associated integration time, T_K. Using this value we compute the variance for both regions. We then do the same for the other region. Also we compute the number of spikes per second, λ. If the system is in the spike region, the time between spikes should be small compared to the integration time, that is, the system should receive many spikes during the integration time. However, if the system is in the Gaussian region, then there should be very few spikes during the integration time.

The region of operation is then found by comparing the variances computed above. Since the variance is representative of the noise the operating region is found by choosing the

larger variance. The procedure can be best illustrated by an example.

Example: (B_1 chosen arbitrarily for $S_i/\eta B_1$ = 0dB, i.e., constant BW case.)

a) Initial uncertainty bandwidth, B_o = 53dB-Hz = 200kHz.

b) Signal-to-Noise Density Ratio, S_i/η = 45dB-Hz = 31.6×10^3 W-Hz.

c) Intermediate bandwidths

B_1 = 31.6 kHz ($S_i/\eta B_1$ = 0dB)

B_2 = 3.16 kHz ($S_i/\eta B_2$ = 10dB)

B_3 = 200 Hz = B_F ($S_i/\eta B_F$ = 22dB)

For the spike region with $\gamma = 6$

$$(T_K) = \frac{9B_K}{B_{K+1}^2}\left[\frac{\text{erfc}\sqrt{\rho_K}}{\sqrt{3}} + e^{-\rho_K}\right] \Big/ \left(1-e^{-\rho_K}\right)^2 \qquad (3.4.1)$$

$$\sigma'^2_{sp} = 4\left(1-e^{-\rho_K}\right)^2 \sigma^2_{sp} = \frac{B_K}{T_K}\left(\frac{\text{erfc}\sqrt{\rho_K}}{\sqrt{3}} + e^{-\rho_K}\right) \qquad (3.4.2)$$

For Gaussian region with $\gamma = 6$

$$(T_K)_g: B_{K+1} = \frac{3}{2\pi\sqrt{\rho_K}} \frac{\sqrt{1-\text{Sa}(2\pi B_K T_K)}}{T_K\left(1-e^{-\rho_K}\right)} \qquad (3.4.3)$$

$$\sigma'^2_g = \left(1-e^{-\rho_K}\right)^2 4\sigma^2_g = \left[\frac{1}{\rho_K}\frac{1}{T_K^2}\frac{1}{\pi^2}\right] \cdot [1-\text{Sa}(2\pi B_K T_K] \qquad (3.4.4)$$

In addition, if $\xi_K = 2\pi B_K T_K$ is large, i.e., $\xi_K \geq 32.5\pi$, $Sa(\xi_K) \leq 0.01$ and $(T_K)_g \approx \frac{3}{2\pi} \frac{1}{\sqrt{\rho_K}} \frac{1}{B_{K+1}} \frac{1}{\left(1-e^{-\rho_K}\right)}$. Also

$$\lambda_K = (B_K/2)\left[\operatorname{erfc}\sqrt{\rho_K}/\sqrt{3} + e^{-\rho_K}\right] = 1/T_{SK} \tag{3.4.5}$$

where T_{SK} is the average time between spikes on the K-th iteration. Using Eqs. (3.4.1) through (3.4.5) we find the following:

I. K = 0

$(T_o)_{sp} = .112$ sec; $\sigma'^2_{sp}[(T_o)_{sp}] = 23.7 \times 10^5 Hz^2$;

$\sigma'^2_g[(T_o)_{sp}] = 12.74 Hz^2$

$(T_o)_g = 3.8$ msec; $\sigma'^2_{sp}[(T_o)_g] = 69.9 \times 10^8 Hz^2$;

$\sigma'^2_g[T_o)_g] = 112.35 \times 10^6 Hz^2$

$\lambda_o = 132.9 \times 10^3$ sp/sec; $(T_{S_o}) = 1/\lambda_o = 7.5$ μsec.

From λ_o and the variances we see that the system is definitely in the spike region as would be expected since $\rho_o = -8$dB. Thus $(T_o)_{sp}$ is the first integration time.

II. K = 1

$(T_1)_{sp} = 3.7$ ms; $\sigma'^2_{sp} = 4.44 \times 10^5$; $\sigma'^2_g = 23.7$

$(T_1)_g = .151$ ms; $\sigma'^2_{sp} = 95.9 \times 10^6$; $\sigma'^2_g = 1.14 \times 10^6$

$\lambda_1 = 7250$ sp/sec; $(T_{S_1}) = .138$ ms.

Again from the variances and λ_1 we see that the system is still in the spike region.

III. K = 2

$(T_2)_{sp}$ = 32.14 μsec; $\sigma'^2_{sp} = 4.44 \times 10^3$; $\sigma'^2_g = 163 \times 10^3$

$(T_2)_g$ = .755 msec; $\sigma'^2_{sp} = 189.2$; $\sigma'^2_g = 4.249 \times 10^3$

λ_2 = .071 sp/sec; T_{S_2} = 14.1 sec.

Thus as can be seen from λ_2 and the variances, the system is in the Gaussian region.

So the integration times are

T_0 = .112 sec.

T_1 = .0327 sec.

T_2 = .000755 sec.

The processing times are $(T_{PK} = 3/B_K)$

$T_{P0} = 3/(200 \times 10^3)$ = .015 msec = .000015 sec.

$T_{P1} = 3/(3.16 \times 10^3)$ = .095 msec = .000095 sec.

$T_{P2} = 3/(3.16 \times 10^3)$ = .95 msec = .000950 sec.

Defining the sum of the N integration times as $S_I(N)$ and $S_P(N)$ as the sum of the N processing times we have

$$S_I(N = 3) = \sum_{K=0}^{N-1=2} T_K = 0.145455; \quad S_P(N = 3) = \sum_{K=0}^{2} T_{PK} = 0.00106$$

so that $T_{ACQ} = S_I(3) + S_P(3) = 0.146515$ seconds. We note that for the case of low initial SNR, for example -8dB, the

processing time in the spike region is generally negligible compared to the integration time. For high initial SNR, however, such is not the case as will be seen shortly. For the Gaussian region we find that one iteration suffices since $T_K < T_{PK}$ in this case. Thus, it is only detrimental to iterate more than once and as such increase the processing time.

If we used one iteration to accomplish the complete process of decreasing the bandwidth from B_o = 200kHz to B_F = 3.16kHz we find that T_{ACQ} = 11.22 seconds. Thus we see the savings in time made by iterating.

Also, using the minimization technique for the spike region we find, from Eq. (3.3.50), B_1^* = 35.8kHz. For this value of B_1 we have T_o = 77.88 msec, T_1 = 48.84 msec, and T_2 = .755 msec as before. Thus, $S_I(N)$ = .127479, $S_P(N)$ = .001049 and T_{ACQ}^* = 0.128528 sec. which is approximately 12 msec faster than the previous case.

As a check on the minimization of T_{ACQ}, the solutions for several B_1^* were perturbed. For the cases chosen, B_1^* produced the minimal result although some cases were extremely close. For example, the 2 stage spike process for B_1^* produced $T_o^* + T_1^* + T_{P_o}^* + T_{P_1}^*$ = 0.1268857. For B_1 = 35kHz, $T_o + T_1 + T_{P_o} + T_{P_1}$ = 0.1270344. The difference between the above two times is less than 0.12%.

In some instances we find that λ is small and so we do not receive many spikes during the integration time. This usually occurs for signal-to-noise ratios greater than +4dB. In essence this means the system is operating on the knee of its threshold curve. This occurrence is accounted for in the variance of the spike noise which is proportional to λ. Also for SNRs greater than 4dB, we occasionally find that the variances for the different regions are close in magnitude. For this condition we choose the solution for the integration time from Eq. (3.3.51).

3.4.1 Quasi-Optimal Bandwidth Reduction

In this subsection we examine some computer results for the quasi-optimal bandwidths obtained from the solutions to Eqs. (3.3.15), (3.3.19) and (3.3.49) to (3.3.51). We will examine first the low SNR region and then the high SNR region for a specific set of parameters.

3.4.1-1 Low SNR Region.

For SNR <+10dB it can be shown that the system is dominated by spike noise. We compute the time needed to bring the input SNR to the FMD to +10dB at which time we enter the high SNR region, that is, $S_i/\eta B_K$ = 10dB, using the quasi-optimal bandwidths obtained from the solution to Eq. (3.3.50). These results are shown in Figs. (3.4.1-1) and (3.4.1-2). They are also tabulated in Tables (3.4.1-1) and (3.4.1-2) for N = 1 and 2.

The T_{ACQ} column for $N = 1$ is $T_o + T_{Po}$; for $N = 2$, we show $T'_K = T_K + T_{PK}$ for $K = 0, 1$, and $T_{ACQ} = T'_o + T'_1$. The associated probability of error, $P_N(\varepsilon)$, is shown. The times computed for various SNDR and initial unknown bandwidths. In all cases the threshold bandwidth B_T (B_1 for $N = 1$, or B_2 for $N = 2$) is chosen so that $S_i/\eta B_T = +10dB$.

The intermediate bandwidth, B_1, is shown for $N = 2$, as well as the threshold bandwidth for $N = 1,2$. We see that for different S_i/η, B_T is different. This is so that we can maintain $S_i/\eta B_T$ constant at 10dB. (These results are for $\rho_o < 10dB$ only.)

Note also that the probability of error (as defined in Appendix 1) for two iterations is twice as large as that for one iteration. This is so because $P_N(\varepsilon) \approx 1 - (1-p)^N \approx Np$ for small p (where $p = P_1(\varepsilon)$). For the same probability of error for $N = 1$ and 2, γ would have to be increased to approximately 8 for the two iteration case. Since the integration time is proportional to γ^2 the increase in T_K for $N = 2$ is $(8/6)^2 = 64/36 \approx 2$. Thus the T_K for $N = 2$ would approximately double. However, most systems presently employed today have $P(\varepsilon)$ of less than 10%, 5%, or 1%. In our case, $N = 3$, falls within these specifications for $\gamma = 6$; and for $N = 4$ $P_4(\varepsilon) \approx 1.04\%$.

With regard to Fig. 3.4.1-1 and Tables 3.4.1-1a through 3.4.1-1e we make the following observations. For a Signal-to-Noise Density Ratio (SNDR) below 55dB-Hz the two iteration technique provides substantial improvement over the one iteration scheme even though we are twice as likely to make a mistake. Reductions of acquisition time are on the order of two magnitudes, a considerable savings.

For $S_i/\eta > 55dB$ we see from the Tables that the integration time is of the same or less than an order of magnitude than the processing time. It is at this point that the spike and Gaussian noise powers are approximately equal. Thus we might do better in this case by using a single iteration from B_1 to B_F rather than to an intermediate value as B_2 where B_2 is the bandwidth such that $S_i/\eta B_2 = +10dB$. This will be investigated later on. For $S_i/\eta \geq 55dB\text{-Hz}$, we see that $N = 1$ provides a smaller acquisition time than $N = 2$. This is expected since for $S_i/\eta > 55dB\text{-Hz}$, $S_i/\eta B_o > 0dB$ for $B_o = 300kHz$ and $S_i/\eta B_o > +5dB$ for $B_o = 100kHz$. Thus as the SNDR increases the closer the system approaches the Gaussian region which requires only one integration.

The dashed lines in Fig. 3.4.1-1 for $S_i/\eta > 55dB\text{-Hz}$ indicate extrapolations of their associated curves. (The acquisition times were computed at 4 points-- $S_i/\eta = +45, +50, +55$ and $+60dB\text{-Hz}$.) The limits at $S_i/\eta = 60dB$ are found by

choosing the acquisition time for $N = 1$ and the processing time equal to $3/B_o$. This is so because there is no solution to Eq. (3.3.50) subject to the constraint $B_2 < B_1 < B_o$ except on the boundary. We also note the degenerate case of $B_o = 100\text{kHz}$ and $S_i/\eta = 60\text{dB-Hz}$. Since for this set of parameters $B_2 = 100\text{kHz}$, we have $S_i/\eta B_2 = +10\text{dB}$ and so the system is already out of the spike region.

In Fig. 3.4.1-2 and Table 3.4.1-2 we show T_{ACQ} vs S_i/η and B_T for $B_o = 4\text{kHz}$ for $N = 1$ and 2. Note here we chose to vary $S_i/\eta B_o$ directly instead of S_i/η. This is the system which will be examined in Chapter 4 as a hardware system. From Fig. 3.4.1-2 we see a similar trend as for the previous case. For $S_i/\eta > 40.8\text{dB-Hz}$ one iteration provides a smaller T_{ACQ} than does two iterations. Also for $S_i/\eta = 31\text{db-Hz}$ we see an improvement in T_{ACQ} for $N = 2$ over $N = 1$ of about 35 to 1. However, we must also examine an additional set of parameters.

In Tables 3.4.1-3a through 3.4.1-3e and Table 3.4.1-4 we compare the following parameters: the average interarrival time between spikes, $\bar{T}_I = \lambda^{-1}$; the worst case (longest) spike width $T_{SP} = 2/B_K$; the ratio between the integration time and the spike widths $R_1 \triangleq T_K/T_{SP}$; the ratio between the integration time and the average interarrival time $R_2 \triangleq T_K/T_I$; the ratio of the spike variance to the Gaussian variance using

T_K assuming spike region operation, S_1; the ratio of the spike variance to the Gaussian variance using T_K assuming operation in Gaussian region S_2. The relationship of T_I, T_{SP} and T_K is shown in Fig. 3.4.1-3 for the case $T_K >> T_I$ or T_{SP}.

In all cases, for $S_i/\eta \leq 50dB$ corresponding to $S_i/\eta B_o \leq 0dB$ we see that R_1 and R_2 are large compared to unity. In the case of R_1 this means that for most of the spikes received during the integration period the entire spike will be included. In the case of R_2 this means that many spikes will be present and so the assumption that the Poisson process of spikes will tend toward a Gaussian at the integrator output is valid.

However, we notice that for $S_i/\eta \geq 55dB$ R_1 and R_2 become comparable to and less than unity in some cases. When R_1 becomes less than one, the integration is carried over only a portion of the spike. In these cases though, we find, in addition, that R_2 is much less than unity. Thus the probability of this happening is small. Also in this region the integrator will receive few spikes if any during the integration period. Therefore we find that the assumption that the integrator output due to the spikes is Gaussian is no longer valid.

This stems from the fact that we violate the conditions necessary for the Central Limit Theorem to hold. But even

in the case for which it holds we see that we are concerned with the tails of the distribution which are in general not Gaussian. In fact, the entire technique is based on the heuristic model established by Rice [18] and is useful because experimental results closely follow the model. Therefore in this region we cannot use only the acquisition curves of Figs. 3.4.1-1 and 3.4.1-2 but we need to consider the parameter comparison of Tables 3.4.1-3. For cases in which S_1 and S_2 are approximately equal and which also have R_1 and R_2 less than unity, we must re-examine the situation.

First we note that this occurs for $S_i/\eta \geq 55$dB-Hz. Therefore the value of B_T is correspondingly higher so that $S_i/\eta B_T = +10$dB. Now B_T becomes the new initial unknown bandwidth. This bandwidth is much larger for $S_i/\eta \geq 55$ than it must be for $S_i/\eta < 55$ while maintaining $S_i/\eta B_T = +10$dB. Thus the IF bandwidth for the case of $S_i/\eta > 55$ is much larger than that for $S_i/\eta < 55$. We know [23] that for an FM discriminator whose input is a sinusoidally modulated signal, that if B is increased so is the modulation index β. As β increases, for a fixed input SNR the threshold increases but the output SNR increases also. Thus FM as we know trades off SNR for bandwidth. We experience a similar phenomenon. That is as we increase B_T while maintaining $S_i/\eta B_T$ fixed the threshold increases because $N_T = \lambda$ increases (see

(Eq. (3.3.31)). As λ increases the discrimination process generates more spikes per second and the (average) time between spikes decreases. As such for a given amount of time there is an increase in the spike noise power and thus a higher input SNR ($S_i/\eta B_T$) is needed to overcome this increase in threshold. So the figure of +10dB as a division between spike and Gaussian noise regions is not a hard and fast rule. It may need to be modified when cases as those cited above arise.

Of course this whole problem of "threshold" chosen for minimization and the utilization of different regions for solution to the question of this acquisition aid technique would not arise if we could solve the original system which includes both regions (Eqs. (3.3.3a, 3.3.12b, 3.3.15, and 3.3.47)). This would produce the solution valid over all regions. However, this is an arduous task and so we must be content with the present solution.

From Fig. 3.4.1-1, we find for SNR $\geq$ 55, that the reduction in acquisition time for $B_o \leq$ 250kHz is less than 6.5:1 for N = 2 to N = 1. For B_o = 300kHz the gain is 8.4:1. This does not warrant an additional iteration since the probability of error increases by a factor of two. We will choose a gain of a minimum of ten to one in acquisition time to justify an additional iteration.

However, we must remember that this is still not the entire process. Thus far we have only brought the system of the spike noise dominated region. We must yet narrow the bandwidth to B_F, that is, the acquisition bandwidth, while the system is in the Gaussian region. Since a desired final operating SNR is 20 to 30dB, the intermediate bandwidth for which the SNR is 10dB, will have to be reduced further by a factor of 10 to 100. In this way we move the system well up into the Gaussian region. We will explore this in the next subsection.

3.4.1-2. High SNR Case.

For signal-to-noise ratios greater than +10dB the system is operating in the Gaussian region. We compute the quasi-optimal B_K's by assuming that only the Gaussian noise power term is significant. We then compute the acquisition time for $N = 1$ and $N = 2$. For the $N = 2$ case we do so only for a final acquisition loop bandwidth, B_F, such that $\rho_F = S_i/\eta B_F$ is +30dB. The reason we do this can be seen from Table 3.4.1-5a.

Here we show T_o, T_{P_o} and T_{ACQ} for $S_i/\eta B_F$ = +20, +25, and +30 dB. For the case of ρ_F = +20dB, the processing time is greater than the integration time; thus iterating more would only increase T_{ACQ}. For ρ_F = +25dB we see that the processing time and integration time are on the same order

of magnitude with T_o slightly greater than T_{P_o}. Thus little or no gain could be made by iterating. However, in the case of $\rho_F = +30dB$ we suspect we may decrease T_{ACQ} by iterating since T_o is nearly an order of magnitude greater than T_{P_o}. In Table 3.4.1-5b we tabulate these results and find little advantage in using two iterations. A comparison of the T_{ACQ} column in Tables 3.4.1-5a and 3.4.1-5b shows this to be so.

Also here we tried perturbations about B_1 and found slightly better acquisition times could be achieved by a different choice of B_1. However, the advantage was insignificant. For example, for $B_o = 3.16kHz$ and $B_1 = 2.0kHz$ we found, for $S_i/\eta = 45dB\text{-}Hz$

$$T_o = .5696 \times 10^{-6},\ T_{P_o} = .9494 \times 10^{-3},\ T_o' = .94994 \times 10^{-3}$$

$$T_1 = .38376 \times 10^{-2},\ T_{P_1} = .15 \times 10^{-2},\ T_1' = .53376 \times 10^{-2}$$

and

$$T_{ACQ} = 6.2875 \times 10^{-3}.$$

Comparing this with the figure in Table 3.4.1-5b we see a difference of .0024ms or 2.4μsec, or a percentage change of less than .0382%.

In addition, for the first iteration we see an extremely short integration time. When we compare the noise powers for spike and Gaussian noise using T_o we find the spike power greater than the Gaussian power. This also

reinforces our judgement to use only one iteration. In Table 3.4.1-6 we show the acquisition times for B_o = 4kHz when operating in the high SNR region. Note here that for ρ_F = +30, T_{ACQ} is approximately five times as large as that for ρ_F = 20dB, just as it was for the previous case. Here also, for the reasons given above, one iteration suffices. As an example here we find that for N = 2, with B_o = 126.5, B_1 = 53, and ρ_F = 30dB that T_{ACQ} = 157.2ms as opposed to 162ms for N = 1. Thus the decrease in T_{ACQ} is negligible.

3.4.1-3. Overall System Acquisition Time

To find the total acquisition time for some unknown initial bandwidth B_o to a final loop bandwidth B_F, we must add together the acquisition times in both regions. These results are shown in Fig. 3.4.1-6 and Table 3.4.1-7 for ρ_F = +20, +25, and +30dB. From these figures, for different ρ_F one notices little change for the acquisition time for any given B_o for S_i/η < 55dB-Hz. However, for S_i/η = 55 and N = 3 we see a change of the order of 3 or 5 to 1 between the ρ_F = 20dB and 30dB curves. Similarly for N = 2, we see a change somewhere between 1.1 to 3.4 to 1. The reason for this is that the processing time has a more pronounced effect on T_{ACQ} for S_i/η > 55. Thus we conclude that for S_i/η < 55 we shall use three iterations and for $S_i/\eta \geq 55$, two iterations suffice. Note also that for each ρ_F the curves tend to coalesce for $S_i/\eta \geq 55$ for the same reason as stated above.

If one compares these curves with those of Fig. 3.4.1-1 we see that for $S_i/\eta \geq 55$dB-Hz the acquisition time increases markedly with increasing ρ_F. This is also due to the processing time influencing the acquisition time for each iteration in the high SNR region. Similar results are shown in Table 3.4.1-8 and Fig. 3.4.1-7, $B_o = 4$kHz.

One may ask if it is beneficial to move the system from B_1 to B_F without first going to the Gaussian region or how does the above compare to moving the system directly from B_o to B_F. We examine these possibilities now. We find first the solution to Eq. (3.3.51) for the acquisition time in the latter case. These times are tabulated in Table 3.4.1-9 for $B_o = 100$kHz and $B_o = 300$kHz, that is, the smallest and largest B_o we have considered. A glance at this table reveals immediately the large range over which the acquisition time varies for different signal-to-noise density ratios. The inordinately long times needed for $S_i/\eta < 50$dB-Hz show immediately the inefficiency of this technique at low SNDR for both extremes of bandwidth. One notices marked improvement, however, as S_i/η gets larger. For $B_o = 100$kHz and $S_i/\eta = 60$dB-Hz, we see the acquisition times for the high SNR case of Table 3.4.1-7. This is because for $B_o = 10^5$Hz and $S_i/\eta = 60$, $S_i/\eta B_o = +10$dB and so the system is in the high SNR region. Further comparison of Tables 3.4.1-7 and 3.4.1-9 reveals the following: For

$S_i/\eta < 55$, the iterative approach is much better in all cases. For $S_i/\eta = 60$dB-Hz and $B_o = 300$kHz the system does better using the iterative approach. It does equally well for $B_o = 100$kHz because $S_i/\eta B_o = +10$dB for this case. Thus we conclude that for $S_i/\eta B_o < 10$dB it is best to acquire through iteration. The determination whether to use one or two iterations in the spike region (and thus two or three respectively for the total acquisition process) is to be made from performance curves of the form of Fig. 3.4.1-6.

Table 3.4.1-10 and Fig. 3.4.1-8 illustrate the acquisition times for $B_o = 4$kHz for S_i/η varying between 31 and 41dB-Hz for $\rho_F = +20$, +25, and +30dB. Again we see a similar trend as in the previous case. We see that for low S_i/η the system takes entirely too long to acquire and improves greatly as S_i/η increases. Nevertheless the iterative scheme works better in all cases.

We next examine the possibility of decreasing the bandwidth in the spike region from B_o to B_1^* and then proceeding from B_1^* directly to B_F bypassing the 10dB bandwidth B_2. To do this we use the value of T_K' in Table 3.4.1-1 for which $N = 2$ and $K = 0$. We then use Eq. (3.3.51) to find the time required to traverse the bandwidth from B_1^* to B_F. These results are shown in Table 3.4.1-11 for $\rho_F = 20$dB. When we compare these times with those in Table 3.4.1-9 we see a marked

improvement over the preceeding technique. This is expected because this technique does use the iteration method. However, on an absolute basis the acquisition times achieved are still long. Next we compare these times with those of Table 3.4.1-7a. Notice that the acquisition times for the above method for $S_i/\eta \leq 50$ are better than or approximately equal to those obtained for $N = 2$ in Table 3.4.1-7a. For $S_i/\eta = 55$dB-Hz and the one case for 60dB-Hz, we find that the previous method allows for acquisition times of about 1/5 as long as the new method. However, the $N = 3$ method provides substantial improvement for $S_i/\eta \leq 50$dB. Thus it would seem that a good strategy for acquisition is to use the $N = 3$ method (i.e., using two iterations in the spike region and one iteration in the Gaussian region) for $S_i/\eta \leq 50$ and the $N = 2$ method (that is using one iteration in the spike region and one iteration in the Gaussian region) for $S_i/\eta > 50$. This is the strategy we arrived at in a previous discussion. Of course we sacrifice some probability of error by using $N = 3$ rather than $N = 2$ but the tradeoff in terms of acquisition time versus probability of error justifies this decision. We note that we need not consider $\rho_F > 20$dB since the acquisition times for higher ρ_F must be longer.

Another interesting point can be made if we look again at Fig. 3.4.1-1. If we draw a curve through the points for

which T_{ACQ}, for $N = 1$, is ten times as large as T_{ACQ} for $N = 2$ we find that the value of $S_i/\eta B_o$ for this to occur is in the range $-1.25 \leq S_i/\eta B_o \leq -0.25$. This is shown in Fig. 3.4.1-9. Similarly, we see from Fig. 3.4.1-2 that for $B_o = 4000$Hz, this occurs for $S_i/\eta B_o = -0.8$dB. Thus we conclude that for $S_i/\eta B_o$ in the range -1 to 0dB we should see a change in spike region acquisition time of about ten to one between the one and two iteration techniques respectively. This seems to be a good choice to decide whether to use one or two iterations. Also it is intuitively appealing because at around this point we see large parameter changes (see Tables 3.4.1-3 and 3.4.1-4) for which we feel that the Gaussian spike noise assumption is questionable. Also note from the parameter comparison, Tables 3.4.1-2a and 3.4.1-3 that for $S_i/\eta B_o = 0$dB ($S_i/\eta = 50$, $B_o = 100$kHz in Table 3.4.1-2a) the parameters R_1, R_2, S_1, and S_2 are very close. Thus this seems to be the common factor regardless of S_i/η or B_o. A good judgement as to the "optimal" approach can be made based upon $\rho_o = S_i/\eta B_o$.

Before we leave the quasi-optimal case we should consider one more aspect. In all of the above cases we kept the final loop SNR constant in order to have a fair comparison for each system. This in turn meant that as S_i/η increased so did the loop bandwidth. In fact for $B_o = 100$kHz and $S_i/\eta = 60$dB-Hz we find that for a ρ_F of +20dB the final bandwidth must be $B_F = 10$kHz. This also is the degenerate case of starting in

the Gaussian region because ρ_o = +10dB. In practice, a system would be specified by the following: (1) A maximum frequency uncertainty, B_o; (2) A range of S_i/η; (3) A final loop bandwidth subject to some minimum desired operating signal-to-noise ratio, $(\rho_F)_{min}$. The system would at worst then be operating at $(\rho_F)_{min}$ for S_i/η its lowest value and $B_K = B_o$. For example, NASA Houston has a system [3] with a $B_o \approx$ 200kHz (±55kHz Doppler, ±20kHz oscillator instability, 30% guard band), $48 \leq S_i/\eta \leq 60$dB-Hz, $B_F = B_L$(acq) = 200Hz and B_L(track) = 50Hz. Thus, the worst case ρ_F is $(\rho_F)_{min} = 48/23 = +25$dB with $(\rho_o)_{worst} = -5$dB. If S_i/η is +60 then the system may be operating at +37dB but at worst the final SNR will be 25dB. We now examine the applications of our technique to the above system.

First we examine the case for $45 \leq S_i/\eta$(db-Hz) ≤ 60 B_o = 100kHz, 200kHz and 300kHz with $B_F/B_o = 10^{-3}$. We assume in each case that B_T is chosen such that $S_i/\eta B_T = \rho_T$ = +10dB. The results are shown in Table 3.4.1-12a. Here we see some interesting results. The acquisition time is not monotonically decreasing with S_i/η as in the previous cases. This is due to the fact that integration and processing times are on the same order of magnitude. Furthermore if we examine the parameters for these cases we see that, for $S_i/\eta \geq 55$dB, the ratio of spike noise power to Gaussian noise power, S, is near or greater than unity. This means at these values of

SNDR and bandwidth B_T, the system is really still at threshold and a higher B_T or another iteration is needed. Proceeding as before we look to increase B_T. We apply our minimization techniques to find a new bandwidth and use this for B_T. Thus we again have two iterations in the spike region and one in the Gaussian.

The results for this technique are shown in Table 3.4.1-12b. For Si/η=45 and B_o=200kHz and 300kHz there are no entries since we are well within the Gaussian region. From the entries we see that the acquisition time is again monotonically decreasing as expected. Note though that since B_F is not the same for each B_o we find that for a particular S_i/η, T_{ACQ} decreases with increasing B_o. This is expected since we know T_{ACQ} varies inversely as B_F. Thus a higher B_F produces a lower T_{ACQ}. When we compare Tables 3.4.1-12a and 3.4.1-12b we see improvement in T_{ACQ} for $S_i/\eta \geq$ 55db-Hz as expected.

Although these values are not substantially less (at most a 5:1 ratio) we must consider them since their associated parameter, S, is the proper value. For these values of B_F we find that the threshold occurs above ρ = +13dB for $S_i/\eta \geq 55$. The total acquisition time is shown in Table 3.4.1-13 which uses the results of Table 3.4.1-1 as follows: For S_i/η equal to 45 or 50dB-Hz, we use for the overall acquisition time the sum of T_{ACQ} for N = 2 from Table 3.4.1-1 and N = 1 from Table 3.4.1-12a. For S_i/η = 55 or 60 dB-Hz we use the sum of

T_{ACQ} for N = 1 from Table 3.4.1-1 and N = 2 from Table 3.4.1-12b. The results are shown in Fig. 3.4.1-10. We see a similar trend here as we did for the previous cases except for S_i/η about 57.5dB-Hz where the curves exhibit a marked difference. This behavior exists because we did not choose B_F as before. There B_F was chosen so that $S_i/\eta B_F$ was equal. Here we have a difference. The reason this cccurs at high S_i/η only is because the 10dB point is not optimal and exhibits this more at high SNDR where the processing times are more influential on the total acquisition times.

We examine now the process using constant bandwidth reduction in the next section.

3.4.2. Constant Bandwidth Reduction (CBR).

We now try another approach to minimize the acquisition time. This technique is simpler since it requires only a fixed set of filters for any S_i/η once B_o and B_F are known. In this method we start with a given B_o and reduce the bandwidth to B_1, some fixed fraction of B_o. We then proceed to reduce B_1 to B_2 some fixed arbitrary fraction of B_1. We continue this process until B_F is reached. For example, if B_o = 100kHz and B_F is 100Hz we might use two iterations to reduce B_o to B_1 = 10kHz and increase ρ by +10dB, and then reduce B_1 to $B_2 = B_F$ = 100Hz. For N = 3,

we might proceed to reduce the bandwidth by the constant ratio $B_{K+1} = 0.1B_K$. Of course, if ρ gets large and we enter the Gaussian region we must be sure a solution exists as was discussed earlier.

The question arises as how to choose the reduction factors so that the acquisition time remains small but the implementation becomes simpler (i.e., less filter settings for different parameters). From our previous analysis (Sec. 3.4.1) we see initially a good choice for the first reduction factor is one-tenth. Again let us choose a $B_F/B_o = 10^{-3}$ and $N = 2$ so that our second reduction factor is one hundred to one. We examine the procedure from B_o = 100kHz, 200kHz and 300kHz as before. The results are shown in Table 3.4.2-1 and Fig. 3.4.2.1.

We see from Table 3.4.2-1 we find that the acquisition time is much higher than those of Table 3.4.1-13 (B_F is the same for each case) for $S_i/\eta = 45$, five to ten times for $S_i/\eta = 50$, about equal for $S_i/\eta = 55$ and 60. Thus for S_i/η larger than 55 it seems that the constant reduction cases suffices. Also we must remember this process used only two iterations while that in Table 3.4.1-13 used three. A good approach to the total problem would be to use $N = 3$ and for example, a relation such as $B_{K+1} = 0.1B_K$ for $S_i/\eta \leq 50$dB-Hz in the CBR technique. This would substantially reduce the acquisition time for low S_i/η. For $S_i/\eta \geq 55$db-Hz the system

would use the $N = 2$ case as shown in Table 3.4.2-1. Since the process needs the value of S_i/η in any event, it would be simple to program this capability into the system controller.

The CBR approach is simpler to implement; that is, one need not have many filters, or if using digital filters, store many coefficients as one needs in the quasi-optimal technique. Thus a practical and economical approach seems to be the CBR method.

3.5. Comparison with Known Techniques.

It is interesting to compare present techniques with the scheme described above. The swept VCO technique is one which used quite frequently. This involves sweeping the VCO slowly over the entire uncertainty and acquiring lock when the difference frequency falls in a narrow passband, that is, B_L. At this time the sweep oscillator would be halted but the frequency shift caused by it would be held at the VCO input terminal. An estimate on the time for acquisition with this method may be found in various references [9, 14, 26]. This technique is currently used by NASA for the Space Shuttle [2]. The parameters for that particular system are acquisition time in six second with a probability of acquisition $P_A > 0.9$ ($P(\varepsilon) < 0.1$). The initial unknown bandwidth is 150kHz and the maximum sweep rate is 5kHz/sec.

An alternate technique which produces approximately the same acquisition time is the dwell technique or stepping correlator. It may also be called a sliding correlator although this terminology is not really indicative of the process. In this technique the system is held for a time in a small frequency cell over which the loop could lock if the carrier were present. When lock is achieved, the process is stopped. Suppose we consider an initial unknown bandwidth B_o, consisting of M cells of width B_L, that is, the loop bandwidth, such that $MB_L = B_o$, M an integer. If we assume the cell is a filter, and that the filter response time T_{fr} is inversely proportional to the filter bandwidth then the acquisition time, T_a, assuming we try all cells is

$$T_a = \frac{M}{B_L} = \frac{B_o}{B_L^2} \tag{3.5.1a}$$

Actually, since each cell is evenly likely to contain the carrier the average value of T_a is

$$\overline{T_a} = \frac{M}{2B_L} = \frac{B_o}{2B_L^2} \tag{3.5.1b}$$

The interesting point here is the form of Eq.(3.4.1). If $B_L = B_1$, then Eq. (3.5.5) is of the form B_K/B_{K+1}^2 which is

similar to Eq. (3.3.49). The difference here is that in Eq. (3.3.49) there is a weighting factor. However, $B_{K+1} \neq B_L$ necessarily and so herein lies the gain. It is intuitively pleasing, however, that the form of the equations is similar.

Viterbi [26] has examined a technique such as this. In this technique he has M uncertainty windows of bandwidth $B = 1/2T$ Hz, where T is a time in seconds for integration. The total uncertainty bandwidth is W-Hz so that M is $\lceil 2WT \rceil$ where $\lceil x \rceil$ indicates the least integer greater than or equal to x. That is M is the integer in the range $2WT \leq M < 2WT + 1$. This system processes the incoming signal envelope in a correlation-type device and chooses the window with the largest value. To make an equal comparison we must use one filter and process serially. Thus $T_{ACQ} = (2WT+1)T$. He shows that the probability of error is $P < WT \exp(-4\rho T/\pi^2)$ where ρ is the signal-to-noise density ratio.

We see that for our system, $B_o = W$, $\rho = S_i/\eta B$ and $B_F = B$. If we use $S_i/\eta B_o = 0$dB, $W = 4000$Hz, $B_L = 400$, we have an equivalent condition for driving the system out of the spike region. For the above we have that $T = 1/2B_L = 1.25 \times 10^{-3}$sec and $P \approx 5e^{-2} = 0.677$. This is a very high probability of error. We find that $T_{ACQ} = 13.25$msec. Our technique for $N = 2$ takes 27.65msec or approximately twice as long but

$P(\varepsilon) = 1 - (.997)^2 = 6 \times 10^{-3}$. The reason Viterbi's method results in a high $P(\varepsilon)$ is that $S_i/\eta B$ is low. A more realistic figure would be $B = 40Hz$ so that $S_i/\eta B = +20dB$. Using one iteration we find that T_{ACQ}=258msec or approximately twenty times as long as the correlation technique with a $P(\varepsilon) = 3 \times 10^{-3}$. Even though the time difference here is large the high $P(\varepsilon)$ in the correlation case does not warrant its use. Thus the iteration method performs better. Also if $\rho_o = -10dB$ while all other parameters are maintained constant, the correlation procedure produces as a $P(\varepsilon) > 1$. This is because $S_i/\eta B_o$ is too low and the approximations used to find $P(\varepsilon)$ do not hold. Thus this technique is not valid for all SNR.

The next point to consider is suppose we set $T_{ACQ} = 27.65$ or $\approx$ 28msec. For this time we find, with $W = 4000$, $\rho_o = 0.0dB$ that $(2WT+1)T \approx 2WT^2 = 28 \times 10^{-3}$ or $T = 1.87msec$. The corresponding $B_L = 267.2Hz$ and $P(\varepsilon) = 0.375$. This is also not acceptable since both B_L and $P(\varepsilon)$ are large.

Let us now consider the case $\rho_o = 0dB$, $W = 4kHz$ and $B_L = 40Hz$. Proceeding as before we find $T_{ACQ} = 1.25sec$ and the $P(\varepsilon) = 10^{-7}$ for the correlation case. This is a small $P(\varepsilon)$ but long T_{ACQ}. Using the iteration procedure with two iterations only (one in the spike region and one in the Gaussian region) we find that $T_{ACQ} = 260 + 11 = 271msec$, which is about one-fifth as long as the above. The associated

$P(\varepsilon)$ is $P(\varepsilon) < 6 \times 10^{-3}$. Thus we see a tradeoff in acquisition time and probability of error.

Using the iterative technique to obtain a probability of error of approximately 10^{-7} requires a new γ, γ', of 12(±6 S.D.) for $N = 2$ or 3. Using this let us find the acquisition time needed to reduce the bandwidth from 4kHz to 40Hz by the iteration method. First using $N = 2$ we find that $T_{ACQ} \approx (\gamma'/\gamma)^2 T_{ACQ}(\gamma = 6) = 4.26 = 1.024$sec. Using $N = 3$ we find that B_1 is approximately the same as for $\gamma = 6$ since the processing time is small for this case. Thus we find, using two iterations in the spike region and one iteration in the Gaussian region that $T_{ACQ} = .741$ seconds which is slightly less than one-half the time using the correlation technique for a $P(\varepsilon) = 10^{-7}$.

An important point to note is as follows. This analysis was geared toward aiding a Costas Loop receiver to acquire a signal imbedded in noise. In particular, the input signal was to be modulated after the receiver locked to the signal. The modulation is PSK or FSK. However, during the acquisition process, the modulation had to be absent so that lock could be obtained. We considered the problem of acquisition for a PLL receiver because it is simpler to analyze than a Costas Loop. The main reason for doing so is to next apply the principle learned from the PLL to the Costas Loop. But even more importantly is to ascertain whether or not an acquisition

technique could be developed for which lock could be achieved when data is present.

Currently, using the sweep method [2], which is similar to the correlation method, there is a problem of locking onto a signal sideband if the carrier is modulated. This is due to the fact that in either case the system "looks" over a small portion of the frequency spectrum. Thus, if a (large) sideband is present the acquisition process will lock onto it as if it were the true carrier. Thus with either of these systems or any other employed today, modulation cannot be present during acquisition.

However, the possibility of having data present in our iterative scheme is a plausible one which must be investigated as future work. The possibility exists here because the acquisition process spans the entire possible frequency spectrum during each iteration. Thus, if we assume random data, and that the data rate is high compared to the acquisition process time, then we expect on the average that the sideband problem will be alleviated and so the system can lock on the carrier signal even with modulation.

This possibility needs to be investigated further for both the PLL and Costas Loop receiver designs. If a positive result is found, it would be an advancement in the application of phase lock principle receiving devices.

Table 3.2.1

SLOPE OF THE CALIBRATION CURVES

$Si/\eta B$ (dB)	$(Si/\eta B)$	$\zeta = (1 - e^{-Si/\eta B})$
∞	∞	1.000
+10.0	10.000	0.999(95)
+ 5.0	3.162	0.957
+3.0	1.995	0.865
+2.0	1.585	0.795
+1.0	1.259	0.716
+0.0	1.000	0.632
-1.0	0.794	0.548
-2.0	0.631	0.468
-3.0	0.501	0.394
-5.0	0.316	0.271
-10.0	0.100	0.095(16)
$-\infty$	$-\infty$	0.000

Table 3.4.1.1(a)

ACQUISITION TIMES FOR SPIKE REGION ONLY, B_o = 100kHz

N = 1; $P_1(\varepsilon) = 2.6\times10^{-3}$

K= N-1	Si/η (dB Hz)	$Si/\eta B_k$ (dB)	B_1 (kHz)	T_o (sec)	T_{P_o} (sec)	T_{ACQ} (sec)
0	45.0	- 5.0	3.16	1.19754	3.0×10^{-5}	1.19757
	--	--	--	--	--	--
0	50.0	0.0	10.0	1.03321×10^{-2}	3.0×10^{-5}	1.03621×10^{-2}
	--	--	--	--	--	--
0	55.0	+ 5.0	31.6	5.00493×10^{-5}	3.0×10^{-5}	8.00493×10^{-5}
	--	--	--	--	--	--
0	60.0	+10.0	100.0	--	--	--
	--	--	--	--	--	--

Note: $Si/\eta B_N$ = +10 dB

Table 3.4.1.1(a')

ACQUISITION TIMES FOR SPIKE REGION ONLY, B_o = 100kHz

N = 2; $P_2(\varepsilon) = 5.2\times10^{-3}$

K= N-1	Si/η (dB Hz)	$Si/\eta B_k$ (dB)	B_{k+1} (kHz)	T_k (sec)	T_{P_k} (sec)	T'_k (sec)	T_{ACQ} (sec)
0	45.0	- 5.0	23.712	2.1269×10^{-2}	3.0×10^{-5}	2.1299×10^{-2}	--
1	--	+ 1.25	3.16	1.2738×10^{-2}	12.65×10^{-5}	1.2864×10^{-2}	3.4163×10^{-2}
0	50.0	0.0	38.639	6.9257×10^{-4}	3.0×10^{-5}	7.2257×10^{-4}	--
1	--	+ 4.13	10.0	3.6220×10^{-4}	$7.764\ 10^{-5}$	4.3984×10^{-4}	1.1624×10^{-3}
0	55.0	+ 5.0	73.695	1.02833×10^{-5}	3.0×10^{-5}	4.02833×10^{-5}	--
1	--	+ 6.32	31.6	1.43378×10^{-5}	$4.0701\ 10^{-5}$	5.505×10^{-5}	9.53294×10^{-5}
0	60.0	+10.0	--	--	--	--	--
1	--	--	--	--	--	--	--

Note: $Si/\eta B_N$ = +10 dB

Table 3.4.1.1(b)

ACQUISITION TIMES FOR SPIKE REGION ONLY, B_o = 150 kHz

N = 1; $P_1(\epsilon) = 2.6\times10^{-3}$

K= N-1	Si/η (dB Hz)	Si/ηB_k (dB)	B_1 (kHz)	T_o (sec)	T_{P_o} (sec)	T_{ACQ} (sec)
0	45.0	-6.76	3.16	4.15182	2×10^{-5}	4.15184
	--	--	--	--	--	--
0	50.0	-1.76	10.0	3.7446×10^{-2}	2×10^{-5}	3.7466×10^{-2}
	--	--	--	--	--	--
0	55.0	+3.24	31.6	2.5429×10^{-4}	2×10^{-5}	2.7429×10^{-4}
	--	--	--	--	--	--
0	60.0	+8.24	100.0	3.8844×10^{-7}	2×10^{-5}	2.038844×10^{-5}
	--	--	--	--	--	--

Table 3.4.1.1(b')

ACQUISITION TIMES FOR SPIKE REGION ONLY, B_o = 150kHz

N = 2; $P_1(\epsilon) = 5.2\times10^{-3}$

K= N-1	Si/η (dB Hz)	$Si/\eta B_k$ (dB)	B_{k+1} (kHz)	T_k (sec)	T_{P_k} (sec)	T'_k (sec)	T_{ACQ} (sec)
0	45.0	-6.76	30.165	4.5563×10^{-2}	2×10^{-5}	4.5583×10^{-2}	--
1	--	0.20	3.16	2.8133×10^{-2}	9.95×10^{-5}	2.8232×10^{-2}	7.38155×10^{-2}
0	50.0	-1.76	48.529	1.5904×10^{-3}	2×10^{-5}	1.6104×10^{-3}	--
1	--	+3.14	10.0	8.7248×10^{-4}	6.18×10^{-5}	9.343×10^{-4}	2.54469×10^{-3}
0	55.0	+3.24	84.193	3.6284×10^{-5}	2×10^{-5}	5.6284×10^{-5}	--
1	--	+5.74	31.6	2.4087×10^{-5}	3.563×10^{-5}	5.972×10^{-5}	1.16×10^{-4}
0	60.0	+8.24	--	--	--	--	--
1	--	--	--	--	--	--	--

Note: $Si/\eta B_N$ = +10 dB

Table 3.4.1.1(c)

ACQUISITION TIMES FOR SPIKE REGION ONLY, B_o = 200kHz

N = 1; $P_1(\varepsilon) = 2.6\times10^{-3}$

K= N-1	Si/η (dB Hz)	$Si/\eta B_k$ (dB)	B_1 (kHz)	T_o (sec)	T_{P_o} (sec)	T_{ACQ} (sec)
0	45.0	-8.01	3.16	10.0026	1.5×10^{-5}	10.0027
	--	--	--	--	--	--
0	50.0	-3.01	10.0	9.18186×10^{-2}	1.5×10^{-5}	9.1834×10^{-2}
	--	--	--	--	--	--
0	55.0	+1.99	31.6	7.1379×10^{-4}	1.5×10^{-5}	7.2879×10^{-4}
	--	--	--	--	--	--
0	60.0	+6.99	100.0	0.3136×10^{-5}	1.5×10^{-5}	1.8136×10^{-5}
	--	--	--	--	-- --	--

Note: $Si/\eta B_N$ = +10 dB

Table 3.4.1.1(c')

ACQUISITION TIMES FOR SPIKE REGION ONLY, B_o = 200kHz

N = 2; $P_2(\varepsilon) = 5.2\times10^{-3}$

K= N-1	Si/η (dB Hz)	$Si/\eta B_k$ (dB)	B_{k+1} (kHz)	T_k (sec)	T_{P_k} (sec)	T'_k (sec)	T_{ACQ} (sec)
0	45.0	-8.01	35.810	7.789×10^{-2}	1.5×10^{-5}	7.7905×10^{-2}	--
1	--	-0.54	3.16	4.8840×10^{-2}	8.3775×10^{-5}	4.8924×10^{-2}	1.2683×10^{-1}
0	50.0	-3.01	57.306	2.7963×10^{-3}	1.5×10^{-5}	2.81123×10^{-3}	
1	--	+2.42	10.0	1.5933×10^{-3}	5.235×10^{-5}	1.6457×10^{-3}	4.4569×10^{-3}
0	55.0	+1.99	96.051	7.7543×10^{-5}	1.5×10^{-5}	9.2543×10^{-5}	
1	--	+5.17	31.6	4.2118×10^{-5}	3.1233×10^{-5}	7.335×10^{-5}	1.6589×10^{-4}
0	60.0	+6.99	--	--	--	--	--
1	--	--	--	--	--	--	--

Note: $Si/\eta B_N$ = +10 dB

Table 3.4.1.1(d)

ACQUISITION TIMES FOR SPIKE REGION ONLY, B_o = 250kHz

N = 1; $P_1(\varepsilon) = 2.6\times10^{-3}$

K= N-1	Si/η (dB Hz)	$Si/\eta B_k$ (db)	B_1 (kHz)	T_o (sec)	T_{P_o} (sec)	T_{ACQ} (sec)
0	45.0	-8.98	3.16	19.76	1.2×10^{-5}	19.76
	--	--	--	--	--	--
0	50.0	-3.98	10.0	1.8312×10^{-1}	1.2×10^{-5}	1.8313×10^{-1}
	--	--	--	--	--	--
0	55.0	+1.02	31.6	1.5195×10^{-3}	1.2×10^{-5}	1.5315×10^{-3}
	--	--	--	--	--	--
0	60.0	+6.02	100.0	5.89×10^{-5}	1.2×10^{-5}	1.789×10^{-5}
	--	--	--	--	--	--

Note: $Si/\eta B_N$ = 10 dB

Table 3.4.1.1(d')

ACQUISITION TIMES FOR SPIKE REGION ONLY, B_o = 250kHz

N = 2; $P_2(\varepsilon) = 5.2\times10^{-3}$

K= N-1	Si/η (dB Hz)	$Si/\eta B_k$ (dB)	B_{k+1} (kHz)	T_k (sec)	T_{P_k} (sec)	T'_k (sec)	T_{ACQ} (sec)
0	45.0	-8.98	40.900	1.17956×10^{-1}	1.2×10^{-5}	1.1797×10^{-1}	--
1	--	-1.12	3.16	0.74485×10^{-1}	7.335×10^{-5}	7.456×10^{-2}	1.9253×10^{-1}
0	50.0	-3.98	65.300	4.2947×10^{-3}	1.2×10^{-5}	4.3067×10^{-3}	--
1	--	+1.85	10.0	2.5122×10^{-3}	4.59×10^{-5}	2.558×10^{-3}	6.8648×10^{-3}
0	55.0	+1.02	107.634	1.3118×10^{-4}	1.2×10^{-5}	1.432×10^{-4}	--
1	--	+4.68	31.6	6.82913×10^{-5}	2.787×10^{-5}	9.616×10^{-5}	2.3935×10^{-4}
0	60.0	+6.02	224.287	1.5284×10^{-5}	1.2×10^{-5}	1.353×10^{-5}	--
1	--	+6.49	100.0	4.1078×10^{-6}	1.3376×10^{-5}	1.7484×10^{-5}	3.1012×10^{-5}

Note: $Si/\eta B_N$ = +10 dB

Table 3.4.1.1(e)

ACQUISITION TIMES FOR SPIKE REGION ONLY, B_o = 300kHz

N = 1; $P_1(\varepsilon) = 2.6\times10^{-3}$

K= N-1	Si/η (dB Hz)	$Si/\eta B_k$ (dB)	B_1 (kHz)	T_o (sec)	T_P (sec)	T_{ACQ} (sec)
0	45.0	-9.77	3.16	34.441	1×10^{-5}	34.441
	--	--	--	--	--	--
0	50.0	-4.77	10.0	0.32112	1×10^{-5}	3.2113×10^{-1}
	--	--	--	--	--	--
0	55.0	+0.23	31.6	2.764×10^{-3}	1×10^{-5}	2.774×10^{-3}
	--	--	---	--	--	--
0	60.0	+5.23	100.0	1.2612×10^{-5}	1×10^{-5}	2.2612×10^{-5}
	--	--	--	--	--	

Note: $Si/\eta B_N$ = +10 dB

Table 3.4.1.1(e')

ACQUISITION TIMES FOR SPIKE REGION ONLY, B_o = 300kHz

N = 2; $P_2(\epsilon) = 5.2\times10^{-3}$

K= N-1	Si/η (dB Hz)	$Si/\eta B_k$ (dB)	B_{k+1} (kHz)	T_k (sec)	T_{P_k} (sec)	T'_k (sec)	T_{ACQ} (sec)
0	45.0	-9.77	45.631	0.16517	1×10^{-5}	0.16518	--
1	--	-1.60	3.16	0.10517	6.57×10^{-5}	0.10523	2.7041×10^{-1}
0	50.0	-4.77	72.705	6.075×10^{-3}	1×10^{-5}	6.08513×10^{-3}	--
1	--	+1.38	10.0	3.620×10^{-3}	4.13×10^{-5}	3.6612×10^{-3}	9.7464×10^{-3}
0	55.0	+0.23	118.68	1.961×10^{-4}	1×10^{-5}	2.061×10^{-4}	--
1	--	+4.25	31.6	1.022×10^{-4}	2.53×10^{-5}	1.2748×10^{-4}	3.336×10^{-4}
0	60.0	+5.23	230.589	2.823×10^{-6}	1×10^{-5}	1.2823×10^{-5}	--
1	--	+6.37	100.0	4.395×10^{-6}	1.3×10^{-5}	1.74×10^{-5}	3.023×10^{-5}

Note: $Si/\eta B_N$ = +10 dB

Table 3.4.1.2

ACQUISITION TIMES FOR SPIKE REGION ONLY, B_o = 4kHz

$N = 1;\ P_1(\varepsilon) = 2.6\times10^{-3}$

K= N-1	Si/η (dB Hz)	$Si/\eta B_k$ (dB)	B_1 (hz)	T_o (sec)	T_{P_o} (sec)	T_{ACQ} (sec)
0	31.0	-5.00	126.5	29.842	7.5×10^{-4}	29.843
	--	--	---	--	--	--
0	33.0	-3.00	200.0	4.546	7.5×10^{-4}	4.5468
	--	--	---	--	--	--
0	36.0	0.00	400.0	0.2583	7.5×10^{-4}	2.59×10^{-1}
	--	--	---	--	--	--
0	39.0	+3.00	798.1	1.231×10^{-2}	7.5×10^{-4}	1.306×10^{-2}
	--	--	--	--	--	--
0	41.0	+5.00	1264.9	1.2467×10^{-3}	7.5×10^{-4}	1.997×10^{-3}
	--	--	--	--	--	--

Note: $Si/\eta B_N$ = +10 dB

Table 3.4.1.2'

ACQUISITION TIMES FOR SPIKE REGION ONLY, B_o = 4kHz

N = 2; $P_2(\varepsilon) = 5.2\times10^{-3}$

K= N-1	Si/η (dB Hz)	$Si/\eta B_k$ (dB)	B_{k+1} (Hz)	T_k (sec)	T_{P_k} (sec)	T'_k (sec)	T_{ACQ} (sec)
0	31.0	-5.00	948.9	0.5304	7.5×10^{-4}	5.311×10^{-1}	--
1	--	+1.25	126.5	0.3180	3.16×10^{-3}	3.21×10^{-1}	8.521×10^{-1}
0	33.0	-3.00	1149.0	0.1384	7.5×10^{-4}	1.392×10^{-1}	--
1	--	+2.42	200.48	0.0795	2.611×10^{-3}	8.2117×10^{-2}	2.213×10^{-1}
0	36.0	0.00	1545.9	1.73×10^{-2}	7.5×10^{-4}	1.81×10^{-2}	--
1	--	+4.13	400.0	9.063×10^{-3}	1.94×10^{-3}	1.1×10^{-2}	2.92×10^{-2}
0	39.0	+3.00	2177.87	1.671×10^{-3}	7.5×10^{-4}	2.421×10^{-3}	--
1	--	+5.64	798.1	1.0486×10^{-3}	1.378×10^{-3}	2.426×10^{-3}	4.847×10^{-3}
0	41.0	+5.00	2950.0	2.563×10^{-4}	7.5×10^{-4}	1.006×10^{-3}	--
1	--	+6.32	1264.9	3.582×10^{-4}	1.017×10^{-3}	1.375×10^{-3}	2.382×10^{-3}

Note: $Si/\eta B_N$ = +10 dB

Table 3.4.1.3(a)

PARAMETER COMPARISON FOR B_o = 100kHz

N = 1

K= N-1	Si/η (dB Hz)	T_I (sec)	T_{SP} (sec)	R_1 --	R_2 --	S_1	S_2
0	45	20.5×10^{-6}	20.0×10^{-6}	5.84×10^{4}	5.98×10^{4}	1.457×10^{6}	3.257×10^{2}
	--	--	--	--	--	--	--
0	50	43.6×10^{-6}	20.0×10^{-6}	5.166×10^{2}	2.37×10^{2}	1.87×10^{3}	8.37×10^{1}
	--	--	--	--	--	--	--
0	55	4.05×10^{-3}	20.0×10^{-6}	2.5	1.234×10^{-1}	2.9×10^{1}	4.54
	--	--	--	--	--	--	--
0	60	--	--	--	--	--	
	--	--	--	--	--	--	

Table 3.4.1.3(a')

PARAMETER COMPARISON FOR B_o = 100kHz

N = 2

K= N-1	Si/η (dB Hz)	T_I (sec)	T_{SP} (sec)	R_1 --	R_2 --	S_1 --	S_2 --
0	45	20.5×10^{-6}	20.0×10^{-6}	1.063×10^{3}	1.037×10^{3}	2.59×10^{4}	4.26×10^{1}
1	--	261×10^{-6}	84.0×10^{-6}	1.51×10^{2}	4.83×10^{1}	5.13×10^{3}	5.44×10^{1}
0	50	43.6×10^{-6}	20.0×10^{-6}	3.46×10^{1}	1.58×10^{1}	1.256×10^{3}	2.567×10^{1}
1	--	585.6×10^{-6}	51.7×10^{-6}	6.997	6.18×10^{-1}	1.244×10^{2}	1.164×10^{1}
0	55	4.05×10^{-3}	20.0×10^{-6}	5.14×10^{-1}	2.5×10^{-2}	4.93	3.34
1	--	1.73×10^{-3}	27.14×10^{-6}	5.28×10^{-1}	8.29×10^{-3}	1.76	1.33
0	60	--	--	--	--	--	--
1	--	--	--	--	--	--	--

Table 3.4.1.3(b)

PARAMETER COMPARISON FOR B_o = 150kHz

N = 1

K= N-1	S_i/η_I (dB Hz)	T_I (sec)	T_{SP} (sec)	R_1 --	R_2 --	S_1 --	S_2 --
0	45	12×10^{-6}	13.3×10^{-6}	3.114×10^{5}	3.45×10^{5}	5.74×10^{6}	4.561×10^{2}
	--	--	--	--	--	--	--
0	50	20.3×10^{-5}	13.3×10^{-6}	2.8×10^{3}	1.84×10^{3}	9.7×10^{4}	1.489×10^{2}
	--	--	--	--	--	--	--
0	55	92×10^{-6}	13.3×10^{-6}	1.91×10^{1}	2.76	4.59×10^{2}	1.81×10^{1}
	--	--	--	--	--	--	--
0	60	9.37×10^{-3}	13.3×10^{-6}	2.9×10^{-2}	4.15×10^{-7}	1.97	2.38×10^{-1}
	--	--	--	--	--	--	--

Table 3.4.1.3(b')

PARAMETER COMPARISON FOR B_o = 150kHz

N = 2

K= N-1	Si/η (dB Hz)	T_I (sec)	T_{SP} (sec)	R_1 --	R_2 --	S_1 --	S_2 --
0	45	12×10^{-6}	13.3×10^{-6}	3.4172×10^{3}	3.7867×10^{3}	6.3×10^{4}	4.9×10^{1}
1	--	66.3×10^{-6}	152.0×10^{-6}	4.243×10^{2}	1.85×10^{2}	1.53×10^{4}	8.11×10^{1}
0	50	20.3×10^{-6}	13.3×10^{-6}	1.193×10^{2}	7.83×10^{1}	4.122×10^{3}	2.886×10^{1}
1	--	271.4×10^{-6}	41.2×10^{-6}	2.12×10^{1}	3.2	5.24×10^{2}	1.87×10^{1}
0	55	92×10^{-6}	13.3×10^{-6}	2.72	3.94×10^{-1}	6.61×10^{1}	6.20
1	--	880×10^{-6}	$23.7\times10^{-}6$	1.01	2.7×10^{-2}	6.68	2.18
0	60	--	--	--	--	--	--
1	--	--	--	--	--	--	--

Table 3.4.1.3(c)

PARAMETER COMPARISON FOR B_o = 200kHz

N = 1

K= N-1	Si/n (dB Hz)	T_I (sec)	T_{SP} (sec)	R_1 --	R_2 --	S_1 --	S_2 --
0	45	8.4×10^{-6}	10^{-5}	1.10^{-6}	1.186×10^{6}	1.48×10^{7}	5.623×10^{2}
	--	--	--	--	--	--	--
0	50	12.66×10^{-6}	10^{-5}	9.182×10^{3}	7.251×10^{3}	2.86×10^{5}	2.104×10^{2}
	--	--	--	--	--	--	--
0	55	40×10^{-6}	10^{-5}	7.14×10^{1}	1.78×10^{1}	2.219×10^{3}	3.888×10^{1}
	--	--	--	--	--	--	--
0	60	1.3×10^{-3}	10^{-5}	3.13×10^{-1}	2.4×10^{-3}	9.59×10^{-1}	7.7×10^{-1}
	--	--	--	--	--	--	--

Table 3.4.1.3(c')

PARAMETER COMPARISON FOR B_0 = 200kHz

N = 2

K= N-1	Si/η (dB Hz)	T_I (sec)	T_{SP} (sec)	R_1 -	R_2 --	S_1 --	S_2 --
0	45	8.4×10^{-6}	10^{-5}	7.789×10^{3}	9.232×10^{3}	1.15×10^{5}	4.85×10^{1}
1	--	107×10^{-6}	55.8×10^{-6}	8.745×10^{2}	4.547×10^{2}	3.17×10^{4}	1.015×10^{2}
0	50	12.66×10^{-6}	10^{-5}	2.796×10^{2}	2.21×10^{2}	8.719×10^{3}	3.88×10^{1}
1	--	166×10^{-6}	34.9×10^{-6}	4.56×10^{1}	9.6	1.324×10^{3}	3.10×10^{1}
0	55	40×10^{-6}	10^{-5}	7.75	1.9	2.413×10^{2}	1.03×10^{1}
1	--	482×10^{-6}	20.8×10^{-6}	2.02	8.7×10^{-2}	2.11×10^{1}	3.78
0	60	--	--	--	--	--	--
1	--	--	--	--	--	--	--

Table 3.4.1.3(d)

PARAMETER COMPARISON FOR B_o = 250kHz

N = 1

K= N-1	Si/η (dB Hz)	T_I (sec)	T_{SP} (sec)	R_1 --	R_2 --	S_1 --	S_2 --
0	45	6.47×10^{-6}	8×10^{-6}	2.47×10^{6}	3.05×10^{6}	3.05×10^{7}	6.565×10^{2}
	--	--		--	--	--	--
0	50	9×10^{-6}	8×10^{-6}	2.23×10^{4}	2.02×10^{4}	6.4×10^{5}	2.621×10^{2}
	--	--	--	--	--	--	--
0	55	23×10^{-6}	8×10^{-6}	1.90×10^{2}	6.60×10^{1}	6.576×10^{3}	6.04×10^{1}
	--	--	--	--	--	--	--
0	60	380×10^{-6}	8×10^{-6}	7.37×10^{-1}	1.55×10^{-2}	4.67	1.72
	--	--	--	--	---	--	--

Table 3.4.1.3(d')

PARAMETER COMPARISON FOR B_o = 250kHz

N = 2

K= N-1	Si/η (dB Hz)	T_I (sec)	T_{SP} (sec)	R_1 --	R_2 --	S_1 --	S_2 --
0	45	6.47×10^{-6}	8×10^{-6}	1.47×10^{4}	1.8×10^{4}	1.82×10^{5}	5.16×10^{1}
1	--	83.6×10^{-6}	48.9×10^{-6}	1.52×10^{3}	8.9×10^{2}	5.44×10^{4}	1.261×10^{2}
0	50	9×10^{-6}	8×10^{-6}	5.368×10^{2}	4.748×10^{2}	1.5×10^{4}	2.6×10^{3}
1	--	116×10^{-6}	30.6×10^{-6}	8.2×10^{1}	2.15×10^{1}	3.9×10^{1}	3.97×10^{1}
0	55	23×10^{-6}	8×10^{-6}	1.64×10^{1}	5.7	5.643×10^{2}	1.68×10^{1}
1	--	299.8×10^{-6}	18.5×10^{-6}	3.7	2.3×10^{-1}	5.3×10^{1}	6.5
0	60	380×10^{-6}	8×10^{-6}	4×10^{-3}	4.67	2.33	2.18
1	--	675×10^{-6}	8.9×10^{-6}	4.6×10^{-1}	6.1×10^{-3}	1.22	1.16

Table 3.4.1.3(e)

PARAMETER COMPARISON FOR B_o = 300kHz

N = 1

K= N-1	Si/η (dB Hz)	T_I (sec)	T_{SP} (sec)	R_1 --	R_2 --	S_1 --	S_2 --
0	45	5.23×10^{-6}	6.6×10^{-6}	5.17×10^{6}	6.58×10^{6}	5.47×10^{7}	7.387×10^{2}
	--	--	--	--	--	---	--
0	50	6.976×10^{-6}	6.6×10^{-6}	4.82×10^{4}	4.6×10^{4}	1.21×10^{6}	3.10×10^{2}
	--	--	--	--	--	--	--
0	55	15.4×10^{-6}	6.6×10^{-6}	4.15×10^{2}	1.80×10^{2}	1.49×10^{4}	8.1×10^{1}
	--	--	--	--	--	--	--
0	60	161×10^{-6}	6.6×10^{-6}	1.89	7.8×10^{-2}	1.91×10^{1}	3.56
	--	--	--	--	--	--	--

Table 3.4.1.3(e')

PARAMETER COMPARISON FOR B_o = 300kHz

N = 2

K= N-1	Si/η (dB Hz)	T_I (sec)	T_{SP} (sec)	R_1	R_2 --	S_1 --	S_2 --
0	45	5.23×10^{-6}	6.6×10^{-6}	2.48×10^{4}	3.15×10^{4}	2.62×10^{5}	5.05×10^{1}
1	--	68.7×10^{-6}	43.8×10^{-6}	2.399×10^{3}	1.53×10^{3}	8.376×10^{4}	1.474×10^{2}
0	50	6.976×10^{-6}	6.6×10^{-6}	9.11×10^{2}	8.71×10^{2}	2.29×10^{4}	4.399×10^{1}
1	--	89×10^{-6}	27.5×10^{-6}	1.32×10^{2}	4.1×10^{1}	4.41×10^{3}	4.898×10^{1}
0	55	15.4×10^{-6}	6.6×10^{-6}	2.94×10^{1}	1.28×10^{1}	1.057×10^{3}	2.4×10^{1}
1	--	206×10^{-6}	16.8×10^{-6}	6.06	4.97×10^{-1}	1.04×10^{2}	1.03×10^{1}
0	60	161×10^{-6}	6.6×10^{-6}	4.23×10^{-1}	1.75×10^{-2}	3.04	3.06
1	--	580×10^{-6}	8.6×10^{-6}	5.07×10^{-1}	7.57×10^{-3}	1.54	1.28

Table 3.4.1.4

PARAMETER COMPARISON FOR B_o = 4kHz

N = 1

K= N-1	Si/η (dB Hz) Si/ηB_o (dB)	T_I (sec)	T_{SP} (sec)	R_1 --	R_2 --	S_1 --	S_2 --
0	31	0.512×10^{-3}	0.5×10^{-3}	5.97×10^{4}	5.82×10^{4}	1.45×10^{6}	3.25×10^{2}
		--	--	--	--	--	--
0	33	0.634×10^{-3}	0.5×10^{-3}	9.09×10^{3}	7.17×10^{3}	2.84×10^{5}	2.11×10^{2}
		--	--	--	--	--	--
0	36	1.09×10^{-3}	0.5×10^{-3}	5.17×10^{2}	2.37×10^{2}	1.87×10^{4}	8.37×10^{1}
		--	--	--	--	--	--
0	39	3.07×10^{-3}	0.5×10^{-3}	2.5×10^{1}	4.0	6.31×10^{2}	1.99×10^{1}
		--	--	--	--	--	--
0	41	10.2×10^{-3}	0.5×10^{-3}	2.5	1.23×10^{-1}	2.88×10^{1}	4.5
		--	--	--	--	--	--

Table 3.4.1.4'

PARAMETER COMPARISON FOR B_o = 4kHz

N = 2

K= N-1	Si/η (dB Hz) Si/ηB_o (dB)	T_I (sec)	T_{SP} (sec)	R_1 --	R_2 --	S_1 --	S_2 --
0	31	0.512×10^{-3}	0.5×10^{-3}	1.061×10^{3}	1.034×10^{3}	2.58×10^{4}	4.2×10^{1}
1	-5	6.53×10^{-3}	2.1×10^{-3}	1.51×10^{2}	4.87×10^{1}	5.12×10^{3}	5.44×10^{1}
0	33	0.634×10^{-3}	0.5×10^{-3}	2.77×10^{2}	2.18×10^{2}	8.64×10^{3}	3.88×10^{1}
1	-3	8.28×10^{-3}	1.74×10^{-3}	4.57×10^{1}	9.6	1.32×10^{3}	3.1×10^{1}
0	36	1.09×10^{-3}	0.5×10^{-3}	3.5×10^{1}	1.59×10^{1}	1.255×10^{3}	2.56×10^{1}
1	0	14.6×10^{-3}	1.3×10^{-3}	7.00	6.2×10^{-1}	1.25×10^{2}	1.16×10^{1}
0	39	3.07×10^{-3}	0.5×10^{-3}	3.3	5.4×10^{-1}	8.3×10^{1}	6.75
1	+3	31.1×10^{-3}	0.92×10^{-3}	1.1×10^{-1}	3.4×10^{-2}	9.3	2.4
0	41	10.2×10^{-3}	0.5×10^{-3}	5.13×10^{-1}	2.52×10^{-2}	4.89	3.34
1	+5	43.2×10^{-3}	0.68×10^{-3}	5.3×10^{-1}	8.3×10^{-3}	1.76	1.34

Table 3.4.1.5(a)

ACQUISITION TIMES FOR GAUSSIAN REGION ONLY

B_o = [100kHz, 300kHz]

$Si/\eta B_F$	Si/η (dB-Hz)	B_2 (kHz)	B_F (kHz)	T_o (ms)	T_{p_o} (ms)	T_{ACQ} (ms)
20	45	3.16	0.316	0.494	0.949	1.443
	50	10.0	1.000	0.156	0.3	0.456
	55	31.6	3.160	0.0494	0.0949	0.1443
	60	100.0	10.000	0.0156	0.03	0.0456
25	45	3.16	0.100	1.583	0.949	2.532
	50	10.0	0.316	0.501	0.300	0.801
	55	31.6	1.000	0.158	0.0949	0.253
	60	100.0	3.160	0.05	0.03	0.08
30	45	3.16	0.0316	5.549	0.949	6.498
	50	10.0	0.100	1.754	0.3	2.054
	55	31.6	0.316	0.555	0.0949	0.650
	60	100.0	1.000	0.175	0.03	0.205

Table 3.4.1.5(b)

ACQUISITION TIMES FOR GAUSSIAN REGION ONLY

$N = 2$, B_o = [100kHz - 300kHz]

k'	Si/η(dB Hz)	$B_{k'}$(kHz)	$B_{k'+1}$(kHz)	$T_{k'}$ (sec)	$T_{pk'}$ (sec)	T'_k (sec)	T_{ACQ}(msec)
0	45	3.16	1.3243	0.5562×10^{-5}	0.9494×10^{-3}	0.9493×10^{-3}	
1		1.3243	0.0316	0.3069×10^{-2}	0.2266×10^{-2}	0.5335×10^{-2}	6.2899
0	50	10.0	4.190	0.1759×10^{-5}	0.3×10^{-3}	0.30176×10^{-3}	---
1		4.190	0.100	0.9699×10^{-3}	0.716×10^{-3}	0.16859×10^{-2}	1.9876
0	55	31.6	13.243	0.555×10^{-6}	0.9494×10^{-4}	0.9493×10^{-4}	
1		13.243	0.316	0.3069×10^{-3}	0.2266×10^{-3}	0.5335×10^{-3}	0.62895
0	60	100.0	41.900	0.1757×10^{-6}	0.3×10^{-4}	0.30176×10^{-4}	---
1		41.900	1.000	0.9699×10^{-4}	0.716×10^{-4}	0.16855×10^{-3}	0.19876

Note: $Si/\eta B_F$ = +30 dB $Si/\eta B_{k'}$ = +10 dB

Table 3.4.1.6

ACQUISITION TIMES FOR GAUSSIAN REGION ONLY

B_o = 4kHz

$Si/\eta B_F$	Si/η	B_2(Hz)	B_F(Hz)	T_o(ms)	T_{po}(ms)	T_{ACQ}(ms)
+20	31	125.5	12.65	12.34	23.72	36.1
	33	200.48	20.05	7.79	14.96	22.75
	36	400.00	40.00	3.9	7.5	11.40
	39	798.1	79.81	1.96	3.75	5.72
	41	1264.9	126.5	1.23	2.37	3.61
+25	31	126.5	4.00	39.56	23.72	63.3
	33	200.48	6.35	24.94	14.96	39.91
	36	400.00	12.65	12.51	7.5	20.00
	39	798.1	25.25	6.28	3.75	10.03
	41	1264.9	40.0	3.96	2.37	6.33
+30	31	126.5	1.265	138.6	23.72	162.3
	33	200.48	2.00	87.45	14.96	102.4
	36	400.00	4.00	43.84	7.5	51.3
	39	798.1	7.98	21.97	3.75	25.7
	41	1264.9	12.65	13.8	2.37	16.23

Note: $Si/\eta B_2$ = +10 dB

Table 3.4.1.7(a)

TOTAL ACQUISITION TIME, ρ_F = 20 dB

B_o = [100kHz - 300kHz]

			T_{ACQ} (sec)				
N	Si/η(dB-Hz)	B_F(kHz)	100kHz	150kHz	200kHz	250kHz	300kHz
2	45	0.316	1.19013	4.15328	10.004	19.76144	34.442
	50	1.000	1.0818×10^{-2}	3.792×10^{-2}	9.229×10^{-2}	1.8359×10^{-1}	3.21586×10^{-1}
	55	3.160	2.2435×10^{-4}	4.1859×10^{-4}	8.7309×10^{-4}	1.6758×10^{-3}	2.9183×10^{-3}
	60	10.000	(4.56×10^{-5})	6.5988×10^{-5}	6.3736×10^{-5}	6.349×10^{-5}	6.8212×10^{-5}
3	45	0.316	3.5606×10^{-2}	7.52585×10^{-2}	1.28273×10^{-1}	1.93973×10^{-1}	2.71853×10^{-1}
	50	1.000	1.6184×10^{-3}	2.97069×10^{-3}	4.9129×10^{-3}	7.3208×10^{-3}	1.0202×10^{-2}
	55	3.160	2.39629×10^{-4}	2.603×10^{-4}	3.1019×10^{-4}	3.8365×10^{-4}	4.779×10^{-4}
	60	10.000	--	--	--	7.6612×10^{-5}	7.583×10^{-5}

Table 3.4.1.7(b)

TOTAL ACQUISITION TIME, ρ_F = 25 dB

B_o = [100kHz - 300kHz]

N	Si/η(dB Hz)	B_F(kHz)	T_{ACQ} (sec) 100kHz	150kHz	200kHz	250kHz	300kHz
2	45	0.100	1.200	4.1544	10.00523	19.7625	34.4435
	50	0.316	1.1163×10^{-2}	3.8267×10^{-2}	9.2635×10^{-2}	1.8919×10^{-1}	3.2192×10^{-1}
	55	1.000	3.3305×10^{-4}	5.273×10^{-4}	9.8179×10^{-2}	1.7845×10^{-3}	$3.027\times10^{=3}$
	60	3.160	($8.0\ 10^{-5}$)	1.0039×10^{-4}	9.8136×10^{-5}	9.789×10^{-5}	1.026×10^{-4}
3	45	0.100	3.6695×10^{-2}	7.6348×10^{-2}	1.2936×10^{-1}	1.9506×10^{-1}	2.7294×10^{-1}
	50	0.316	1.9634×10^{-3}	3.3457×10^{-3}	5.2579×10^{-3}	7.6658×10^{-3}	1.0547×10^{-2}
	55	1.000	3.4833×10^{-4}	3.69×10^{-4}	4.1889×10^{-4}	4.9235×10^{-4}	5.866×10^{-4}
	60	3.160	--	--	--	1.11×10^{-4}	1.1023×10^{-4}

Table 3.4.1.7(c)

TOTAL ACQUISITION TIME, ρ_F = +30 dB

B_o = [100kHz - 300kHz]

			T_{ACQ} (sec)				
N	Si/η(dB Hz)	B_F(kHz)	100kHz	150kHz	200kHz	250kHz	300kHz
2	45	.0316	1.2041	4.15834	10.0092	19.7665	34.4475
	50	.1000	1.2416×10^{-2}	3.952×10^{-2}	9.3888×10^{-2}	1.852×10^{-1}	3.232×10^{-1}
	55	.3160	7.3×10^{-4}	9.243×10^{-4}	1.3788×10^{-3}	2.1815×10^{-3}	3.424×10^{-3}
	60	1.000	(2.05×10^{-4})	2.254×10^{-4}	2.2314×10^{-4}	2.2289×10^{-4}	2.276×10^{-4}
3	45	.0316	4.0661×10^{-2}	8.0314×10^{-2}	1.3333×10^{-1}	1.9903×10^{-1}	2.7691×10^{-1}
	50	.1000	3.2164×10^{-3}	4.59869×10^{-3}	6.511×10^{-3}	8.9×10^{-3}	1.18×10^{-2}
	55	.3160	7.4533×10^{-4}	7.66×10^{-4}	8.1589×10^{-4}	8.894×10^{-4}	9.836×10^{-4}
	60	1.000	--	--	--	2.36×10^{-4}	2.352×10^{-4}

Table 3.4.1.8

TOTAL ACQUISITION TIME

B_o = 4kHz

			T_{ACQ} (sec)		
N	$Si/\eta B_0$	Si/η(dB-Hz)	ρ_F = 20 dB	ρ_F = 25 dB	ρ_F = 30 dB
2	-5	31	29.8791	29.9053	30.0153
	-3	33	4.56955	4.58671	4.6492
	+0	36	2.704×10^{-1}	2.79×10^{-1}	3.102×10^{-1}
	+3	39	1.878×10^{-2}	2.31×10^{-2}	3.876×10^{-2}
	+5	41	5.61×10^{-3}	8.327×10^{-3}	1.823×10^{-2}
3	-5	31	8.882×10^{-1}	9.154×10^{-1}	1.0144
	-3	33	2.441×10^{-1}	2.612×10^{-1}	$3,237\times10^{-1}$
	+0	36	4.06×10^{-2}	4.92×10^{-2}	8.05×10^{-2}
	+3	39	1.0567×10^{-2}	1.4877×10^{-2}	3.055×10^{-2}
	+5	41	5.992×10^{-3}	8.712×10^{-3}	1.861×10^{-2}

Table 3.4.1.9

TOTAL ACQUISITION TIME, N = 1 -- B_o TO B_F DIRECTLY

B_o = [100, 300]kHz

		T_{ACQ} (sec)					
		B_o = 100kHz			B_o = 300kHz		
Si/η(dB Hz)	Si/η(W-Hz)	ρ_F = 20 dB	ρ_F = 25 dB	ρ_F = 30 dB	ρ_F = 20 dB	ρ_F = 25 dB	ρ_F = 30 dB
45	31.6×10^{3}	1.1975×10^{2}	1.1958×10^{3}	1.1975×10^{4}	3.44×10^{3}	3.44×10^{4}	3.44×10^{5}
50	1×10^{5}	1.033	1.035×10^{1}	1.033×10^{2}	3.21×10^{1}	3.22×10^{2}	3.21×10^{3}
55	316×10^{3}	4.88×10^{-3}	4.84×10^{-2}	4.83×10^{-1}	2.764×10^{-1}	2.76	2.76×10^{1}
60	1×10^{6}	(4.56×10^{-5})	(8.01×10^{-5})	(2.05×10^{-3})	1.21×10^{-3}	1.203×10^{-2}	1.2×10^{-1}

Table 3.4.1.10

TOTAL ACQUISITION TIME, N = 1 -- B_o TO B_F DIRECTLY

B_o = 4kHz

	T_{ACQ} (sec)		
Si/η(dB Hz)	ρ_F = 20 dB	ρ_F = 25 dB	ρ_F = 30 dB
31	2.98×10^{3}	2.98×10^{4}	2.98×10^{5}
33	4.5×10^{2}	4.5×10^{3}	4.5×10^{4}
36	2.58×10^{1}	2.58×10^{3}	2.58×10^{4}
39	1.23	1.23×10^{1}	1.23×10^{2}
41	1.21×10^{-1}	1.21	1.2×10^{1}

Table 3.4.1.11

TOTAL ACQUISITION TIME FOR N = 2 FROM B_o TO B_1^* TO B_F, ρ_F = +20 dB

B_o = [100kHz, 200kHz, 300kHz]

		B_o = 100kHz		B_o = 200kHz		B_o = 300kHz	
K	Si/η(dB-Hz)	T_k'(sec)	T_{ACQ}(sec)	T_k'(sec)	T_{ACQ}(sec)	T_k'(sec)	T_{ACQ}(sec)
0	45	2.13×10^{-2}	--	7.79×10^{-2}	--	1.65×10^{-2}	--
1		1.2736	1.2949	4.884	4.962	10.516	10.533
0	50	7.226×10^{-4}	--	2.81×10^{-3}	--	6.085×10^{-3}	--
1	--	3.6016×10^{-2}	3.674×10^{-2}	1.59×10^{-1}	1.62×10^{-1}	3.62×10^{-1}	3.681×10^{-1}
0	55	4.05×10^{-5}	--	9.25×10^{-5}	--	2.06×10^{-4}	--
1	--	1.117×10^{-3}	1.157×10^{-3}	4.069×10^{-3}	4.16×10^{-3}	1.015×10^{-2}	1.036×10^{-2}
0	60	--	--	--	--	1.28×10^{-5}	--
1	--	--	--	--	--	3.331×10^{-4}	3.459×10^{-4}

Table 3.4.1.12(a)

ACQUISITION TIMES FOR GAUSSIAN REGION ONLY,

B_o = [100kHz, 200kHz, 300kHz]

$B_F/B_o = 10^{-3}$, N = 1

	T_{ACQ} (sec)		
Si/η(dB Hz)	B_o = 100kHz	B_o = 200kHz	B_o = 300kHz
45	2.532×10^{-3}	1.7065×10^{-3}	1.4819×10^{-2}
50	2.0535×10^{-3}	1.110×10^{-3}	8.214×10^{-4}
55	2.475×10^{-3}	1.0475×10^{-3}	6.85×10^{-4}
60	4.996×10^{-3}	1.5355×10^{-2}	8.421×10^{-4}

Note: $Si/\eta B_T$ = +10 dB

Table 3.4.1.12(b)

ACQUISITION TIMES FOR GAUSSIAN REGION ONLY,

B_o = [100kHz, 200kHz, 300kHz]

$B_F/B_o = 10^{-3}$, N = 2

	T_{ACQ} (sec)		
Si/η(dB-Hz)	B_o = 100kHz	B_o = 200kHz	B_o = 300kHz
45	3.44×10^{-3}	--	--
50	1.99×10^{-3}	1.362×10^{-3}	1.114×10^{-3}
55	1.27×10^{-3}	0.834×10^{-3}	0.648×10^{-3}
60	0.83×10^{-3}	0.534×10^{-3}	0.418×10^{-3}

Note: $Si/\eta B_T$ = +10 dB

Table 3.4.1.13

TOTAL ACQUISITION TIME, $B_F/B_o = 10^{-3}$

B_o = [100kHz, 200kHz, 300kHz]

	T_{ACQ} (sec)		
Si/η(dB Hz)	B_o = 100kHz	B_o = 200kHz	B_o = 300kHz
45	5.95×10^{-2}	1.285×10^{-1}	2.8523×10^{-1}
50	3.22×10^{-3}	5.567×10^{-3}	1.057×10^{-2}
55	1.35×10^{-3}	1.563×10^{-3}	3.422×10^{-3}
60	8.3×10^{-4}	5.52×10^{-4}	4.4×10^{-4}

Table 3.4.2.1

TOTAL ACQUISITION TIME FOR CONSTANT BANDWIDTH REDUCTION,

$N = 2,\ B_F/B_o = 10^{-3}$

$(B_1/B_o = 0.1,\ B_F/B_1 = 0.01)$

B_o (kHz) / Si/η (dB Hz)	T_{ACQ} (sec)		
	100	200	300
45	6.04×10^{-1}	2.03	3.45
50	1.24×10^{-2}	5.8×10^{-2}	1.71×10^{-1}
55	9.31×10^{-4}	2.55×10^{-3}	3.71×10^{-3}
60	5.84×10^{-4}	5.44×10^{-4}	5.17×10^{-4}

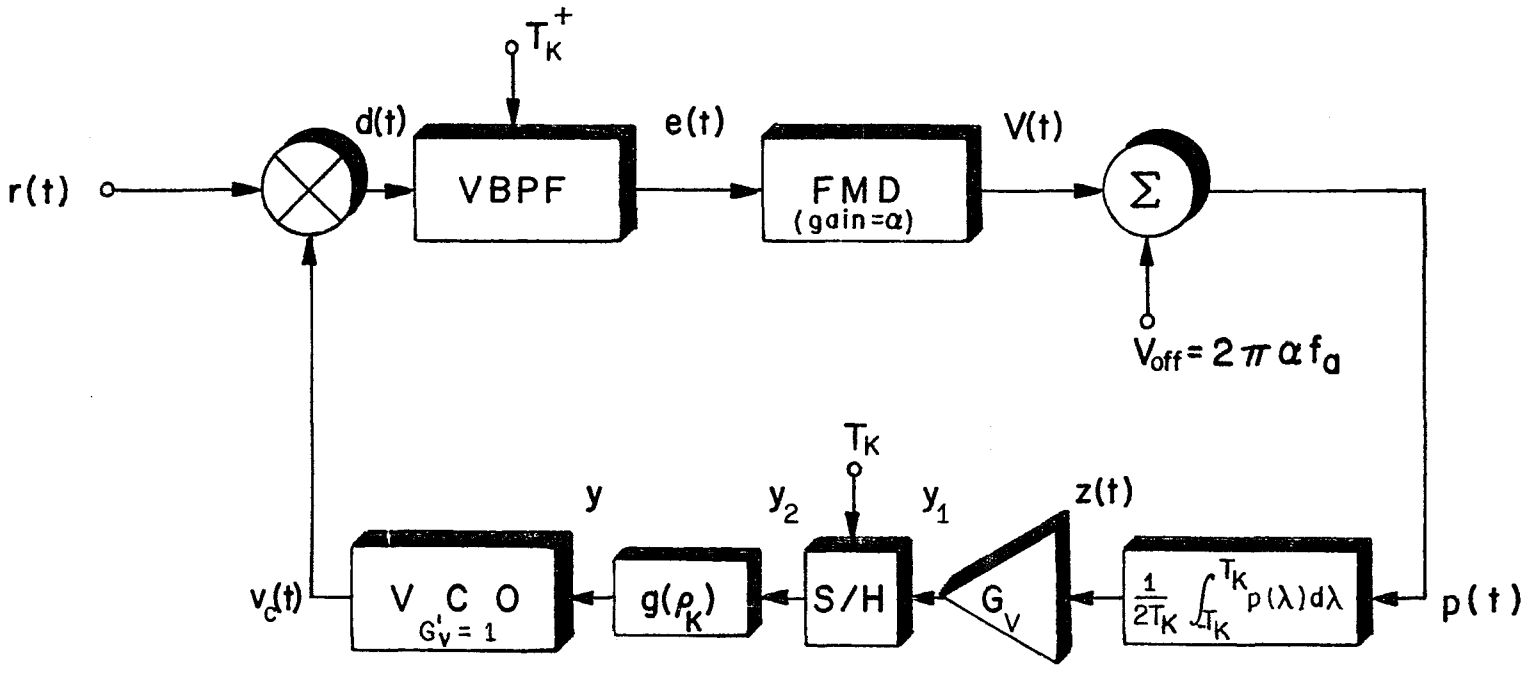

Figure 3.1.1 Acquisition Loop Configuration

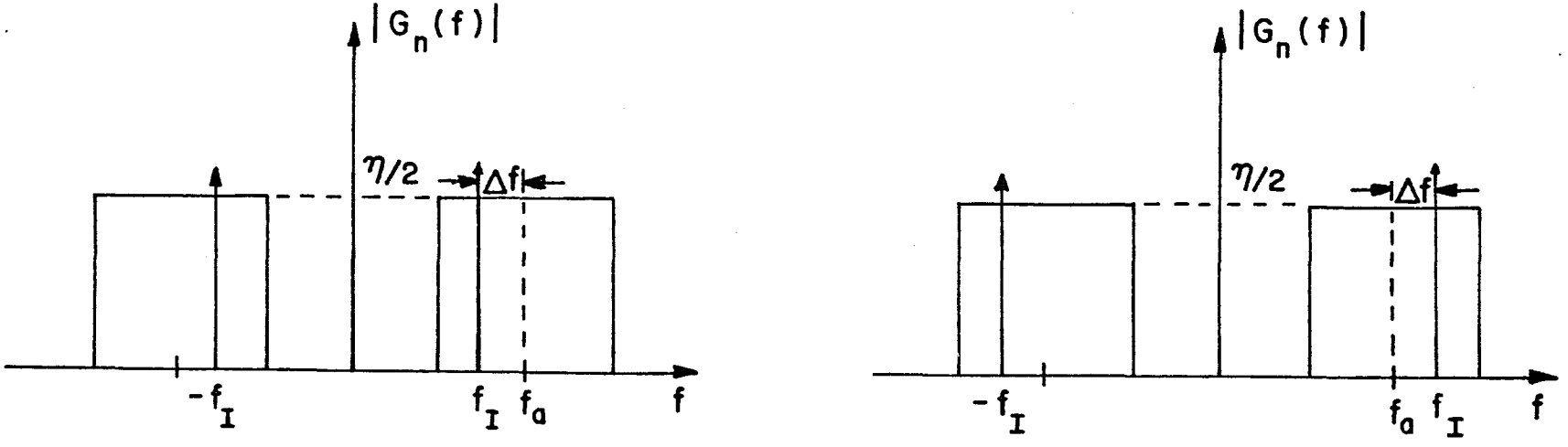

Figure 3.1.2 Illustrating Two Possible Locations of Carrier Signal

(a) Actual Carrier Below Center Band - $\Delta f = -f_D$

(b) Actual Carrier Above Center Band - $\Delta f = +f_D$

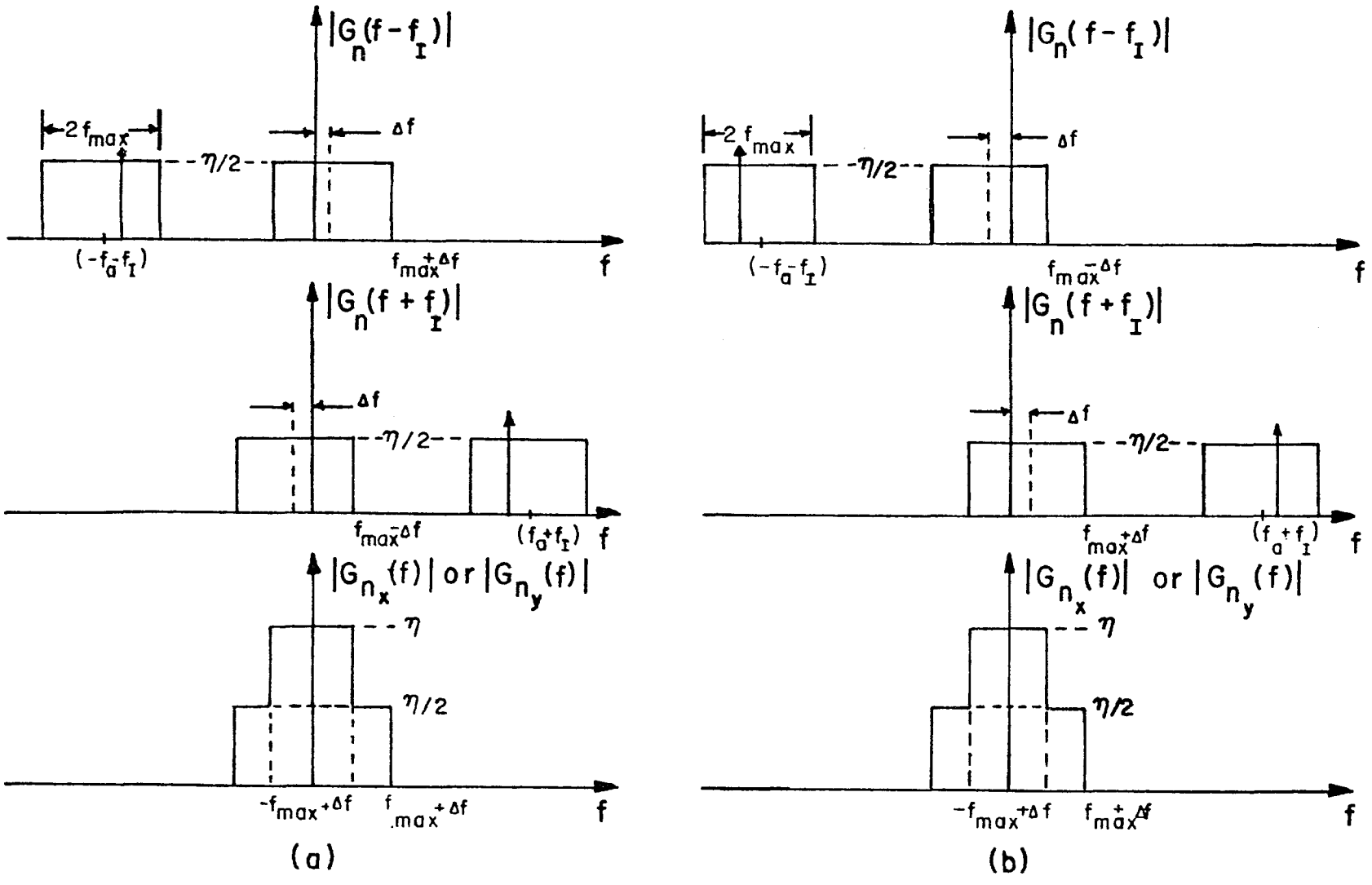

Figure 3.1.3 Determination of $G_{n_x}(f)$ or $G_{n_y}(f)$ (a) $\Delta f = -f_D$ (b) $\Delta f = +f_D$

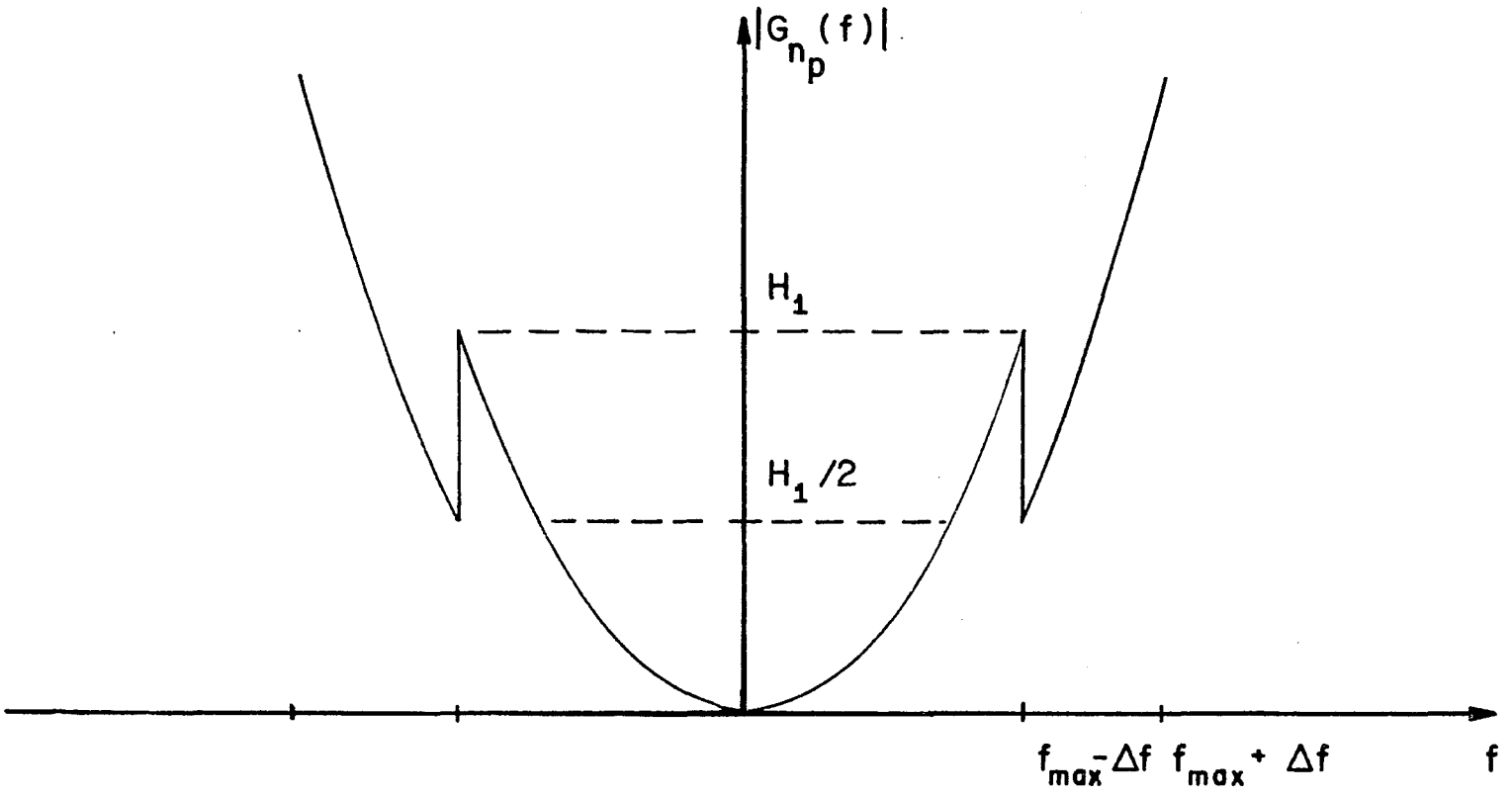

Figure 3.1.4 Power Spectral Density of the Discriminator Output Noise for High Signal-to-Noise Ratio

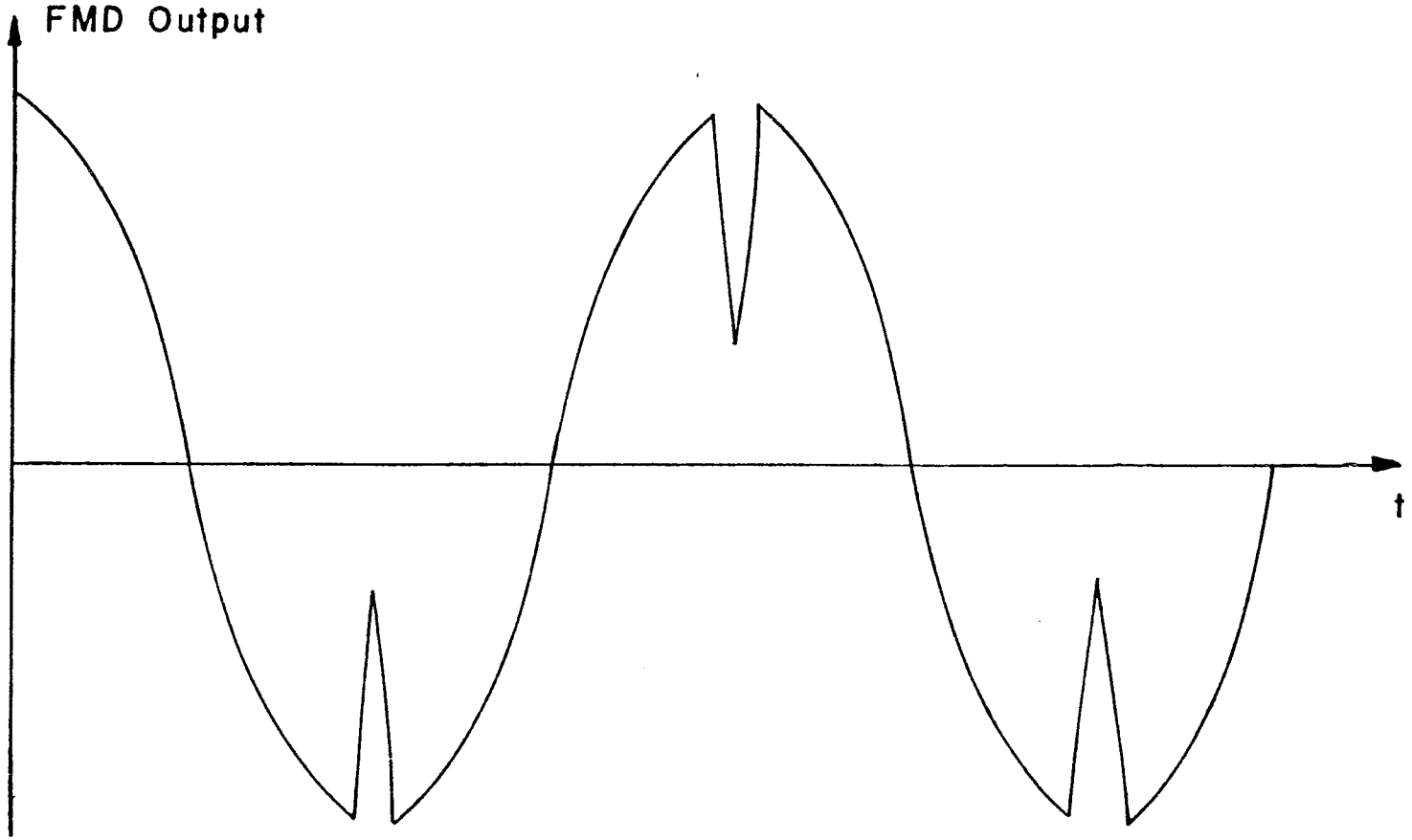

Figure 3.1.5 Illustrating δN for a Sinusoidally Modulated Carrier

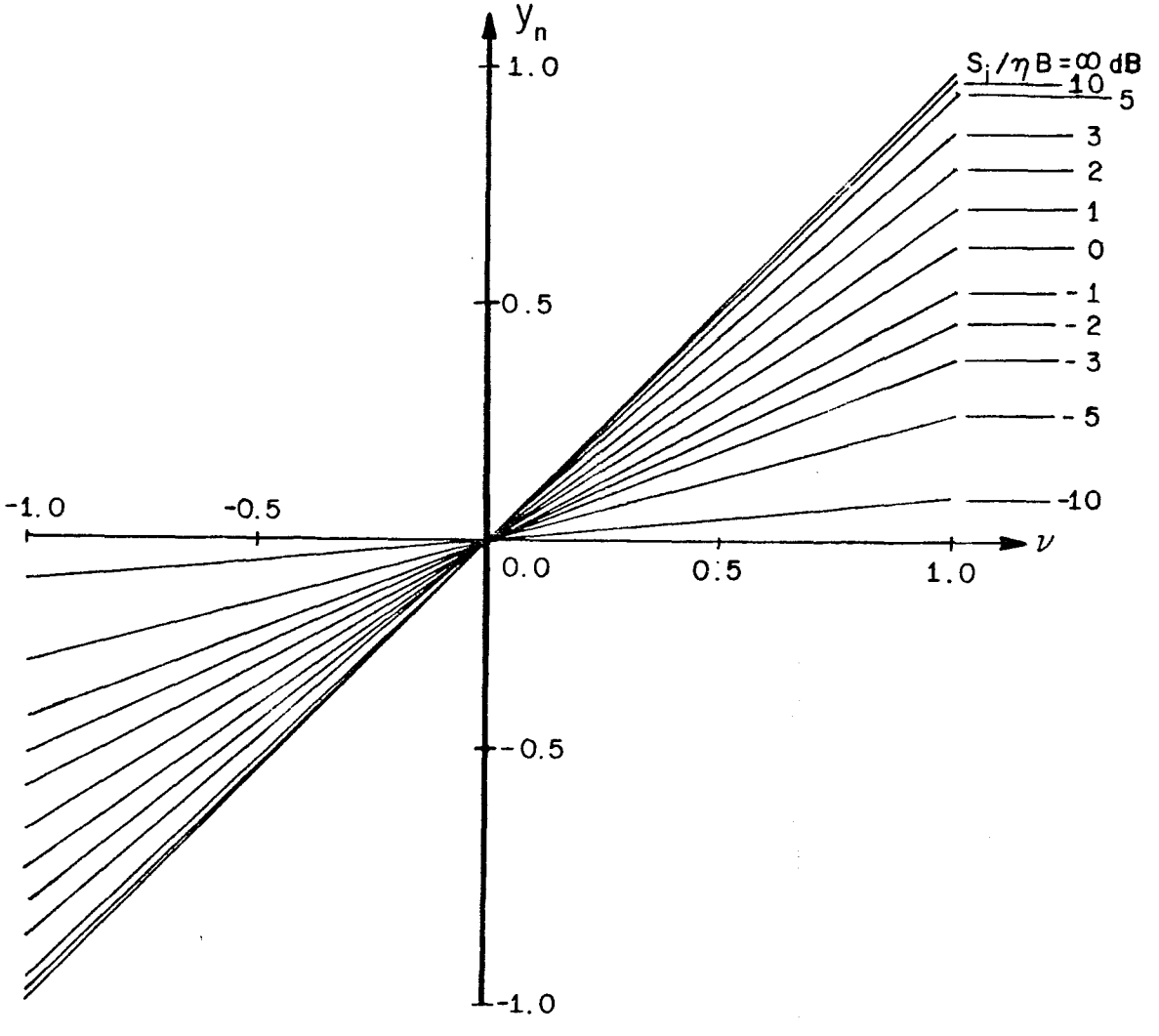

Figure 3.2.1 Normalized Integrator Output vs. Normalized Frequency Offset

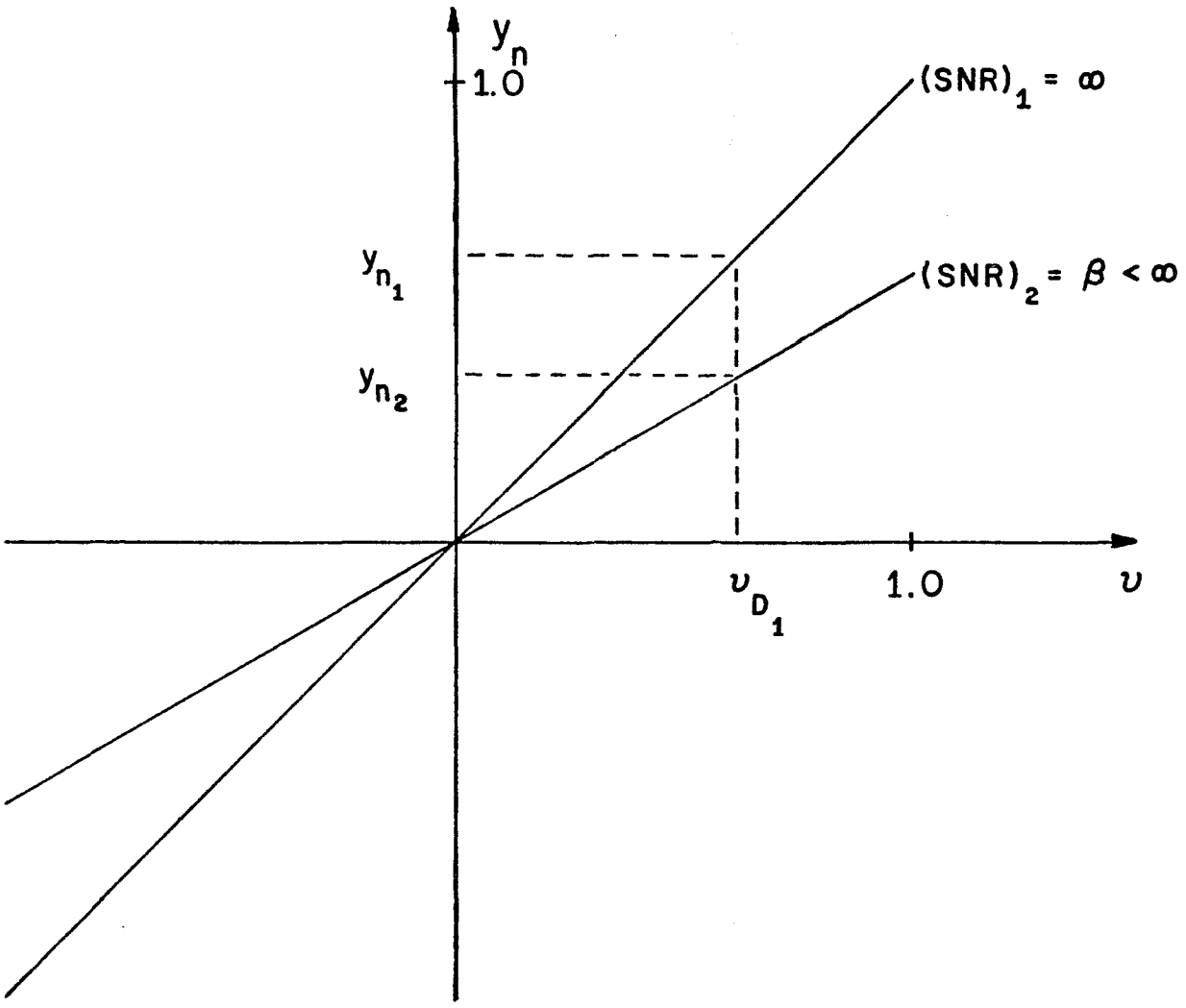

Figure 3.2.2 Illustrating Two Particular Calibration Curves

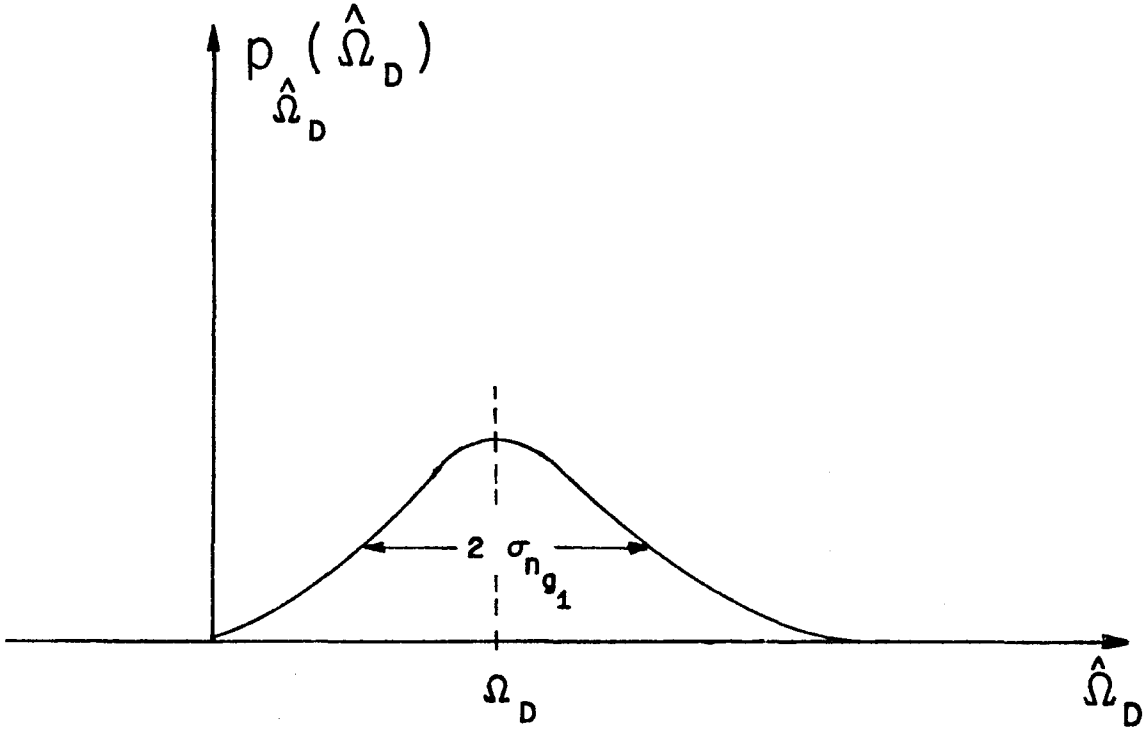

Figure 3.3.1 Distribution of the Frequency Estimate, $\hat{\Omega}_D$ – High SNR

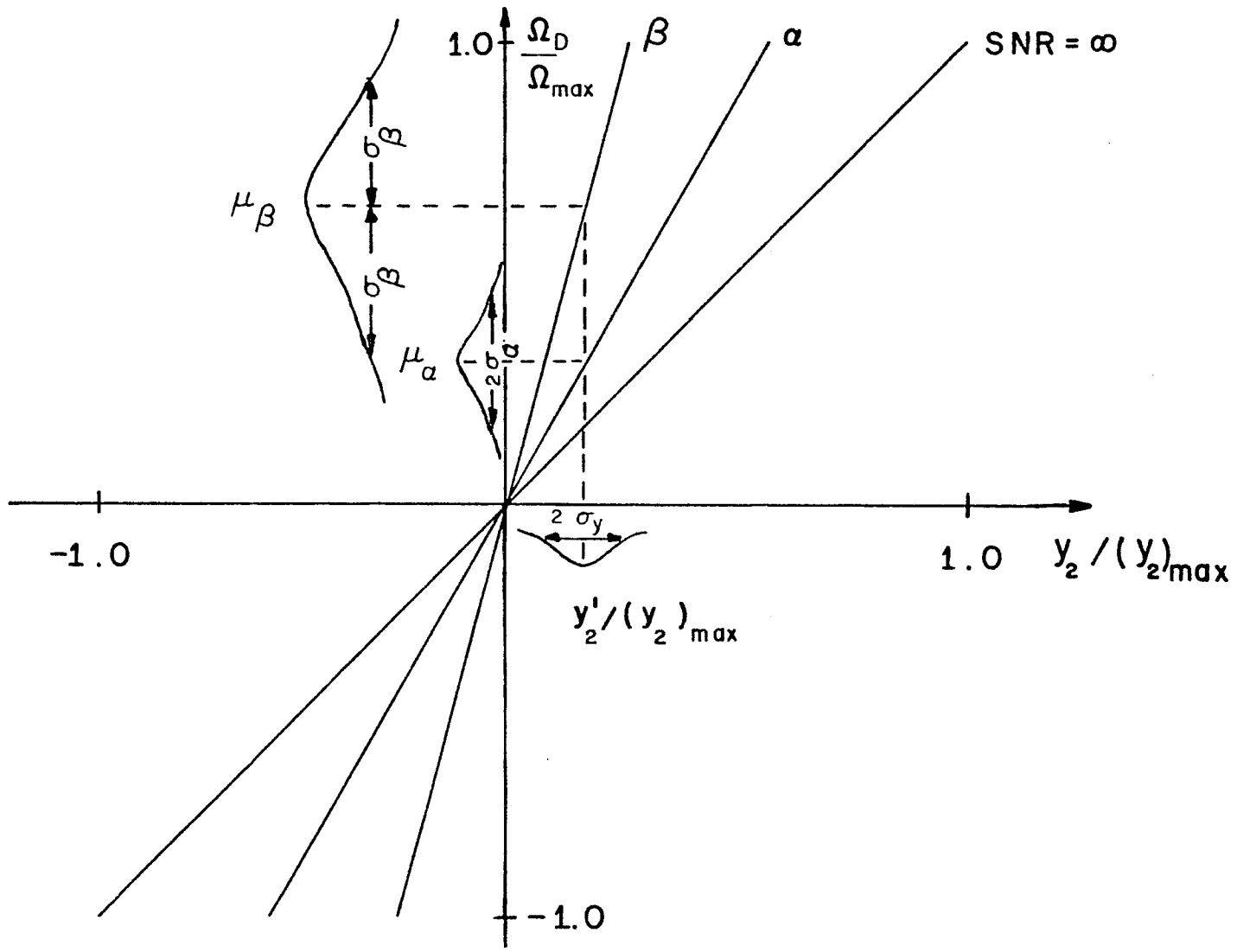

Figure 3.3.2 Illustration of the Uncertainty Bandwidth

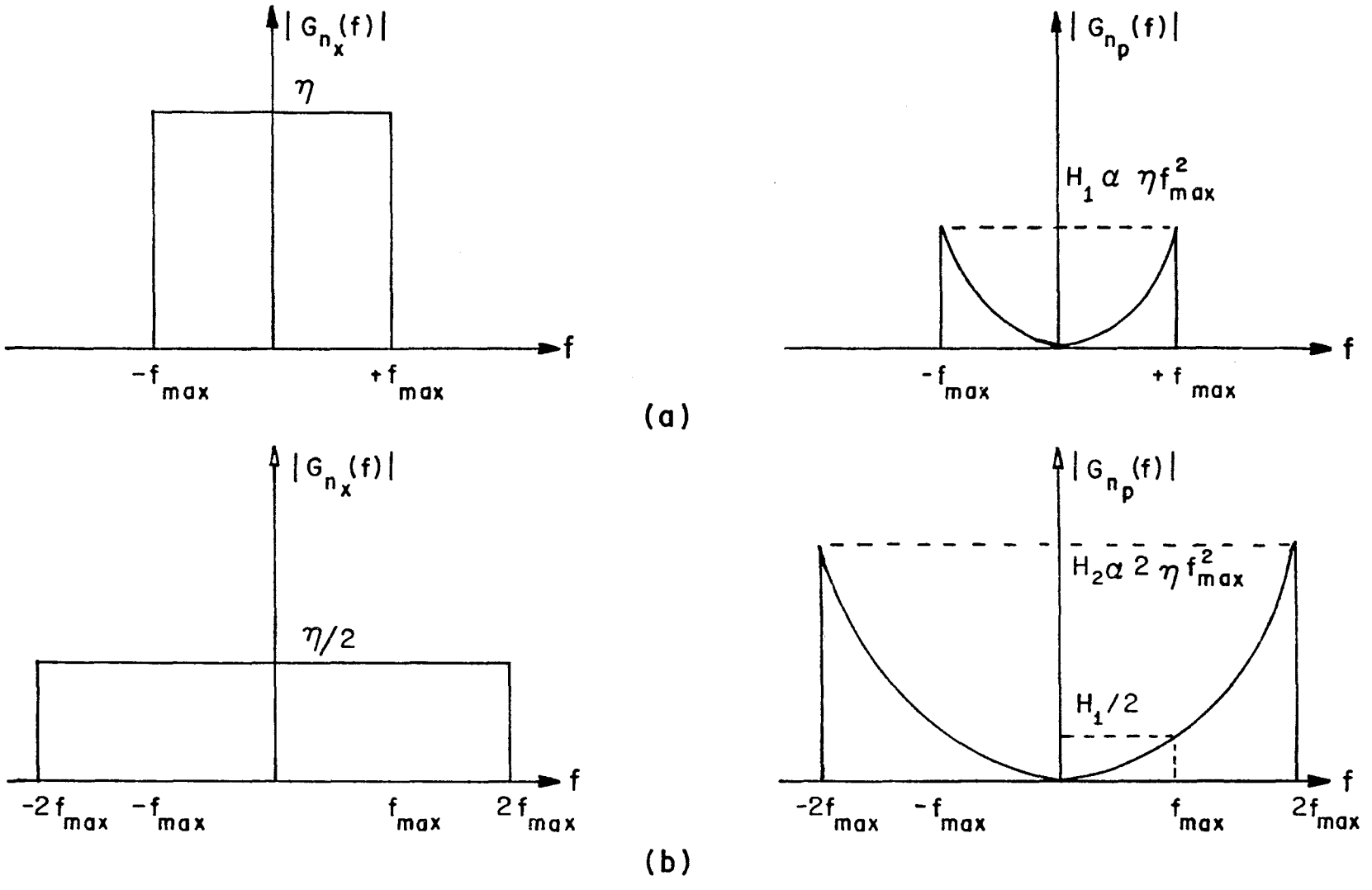

Figure 3.3.3 The Associated Power Density Spectra of $n_x(t)$ and $n_p(t)$ (a) $\Delta f = 0$ (b) $\Delta f = f_{max}$

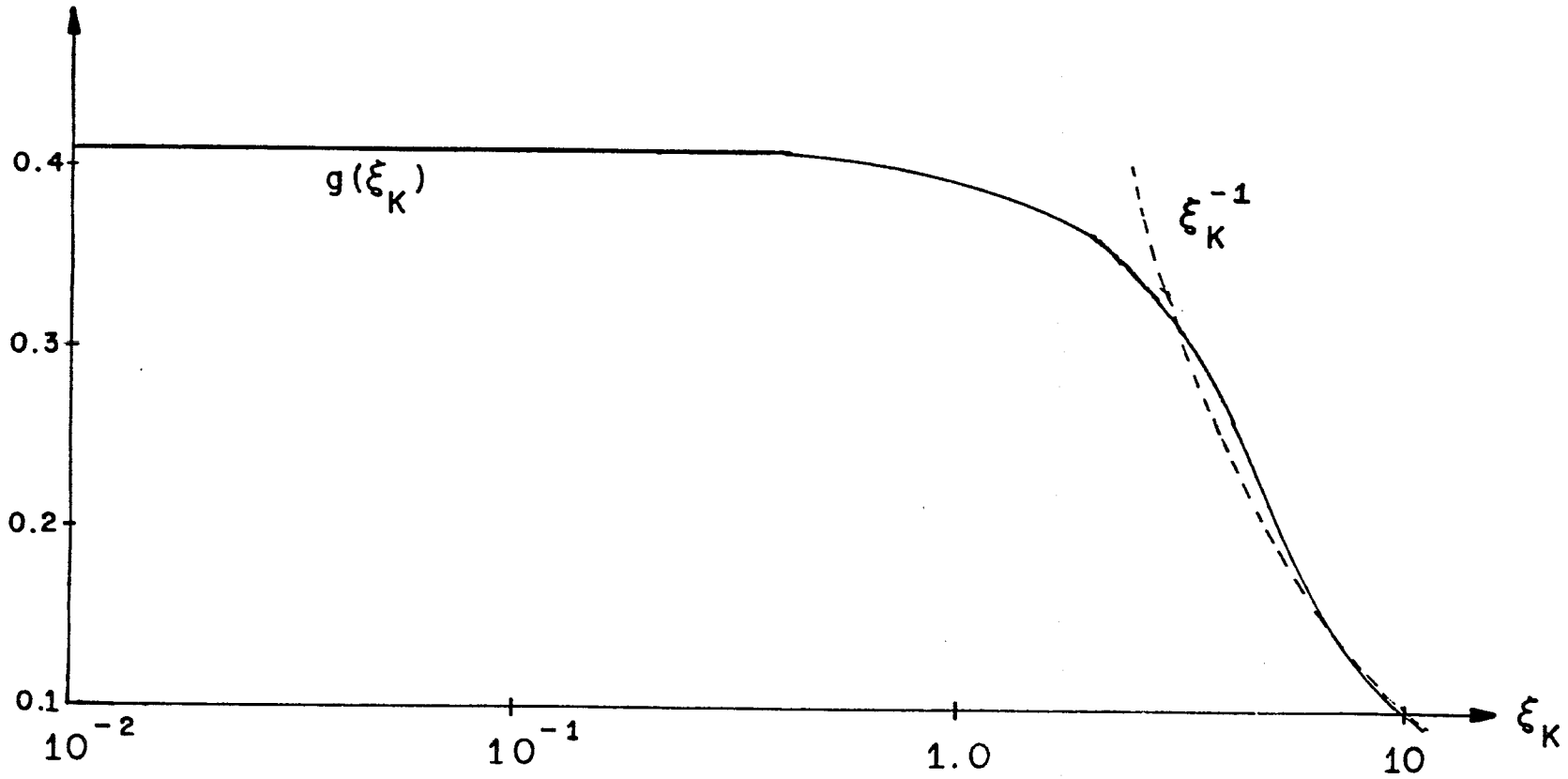

Figure 3.3.4 $g(\xi_K)$ and ξ_K^{-1} vs. ξ_K

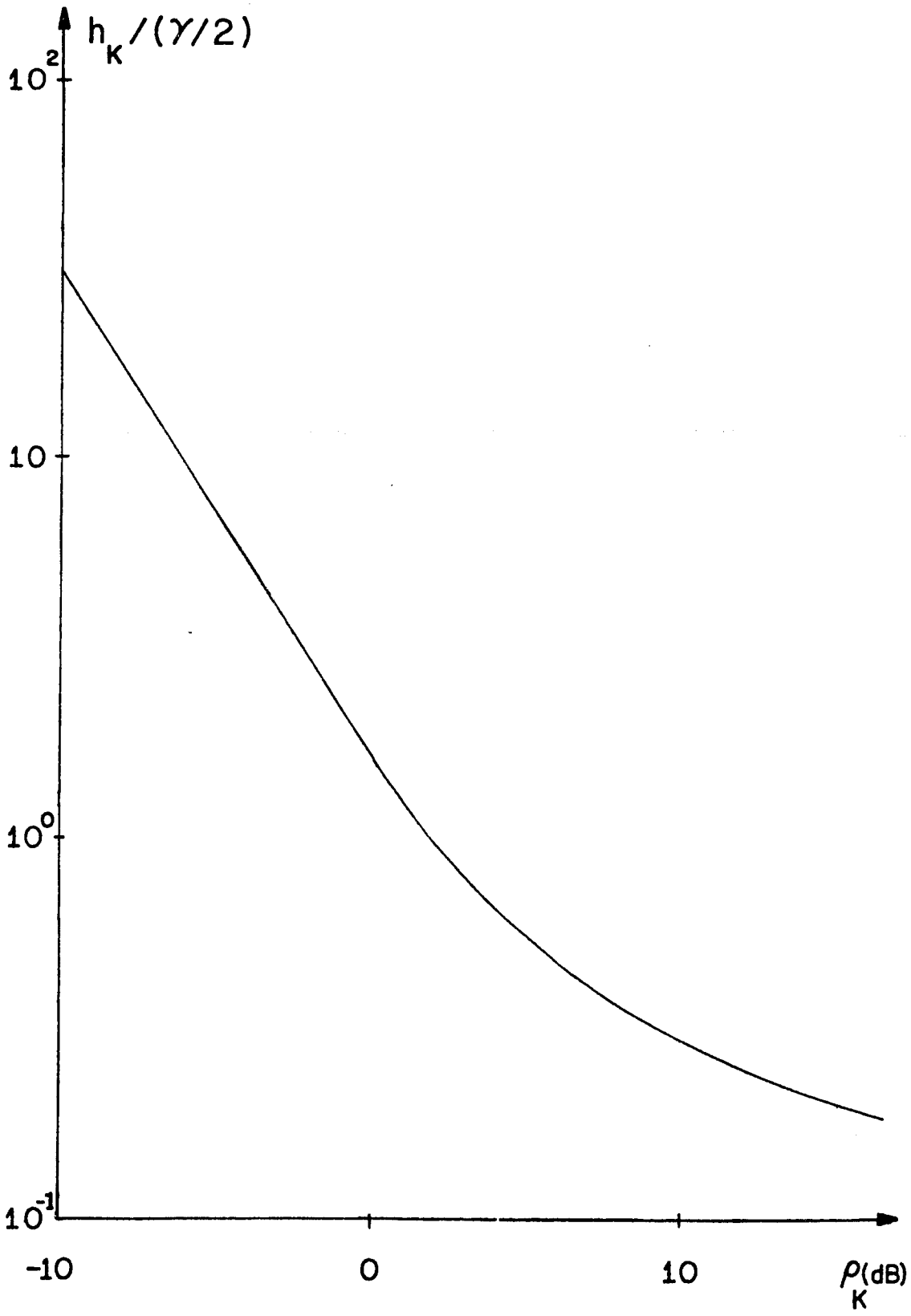

Figure 3.3.5 $h_K/(\gamma/2)$ vs. ρ_K

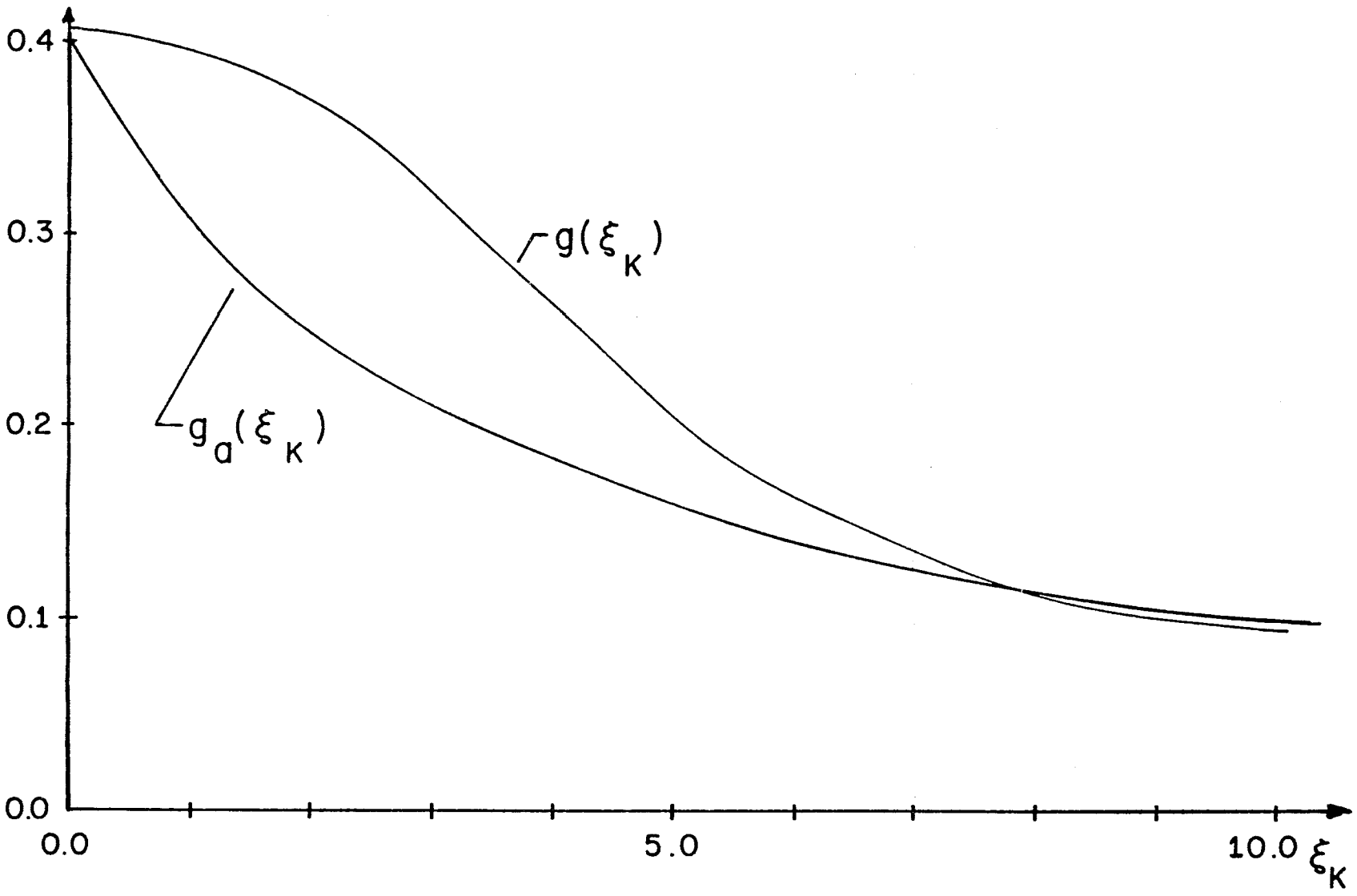

Figure 3.3.6 The Functions $g(\xi_K)$ and $g_a(\xi_K)$ vs. ξ_K

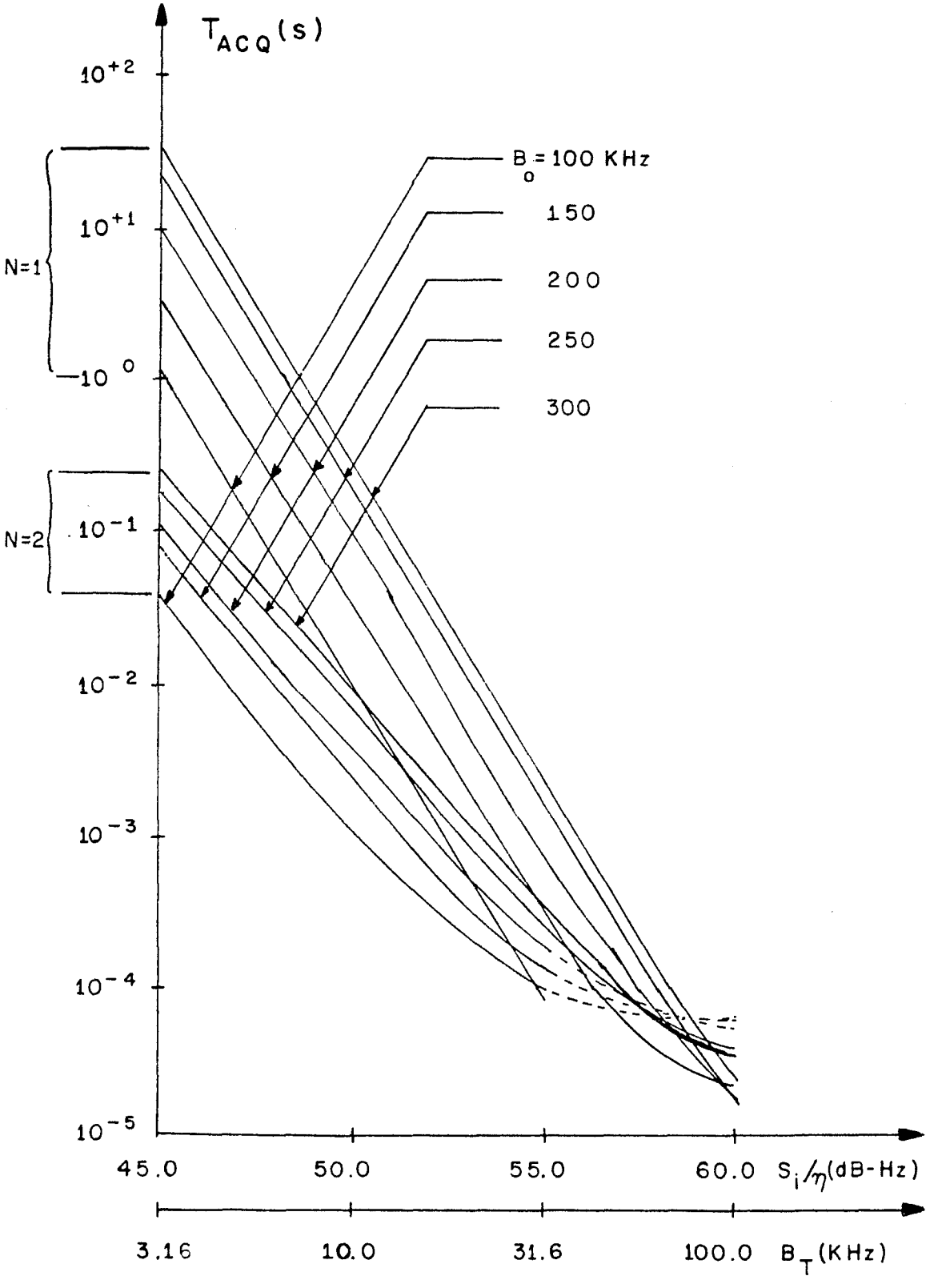

Figure 3.4.1.1 Acquisition Time vs. SNDR and B_T for Spike Region Only - One and Two Iterations

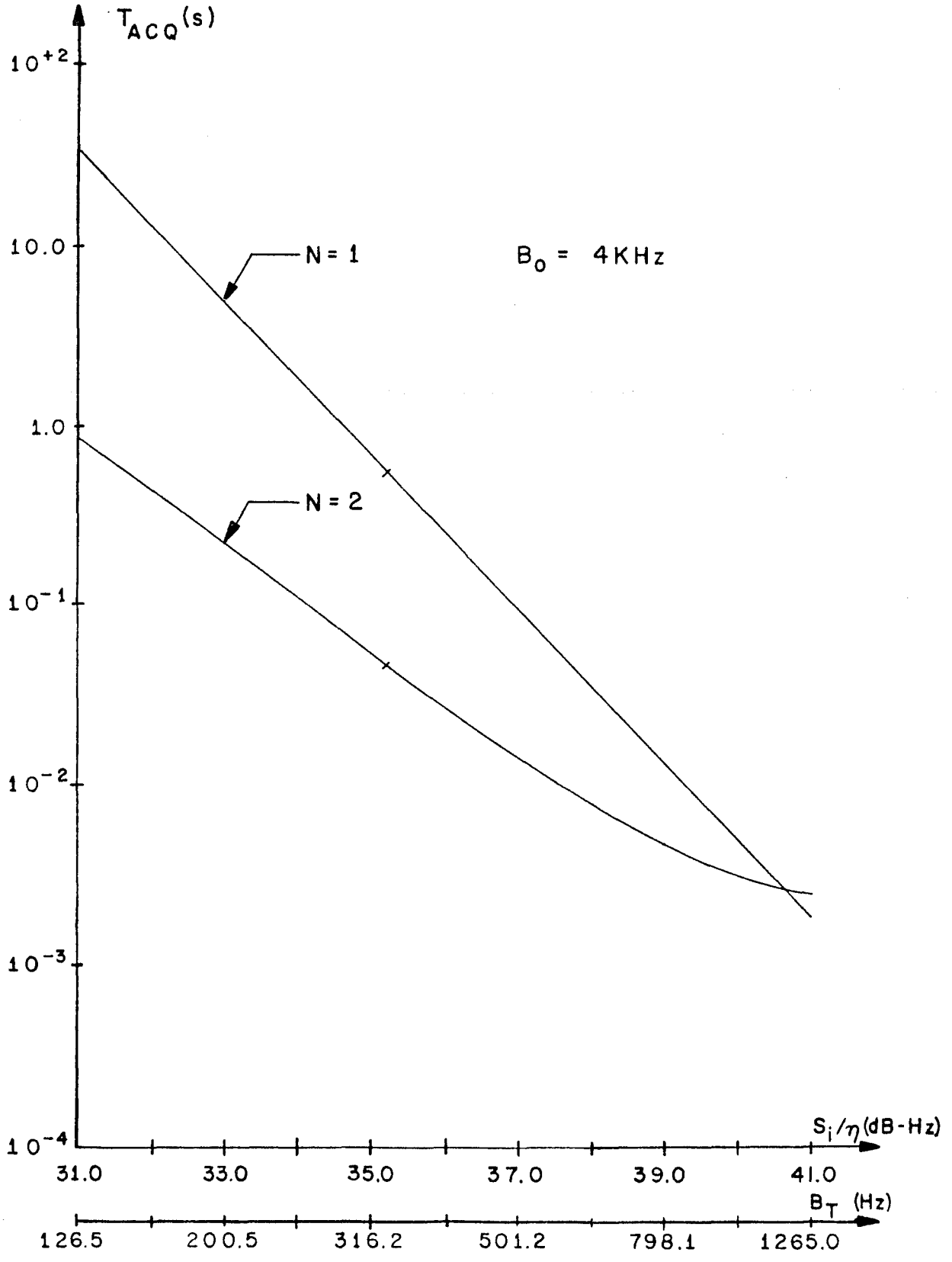

Figure 3.4.1.2 Acquisition Time vs. SNDR and B_T - for Spike Region Only - One and Two Iterations

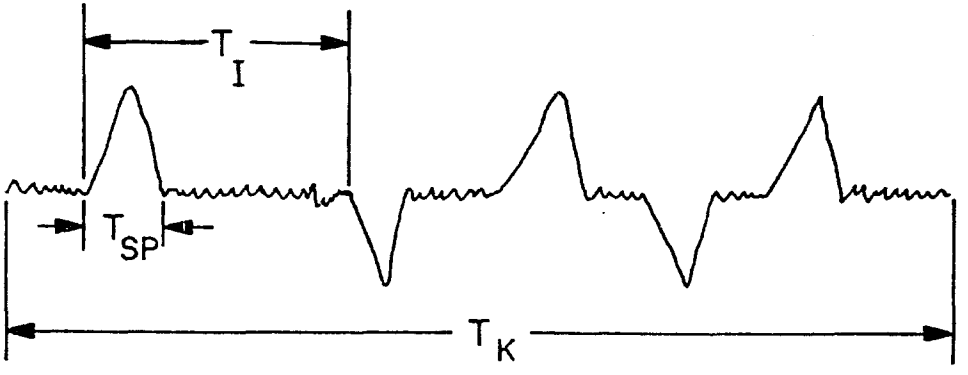

Figure 3.4.1.3 Relationship of T_K, T_I, and T_{SP}

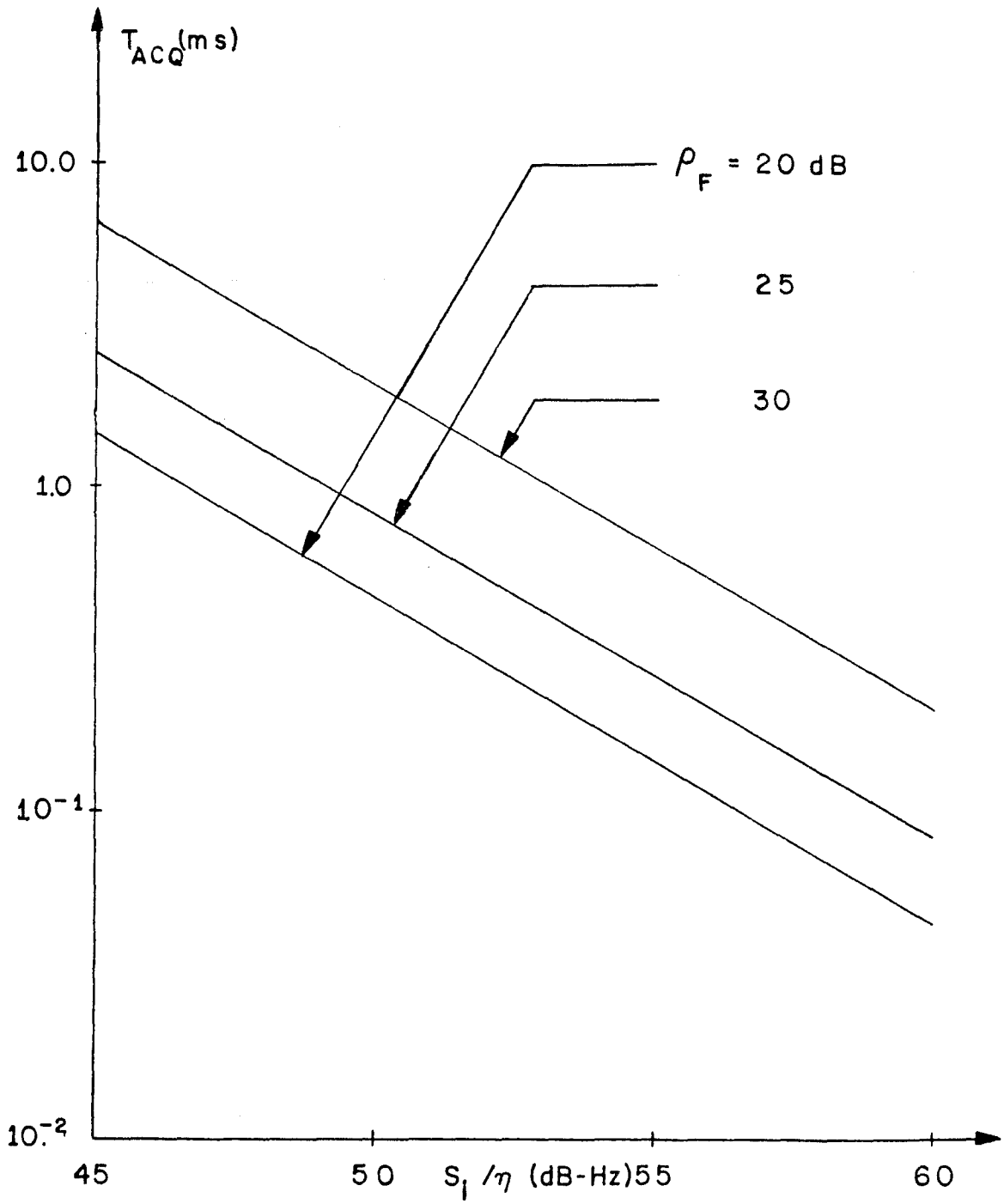

Figure 3.4.1.4 Acquisition Time for High SNR Region, B_o= [100 - 300]KHz

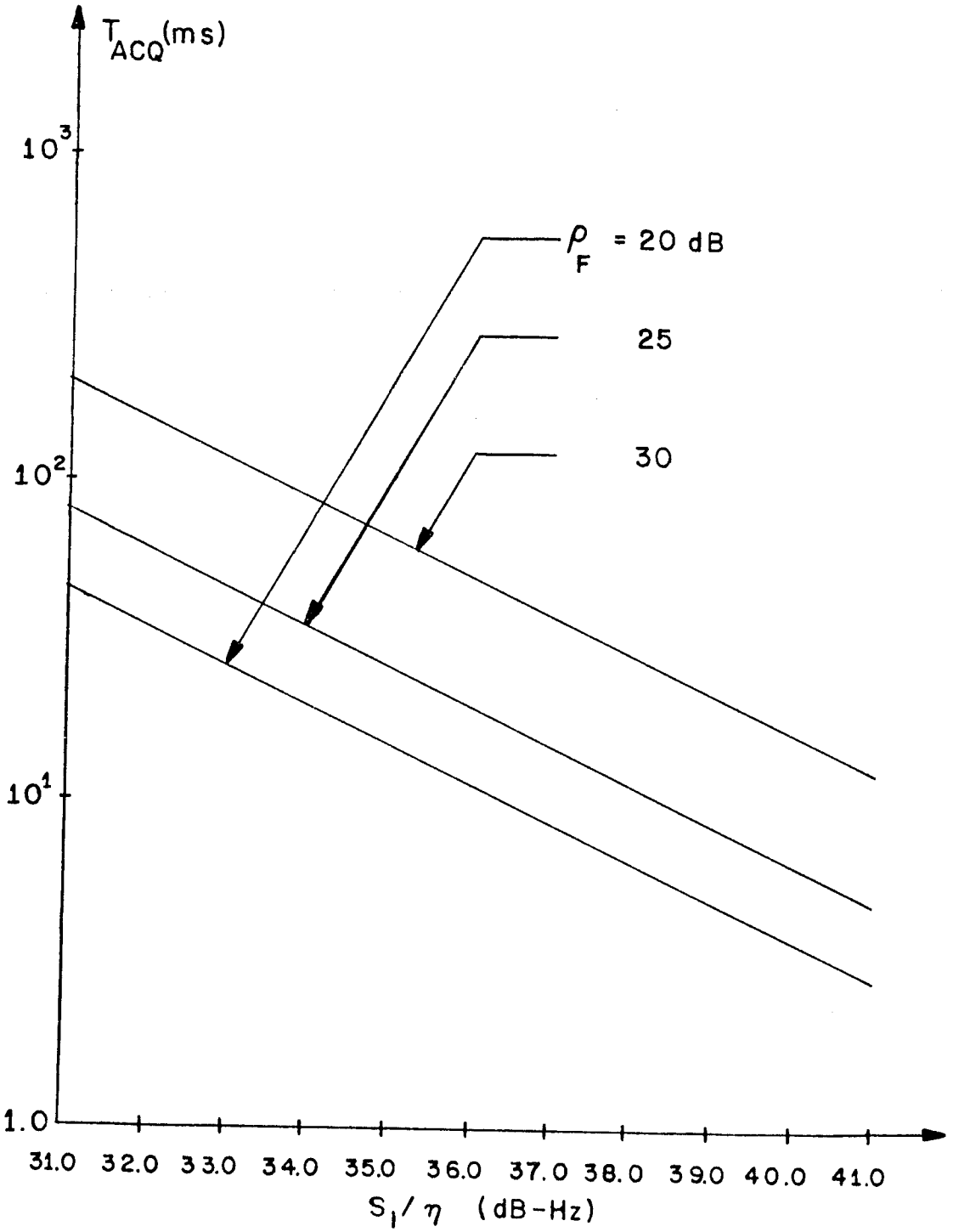

Figure 3.4.1.5 Acquisition Time for High SNR Region, B = 4KHz

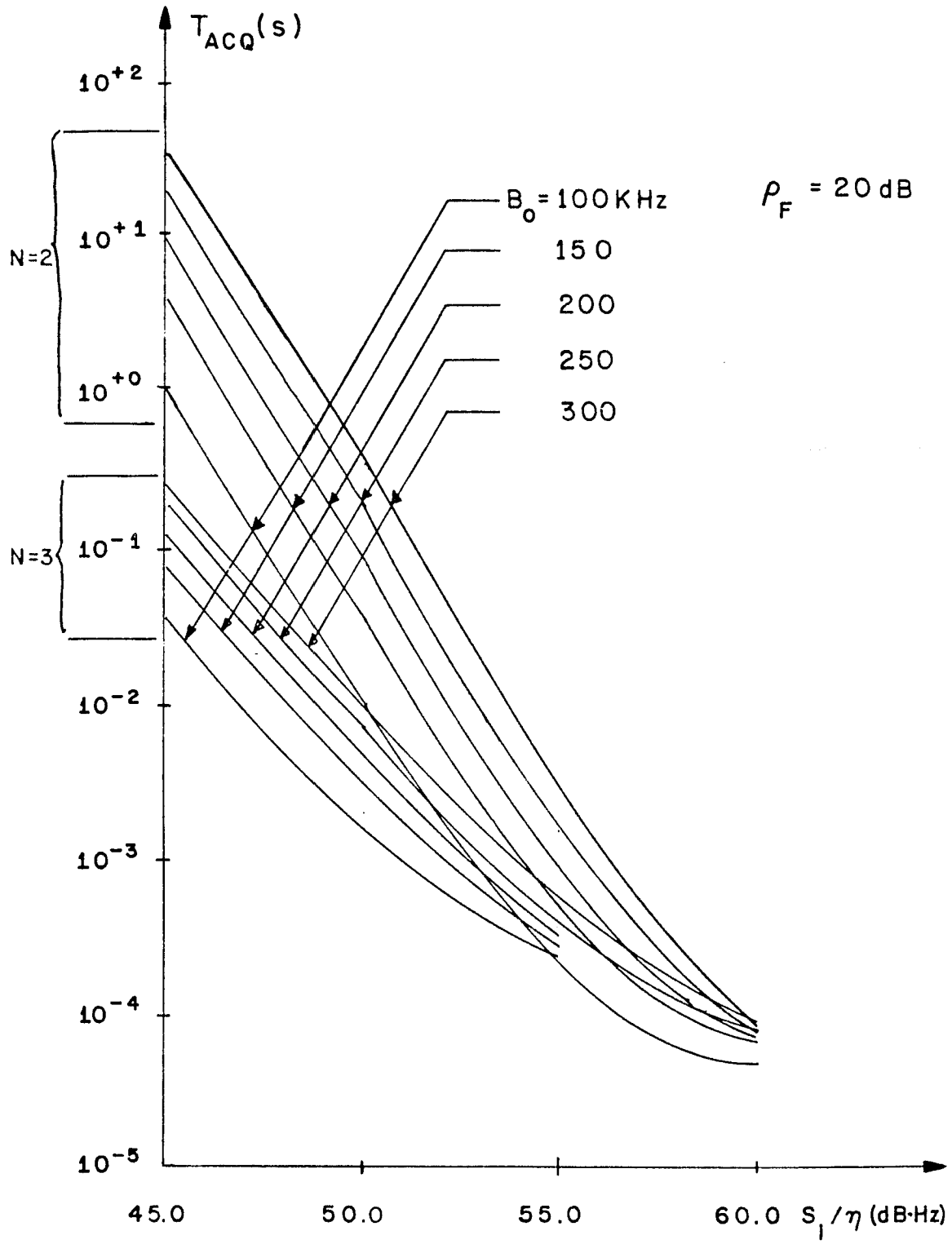

Figure 3.4.1.6a Total Acquisition Time

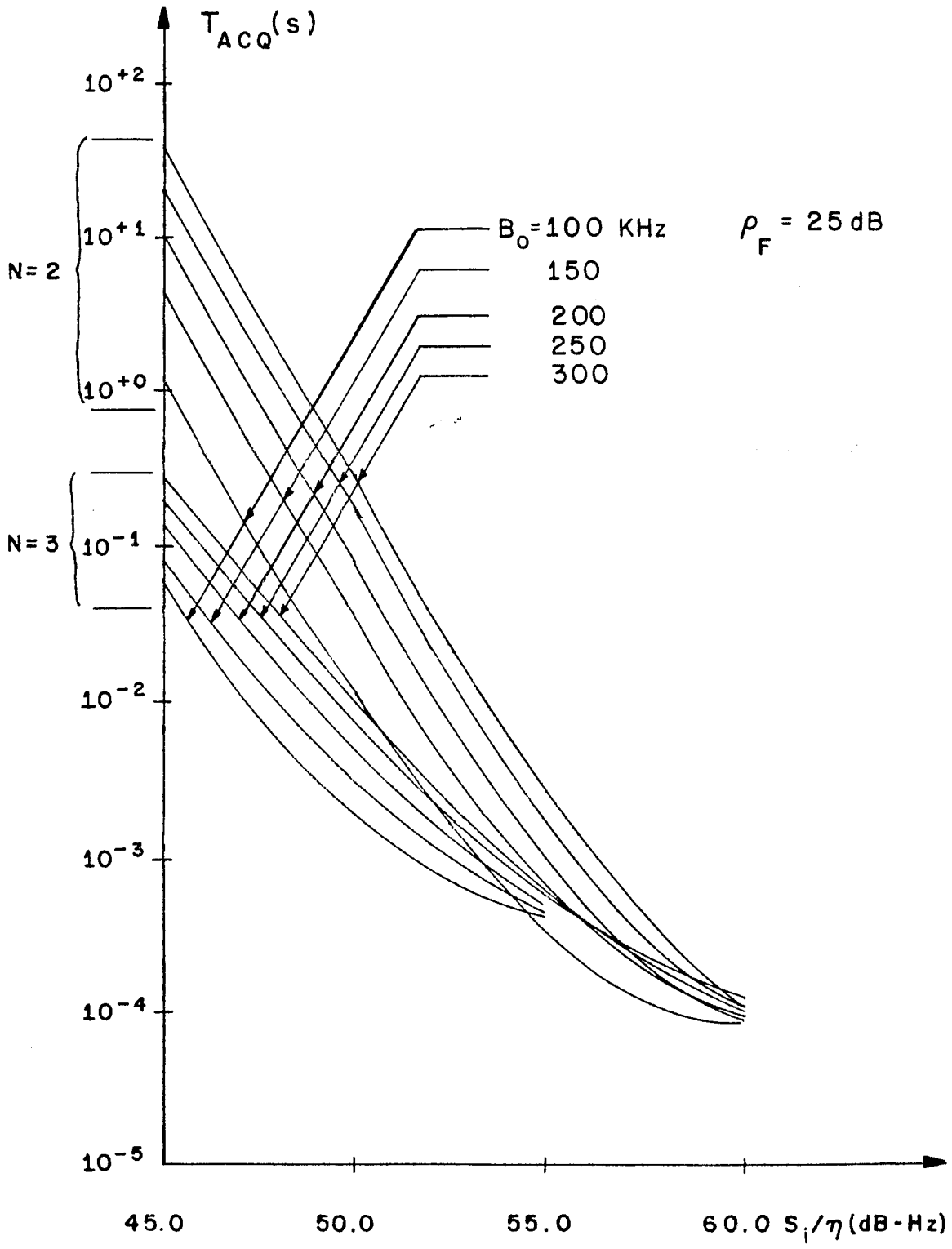

Figure 3.4.1.6b Total Acquisition Time

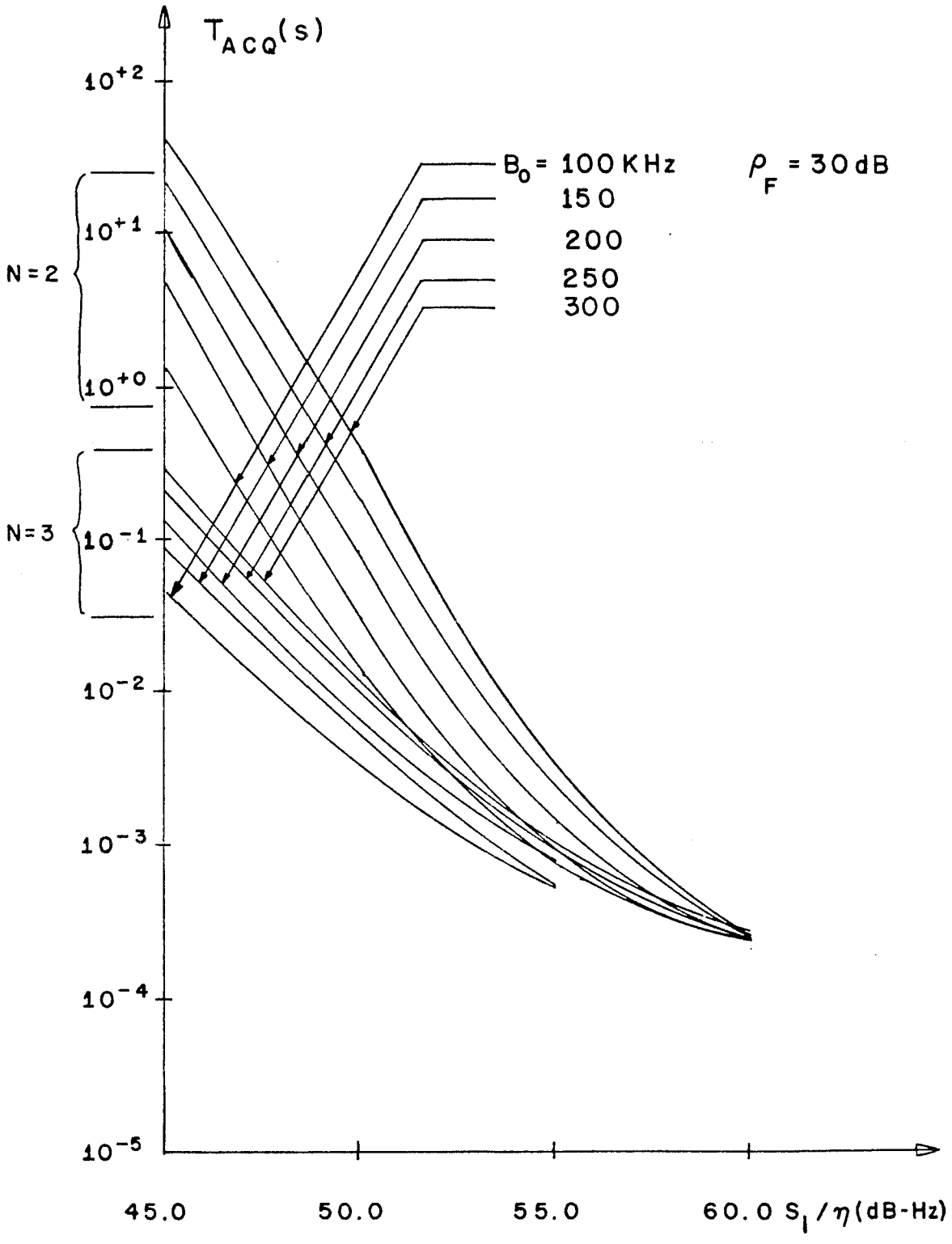

Figure 3.4.1.6c Total Acquisition Time

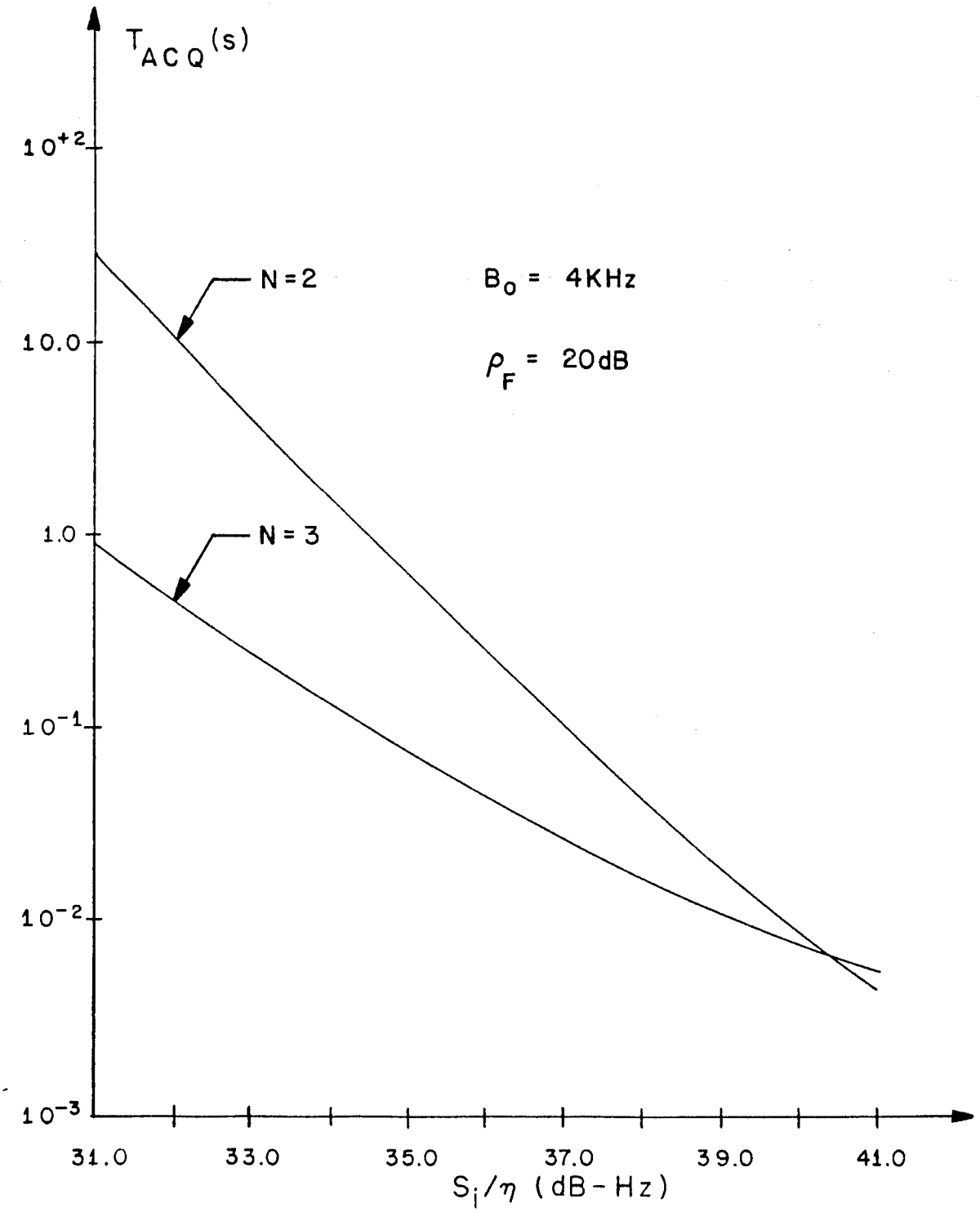

Figure 3.4.1.7a Total Acquisition Time

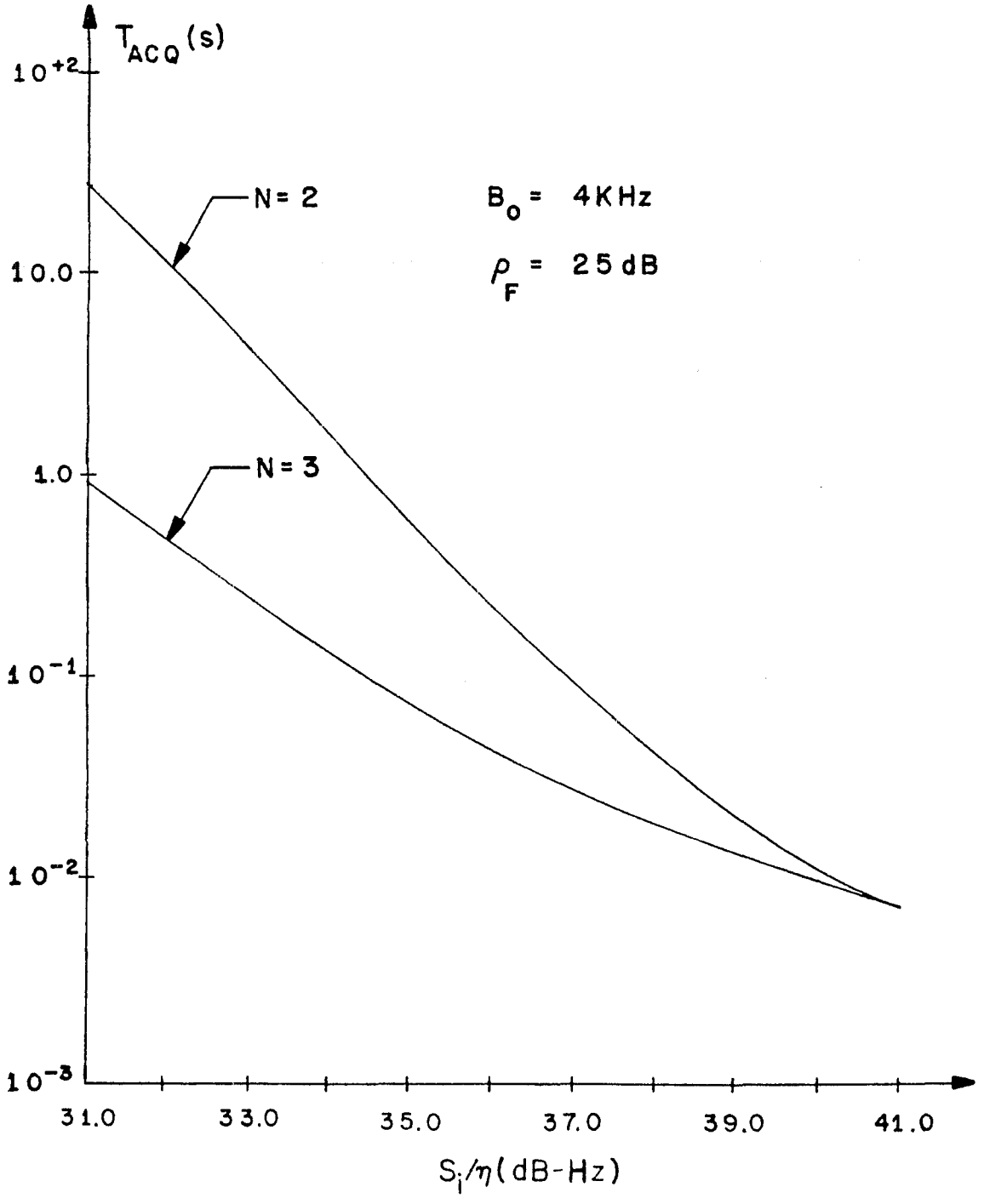

Figure 3.4.1.7b Total Acquisition Time

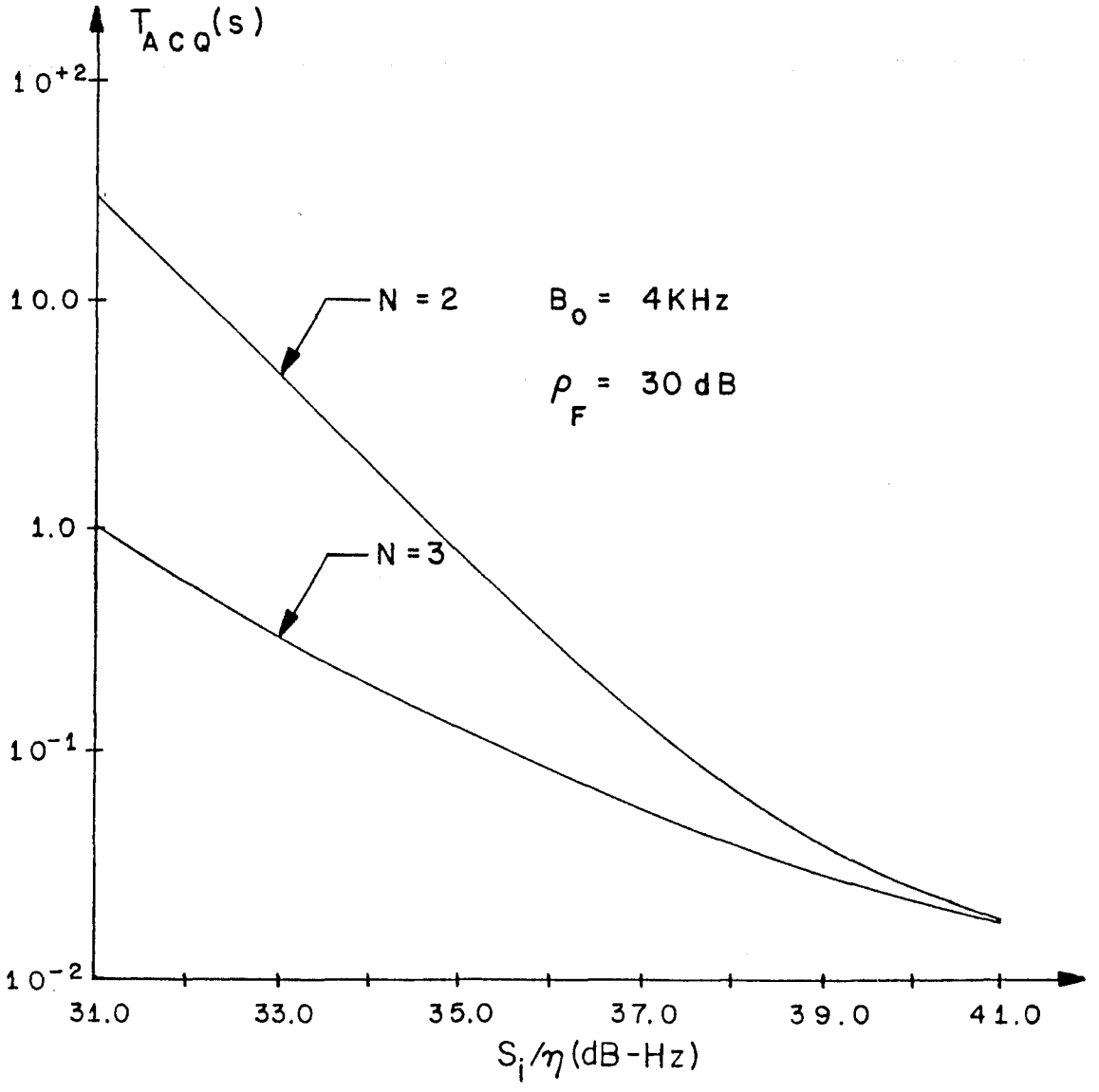

Figure 3.4.1.7c Total Acquisition Time

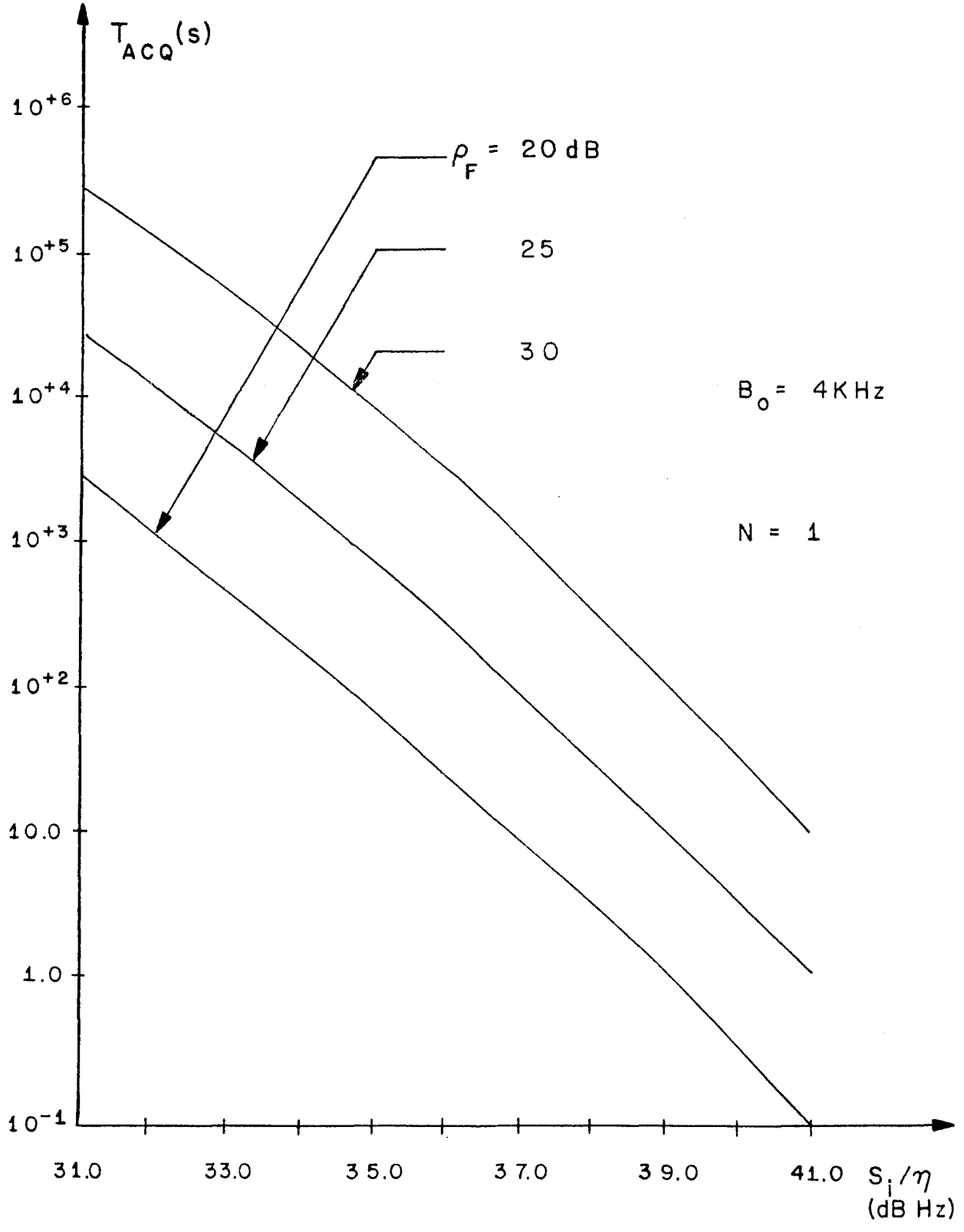

Figure 3.4.1.8 Total Acquisition Time, Directly from B_o to B_F

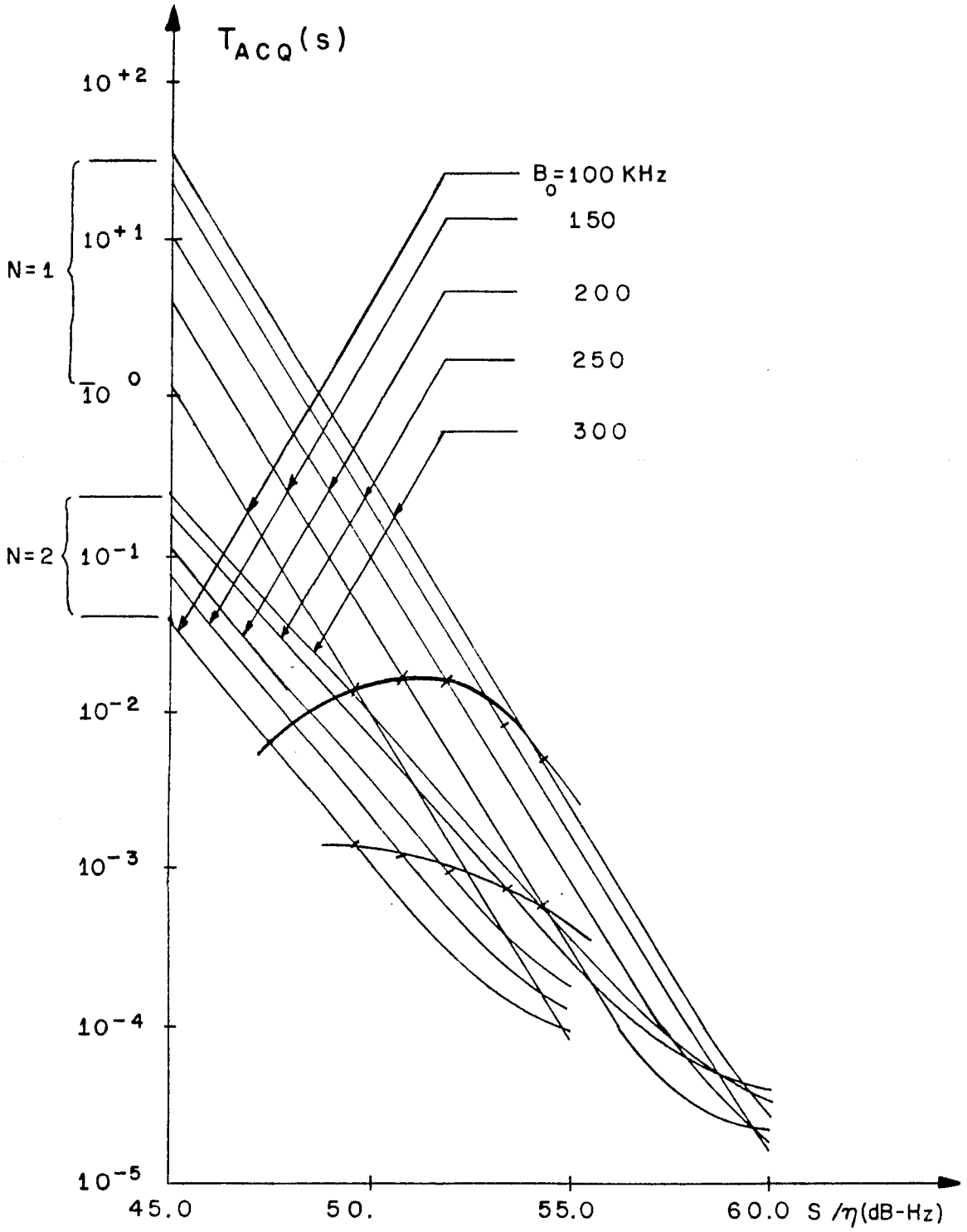

Figure 3.4.1.9 Illustrating $[T_{ACQ}(N=1) / T_{ACQ}(N=2)]=10$ in the Spike Region

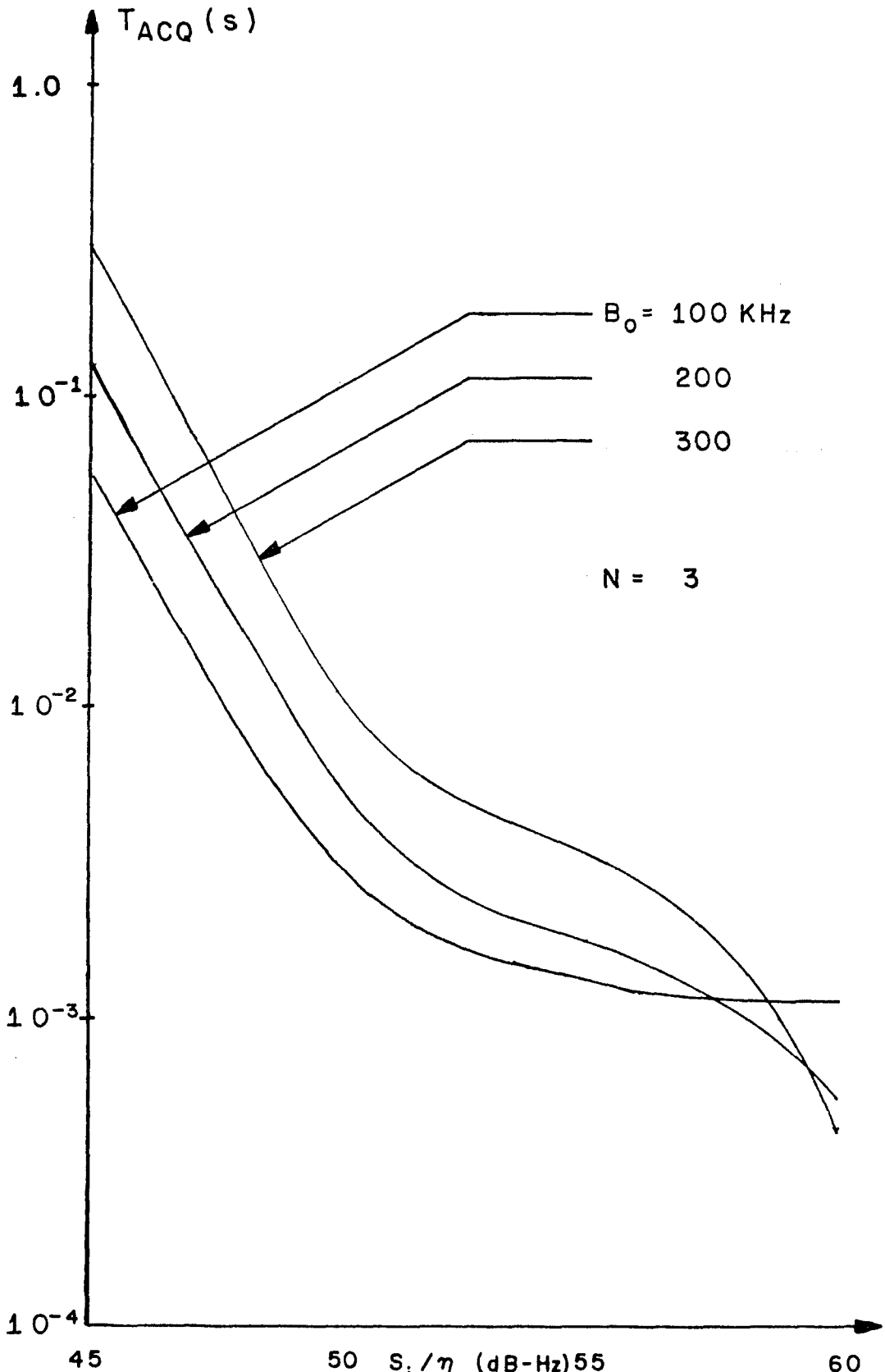

Figure 3.4.1.10 Total Acquisition Time for $B_F/B_o = 10^{-3}$

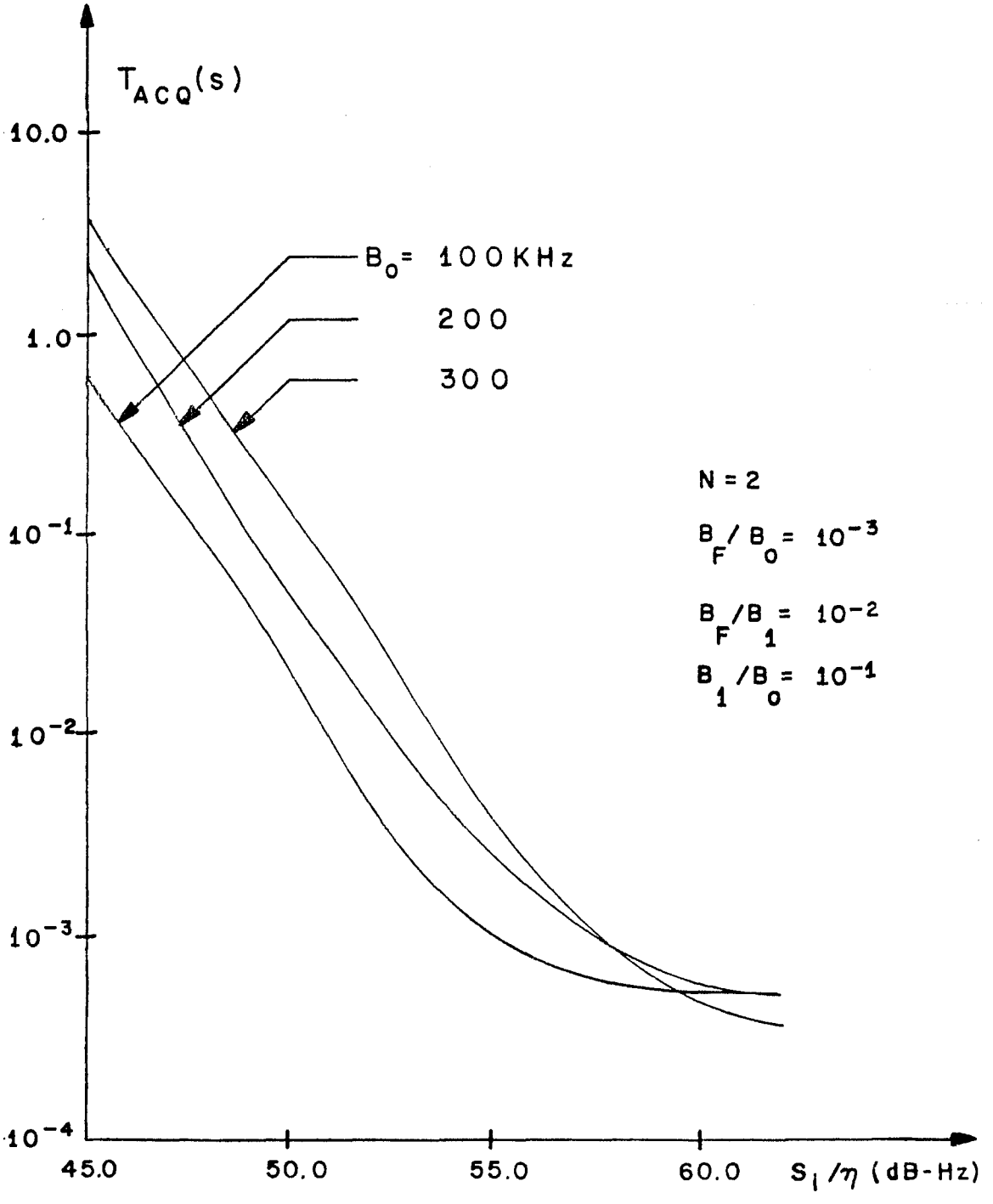

Figure 3.4.2.1 Total Acquisition Time for Constant Bandwidth Reduction

Chapter 4

THE HARDWARE SYSTEM

In this chapter we discuss the hardware system implementation of the PLL acquisition aided structure described in the previous chapters. The integration-sample and hold process is accomplished using a special purpose microprocessor which was built by Dr. Tuvia Apelewicz [1]. This microprocessor was intended for voice processing but can be programmed to perform other functions due to its versatile software capabilities. Such was the case in our application.

The simulation is only a partial one which traverses the spike region using only one iteration. We chose an initial uncertainty bandwidth of 4kHz and initial values of SNR equal to zero and three dB. The reasons for this are the limitations of the equipment available for use. In particular the filters we used exhibited a frequency response characteristic which, coupled with the constraints imposed by the microprocessor, did not afford us a large variety of bandwidths over which the system could operate. However, for the operating states considered we find that the system responds well within the bounds prescribed earlier.

Our original system was designed to operate in a closed loop configuration with a nominal input carrier frequency of

fc = 40kHz and a VCO frequency of f_v = 30kHz. The difference frequency would have been fa = f_c - fv = 10kHz and so m = fa/B_o = 2.5. However, due to restrictions on the noise signal spectrum, which will be examined shortly, we needed to operate open loop. We then chose a signal frequency equal to the value of the difference frequency for the closed loop case. Thus the signal frequency was 10kHz. We also arbitrarily set the VCO frequency at 10kHz. This setting provided a reasonably sensitive VCO gain amenable to the resolution of our system.

We opened the loop of our test system at the phase detector input simply by not connecting the VCO output signal to it. After we calibrated the system, we observed its response in the acquisition aided mode for different values of SNR and frequency offsets. We also varied the integration time keeping the gain-time factor constant.

To determine the frequency acquisition properties of the system we recorded the VCO frequency for the various offset frequencies and signal-to-noise ratios. The system was said to have acquired if the output frequency fell within the new prescribed bandwidth. We repeated this process many times and recorded each value of the output frequency.

4.1 The Hardware Simulation

The system used in the simulation, corresponding to the system of Fig. 3.1.1, is shown in Fig. 4.1.1 in block diagram form. The schematic diagrams of the adder, limiters and

amplifier stages are shown in Fig. 4.1.2. The GR-1142A had been modified by disconnecting the 5kHz RC filter at its output terminals. This was needed to produce a rectangular pulse at the input to limiter 2 and to avoid loading problems at the discriminator output. The operational amplifiers (op-amps) used were ones that were generally available. In most applications a load resistor configuration was needed for stability and linearity.

The signal and noise generators were coupled to the adder through attenuators which were used to change the signal-to-noise ratio at the input to the bandpass filter. This arrangement maintained the proper loading effects during this adjustment. The HP 355D has a range of 0 to 120 dB attenuation in 10 dB steps while the HP 355C has a range of 0 to 12 dB in 1 dB steps. In addition the noise is filtered by a 40kHz low pass filter (Krohn-Hite model 3202) to prevent saturation in the op-amp adder while allowing appreciable noise power into the system for proper operation. Without this filter we found we had to attenuate both signal and noise by an additional 10 dB producing signals too low in power to allow meaningful results.

Figure 4.1.3 shows the waveshape and spectrum of the noise source before and after the 40kHz filter. The pictures of the spectrum were taken as follows. The spectrum was displayed on an HP 140S Spectrum Analyzer display section with a 8553L and 8552A RF and IF section respectively. The vertical output was displayed on a Textronix 549 storage oscilloscope with the horizontal output driven by the spectrum analyzer

sweep circuit.

The spectrum is flat or white for $0 \leq f \leq 70$kHz at the filter input and for $0 \leq f \leq 30$kHz at the filter output. We also see that the noise is down approximately 6 dB at f = 40kHz and 12 dB at f = 45kHz. Thus the frequency rolloff is approximately 24 dB/octave. This is typical of Krohn-Hite filters which are usually 4-pole devices.

Since the spectrum of the noise was white for frequencies only up to 30kHz we did not perform the experimental analysis with the loop closed. In order to operate closed loop we would have needed the noise to be white for frequencies well above 40kHz. Since this was not the case the Clarke-Hess multiplier served only as a buffer amplifier stage. The second input to the multiplier was its own internal d.c. offset voltage.

The two cascaded Krohn-Hite filters were used as the input bandpass filter. We cascaded two stages to improve the frequency response of the filter. However we found that the two stage filter afforded us little improvement over that of the one stage filter. The center frequency of the bandpass filter was set at f_c = 10kHz. The filter passband was set by the filter controls. The lowerside was set at 8kHz while the upperside was set at 12kHz. The frequency response characteristic of the filter is shown in Fig. 4.1.4. It can be seen from the curve that the

peak value of the response occurs at f = 9kHz. The rolloff for frequencies less than 9kHz it is approximately 28 dB/ octave. The lower and upper 3 dB points are 7.0kHz and 12.0kHz respectively. This makes the 3-dB bandwidth 5kHz instead of 4kHz; however, this was the most amenable situation we could achieve. The effective center of band was approximately 9.5kHz. This can be seen to be true if one computes the area under the curve of Fig. 4.1.4 and finds the frequency which divides this area in half. Figure 4.1.5 is a picture of the frequency response of the bandpass filter over the range $0 \leq f \leq 20$kHz. Comparison with Fig. 4.1.4 shows close agreement over the appropriate ranges.

However, the asymmetry of the filter proved to be troublesome since noise components an equal distance away from the center frequency were attenuated differently. This caused an imbalance in the production of spikes especially for offset frequencies (see Section 4.2). Some typical waveforms at the output of the bandpass filter are shown in Fig. 4.1.6. Their associated spectra are shown in Fig. 4.1.7. One can observe the effect of noise on the signal from these figures.

Notice also from Fig. 4.1.7(a) that signal harmonics appear at multiples of the fundamental, that is at 18kHz and 27kHz even though the source is a sine wave. However, this effect does not produce any problems because

the limiter due to its operation, will create harmonics anyway. From Fig. 4.1.7(b) through (e) we notice another phenomena. Although the signal is buried deeper in noise as the SNR decreases and is almost indistinct from noise at SNR = -10 dB, our acquisition system is able to discern its presence. But also notice at the harmonics the noise level increases. This is especially visible in Fig. 4.1.7 (b) decreasing to a lesser degree in (e). (In fact, since the BPF characteristic is approximately flat for frequencies greater than 20kHz the noise in (e) appears almost white for f > 20kHz although we see from (b) to (d) that this is not so.) Thus this effect adds inband noise to the system. Figure 4.1.7(f) shows the noise spectrum with no signal present. Note the flat response in the stopband.

Figure 4.1.8 shows an expanded view of the frequency spectrum of the signal plus noise in the passband of the BPF. Note in Fig. 4.1.8(a) that even for ρ = 0 dB the signal is clearly defined. However in (b) we see that for ρ = -10 dB that the signal is imbedded in noise and is barely distinguishable.

The first limiter was used to shape the input to the FMD. The FMD was a zero crossing type discriminator which produced a constant width pulse of varying period according to the frequency of the input. The d.c. content of this waveform corresponds to the input signal fequency. The range of these pulses was from zero volts to thirty-

five volts negative. The reason for such a large value was that the FMD was a vacuum tube device capable of producing large excursions.

The second limiter reduced this voltage back to the d.c. power supply level of ±6 volts. To adjust the d.c. value at the output of the second limiter we added an offset adjustment as illustrated in Fig. 4.1.2(d). This provided a coarse adjustment for the final d.c. output prior to the microprocessor analog input. The potentiometer used for this purpose was a 10-turn Allen Bradley heliopot.

As can be seen from Figs. 4.1.1 and 4.1.2 this limiter has two outputs. The output labeled "RC Buffer In" in Fig. 4.1.2(d) was applied to the circuit fo Fig. 4.1.2(f). This configuration enabled us to generate the calibration curves for the system. The generation of these curves will be discussed in the next section. The other output, labeled "LPF 1 In" in Fig. 4.1.2(d), was used as an input to the first low pass filter. The voltage divider was used to reduce the input level to the low pass filter to approximately ±2 volts, the reason for this is that the maximum value for the total input voltage to the filter is ±4V. By using the above voltage division we provided a sufficient safety margin.

The bandwidth of this low pass filter (LPF 1) was set at approximately 1kHz for reasons which will be discussed later. To provide appropriate signal levels to the microprocessor (μP) we used the 2 stage buffer amplifier of Fig. 4.1.2(e). The second low pass filter of bandwidth

2kHz was needed to isolate the circuit from the A/D converter clock noise of the microprocessor (We note that the Krohn-Hite 3202 filter must be used at the output of the second limiter and buffer amplifier because it passes the d.c. component of the signal. The Krohn-Hite 3550 does not pass d.c. even in its low pass mode but passes instead frequencies above 0.2Hz).

The integration timing was accomplished as follows. The uP has an external system (A/D) clock and an internal operating clock. Each instruction in a program is carried out at the internal clock rate (approximately 170 nanoseconds per instruction) when the μP finishes its set of programmed instructions it waits in a final location (address 255) for the next A/D clock pulse. Upon the arrival of this pulse it returns to its starting location and again cycles through the program. This process is repeated until the integration period, T_k, which is stored in the μP, is completed. At this time the μP outputs the result to the D/A converter at its analog output. This is accomplished through a latch so that this value is maintained regardless of the input signal variations. Therefore the μP also performs the sample and hold operation. The integration period is set in a register (R_3) as an integer multiple of the A/D clock and this register is decremented at each clock pulse of the system clock. When this register content becomes zero, the the μP outputs the result of the integration to the D/A

converter in proper format, and then ceases its integration process by remaining in an infinite loop. (This loop is terminated manually by the operator in our experiment but this can be accomplished automatically for the next iteration by proper programming. For these applications a special purpose up would have to be built.)

The largest positive (negative) number the μP can store is +511 (-512). For the zero dB case we found with B_o = 4000 and B_1 = 400Hz resp. that the integration time was to be 258 milliseconds. Since 511 is approximately one-half of 258, the A/D clock had to be set at 2kHz. Since the spikes were a pulselike phenomenon, in order to obtain proper sampling we had to set the first low pass filter at 1kHz. This provided the Nyquist rate of sampling. We maintained this sampling rate for the three dB case for comparison purposes even though the integration times were considerably less; this would have allowed us to increase the smapling rate, f_s, but also it would have distorted the results.

The actual integration was performed in the following manner. The signal at the A/D input terminal is brought into the accumulator with the arrival of the clock pulse. The sign of the signal is determined and then the program branches to the appropriate loop. (We will describe the operation for only negative values; positive values go through a similar operation.) The next step is to add the input to the primary counter register (R_o) and test for overflow. If over-

flow occurs we increment the overflow register (R_1) and retain the amount by which the input and R_o differ in R_o. If no overflow occurs we keep the results in R_o. Next we determine if the timing register (R_3) is zero. If so we output the result. If not, we continue the accumulation, or integration. Of course before each run R_o, R_1, R_3 and all other pertinent registers are properly initialized. A complete flow chart and program are shown in Appendix 4.

We note here that we do not allow for processing time in either the zero or three dB case because it is small compared to the integration time (0.75 msec). Also, the μP has an offset null voltage; that is, with no input applied to the μP, if the program is run a d.c. voltage appears at the analog output. To remedy this we simply present an offset voltage at the μP input equal and apposite to μP output null voltage.

The output of the μP is connected to a 2 stage buffered attenuator. This is needed to set the output d.c. at the proper level for the VCO input and to establish the appropriate gain settings.

Some typical spike waveforms appearing at the output of the first LPF are shown in Figs. 4.1.9 and 4.1.10 at signal to noise ratios fo three and zero dB respectively. Note the d.c. level shift with changing frequency. The 10kHz signal is set for zero d.c. volts; this appears at the center of the screen (The system gains are of course

different here than at the μP input. These pictures serve to show the relative size of the spikes.)

From these pictures we make the following observations which bear out some of our previous comments. First note from Fig. 4.1.9(c) that even though we are supposedly at the center of the bandpass filter and we expect to see an equal number of positive and negative spikes we see mostly positive spikes. This suggests that the center of band is slightly higher than 10kHz. We will later see from the calibration curves that the center is higher at approximately 10.2kHz.

There are two reasons for this. One is filter and system drift. (These pictures were taken after the filter frequency response was measured.) The other reason is because the limiter threshold is not zero. Thus not all noise components are treated equally. So we find that the frequency response curve of Fig. 4.1.4 experiences a shift in its frequency center. This is because the frequency for which the filter area is halved would increase. To see this, picture a horizontal line across the response characteristic of Fig. 4.1.4 (or 5) at the zero dB point; due to the effect of the limiter all voltages below this point are reduced; this changes the response characteristic considerably as one can see by finding the frequency for equal area. Thus, this effect on the spikes can be expected.

Another point is that in Figs. 4.1.9 and 4.1.10 we see

that the decrease in SNR manifests itself in an increase in the number of spikes per second (λ) whereas the energy of each spike is constant although the widths and heights vary as we would expect. Figure 4.1.11 shows a comparison of the spike waveforms when offset an equal amount on either side of the center band. The SNR in this case is +4 dB. Note the similarity in the waveshapes even though the band-pass filter was asymmetrical. The variations of course are due in part to this characteristic of the filter.

Figure 4.1.12 is an amplified view of Fig. 4.1.9(c). Here we see more clearly the relative spike heights and widths. Notice the spike triplet one division to the left of center. A triplet occurs when noise causes the phasor, representing the instantaneous phase, to rotate to almost 180° (-180°), back through 0°, then to $-180^{\circ}(180^{\circ})$ and back again through the origin. It does not encircle the origin. Instead it causes a doublet in phase and so a triplet in frequency. As such it does not add significant noise energy to the system when compared to a spike [23]. (Note: all the spike waveforms shown in Figs. 4.1.9 to 4.1.12 are typical waveforms. Many patterns were viewed before the pictures were taken.)

4.2. Experimental Procedure and Results

In this section we describe the experimental procedure and the simulation results. The first item we must check

is the system calibration. To do this we divide the system in three sections and check each section independently. We define the system front end as all components prior to but not including the μP. The intermediate stage is the μP itself and the final stage consists of all components after the μP. We next calibrate the overall system and then perform the statistical study. In each case we periodically check the d.c. level for drift and the signal and noise power levels to maintain the proper SNR. The d.c. drift problem was a major one occurring very frequently. In a practical system one would need stable d.c. sources, potentiometers and circuit elements. Also, due to the filter rolloff the SNR would vary with varying input frequency. In practice this would be similar to a fading channel. Thus an extremely good filter is also necessary so that this problem is reduced.

4.2.1 System Calibration Procedure and Results

In calibrating the front end we first calibrate the FMD using the RC buffer amplifier. The RC time constant is $\tau = RC = 0.82$ second. It is sufficiently long to filter the random effects of the noise. The filter bandwidth of the RC filter is approximately $B = 1/\tau = 1.2$Hz. The following procedure is used to generate the FMD calibration curves.

We first calibrate the system with the only the signal and no noise present. The noise is attenuated to its minimum level (approximately 180 dB down from the signal). The

input signal is applied to the FM input through the RC buffer amplifier. (The rest of the acquisition circuit is connected to the system but is inoperative at this point since we maintain the μP in the stop mode.) The signal frequency is at the assumed center frequency of the band which by measurement we chose to be 9.89kHz. (This value was best in the sense that the number of positive and negative spikes produced at this frequency when observed over a long period of time was equal.) With this frequency we adjust the d.c. offset throughout the system so that the VCO output frequency is at the signal frequency. This is the system null point. We move the input signal frequency either 1kHz above or below the null point; after waiting a sufficient amount of time for the RC filter to settle ($5\tau \simeq 4.1$ sec) we adjust the gain so that the VCO moves to the proper frequency.

Of course we first observed that the sense was correct. That is if the input frequency increased so must the output frequency. Once this is done we check the gain adjustment on the opposite side of the nullpoint. (It was at this point we found that the op-amps behaved non-linearly to d.c. inputs if they did not have some appropriate loading at the output. However, once properly loaded they responded linearly.) Next we introduced the noise and set the signal and noise levels. In order not to overload the multiplier input we chose as our zero dB reference point to set the attenuators at 10 dB down. (The noise would have overloaded

the multiplier with the signal present even at 10 dB down without the 40kHz LPF present.) We next vary the frequency from 8 to 12kHz in 1kHz steps while keeping the SNR fixed. (For each new value of frequency we must check both the signal and noise level due to the attenuation properties of the filter. In this way we maintain the proper SNR.) After waiting for the RC filter to settle we record the frequency at the VCO output. The result of this procedure is shown in the calibration curves of Fig. 4.2.1. Note that the intersection point of these curves is at f = 10.2kHz. This frequency is the filter center frequency. The reason for the increase over the assumed center frequency is due to, as noted before, the effect of the asymmetry of the BPF, the limiter threshold and the harmonics of the input signal due to the generator. We note from these curves the close agreement with the theoretical values. The infinite SNR curve provides an almost perfect one-to-one relationship. The error is less than 0.2% for this curve. If we compare the slopes of the calibration curves with those of the theoretical curves we find that the percentage error is less than 1.6% as is shown in Table 4.2.1. Since the discriminator calibration is finished we remove the RC buffer stage from the system and connect the VCO input to the 2-stage attenuator.

As another check on the system center frequency we performed a spike count for a SNR of +5 dB and offset fre-

quencies of 0, ±1 and ±2kHz. The result of these spike counts is shown in Table 4.2.2. We notice that at "mid-band," that is at f = 10kHz we have more negative spikes than positive. This seems to indicate that the center should be somewhat lower than 10kHz as far as spike production was concerned. This is another example of filter drift that we found. Also we see that at 9 and 11kHz the spike production is about equal while at the outer limits of 8 and 12kHz there is a difference of about 1.3 to one. Although this is not a substantial difference (especially for only 20 trials) we decided for the statistical experiments to use ±1kHz offsets only.

We must now finish the adjustment of the front end section. The system is returned to the null point and we adjust the d.c. offsets so that the output of the second LPF cancels the inherent offset at the μP output. Again we displace the system from the null point, adjust the gain for proper d.c. levels and check the linearity for various signal frequencies. The microprocessor analog input has a dynamic range of approximately ±5 volts. We chose to use slightly less than half this voltage, that is about ±2.0 volts, to cover the range of input frequencies (8 to 12kHz). Since the gain of LPF 2 at d.c. is close to unity the voltage levels at its input were also about ±2.0 volts. This level is sufficiently within the dynamic range of the filter. Because B_o was 4kHz, these levels gave us a sensitivity for

the front end of 1 Hz/mv.

We next calibrated the μP. The A/D converter at the μP input is sensitive to level changes of approximately 10 mv. Therefore uP could detect a minimum change of 10Hz. The integration routine was checked by applying a d.c. voltage to the analog input of the μP and running the program. The output circuit, or final stage, was checked similarly. A d.c. voltage was applied at its input and the output was noted. Figure 4.2.2 displays the microprocessor integration routine results. The integration routine is seen to have a one-to-one correspondence, that is a slope of unity. (Note here that we have plotted output voltage versus the difference between the input voltage and uP offset merely so that the curve passes through the origin.

We are now ready to test the frequency aided acquisition structure. We perform a final calibration check properly adjusting the d.c. offsets and gains as before. Starting at the system nullpoint we initiate the program and adjust the d.c. so that the VCO is at its quiescent frequency that is the signal generator frequency. We adjust the gain as before. Figure 4.2.3 shows the input-output characteristic of the system for no noise, that is the overall system calibration curve. This was performed with an integration time period of 256 msec. Note the excellent correspondence between the input and output frequency.

To obtain a measure of the system sensitivity we varied the input frequency in small steps and observed the output frequency of the VCO when the μP program was run. We found that the system needed approximately a 10Hz change in input frequency to produce a change (of 10Hz) in the VCO output frequency. Thus the overall system would detect changes of ±10Hz.

At this juncture we are ready to introduce noise into the system and observe the statistical behavior of our acquisition aided structure.

4.2.2 Statistical Study and Results

To study the operation of our acquisition aided Phase Lock Loop we observed the output frequency variation of the VCO when stimulated by the input signal for various combinations of parameters. We did this for many trials and found the statistical mean and variance of the data.

Both the gain and time period for integration were set for the no noise case as per the description in Section 4.2.1. We then chose the appropriate SNR and modified the gain accordingly. To do this is rather simple. Since ρ is known $(1 - e^{-\rho})^{-1}$ is known. This represents the increase in gain needed to map the associated calibration curve to the no noise curve. We increase the loop gain this amount by simply increasing the voltage on the second stage amplifier of Fig. 4.1.2(f). We created a parallel

circuit with the appropriate gains so that we merely had to move the first stage output to the new configuration and add the noise. In this way we could periodically return to the no noise circuit and (after attenuating the noise of course) check for drift.

For each of the different parameter settings used we performed fifty (50) acquisition attempts or "runs". The μP was initialized prior to each run and then the program was started. We also performed the same test with 150 trials at a frequency of 8.89kHz. This was used for a Chi-square (χ^2) goodness of fit test. The results follow.

We performed the experiment for two values of SNR. that is at ρ = 0 dB and ρ = +3 dB. In both cases we chose to reduce the bandwidth from its initial value of 4000Hz to a value of 400Hz that is B_o = 4000Hz and B_1 = 400Hz. With these parameters chosen we obtain the integration times from Eq. (3.3.49). The value of B_1 is the value of the "threshold" bandwidth for the zero dB case such that $\rho_1 = Si/\eta B_1$ = +10 dB when ρ_o = 0 dB. Using this value for B_1 in both cases provides us with a common value with which to compare the results for the two values of SNR.

In addition, to determine the effect of reduced integration time on the system's output response we performed the same test at one-half the integration time for the zero dB case and one-fourth the integration time for the three dB case. For each of these tests we adjusted the gain for

proper operation with each chosen value of integration time period as per the procedure outlined in the previous section. Thus, from Eq. (3.3.49) we find the full and half-time integration periods for ρ = 0 dB are 255 and 128 msec resp. whereas, for the ρ = +3 dB case we find the full and one-fourth integration times to be 48 and 12 msec. resp. We again mention here that in all cases we did not wait the processing time. For the zero dB times this value is not significant since it is $3/B_o$ = 0.75 msec. which is 0.3% of 255 and 1.2% of 128. However it may be significant for the three dB case since it is 1.6% of 48 and 6.4% of 12.

Also notice that the value of integration time for the three dB, one-fourth period case is the value needed for reducing the bandwidth to 798.1Hz, that is the (+10 dB) threshold value for $Si/\eta B_o$ = +3 dB. Thus we can use the same results for the one-fourth time reduction case as data for the above mentioned parameter set.

The results of the experiment are shown in Tables 4.2.3, 4.2.4 and 4.2.5. In these Tables we record the mean frequency, $\bar{f}$, and the population Standard Derivation (S.D.), σ_f where

$$\bar{f} \triangleq \frac{1}{L} \sum_{\ell=1}^{L} f_\ell \qquad (4.2.1)$$

and

$$\sigma_f^2 \triangleq \frac{1}{L} \sum_{\ell=1}^{L} f_\ell^2 - \bar{f}^2 \qquad (4.2.2)$$

and L is the number of data points, f_ℓ. Also shown are: $\Delta_D f$, the difference between the input frequency, f_{IN} and the mean frequency; $\Delta_P f_{max}$, the maximum positive deviation from the mean; $\Delta_N f_{max}$, the maximum negative deviation from the mean, and R_f the total range of frequency deviation. Thus,

$$\Delta_D f = f_{IN} - \bar{f} \tag{4.2.3}$$

$$\Delta_P f_{max} = \max(f_\ell) - \bar{f} \tag{4.2.4}$$

$$\Delta_N f_{max} = \min(f_\ell) - \bar{f} \tag{4.2.5}$$

and

$$R_f = \max(f_\ell) - \min(f_\ell) \tag{4.2.6}$$

Let us consider Table 4.2.3. Initially we note that the first frequency entry for both the full and half time integration is 8.992kHz while the last frequency entry in the half time period is 10.992kHz. These are 900Hz and 1100Hz above f = 9.89kHz. The frequencies should have been chosen as 8.892 and 10.892kHz resp. but were simply set incorrectly. However they provide us with ample data. Furthermore, the χ^2 test performed later used f = 8.89kHz.. So we can compare this data also.

The first thing we notice is that, if we compare the full time mean value frequency for a particular offset fre-

quency with its respective counterpart for half-time integration we see very good agreement. The worst difference appears at the upper value of offset. (We experienced the most trouble at the high frequency and with many measurements. We attribute the asymmetry of the filter to much of this problem. A symmetrical filter at least should alleviate some of this discrepancy. A symmetric "brick wall" filter is certainly desirable.) From the third entry in the Table we see that, in each case, the mean value frequency is about 100Hz above the input frequency. This is because we calibrated the system for a center frequency of 9.89kHz while the actual center is at 10.2kHz. This 300Hz offset of center caused the estimate to be above the "true" mean. If the system calibration was such that the zero d.c. point were at 10.2kHz we would not expect to see such a large difference between $\bar{f}$ and f_{IN} although due to the random nature of the process we would not expect a perfect match either. The reason that $\bar{f}$ is higher than f_{IN} can be seen from the calibration curves. The natural center of the band is at 10.2kHz; that is, the noise, due to the filter shape tends to push the estimate to this higher point. Similarly, if we set the zero d.c. point above the natural center we would expect that $\bar{f}$ would be less than f_{IN} since the noise would tend to push the estimate back toward the center.

Now let us compare the second entry, that is, the

standard deviation. We expect the standard deviation to increase if the integration time were reduced. From Eq. (3.3.46) we see that we can expect an increase of about $\sqrt{2} = 1.414$ to one. From Table 4.2.3 we see that for the low frequency offset ($\Delta f = -.9$kHz or $f = 8.992$kHz), the ratio of standard deviations is $74/48.3 \simeq 1.5$ which is comparable to $\sqrt{2}$. We would next like to compare the S.D. at the different offsets for each integration time. However, this is not really fair since the offsets are -.9 and +1.0kHz for the full time integration, whereas for the half time we have -.9 and +1.1. However in Table 4.2.5 we show the same statistics for the case of zero dB, full time integration at $\Delta f = -1$kHz, i.e. $f = 8.892$kHz. Thus we can compare this S.D. with that of the corresponding one in Table 4.2.3. Doing so we see that the values are comparable: 62.4 compared to 64.2.

Another important point to note is the (absolute value) of the maximum frequency deviation. From Table 4.2.3 we see that for all but two cases this value is less than the required 200Hz even in the half time integration period. We also indicate in parenthesis next to the two values greater than 100 the next farthest point. These points are well within the 200Hz limit. Thus in 300 test "runs," only two points fell outside the prescribed region. Finally, if we examine R_f we see that the sytem is well within the 400Hz limit in all cases.

Next let us consider Table 4.2.4 which shows the results for = +3 dB. In this case notice that we have

adjusted for the proper offsets, that is $\pm$1kHz from $f = 9.892$kHz. Again we see that the mean frequencies in the corresponding integration periods compare well except for the positive offset. In fact for $f_{IN} = 10.892$kHz, $\bar{f}$ is less than f_{IN} as seen from the third entry in Table 4.2.3. This is the only occurrence of this kind in all the tests. We note it occurs on the high frequency side. Since T_k is very small this does not surprise us.

In fact if we view the raw data for the 1/4-time case we find that very few different frequencies were recorded. Two extreme values, one at 10.404kHz and the other at 11.168kHz were found. Sixteen occurrences of frequencies varying from 10.657 to 10.667kHz appeared at the output and the remaining thirty points varied over the range 10.901 to 10.909kHz. The mode was quite marked with twenty three values at 10.907kHz, its next leading competitor with ten values at 10.657kHz. (Note: the 10.907kHz value is rather close to f_{IN}.) From this data we expect that the system was receiving very few spikes. As a matter of fact it is conjectured that a particular number of spikes caused the output frequency to have a multimodal configuration. Note that the two values of f with the highest rate of occurrence are on opposite sides of the mean. The low value of frequency is 165Hz from $\bar{f}$ while the high value of frequency is 185Hz above $\bar{f}$. It seems here that for $\rho = 3$ dB and small T_k the Gaussian probability assumption fails. But we predicted

this possibility under the above conditions.

Another point to remember is that we did not allow for processing time in the ρ = 3 dB case also. Here T_{pk} is more critical since T_k is less. As mentioned before in the zero dB case T_{pk} was only 0.3% and 1.2% of T_k in the full and half time integration tests. However for the three dB case we find that T_{pk} about 1.6% and 6.4% for the full and one fourth-integration tests. Thus it is much more crucial to wait the processing time for ρ = 3 dB.

We next examine the S.D. Surprisingly we find a larger deviation than in the zero dB case even though the system is operating at a higher SNR. However a careful examination of the data points reveal that this large deviation is caused by one or two data points which are far removed from the mean. This can be seen from $\Delta_P f_{max}$ and $\Delta_N f_{min}$. The next closest data points are indicated in parenthesis. These are seen to be well within the $\pm$200Hz bandwidth. Also the number in the parenthesis in the S.D. row of Table 4.2.4 shows the S.D. if the extreme points are omitted. We see that these values are more reasonable and on the same order as the zero dB case. Notice also if the extreme values are omitted R_f is < 400Hz whereas when they are considered R_f > 800 for the offsets.

One possible reason for these extreme points is that for the small integration time the system receives only a few spikes. Furthermore they may all be in a direction as

to increase the frequency estimate. Another cause may be the μP itself. During the calibration procedure we noticed that sometimes the microprocessor output did not change or changed irratically. Since during the calibration procedure there is no noise, these events were caused by the μP. The μP control is accomplished through a series of toggle switches which may pick up noise or not set correctly thus causing these errors. Thus it is not surprising to see such oddities occur. Due to this we view the extremum data carefully. Note also that the means do not vary much except at the high offset frequency of f = 10.892kHz when these points are excluded (the values for the mean frequency, $\bar{f}$, without the extremum points are shown in parenthesis, next to their associated values.

In the one-fourth time integration case we make the following observations. First at the "center" frequency not once in fifty attempts at locking did the injection locked system fail to produce the correct value of f_{IN}; i.e. $\hat{f} = f_{IN}$ for all the runs. This is due to the fact that at the center very few, if any at all, spikes entered the system (we monitored the waveform on an oscilloscope for the period of integration and saw no spikes). Thus the system had to contend only with Gaussian noise and did quite well with the resolution available ($\simeq$ 10Hz).

Now we must examine the offset frequencies for the 1/4-time case. First we see that the highend offset had the largest range, R_f. However if we recall that the 1/4

integration time period is the period for the bandwidth to be within $\pm$399Hz of the center we see that it almost meets this requirement (the $\Delta_N f_{min}$ = -418 is the only value outside this $B_k/2$ limitation). It does meet the 798kHz requirement on R_f though. Due to these considerations we expect that the extreme values here are valid points and not caused by μP failure.

If we compare the "new" value of σ_f (the value in parenthesis) for each integration period, we see that, for the corresponding frequency offsets, the increase is almost 2 to 1 for f = 10.892kHz and about 1.3 to 1 for f = 8.892kHz. We expect a worst case increase of about 2 to 1 in σ_f. Thus these values are commensurate with our expectations.

One final test was performed. In order to find out if the noise processes at the system output could come from a Gaussian distribution we performed a χ^2-goodness of fit test [13]. The raw data was taken for a SNR of zero dB at an offset frequency of 8.891kHz, and T_k = 255 msec. We generated a total of L = 149 data points whose mean value and S.D. were $\bar{f}$ = 9.034kHz and σ_f = 62.4Hz resp. (see Table 4.2.5).

The null hypothesis, H_o, and the alternate hypothesis, H_1 are as follows:

H_o: Data is from a Gaussian distribution

H_1: Data is not from a Gaussian distribution.

The intervals for the χ^2-test were chosen to be 10Hz. This

produced 29 distinct intervals for the 149 data points. According to rules for the χ^2-test some intervals had to be grouped together in order to have at least five data points contained in them. This produced a total of 20 test intervals, I_T. We had to estimate r = 2 parameters, that is $\bar{f}$ and σ_f, thus we had $F = I_T - r - 1 = 17$ degrees of freedom. We chose the 95% significance level for the χ^2 test. From standard tables for the χ^2-distribution we find that, for H_o to be true the χ^2-test as performed on the data must yield a value less than c = 27.59. Performing the appropriate operations on the data we find our test variable to be 12.54. Since 12.54 < c we accept the hypothesis H_o. This of course does not mean the distribution of the data is definitely normal; it only means that it is normal with a probability of .95 in regard to the χ^2 test. Other distributions may as well be accepted by the test. Thus in this sense we really are stating that we do not reject the hypothesis H_o.

The experimental results were satisfying. We see that in most cases the system, in the full-time integration mode produced resultant frequencies within the band of operation. The statistics show that the distribution has a high likelihood of being Gaussian and that the system behaves in a predictable manner.

The sources of error in the test are (1) the filter asymmetry, coupled with (2) the limiter clipping properties,

(3) the μP quantization, (4) the off-center calibration, (5) d.c. drift, and finally (6) the gain setting adjustment when operating with noise. This corresponds to changing the gain by the factor $(1 - e^{-\rho})^{-1}$. As we mentioned before this was done by increasing the voltage on a potentiometer. This adjustment was made in the tens of millivolts region. Thus a noisy "pot" or a slight misalignment produces a considerable error in the output frequency estimate. So here too is a reason why, in a practical system, highly accurate and reliable components are needed.

Table 4.2.1

COMPARISON OF THEORETICAL AND EXPERIMENTAL

CALIBRATION CURVE SLOPES

	Signal-to-Noise Ratio (dB)					
Slopes	∞ (and +10)	+5.0	+3.0	0.0	-3.0	-5.0
Experimental	1.0015	0.9460	0.8503	0.6285	0.3910	0.2688
Theoretical(ζ)	1.0000	0.9580	0.8640	0.6322	0.3942	0.2711
1% error | worst* case	0.15	1.22	1.59	0.573	0.810	0.8521

*worst case means numbers rounded off to give largest error, and % error rounded higher."

e.g., for ρ = +5 dB, ζ = 0.9576707

% error was computed as follows

% error = [|0.9576708 - 0.946|/0.9576706] × 100% = 1.21866%

Table 4.2.2

SPIKE COUNT FOR SNR OF +5 dB (P $\triangleq$ positive, N $\triangleq$ negative)

	Frequency (kHz)									
Trial	8.0		9.0		10.0		11.0		12.0	
Number	P	N	P	N	P	N	P	N	P	N
1	13	0	4	0	3	1	0	4	0	10
2	11	0	3	0	0	1	0	3	0	7
3	9	0	1	0	0	1	0	3	0	7
4	10	0	4	1	0	1	0	7	0	10
5	5	0	5	0	0	3	0	3	0	5
6	13	0	3	0	0	3	0	4	0	11
7	12	0	5	0	0	1	0	5	0	9
8	10	0	3	0	1	1	0	5	0	6
9	8	0	3	0	1	2	0	6	0	6
10	11	0	3	1	0	3	0	8	0	6
11	10	0	6	0	0	2	0	6	0	8
12	11	0	2	2	1	3	0	2	0	7
13	12	0	4	0	2	4	0	7	0	10
14	14	0	6	1	0	2	0	3	0	4
15	8	0	6	0	0	2	0	1	0	4
16	15	0	2	0	1	3	0	3	0	13
17	11	0	4	0	0	3	0	5	0	8
18	10	0	5	0	0	0	0	4	0	10
19	7	0	5	0	1	3	1	4	0	8
20	10	0	4	0	1	2	0	2	0	8
Sub Total	210	0	78	5	11	40	1	85	0	157
Total	210	0	83		51		86		157	

Table 4.2.3

VCO OUTPUT FREQUENCY STATISTICS, ρ = 0 dB (50 trials)

	Full Time Integration			Half Time Integration		
frequency (kHz) / Parameter	Δf=-900Hz 8.992	Δf=0.0Hz 9.890	Δf=1000Hz 10.892	Δf=-900Hz 8.992	Δf=0.0Hz 9.89	Δf=1100Hz 10.992
$\bar{f}$ (mean value), kHz	9.100	9.967	11.027	9.100	9.972	11.096
σ_f (St.dev.), Hz	48.3	52.2	64.2	73.97	52.6	78.5
$\Delta_D f$ ($f_{IN}-\bar{f}$), Hz	-108.0	- 77.4	-134.5	-108.0	- 80.9	- 96.5
$\Delta_P f_{max}$[max(f_ℓ)-$\bar{f}$], Hz	+149	+117	+166	+136	+ 88	+108
$\Delta_N f_{max}$[min(f_ℓ)-$\bar{f}$, Hz	- 88	-122	-224 (-80)	-218 (-112)	-104	-165
R_f ($\Delta_P f_{max}-\Delta_N f_{min}$), Hz	237	239	390 (246)	354 (248)	192	328

Table 4.2.4

VCO OUTPUT FREQUENCY STATISTICS, ρ = 3 dB (50 trials)

	Full Time Integration			One-Fourth Time Integration		
frequency (kHz) / Parameter	Δf=-1kHz 8.892	Δf=0 9.892	Δf=+1kHz 10.892	Δf=1kHz 8.892	Δf=0 9.892	Δf=+1kHz 10.892
$\bar{f}$, kHz	8.940(8.948)	9.908(9.902)	10.973(10.952)	8.906	9.892	10.822
σ_f , Hz	111.0(62.9)	57.2(39.1)	130.3(74.1)	78.9	0	137.7
$\Delta_D f$, Hz	-48.0	-10.0	-81.0	-14.0	0	+70
$\Delta_P f_{max}$, Hz	+272(103)	+300(118)	+589(157)	+241	0	+346(87)
$\Delta_N f_{max}$, Hz	-596(147)	-67	-159(-159)	-267	0	-418(-165)
R_f , Hz	868(250)	367(185)	748(316)	508	0	754(252)

Table 4.2.5

VCO OUTPUT FREQUENCY STATISTICS

ρ = 0 dB (149 trials), f = 8.89kHz

Parameter			Full Time Integration
$\bar{f}$	,	kHz	9.034
σ_f	,	Hz	62.4
$\Delta_D f$	,	Hz	-142
$\Delta_P f_{max}$	,	Hz	+139
$\Delta_N f_{max}$	,	Hz	-144
R	,	Hz	283

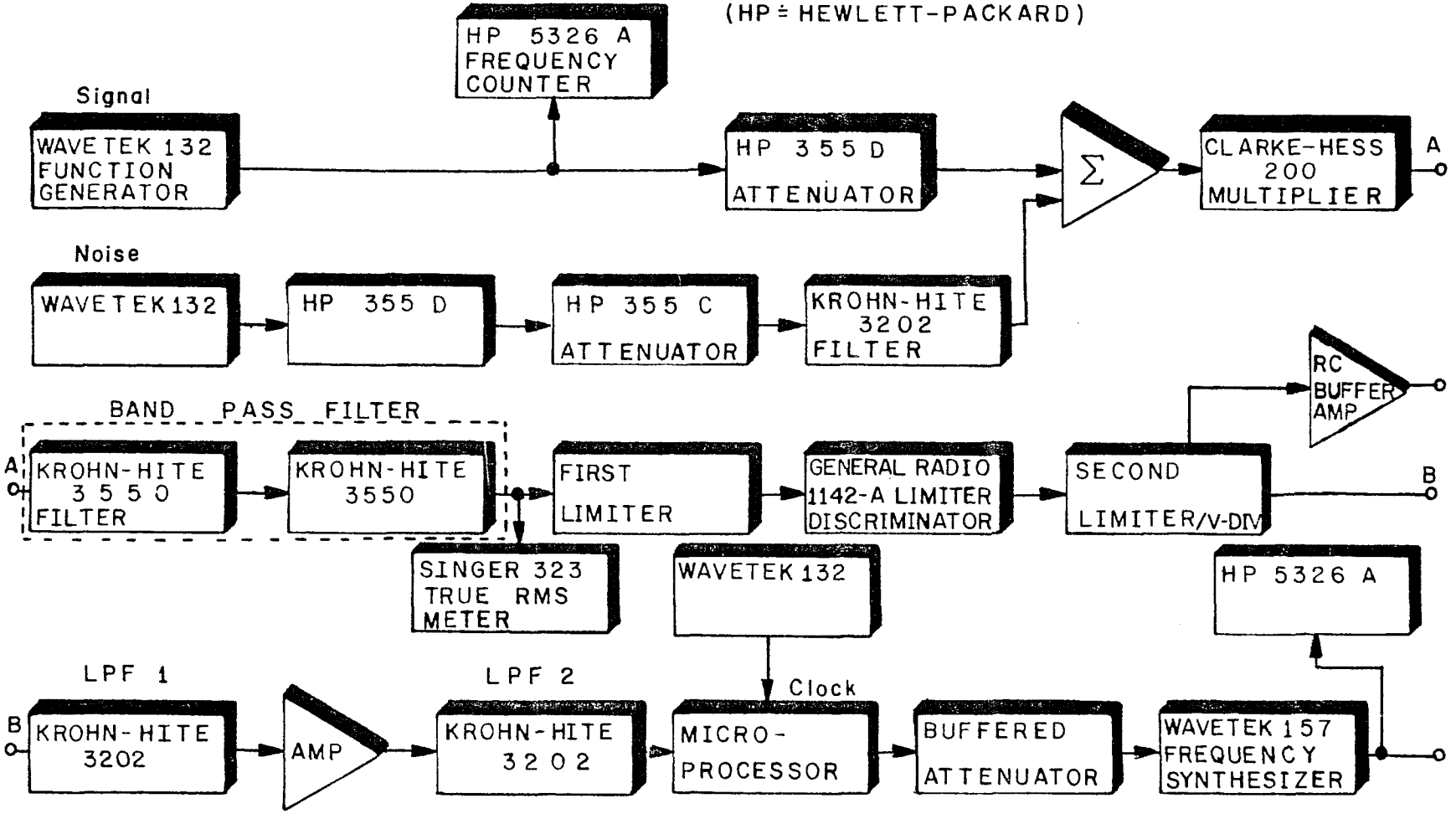

Figure 4.1.1 Block Diagram of the Test Facility for the Acquisition-aided PLL

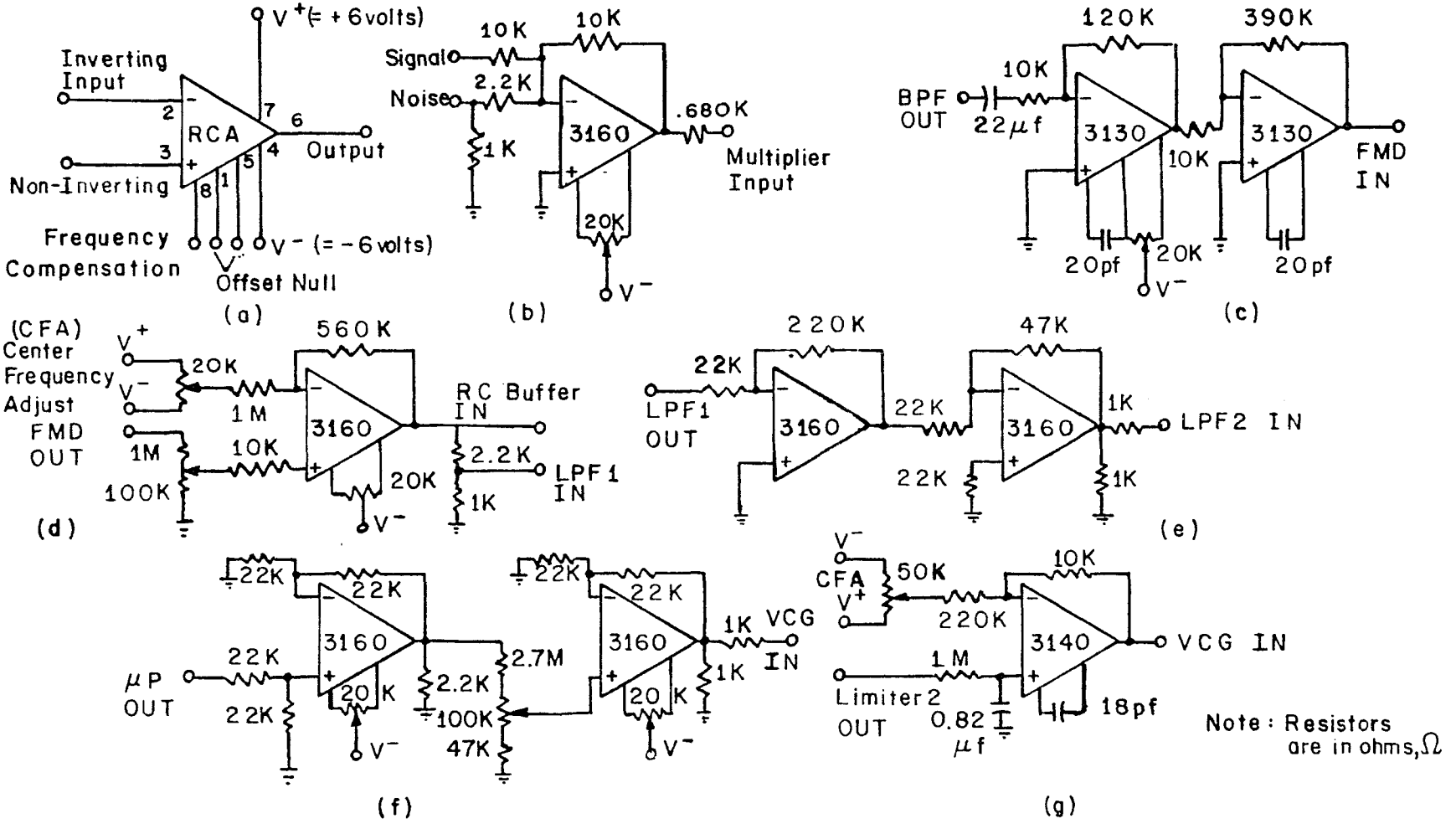

Figure 4.1.2 Circuit Schematics for System Implementation (a) General Pin Configuration (b) Adder (c) First Limiter (d) Second Limiter/Voltage Divider (e) 2-Stage Buffur amplifier (f) Buffered-Attenuator (g) RC Buffer Amplifier

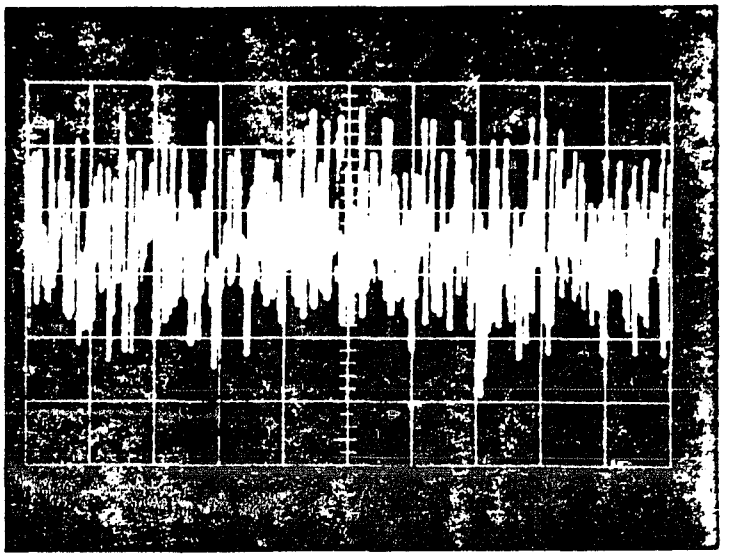

(a)

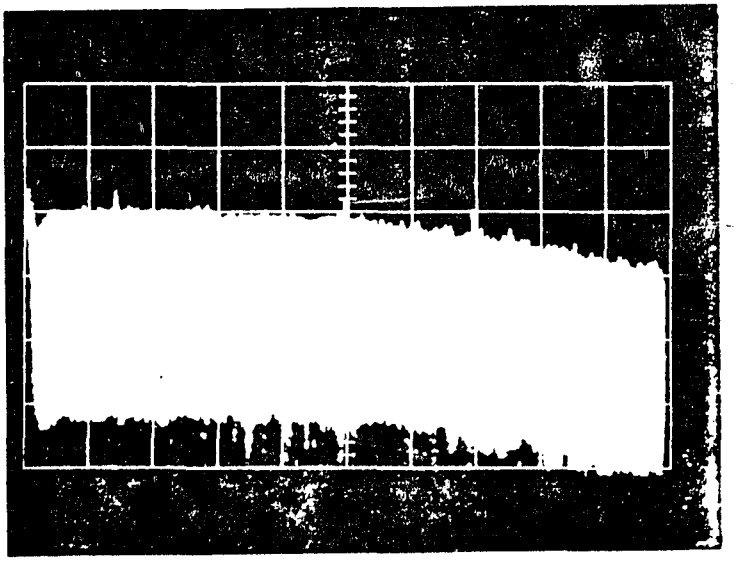

(b)

Figure 4.1.3 Noise characteristics
(a) Waveshape at filter input
(Vert. = 0.5v/div, Horiz. = 0.2 msec/div)
(b) Spectrum at filter input
(Vert. = 10 dB/div, Horiz. = 10kHz/div)

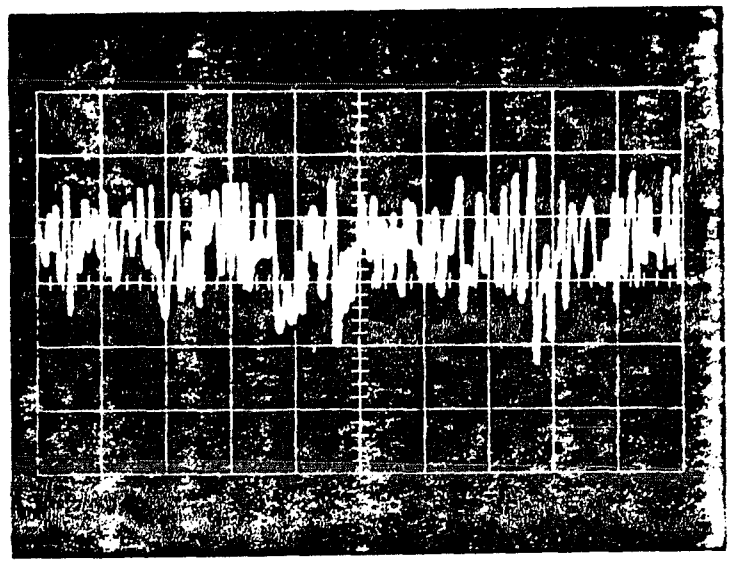

(c)

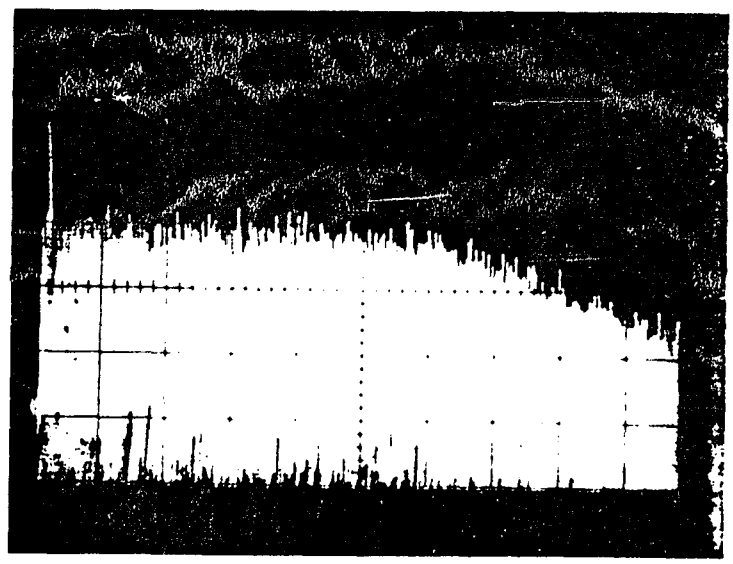

(d)

Figure 4.1.3 (cont'd.)
(c) Waveshape at filter output
(Vert. = 0.5v/div, Horiz. = 0.2msec/div)
(d) Spectrum at filter output
(Vert. = 10 dB/div, Horiz. = 5kHz/div)

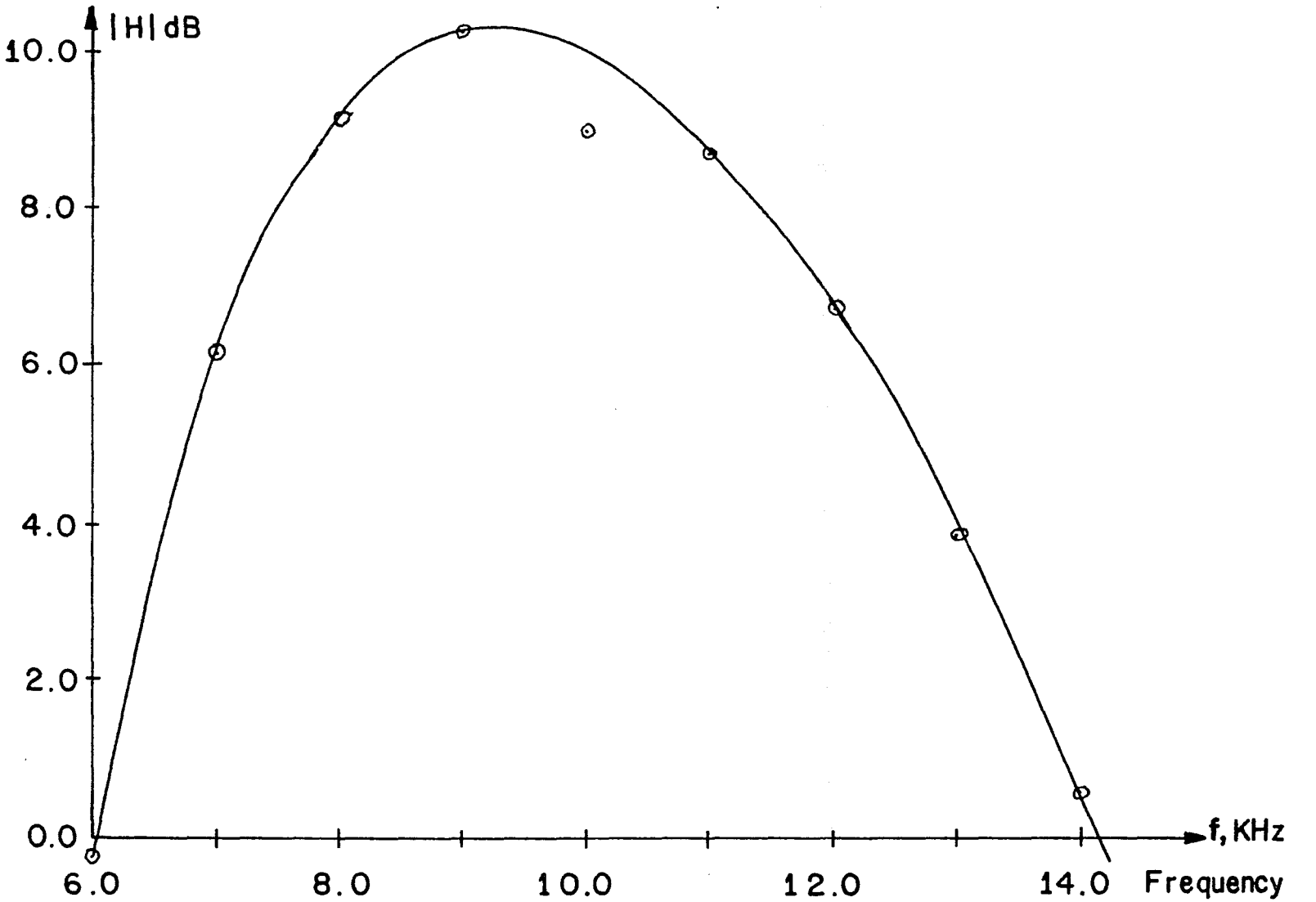

Figure 4.1.4 Filter Characteristic for Acquisition Process (Cascade)

Figure 4.1.5 Frequency response of bandpass filter 0 to 20kHz
(Vert. = 10 dB/div; Horiz. = 2kHz/div)

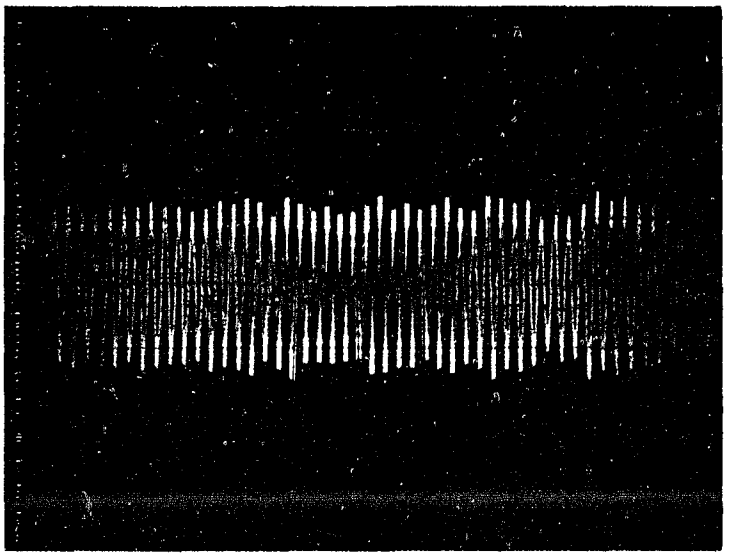

(a)

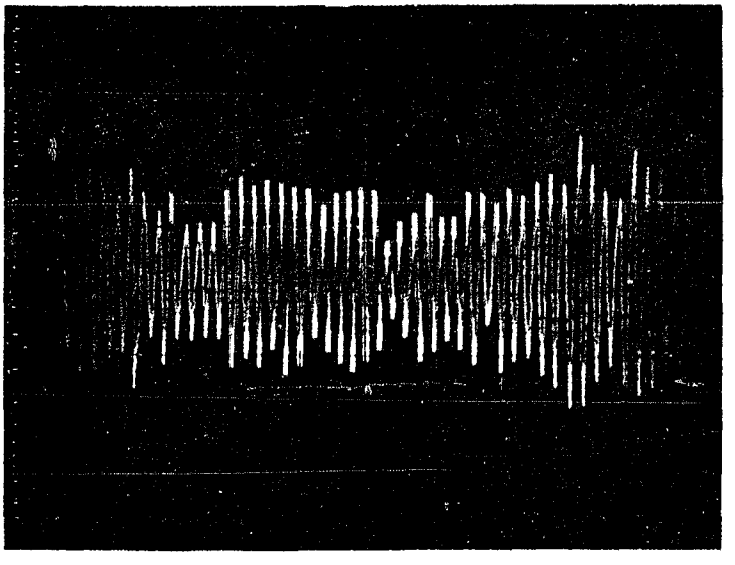

(b)

Figure 4.1.6 Signal and noise at output of BPF vs. time:
Signal frequency = 9kHz
(a) ρ = +20 dB (b) ρ = +10 dB
[(a) and (b) Vert. = 50mv/div; Horiz. = 500μs/div]

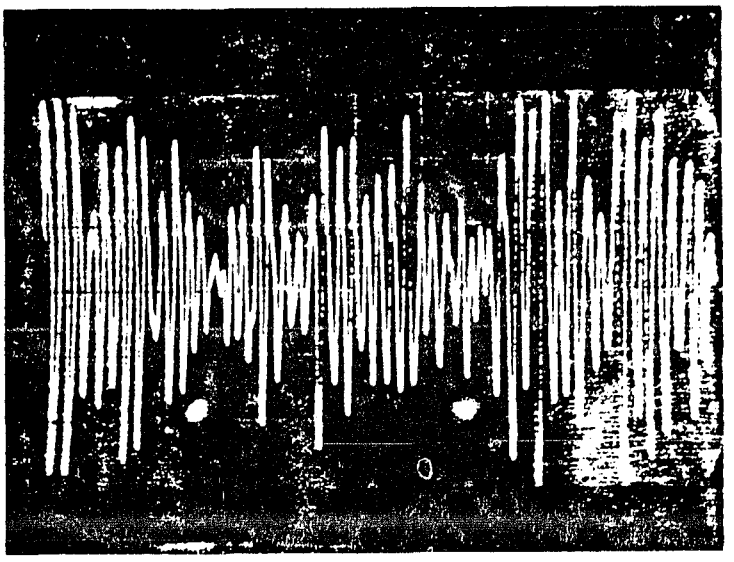

(c)

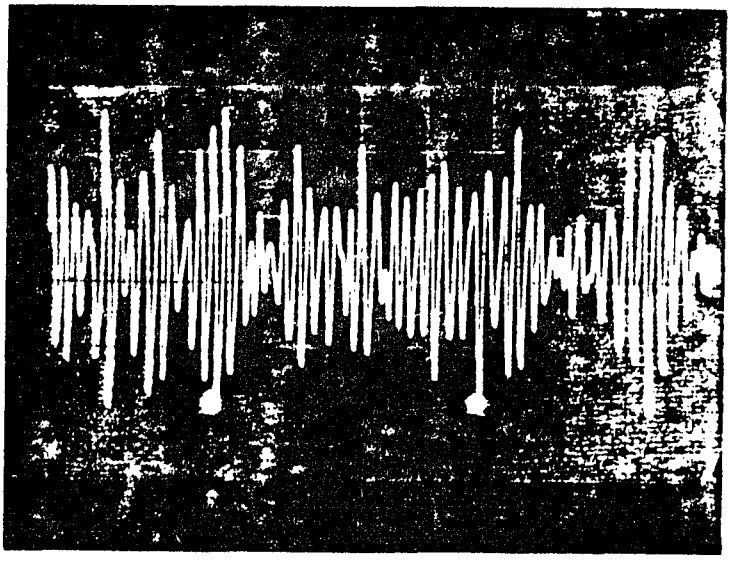

(d)

Figure 4.1.6 Signal and noise at output of BPF vs. time:
Signal frequency = 9kHz
(c) ρ = 0 dB (d) ρ = -3 dB
[(c) Vert. = 50mv/div; Horiz. = 500μs/div;
(d) Vert. = 10mv/div; Horiz. = 500μs/div]

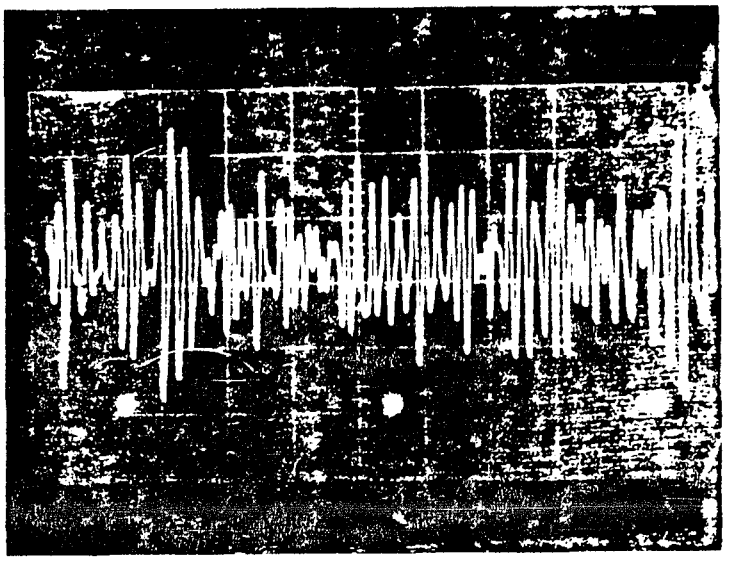

(e)

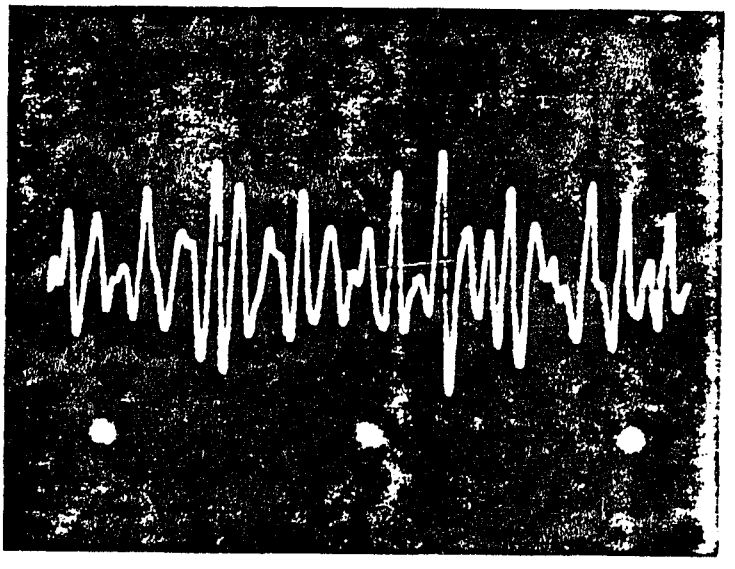

(f)

Figure 4.1.6 Signal and noise at output of BPF vs. time:
Signal frequency = 9kHz
(e) ρ = -10 dB (f) Noise only
[(e) Vert. = 200mv/div; Horiz. = 500μs/div;
(f) Vert = 100mv/div; Horiz. = 200μs/div]

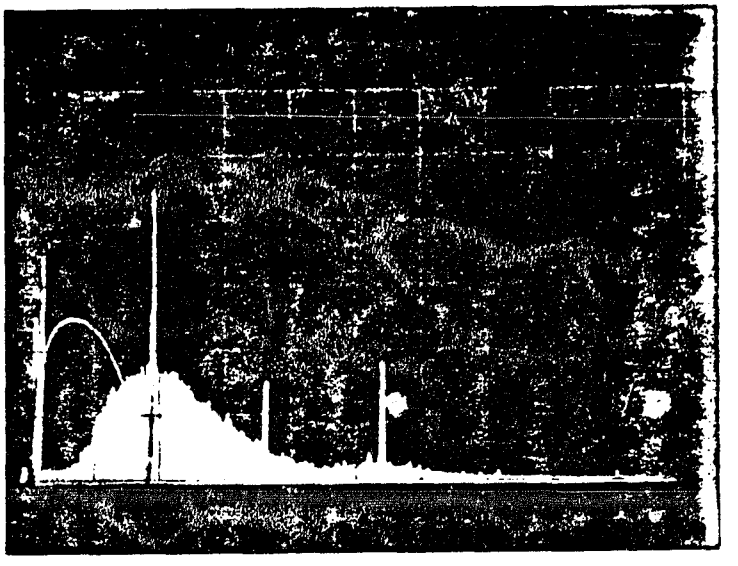

(a)

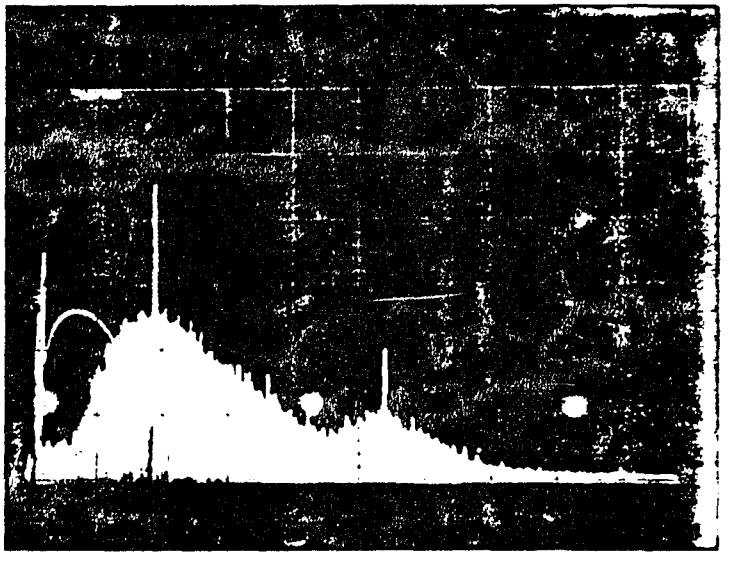

(b)

Figure 4.1.7 Spectrum of signal plus noise at output of BPF
Signal frequency = 9kHz
(a) ρ = +20 dB (b) ρ = +10 dB
(Vert. = 10 dB/div; Horiz. = 5kHz/div)

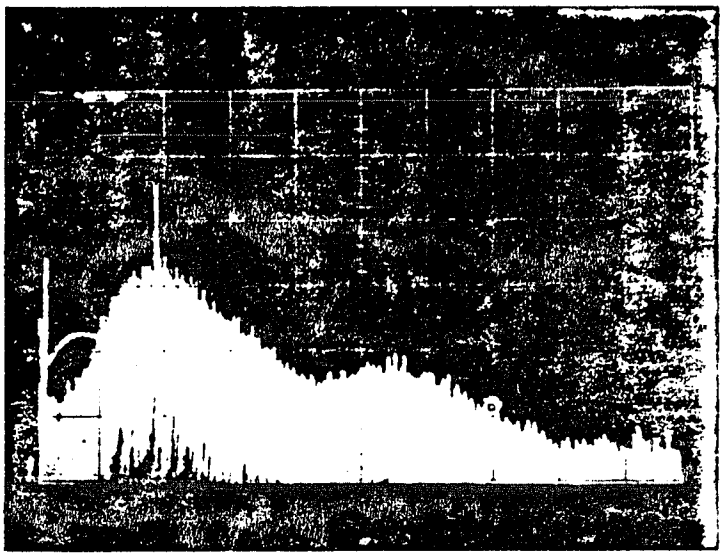

(c)

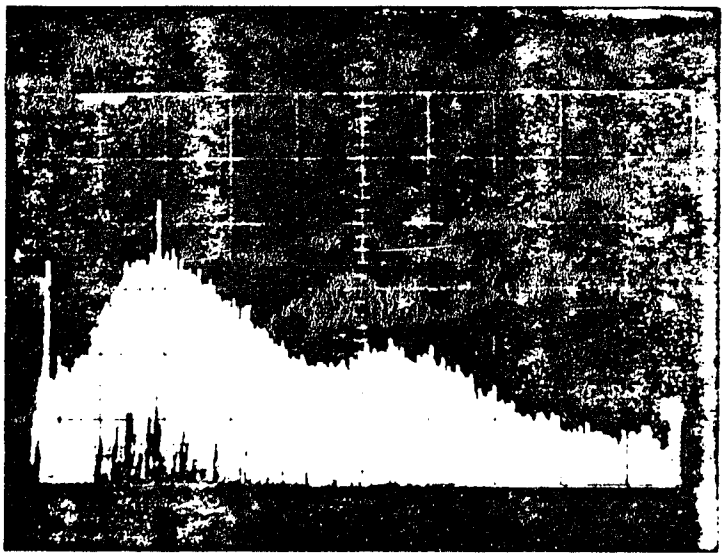

(d)

Figure 4.1.7 Spectrum of Signal plus noise at output of BPF
Signal frequency = 9kHz
(c) ρ = 0 dB (d) ρ = -3 dB
(Vert. = 10 dB/div; Horiz. = 5kHz/div)

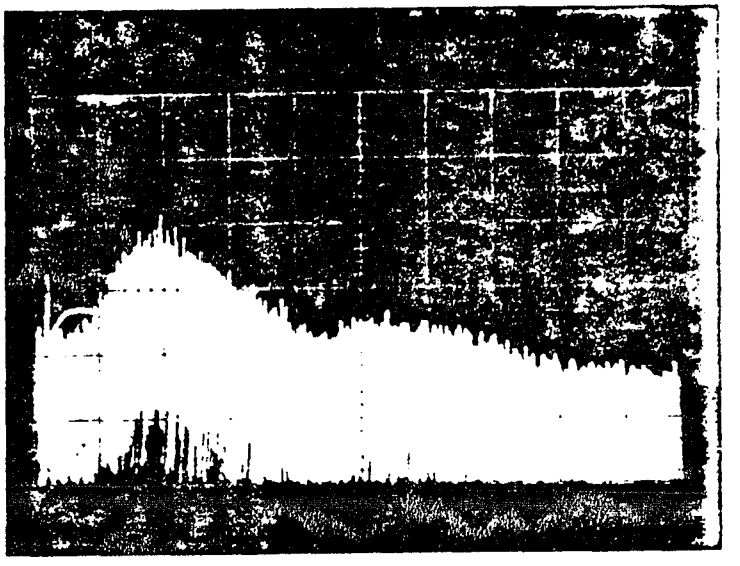

(e)

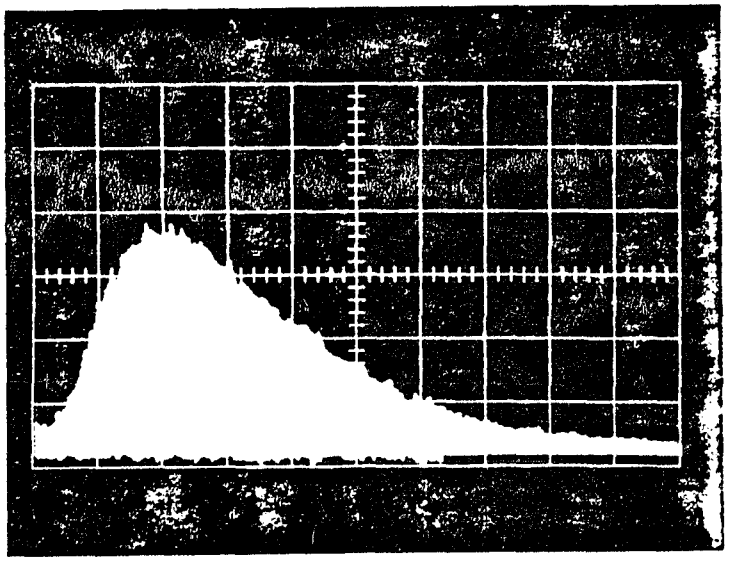

(f)

Figure 4.1.7 Spectrum of signal plus noise at output of BPF
Signal frequency = 9kHz
(e) ρ = -10 dB (f) Noise only
(Vert. = 10 dB/div; Horiz. = 5kHz/div)

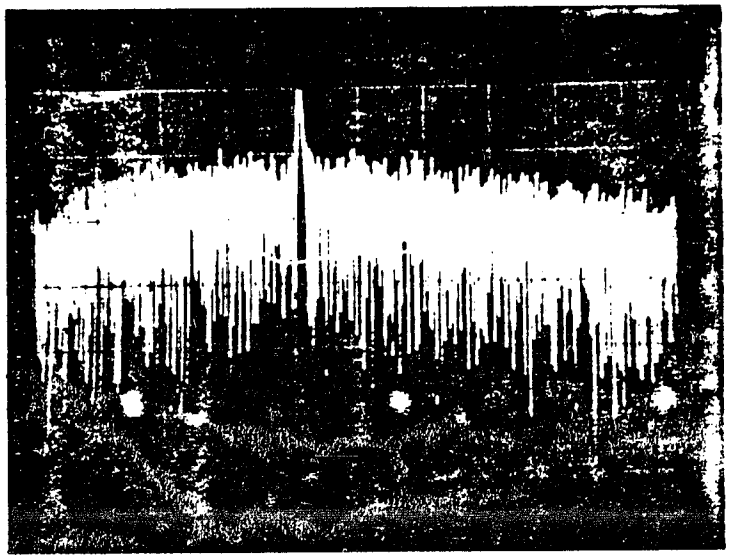

(a)

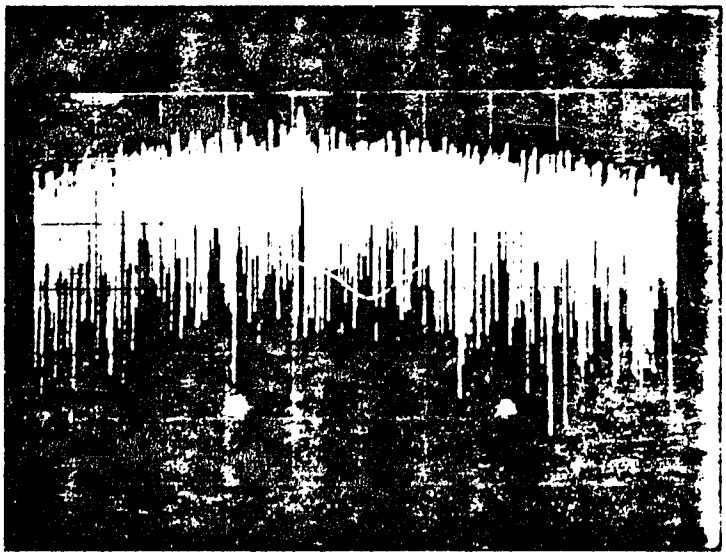

(b)

Figure 4.1.8 Expanded view of spectrum of signal plus noise at BPF output (Signal frequency = 9kHz)
(a) ρ = 0 dB (b) ρ = -10 dB
(Vert. = 10 dB/div; Horiz. = 1kHz/div)

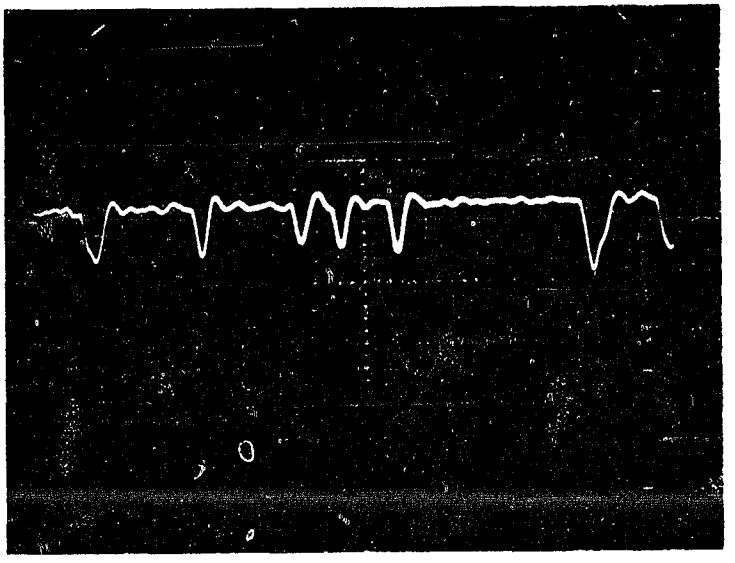

(a)

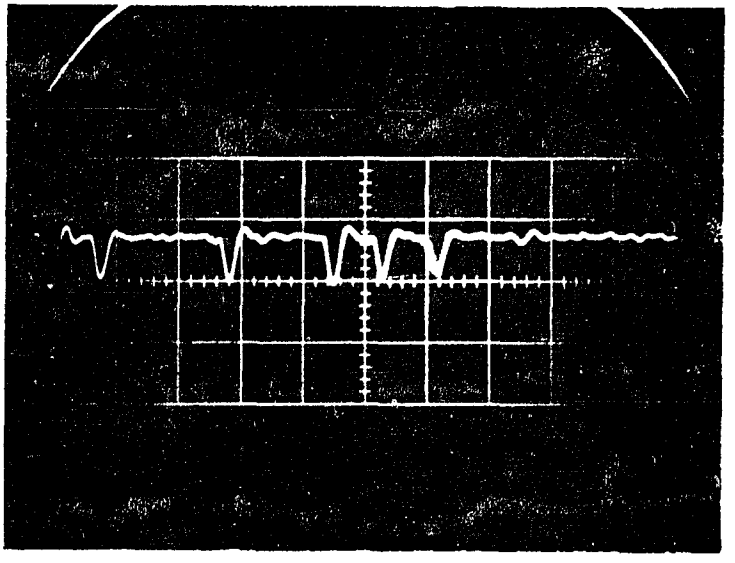

(b)

Figure 4.1.9 Spike waveforms for ρ = 3 dB, Input frequency
(a) 8kHz (b) 9kHz

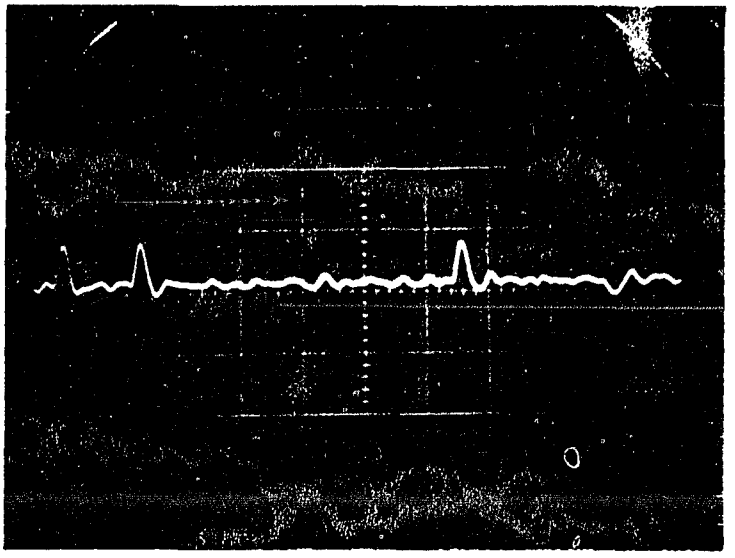

(c)

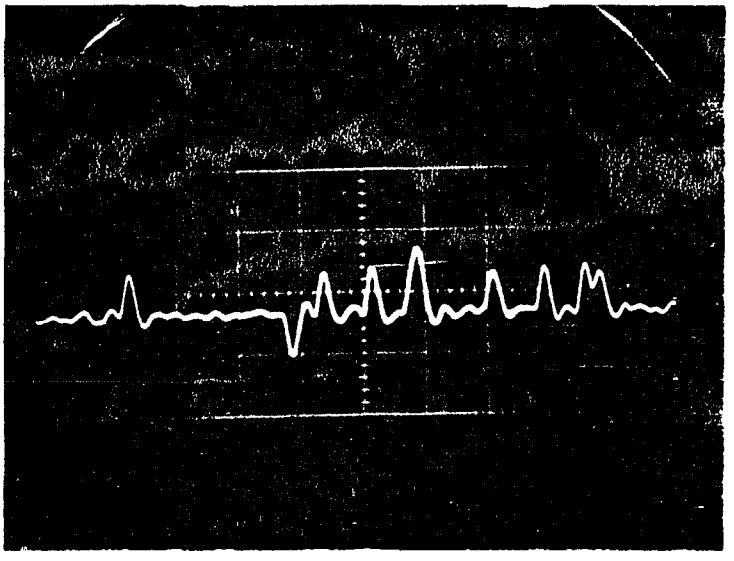

(d)

Figure 4.1.9 Spike waveforms for ρ = 3 dB, Input frequency
(c) 10kHz (d) 11kHz

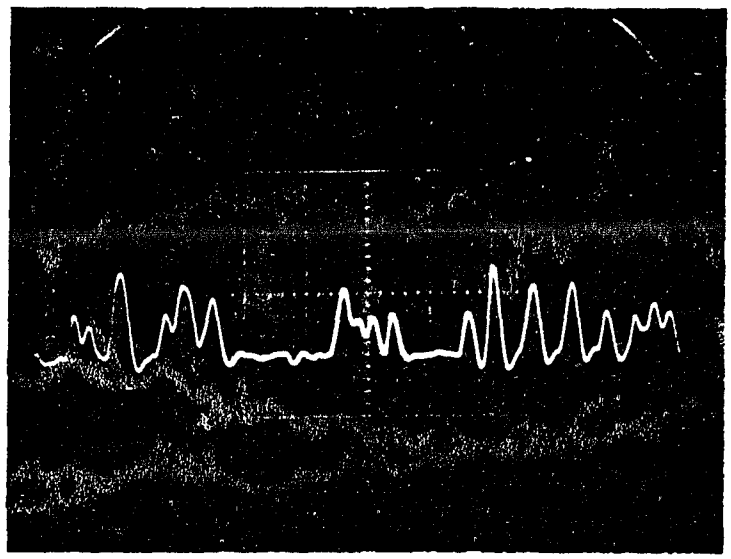

(e)

Figure 4.1.9 Spike waveforms for ρ = 3 dB, Input frequency
(e) 12kHz

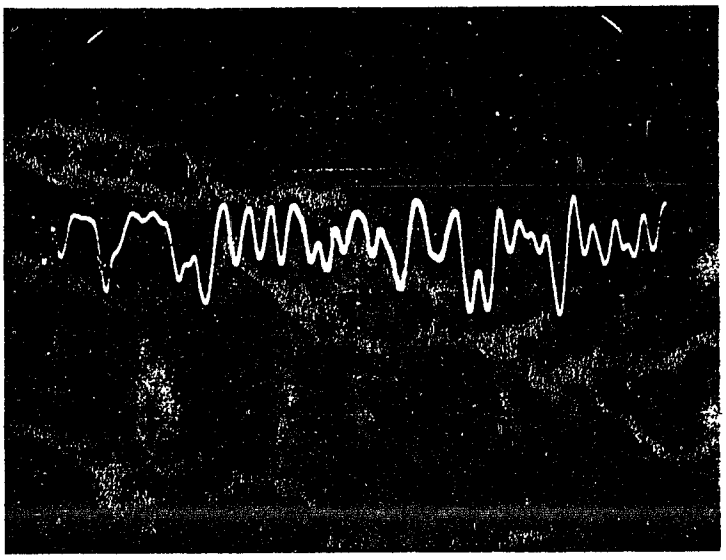

(a)

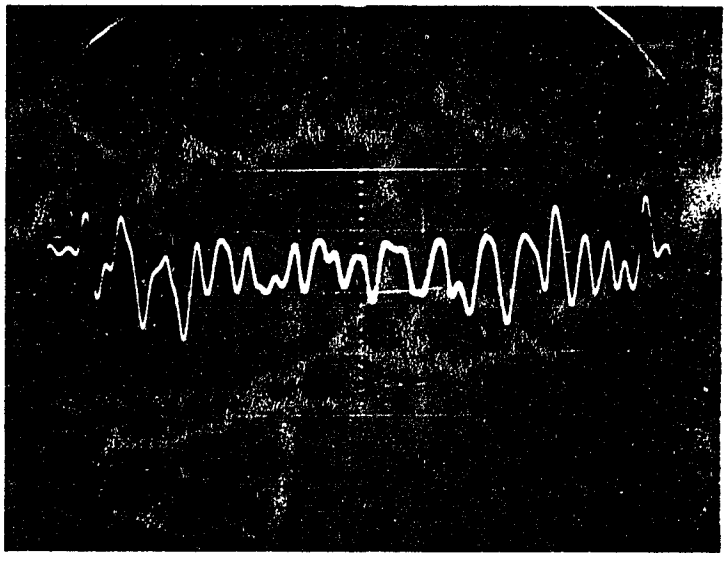

(b)

Figure 4.1.10 Spike waveforms for ρ = 0 dB, Input frequency
(a) 8kHz (b) 9kHz

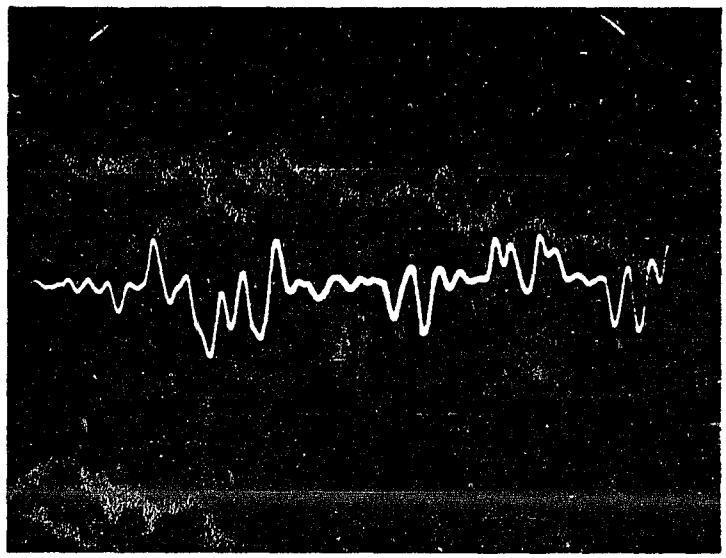

(c)

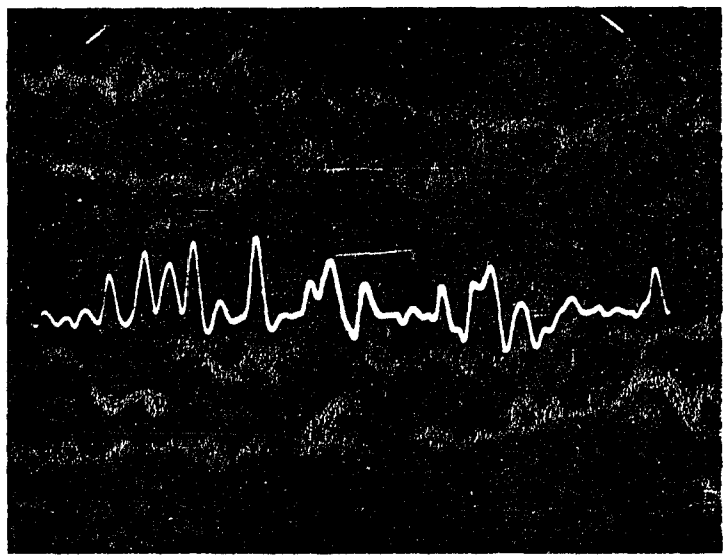

(d)

Figure 4.1.10 Spike waveforms for ρ = 0 dB, Input frequency
(c) 10kHz (d) 11kHz

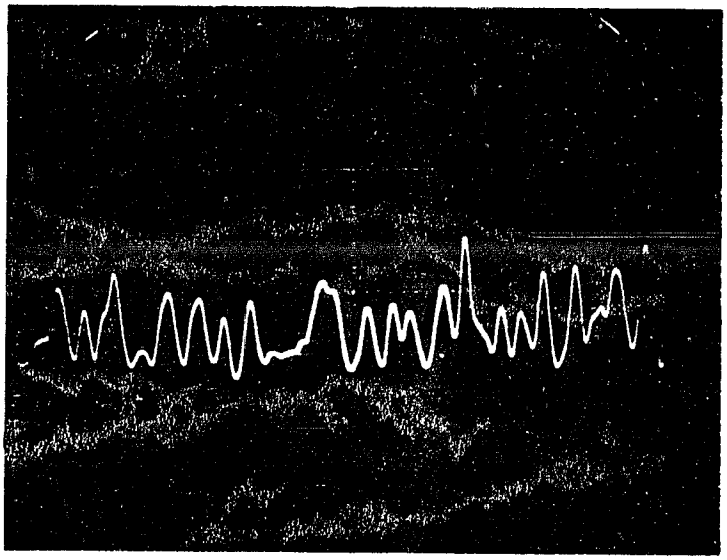

(e)

Figure 4.1.10 Spike waveforms for ρ = 0 dB, Input frequency (e) 12kHz

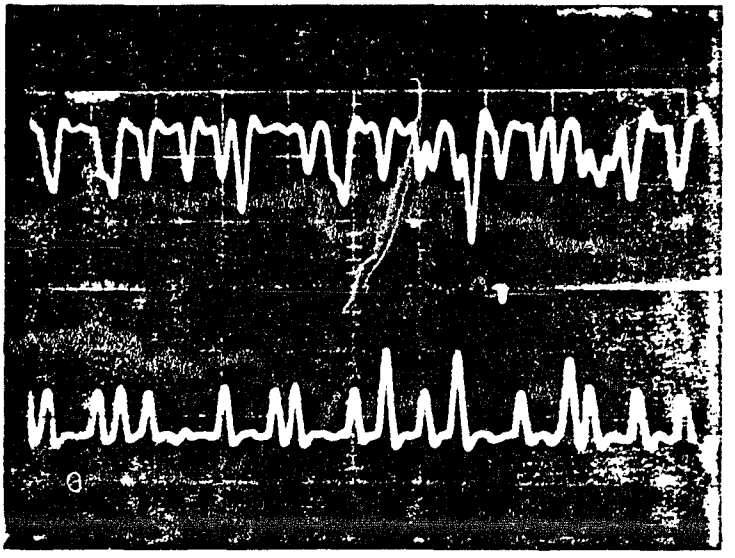

(a)

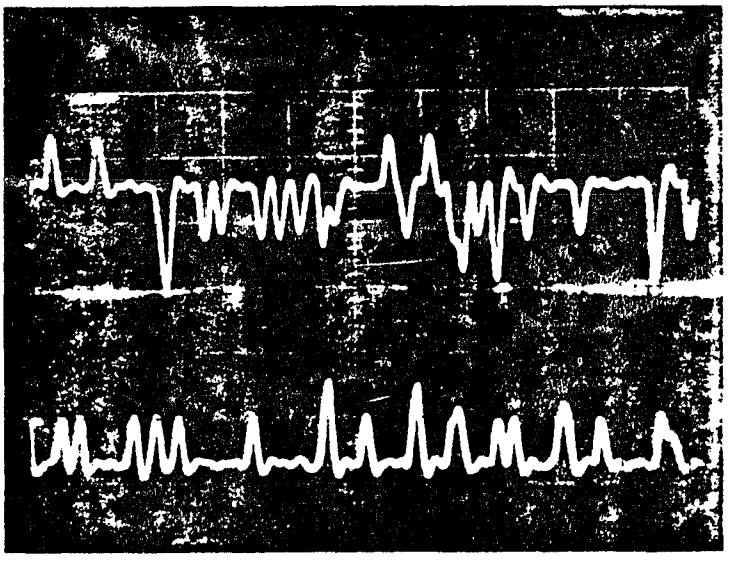

(b)

Figure 4.1.11 Spike comparisons
(a) Top: 11kHz; Bot.: 9kHz
(b) Top: 12kHz; Bot.: 8kHz
(Vert. = 10mv/div; Horiz. = 10ms/div)

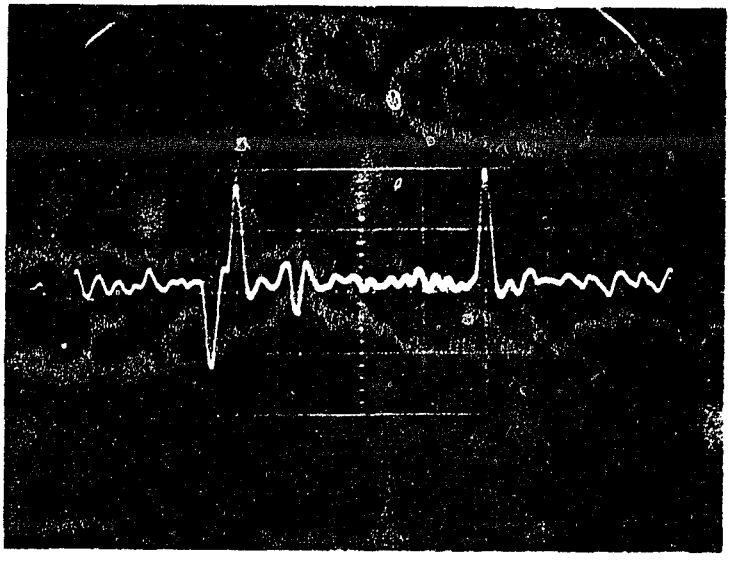

Figure 4.1.12 Spikes for ρ = +3 dB
Signal frequency = 10kHz
(Vert. = 200mv/div; Horiz. = 5ms/div)

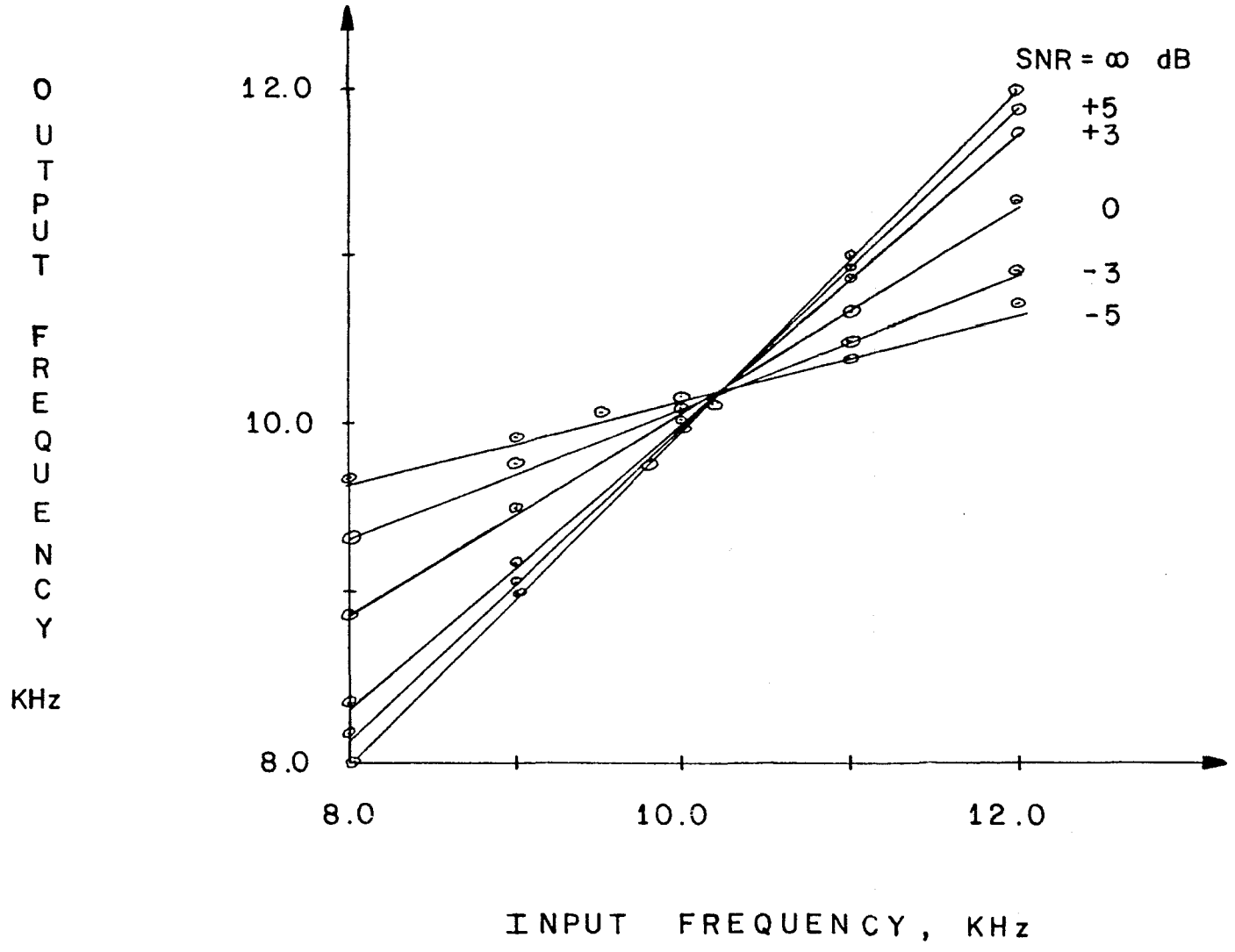

Figure 4.2.1 FMD (RC) Calibration Curves

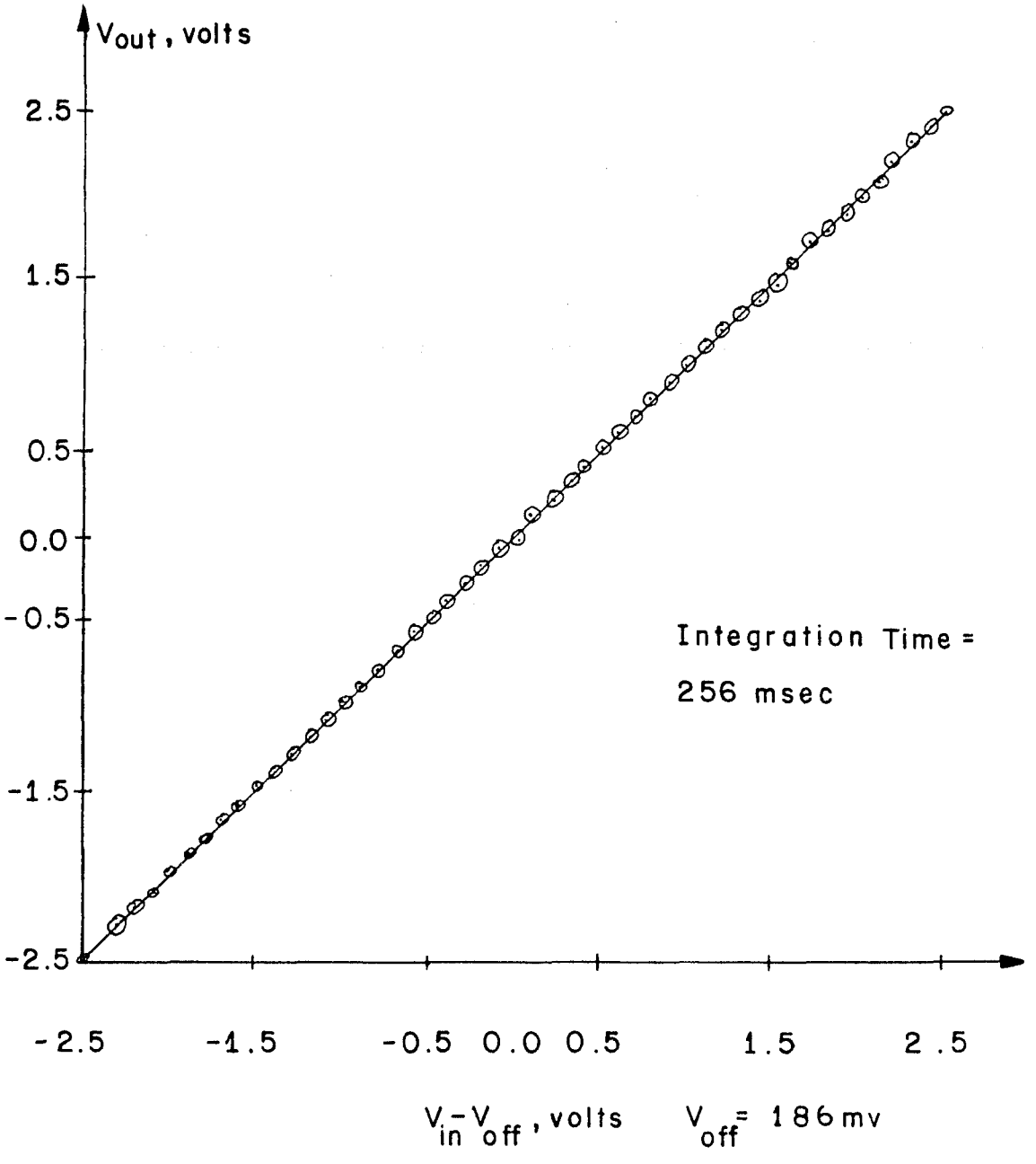

Figure 4.2.2 Microprocessor Integration Program

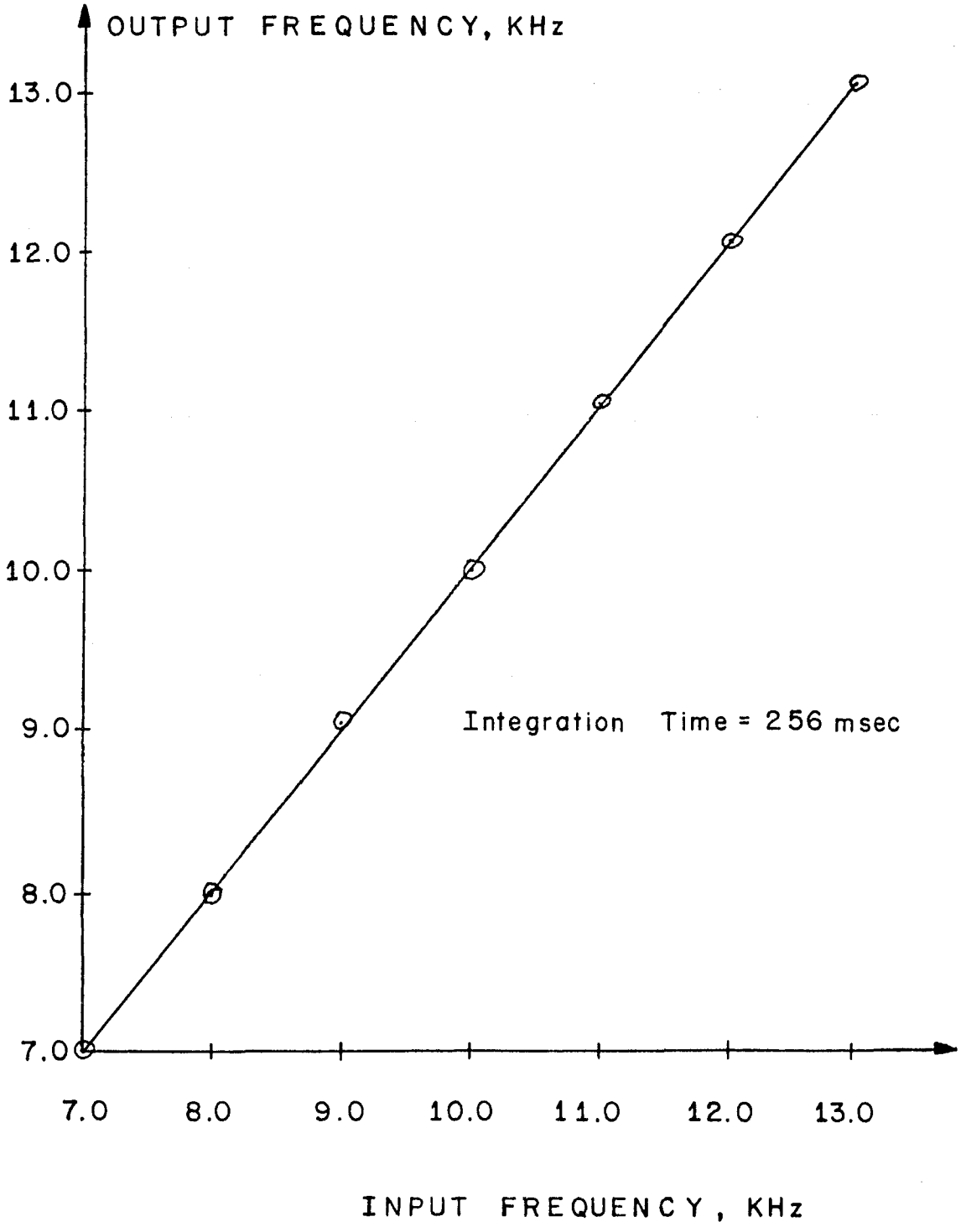

Figure 4.2.3 Frequency Calibration Using Microprocessor – No Noise

Chapter 5

CONCLUSIONS

5.1. Conclusions

In this final and concluding chapter we present a summary of the contributions of this thesis. In addition we provide a brief comparison of the system with other techniques. A discussion of new problems which are generated as a consequence of the work presented herein is also given.

In this dissertation we addressed ourselves to the problem of acquiring an unmodulated carrier signal when it is deeply embedded in noise. In Chapter 2 we outlined the development of a system used to perform an injection locking function as an acquisition aid in a phase lock loop. We defined the structure and explored the system design considerations for proper operation. The injection locking portion of the structure used an FM discriminator, an integrator and a variable bandpass filter. The controller for these functions was assumed to be available as, for example, a microprocessor. We discussed the tradeoff between system resolution and processing time. We also discussed the effect of noise on the system operation. Since in an FM discriminator operating below threshold we find the occurrence of both Gaussian and Poisson (Spike) noise, we presented an

argument which allows us to make use of the spike noise in an FM discriminator whereas we could not do so in a phase lock loop. We state that the technique is an iterative one and pose the problems of determining (1) the particular number of iterations, (2) integration times and (3) bandwidths to be used and (4) the methods for resolving these problems when given a particular set of parameters. We also posed the question of minimizing the acquisition time.

In Chapter 3 we present the analysis and theoretical results for the acquisition aided technique. We developed relationships to answer the problems presented in Chapter 2. In particular, with the aid of Rice's Theory [18], we formulated the means by which the acquisition time could be minimized and the number of iterations chosen. We also examined a technique which was simpler to implement than the minimization technique but which also reduced the acquisition time. When properly set up this simpler system could produce quite adequate results with a reduction in hardware complexity. We found that generally three iterations are needed for practical systems, two of these iterations being performed in the spike region and one in the Gaussian region. We noted the phenomenon of the moving threshold point in the FMD. We found under these considerations a substantial improvement over existing systems even when the signal is deeply imbedded in noise. We also presented the possibility of using this method when data is present on the carrier. Also this technique allows for various types of noise as long as they can

be characterized at the output of an FM discriminator. One major drawback of the system is that the signal-to-noise ratio must be known for proper operation.

In Chapter 4 we presented the hardware simulation and the associated results. We found good agreement with the theoretical analysis despite the many assumptions made. The experiment bore out the moving threshold problem but showed the technique proved effective in all the cases considered. The use of a special purpose microprocessor as an integrator/sample-and-hold device proved very useful since it provided a linear integration and non-fading "hold" unit.

5.2. Suggestions for Future Work

A veritable plethora of problems to be researched was produced by this work the most important of which is the use of a technique similar to the one presented here on a modulated carrier. This work must be first examined for the general phase lock loop structure and then use of the technique for a Costas Loop when no modulation is on the input signal. This requires analysis of the "noise-noise" term present in Costas and Squaring Loops as applied to the output variance of the estimate. Finally, as concerns this problem, the possibility of acquiring a modulated signal with a Costos Receiver must be studied.

Another problem to be considered is the effect of a wrong estimate of S_i/η on the system performance. Here all systems could be considered -- both the standard PLL

and Costas Loop receiver under the conditions of both modulation and no modulation.

A point also to be considered is the use of an adaptive estimator. The work contained in this dissertation assumed a worst case condition. For this situation the integration period is longer for any value of Doppler except the maximum. Thus the technique "pushes" the estimate farther away from the actual signal frequency. An adaptive estimator which accounts for this behavior would be beneficial.

A major problem is that of choosing a "proper" threshold for a particular set of parameters. Basically this problem would be resolved if a minimization could be performed for the general system equation without resorting to different regions of operation. Some dynamic and/or nonlinear programming could be helpful here. The solution to this problem would remove the one of the adaptive estimator completely.

We also pose the question of determining the response of an acquisition structure such as the one described here without a Sample and Hold unit present. This structure was mentioned by us as a possible means of acquisition but was rejected because of the possibility of driving the system out of lock. However, such a structure was not tested. Of course in such a structure the variable bandpass filter would be continuously narrowed until the loop bandwidth was reached. The rate at which this should be done is one particular problem which arises here.

A final problem brought up here but by no means the last

one that may come to mind is related to a previously discussed issue. The question is what can be done if S_i/η is unknown (this is related to estimating S_i/η incorrectly). A possibility is to assume that the worst case exists and integrate the longest possible time. Perhaps it is only best to find the proper direction of the offset frequency here. In any event all these problems can be examined by an interested researcher.

Appendix 1

DERIVATION OF THE PROBABILITY OF ERROR FOR $\hat{f}_D$

In this appendix we find the probability of error for our estimate, $\hat{f}_D$, after the n^{th} iteration.

Consider the following. The frequency of the incoming signal, f_D, is known to lie in an uncertainty bandwidth, B_o. We make an estimate of f_D, $\hat{f}_D$ which has known statistics. We want this estimate to be within a new bandwidth B_1 with some probability. Let p be the probability of making an error in f_D on the k^{th} iteration such that $|f_D - \hat{f}_D|_k > \frac{1}{2}B_k$, given that f_D lies in a bandwidth B_{k-1}.

Consider making repeated estimates of f_D each in an smaller window, B_{k+1}. We wish to determine the probability of error after n iterations. With ε_n the event that we are in error after n iterations we want $Pr(\varepsilon_n)$, where $Pr(\varepsilon_n)$ means the probability of event ε_n.

Defining p mathematically we have

$$Pr[(|f_D - \hat{f}_D|_k \,|\, f_D \text{ in } B_{k-1}) > \tfrac{1}{2}B_k] = p \qquad \text{(A1.1)}$$

where the bar (|) denotes conditional probability. The probability of making an error after the first iteration is simply p; that is

$$Pr(\varepsilon_1) = Pr(\text{after one iteration}) = p. \qquad \text{(A1.2a)}$$

After the second iteration an error is made in possibly two ways. The first is that there was an error after the first

iteration in which case the overall estimate will be in error. This is true because we are estimating $\hat{f}_D$ in a band in which it cannot be. The other possibility is that we make an error after the second iteration only. Let C_i be the event that there was no error after the i^{th} iteration. Then the $Pr(\varepsilon_2)$ is given by

$$Pr(\varepsilon_2) = Pr(\varepsilon_1) + Pr(\varepsilon_2|C_1)Pr(C_1). \tag{A1.2b}$$

Thus we have the recursive relation

$$Pr(\varepsilon_n) = Pr(\varepsilon_{n-1}) + Pr(\varepsilon_n|C_{n-1})Pr(C_{n-1}). \tag{A1.3}$$

However, $Pr(\varepsilon_n|C_{n-1}) = p$ (see Eq. (A1.1)). If we let

$$P_n \triangleq Pr(\varepsilon_n), \tag{A1.4a}$$

then

$$Pr(C_n) = 1 - P_n. \tag{A1.4b}$$

Using Eq. (A1.4) in Eq. (A1.3) we have

$$P_n = P_{n-1} + p(1 - P_{n-1}) \tag{A1.5a}$$

or

$$P_n = (1 - p)P_{n-1} + p. \tag{A1.5b}$$

Equation (A1.5b) is a first order linear nonhomogenous difference equation with initial condition $P_1 = p$ and is defined

for all integer n, $n \geq 1$. Solving Eq. (A1.5b) we find

$$P_n = 1 - (1 - p)^n. \qquad \text{(A1.6)}$$

Thus, the probability of error after n iterations is given by Eq. (A1.6). Since $Pr(C_n) = 1 - P_n$, the probability of being correct after n iterations is

$$Pr(C_n) = (1 - p)^n = \prod_{i=1}^{n} (1 - p) = \prod_{i=1}^{n} Pr(C_i) \qquad \text{(A1.7)}$$

Equation (A1.7) tells us that the probability of being correct after n iterations is simply the n-tuple product of being correct after one iteration. Note as $n \to \infty$, $Pr(C_n) \to 0$. Thus, as we intuitively suspect, if we keep estimating f_D, we are bound to make an error.

Appendix 2

DERIVATION OF VARIANCE OF THE INTEGRATOR OUTPUT FOR THE HIGH SNR CASE

To establish Eq. (3.3.6) we proceed as follows.

Consider a stationary process $x(t)$, with mean $\bar{x}(t) = 0$, autocorrelation $R_x(\tau)$ and power spectrum $G_x(f)$. Form a new process

$$W(t) = \frac{1}{2T} \int_{t-\varepsilon}^{t+\varepsilon} x(\lambda)d\lambda \tag{A2.1}$$

which is the average of $x(t)$ over the time interval $[T,-T]$. Consider x as the input to a linear filter with impulse response $h(t)$ the rectangular pulse

$$h(t) = \begin{cases} 1/2\varepsilon & |t| < \varepsilon \\ 0 & |t| > \varepsilon \end{cases}. \tag{A2.2}$$

By the convolution theorem

$$W(t) = \int_{-\infty}^{\infty} h(t-\alpha)x(\alpha)d\alpha. \tag{A2.3a}$$

But if $h(t-\alpha) = 0$ for $|t-\alpha| < \varepsilon$

$$W(t) = \int_{t-\varepsilon}^{t+\varepsilon} h(t-\alpha)x(\alpha)d\alpha = \frac{1}{2\varepsilon} \int_{t-\varepsilon}^{t+\varepsilon} x(\ )d \tag{A2.3b}$$

which is identical to Eq. (A2.1). Thus $W(t)$ is the output

of a linear system with impulse response h(t) as given by Eq. (A2.2) and input x(t).

The system function which is the Fourier transform of h(t), that is, H(j2πf) is given by

$$H(j2\pi f) = \frac{\sin 2\pi\varepsilon f}{2\pi\varepsilon f}, \quad |f| < \infty. \tag{A2.4}$$

Thus the power spectrum of W is $G_W(f) = |H|^2 G_x(f)$ or

$$G_W(f) = \frac{\sin^2 2\pi\varepsilon f}{(2\pi\varepsilon f)^2} G_x(f), \quad f \in f_D \tag{A2.5}$$

where f_D is the domain of definition for $G_x(f)$. But we know that $R_W(\tau)$ is the Fourier transform of $G_W(f)$. Since the inverse transform of $(\sin^2 2\pi\varepsilon f)/(2\pi\varepsilon f)^2$, $h_1(t)$ is a triangle

$$h_1(\lambda) = \begin{cases} (1 - |\lambda|\ 2\varepsilon)/2\varepsilon & |\lambda| < 2\varepsilon \\ 0 & |\lambda| > 2\varepsilon \end{cases} \tag{A2.6}$$

by the convolution theorem we have

$$R_W(\tau) = \frac{1}{2\varepsilon} \int_{-2\varepsilon}^{2\varepsilon} \left(1 - \frac{|\lambda|}{2\varepsilon}\right) R_x(\tau-\lambda)\, d\lambda. \tag{A2.7}$$

If $t = 0$, $\varepsilon = T_k$ and $q = W(0)$ Eq. (A2.1) becomes

$$q = \frac{1}{2T_k} \int_{-T_k}^{T_k} x(\alpha)\, d\alpha. \tag{A2.8}$$

which is the form of our integrator. Thus since $\bar{q} = 0$, $E(q^2) = \sigma_q^2 = \overline{W(0)^2} = R_W(0)$, we have

$$R_W(0) = \sigma_q^2 = \frac{1}{2T_k} \int_{-2T_k}^{2T_k} 1 - \frac{|\tau|}{2T_k} R_x(\tau)d\tau. \qquad \text{(A2.9)}$$

Equation (A2.9) is the same as Eq. (3.3.5b). Therefore, σ_q^2 is the total area under $G_W(f)$ for $x(t) = n_p(t)$ or

$$\sigma_{n_g}^2 = \int_{-\infty}^{\infty} \frac{\sin^2 2\pi T_k f}{(2\pi T_k f)^2} G_{n_p}(f)df. \qquad \text{(A2.10)}$$

Using Eq. (3.1.13b) we have

$$\begin{aligned} \sigma_{n_g}^2 = {} & 2 \int_0^{f_{max}-\Delta f} \frac{4\pi^2\alpha^2}{A^2}\eta f^2 \frac{\sin^2 2\pi T_k f}{(2\pi T_k f)^2}df \\ & + 2 \int_{f_{max}-\Delta f}^{f_{max}+\Delta f} \frac{4\pi^2\alpha^2}{A^2} \frac{\eta}{2} f^2 \frac{\sin^2 2\pi T_k f}{(2\pi T_k f)^2}df \end{aligned} \qquad \text{(A2.11)}$$

Letting $B_o^2 = (\eta\alpha^2)/(AT_k)^2$, $L_1 = f_{max} - \Delta f$, $L_2 = f_{max} + \Delta f$, using the trigometric identity $2 \sin^2 \theta = 1 - \cos 2\theta$, and performing the integration in Eq. (A2.11) we find

$$\sigma_{n_g}^2 = \frac{\beta_o^2}{2}\left[(L_1+L_2) - \left[\frac{\sin 4\pi T_k L_1}{4\pi T_k} + \frac{\sin 4\pi T_k L_2}{4\pi T_k}\right]\right] \qquad \text{(A2.12)}$$

Substituting for β_o^2, L_1 and L_2 and using the trignometric identity for the sum of two sines we have

$$\sigma_{n_g}^2 = \frac{\eta\alpha^2}{2A^2T_k^2}\, 2f_{max}\left[1 - \frac{\sin 2\pi(2f_{max})}{2\pi(2f_{max}T_k)}T_k \cos 4\pi\, \Delta f T_k\right] \qquad \text{(A2.13)}$$

Noting that on any iteration $2f_{max} = B_k$, and that $Si = A^2/2$ we find

$$\sigma_{n_g}^2 = \frac{\alpha^2}{\frac{4Si}{\eta B_k}T_k^2}\left[1 - \frac{\sin 2\pi B_k T_k}{2\pi B_k T_k}\cos 4\pi\, \Delta f T_k\right] \qquad \text{(A2.14)}$$

which is Eq. (3.3.6).

Another way to arrive at this result is as follows. The noise at the discriminator output is from Eq. (3.1.12)

$$n_p(t) = \frac{\alpha}{A}\dot{n}_c. \qquad \text{(A2.15)}$$

The integrator output due to the noise $n_p(t)$ is

$$n_g = \frac{\alpha}{2T_kA}\int_{-T_k}^{T_k}\frac{dn_c}{dt}(t)dt = \frac{\alpha}{2T_kA}\int_{-T_k}^{T_k}(dn_c) \qquad \text{(A2.16a)}$$

or

$$n_g = \frac{\alpha}{2T_kA}[n_c(T_k) - n_c(-T_k)]. \qquad \text{(A2.16b)}$$

Thus the variance $\sigma_{n_g}^2$ is

$$\sigma^2_{n_g} = \frac{\alpha^2}{(2T_kA)^2}\left[\overline{n_c^2(T_k)} + \overline{n_c^2(-T_k)} - 2\,\overline{n_c(T_k)n_c(-T_k)}\right]. \qquad \text{(A2.17)}$$

Since $n_c(t)$ is stationary $n_c^2(T_k) = n_c^2(T_k) = R_{n_c}(0)$ where $R_{n_c}(\tau)$ is the autocorrelation function of $n_c(t)$. Also $E(n_c(T_k)n_c(-T_k)) = R_{n_c}(\tau = 2T_k)$. Therefore

$$\sigma^2_{n_g} = \frac{\alpha^2}{4A^2T_k^2}[2R_{n_c}(0) - 2R_{n_c}(2T_k)]. \qquad \text{(A2.18)}$$

Now $R_{n_c}(\tau)$ is the inverse Fourier transform of $G_{n_c}(f)$ given by Eq. (3.1.6b) and shown in Fig. 3.1.3. $G_{n_c}(f)$ can be represented as the sum of two rectangular pulses -- both of height $\eta/2$ -- one extending from $-f_{max} - \Delta f \leq f \leq f_{max} + \Delta f$, and the other from $-f_{max} - \Delta f \leq f \leq f_{max} + \Delta f$. It is known that the Fourier transform of a pulse is of A_m sin x/x form where A_m is some magnitude. In particular, for a pulse waveform of height $\eta/2$ and bandwidth B, $R(\tau)$ is given by

$$R(\tau) = (\eta/2)\frac{\sin \pi B\tau}{\pi\tau}. \qquad \text{(A2.19)}$$

For $B = 2f_{max} + 2\Delta f$ we find

$$R_1(\tau) = (\eta/2) = \frac{\sin 2\pi(f_{max} + \Delta f)\tau}{\pi\tau} \qquad \text{(A2.20a)}$$

and for $B = 2f_{max} - 2\Delta f$

$$R_2(\tau) = \eta/2 \frac{\sin 2\pi(f_{max} - \Delta f)\tau}{\pi\tau}. \qquad \text{(A2.20b)}$$

With $R_{n_c}(\tau) = R_1(\tau) + R_2(\tau)$, and using the trignometric identity for sin(a+b) we find

$$R_{n_c} = \eta \frac{\sin 2\pi f_{max}\tau}{\pi\tau} \cos 2\pi \Delta f\tau. \qquad \text{(A2.20c)}$$

Multiplying the numerator and denominator by $2f_{max}$ to produce a (sin x)/x form and with $B_k = 2f_{max}$ as before

$$R_{n_c}(\tau) = (\eta B_k)\frac{\sin \pi B_K \tau}{\pi B_k \tau} \cos 2\pi \Delta f\tau. \qquad \text{(A2.20d)}$$

Letting $\tau = 0$ we have

$$R_{n_c}(\tau = 0) = R_n(0) = \eta B_K \qquad \text{(A2.21a)}$$

and for $\tau = 2T_k$, we have

$$R_{n_c}(\tau = 2T_k) = R_{n_c}(2T_k) = \eta B_k \frac{\sin 2\pi B_k T_k}{2\pi B_k T_k} \cos 4\pi \Delta f T_k. \qquad \text{(A2.21b)}$$

Thus, from Eqs. (A2.18) and (A2.21) we have

$$\sigma_{n_g}^2 = \frac{\alpha^2}{2A^2T_k^2}\eta B_k \left[1 - \frac{\sin 2\pi B_k T_k}{2\pi B_k T_k} \cos 4\pi \Delta f T_k\right]. \qquad \text{(A2.22)}$$

Substituting $Si = A^2/2$ in Eq. (A2.22) we arrive at the same result as in Eq. (A2.14).

Appendix 3

DERIVATION OF THE MEAN AND VARIANCE OF THE INTEGRATOR OUTPUT FOR THE LOW SNR CASE

Consider the process

$$q_\ell(t) = \sum_\ell a_\ell \delta_D(t - \tau_\ell) \tag{A3.1}$$

where the a_ℓ, and τ_ℓ i.i.d.r.v. and a_ℓ and τ_j are independent of each other for all ℓ and j. With $E(a_\ell) = \bar{A}$ and $E(a_\ell^2) = \overline{A^2}$ we wish to find $E[q_\ell]$ and $E[q_\ell(t_1)q_\ell(t_1 + \tau)]$. Taking the expected value of Eq. (A3.1) we have

$$E(q_\ell) = E[\sum_\ell a_\ell \delta_D(t - \tau_\ell)]. \tag{A3.2}$$

Bringing the expectation inside the summation and using the independence between a_ℓ and τ_ℓ we have

$$E(q_\ell) = \sum_\ell E(a_\ell)E[\delta_D(t - \tau_\ell)]. \tag{A3.3}$$

Since $E(a_\ell) = \bar{A}$ we obtain

$$E(q_\ell) = \bar{A}\, E[\sum_\ell \delta_D(t - \tau_\ell)] \tag{A3.4a}$$

where we have brought the expectation outside the summation However the term inside the brackets is $p_i(t)$, a Poisson impulse process with mean λ. Thus we have

$$E(q_\ell) = \bar{A}\lambda. \tag{A3.4b}$$

To find the autocorrelation of q_ℓ we form $R_q = E[q_\ell(t_1)q_\ell(t_2)]$. Thus

$$R_q(t_1,t_2) = E[\sum_k a_k\delta_D(t_1 - \tau_k)\cdot\sum_j a_j\delta_D(t_2 - \tau_j)] \tag{A3.5}$$

This is equivalent to

$$R_q(t_1,t_2) = E[\sum_k \sum_j a_k a_j\delta_D(t_1 - \tau_k)\delta_D(t_2 - \tau_j)] \tag{A3.6a}$$

or

$$\begin{aligned} R_q(t_1,t_2) = {} & E[\sum_k a_k a_k\delta_D(t_1 - \tau_k)\delta_D(t_2 - \tau_k)] \\ & + E[\sum_k \sum_{j\neq k} a_k a_j\delta_D(t - \tau_k)\delta_D(t - \tau_j)]. \end{aligned} \tag{A3.6b}$$

The first term on the Right Hand Side (RHS) of Eq. (A3.6b) is equal to $E(a_k^2)E[\sum_k \delta_D(t_1 - \tau_k)\delta_D(t_2 - \tau_k)]$. Since $\delta_D(x) = 0$ for $x \neq 0$, the term inside the brackets is zero unless $t_1 = t_2$. Thus, with $\tau = t_1 - t_2$ we have that $\delta_D(t_1 - \tau_k)\delta_D(t_2 - \tau_k) = \delta_D(\tau = t_1 - t_2)\delta(t_1 - \tau_k)$. So the first term on the RHS of Eq. (A3.6b), R_1 is

$$R_1 = E(a_k^2)\delta_D(\tau)E[\sum_k \delta_D(t_1 - \tau_k)] \tag{A3.7a}$$

or

$$R_1 = \lambda\overline{A^2}\delta_D(\tau) \tag{A3.7b}$$

where we have used the fact that $E(a_k^2) = \overline{A^2}$ and $E(p_i(t)) = \lambda$.

We now consider the second term on the RHS of Eq. (A3.6b), R_2. Since $a_k a_j$ are independent of each other for $k \neq j$, we have that

$$R_2 = \overline{A}^2 \, E[\sum_k \sum_{j \neq k} \delta_D(t_1 - \tau_k)\delta_D(t_2 - \tau_j)]. \qquad \text{(A3.8)}$$

To evaluate the expectation in Eq. (A3.8) note that if a_i = constant that is, $a_i = 1$ for all i, such that $\overline{A^2} = \overline{A} = 1$, then $q_\ell = p_i$. It is known that $R_p(\tau) = \lambda\delta_D(\tau)+\lambda^2$. Thus by comparison the expectation in Eq. (A3.8) is λ^2 so that

$$R_q(\tau) = \overline{A^2} \, \lambda_D\delta(\tau) + \overline{A}^2\lambda^2. \qquad \text{(A3.9)}$$

The covariance function $C_q(\tau) = R_q(\tau) - E^2(q)$ is thus

$$C_q(\tau) = \overline{A^2}\lambda\delta_D(\tau). \qquad \text{(A3.10)}$$

Appendix 4

PROGRAMMING AND INSTRUCTIONS FOR THE MICROPROCESSOR ROUTINE

This Appendix illustrates the flow chart and programming for the microprocessor integrate and sample and hold functions. Also the microprocessor instruction set is shown. For a complete list of commands, explanation of the functions and operating structure see [1].

The following registers were used.

R_0 - Primary Counter

R_1 - Overflow Counter

R_3 - Timer Counter

R_8 - Input Storage

AC - Accumulator

T - Temporary Storage

The main program is presented and a typical initialization program is also shown. We note that this particular program is useful only for the special μP we used.

FLOW CHART

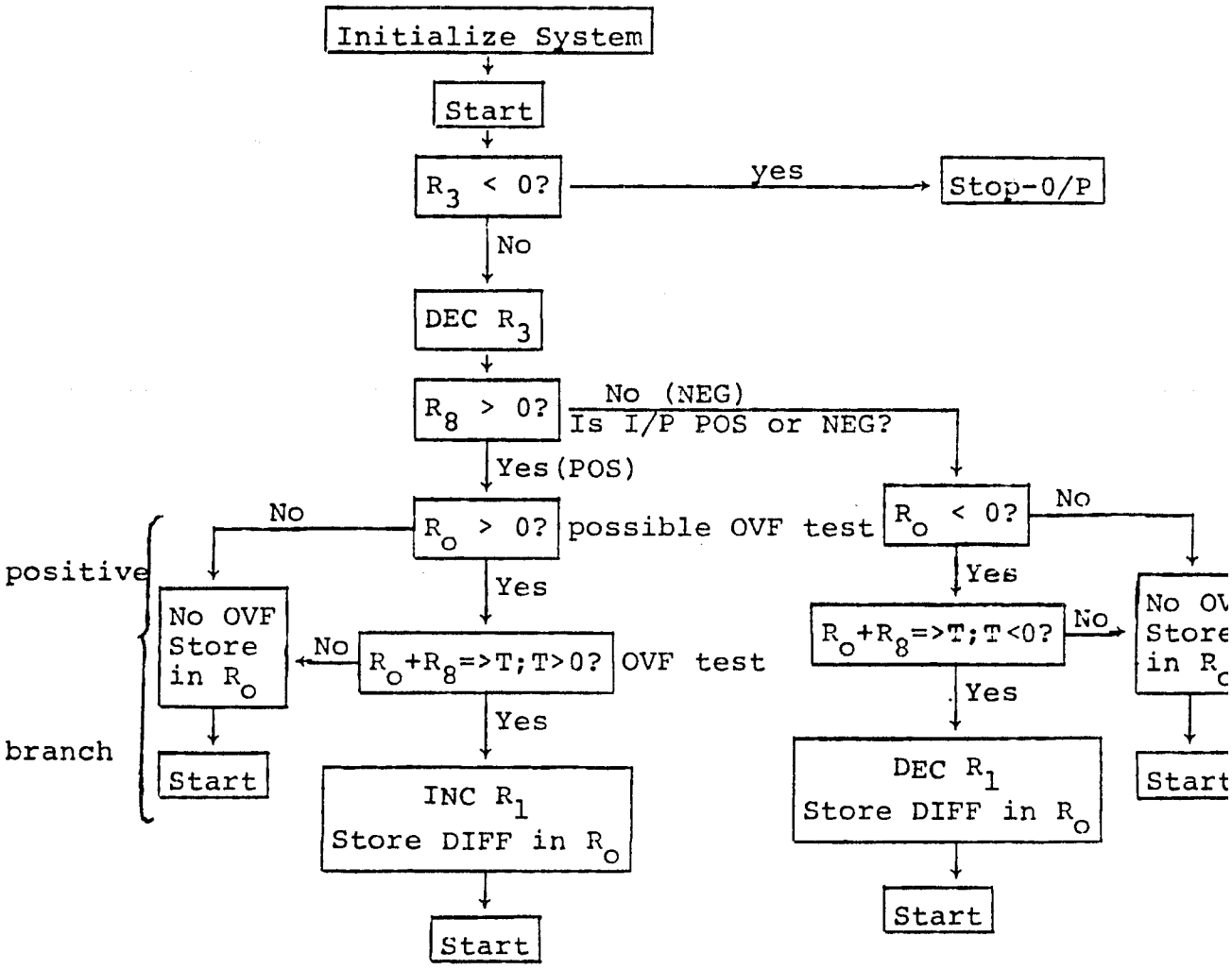

I/P(O/P) - Input(Output)

POS - Positive

NEG - Negative

DIFF - Difference

DEC - Decrement

INC - Increment

OVF - Overflow

MAIN PROGRAM

Location	Label	Mnemonic	Code
47	Start	ILR R_3	000 1 0011 1010
48		ALR AC (Skip-ve)	000 0 1101 1110
49		JMP Continue(51)	001 1 1001 1011
50		JMP 255	111 1 1111 1011
51	Continue	DSM R_3	001 0 0011 1010
52		ILR R_3	000 1 0011 1010
53		ALR AC (Skip-ve)	000 0 1101 1110
54		JMP S (9)	000 1 0100 1011
55		ILR R_1	000 1 0001 1010
56		CMA AC	111 1 1111 1010
57		AC/DA	110 1 0000 1000
58		JMP 255	111 1 1111 1011
9	S	CLA AC	100 1 1101 1010
10		AIA AC	011 0 1111 0010
11		CIA AC	001 1 1111 0010
12		SDR R_8	010 0 1000 0010
13		NOP	110 1 0000 1010
14		NOP	110 1 0000 1010
15		ILR R_8	000 1 1000 1010
16		ALR AC (Skip-ve)	000 0 1101 1110
17		JMP A_1 (31)	000 1 1111 1011
18		ILR R_o	000 1 0000 1010
19		ALR AC (Skip-ve)	000 0 1101 1110
20		JMP A_2 (44)	001 0 0110 1011

MAIN PROGRAM (Continued)

Location	Label	Mnemonic	Code
21		ILR R_o	000 1 0000 1010
22		SDR T	010 0 1100 0010
23		ILR R_8	000 1 1000 1010
24		ALR T	000 0 1100 1010
25		CIA AC	001 1 1111 0010
26		ALR AC(Skip-ve)	000 0 1101 1110
27		JMP A_2 (44)	001 0 0110 1011
28		JMP N (69)	010 1 0010 1011
69	N	ILR T	000 1 1100 1010
70		CIA AC	001 1 1111 0010
71		ALR AC	000 0 1101 1010
72		SRA AC	000 1 1111 1010
73		CIA AC	001 1 1111 0010
74		SDR R_o	010 0 0000 1010
75		JMP BACK N (29)	000 1 1110 1011
29	BACK N	DSM R_1	001 0 0001 1010
30		JMP 255	111 1 1111 1011
31	A_1	ILR R_o	000 1 0000 1010
32		CIA AC	001 1 1111 0010
33		ALRAC (Skip-ve)	000 0 1101 1110
34		JMP A_2	001 0 0110 1011
35		ILR R_o	000 1 0000 1010

MAIN PROGRAM (Continued)

Location	Label	Mnemonic	Code
36		SDR T	010 0 1100 0010
37		ILR R_8	000 1 1000 1010
38		ALR T	000 0 1100 1010
39		ALR AC (Skip-ve)	000 0 1101 1110
40		JMP A_2	001 0 0110 1011
41		JMP P(63)	001 1 1111 1011
63		ILR T	000 1 1100 1010
64		ALR AC	000 0 1101 1010
65		SRA AC	000 1 1111 1010
66		INR AC	011 1 1101 1010
67		SDR R_o	010 0 0000 1010
68		JMP BACK P(42)	001 0 0101 1011
42	BACK P	INR R_1	011 1 0001 0010
43		JMP 255	111 1 1111 1011
44	A2	ILR R_8	000 1 1000 1010
45		ALR R_o	000 0 0000 1010
46		JMP 255	111 1 1111 1011
255		NOP	110 1 0000 1010

INITIALIZATION PROGRAM

(Typical - to load 256 in R_3)

Location	Label	Mnemonic	Code
192	Start Init	CLR AC	100 1 1101 1010
193		INR AC	011 1 1101 0010
194		SRA AC	000 1 1111 1010
195		SRA AC	000 1 1111 1010
196		SDR R_3	010 0 0011 0010
197		CLR R_o	100 1 0000 1010
198		CLR R_1	100 1 0001 1010
199		CLR AC	100 1 1101 1010
200		CMA AC	111 1 1111 1010
201		AC/DA	110 1 0000 1000
202		CLR AC	100 1 1101 1010
203		JMP 255	111 1 1111 1011

INSTRUCTION SET

Mnemonic	Machine Code	Description
Arithmetic Operations		
ADR X	0110 xxxx $\overline{CI}$010	(X)+(Ac)→X
ILR X	0001 xxxx $\overline{CI}$010	CI+(x)→Ac,X
ADD X	0000 xxxx $\overline{CI}$010	CI+(x)+(Ac)→Ac,X
CSR X	0101 xxxx $\overline{CI}$010	CI-1→X
SDR X	0100 xxxx $\overline{CI}$010	(Ac)-1+CI→X
INR X	0111 xxxx $\overline{CI}$010	(X)+CI→X
CLR X	1001 xxxx 1010	0→X
NOP X	1101 xxxx 1010	(X)→X
CMR X	1111 xxxx 1010	$(\overline{X})$→X
RRA Y	0001 yyyy 1010	y(o)→y(n-1),→y(n-i)→y(n-i-1)
CIA Y	0011 yyyy $\overline{CI}$010	$(\overline{y})$+CI→y
DCA Y	0010 yyyy $\overline{CI}$010	(y)-1+CI→y
INA Y	0111 yyyy $\overline{CI}$010	(y)+CI→y
NOP Y	1101 yyyy $\overline{CI}$010	(y)→y
CMA Y	1111 yyyy 1010	$(\overline{y})$→y
Logic Operations		
ANR X	1000 xxxx 1010	(x) Λ(Ac)→x
ORR X	1100 xxxx 1010	(x)V(Ac)→x
XNR X	1110 xxxx 1010	$\overline{(x)(+)(Ac)}$→x
ANI Y	1000 yyyy 1010	(y)Λ$(\overline{I})$→y
ORI Y	1100 yyyy 1010	(y)V(I)→y
XNI Y	1110 yyyy 1010	$\overline{(y)(+)(\overline{I})}$→y

INSTRUCTION SET (Continued)

Input Operations				
LDI	Y	0100 yyyy	CI010	$(\overline{I})-1+CI\rightarrow Y$
AIA	Y	0110 yyyy	CI010	$(\overline{I})+CI+Y\rightarrow Y$
AMA	Z	0000 zzzz	CI010	$(\overline{M})+(Z)+CI\rightarrow Z$
LDI	Z	0001 zzzz	CI010	$(\overline{DI})_{MSB}\rightarrow Z_{MSB}, CI\rightarrow Z_{MSB}$ $z_i=0$ $i\neq 1,n-1$
LDE	Z	1101 zzzz	1010	$(\overline{DI})\rightarrow Z_{MSB}$, $z_i=0$ $i\neq n-1$
LOD	Z	1111 zzzz	1010	$(DI)\rightarrow Z_{MSB}$, $z_i=1$ $i\neq n-1$
Output Operations				
Out	Ac	1101 0000	1000	$(Ac)\rightarrow$D/A
Out	X_d	0011 xxxx	1010	$(X)_{MSB}\rightarrow$Digital output
Branching Operations				
JMP	LOC	$A_7A_6A_5A_o$ $A_4A_3A_2A_1$	1011	unconditional jump to location $A_7A_6A_5A_4A_3A_2A_1A_o$. Next instruction is to be skipped if $(Ac)\geq 0$, providing the instruction to be skipped is not a jump instruction. If it is, then the jump condition is on negative accumulator content [i.e. $(Ac)< 0$].
SKP	AC			

X Y and Z are chosen from Table A1. I is a 10 bit sampled analog input. Ac is the accumulator

Table A1: REGISTER CODES

X	group	Y	group	Z	group
X	xxxx	Y	yyyy	Z	zzzz
R_o	0000	T	1110	T	1010
R_1	0001	Ac	1111	Ac	1011
R_2	0010				
R_3	0011				
R_4	0100				
R_5	0101				
R_6	0110				
R_7	0111				
R_8	1000				
R_9	1001				
T	1100				
Ac	1101				

REFERENCES

[1] Apelewicz, Tuvia, "The Design of a Programmable Real Time ADM Voice Processor and the Formulation of the Autocorrelation Function for the LDM Algorithm", Ph.D. Thesis, Dept. of Elec. Eng., The City University of New York, Sept. 1978.

[2] Bacinski, R. R., and Helgeson, R. J., Orbiter S-Band Communications Subsystem, IEEE Trans. Commun., Vol. COM-26, Part I, Nov. 1978, Special Issue on Space Shuttle Communications and Tracking, pp. 1521-1531.

[3] Batson, B. H., private communication, June, 1978.

[4] Brown, K. H. and Kline, A. J., Jr., "Automatic Signal Acquisition Means for Phase-Lock Loop With Anti-Sideband Lock Protection", U. S. Patent reg. num. 3,768,030, Oct. 23, 1973.

[5] Cahn, C. R. "Improving Frequency Acquisition of a Costas Loop", IEEE Trans. Commun. Vol. COM-25, No. 12, pp. 1453-1460, Dec. 1977.

[6] Cobb, R. F. and Martin, A. R., "A Guide to Acquisition Receiver Selection and Performance", The Microwave Journal, June 1968, pp. 63-68.

[7] Costas, J. P., "Synchronous Communication", Proc. IRE, Vol. 44, pp. 1713-1718, Dec. 1956.

[8] Dixon, R. C., Spread Spectrum Systems, John Wiley & Sons, 1976.

[9] Frazier, J. P. and Page, J., "Phase-Lock Loop Frequency Acquisition Study", Trans. IRE, SET-8, Sept. 1962, pp. 210-227.

[10] Gardner F. M., Phase-Lock Techniques ,John Wiley and Sons, 1966.

[11] _____, pp. 52-3 and 96.

[12] Gupta, S. C., "Phase-Locked Loops", Proc. of the IEEE, Vol. 63, No. 2, pp. 291-306, Feb. 1975.

[13] Kreyszig, E., Advanced Engineering Mathematics, Third Edition, John Wiley and Sons, pp. 817-819, 1967.

[14] Lindsey, W. C., Synchronization Systems in Communication and Control, Prentice-Hall, 1972.

[15] _____, pp. 468-473.

[16] Papoulis, A., Probability, Random Variables and Stochastic Processes, McGraw-Hill, 1965, p. 325.

[17] _____, p. 287.

[18] Rice, S. O., Time Series Analysis, John Wiley and Sons, Chap. 25, 1963.

[19] Richman, D., "The DC Quadricorrelator: A Two-Mode Synchronization System", Proc. of the IRE, pp. 288-299, Jan. 1954.

[20] Ringdahl, I. and Schilling, D. L., "On the Distribution of the Spikes Seen at the Output of an FM Discriminator Below Threshold", Proc. IEEE, Vol. 52, pp. 1756-1757, Dec. 1964.

[21] Sage, P. and White, C. C., Optimum Systems Control, Prentice-Hall, Chap. 6, 1977.

[22] Taub, H. and Schilling, D. L., Principles of Communication Systems, McGraw-Hill, 1971.

[23] _____, pp. 335-337.

[24] _____, pp. 320-335.

[25] _____, pp. 256-258.

[26] Viterbi, A. J., Principles of Coherent Communication, McGraw-Hill, 1966.

[27] _____, p. 186.

[28] _____, pp. 50, 12 and 13.

[29] _____, pp. 28-33.

[30] Williamson, D., "Improved Phase-Locked Loop Performance Via Non-Linear Loop Filters", IEEE Trans. Commun., Vol. COM-27, No. 3, pp. 542-556, March 1979.

[31] Wozencraft, J. M., and Jacobs, I. M., Principles of Communication Engineering, John Wiley and Sons, 1967.

[32] _____, pp. 144-147, 106-109.

[33] _____, pp. 650-655.

TIEGERMAN, ELLENMORRIS

A COMPARISON OF THREE PLAY PROCEDURES IN THE MANIPULATION OF GAZE BEHAVIOR AND OBJECT USE WITH AUTISTIC CHILDREN

City University of New York PH.D. 1979

A COMPARISON OF THREE PLAY PROCEDURES IN THE MANIPULATION OF GAZE BEHAVIOR AND OBJECT USE WITH AUTISTIC CHILDREN

by

Ellenmorris Tiegerman

A Dissertation Submitted to
The Graduate Faculty in Speech and Hearing Sciences
in Partial Fulfillment of the Requirements
for the Degree of
Doctor of Philosophy

The City University of New York

1979

This manuscript has been read and approved for the Graduate Faculty in Speech and Hearing Sciences in satisfaction of the dissertation requirement for the degree of Doctor of Philosophy.

Sept 17, 1979
date

James K. Stark
Chairman of Examining Committee

Sept 17 1979
date

Irving Hochberg
Executive Officer

Joel Stark, Ph.D.

Harvey Halpern, Ph.D.

Marie Meier, Ph.D.
Supervisory Committee

The City University of New York

ABSTRACT

A COMPARISON OF THREE PLAY PROCEDURES IN THE MANIPULATION OF GAZE BEHAVIOR AND OBJECT USE WITH AUTISTIC CHILDREN

by
Ellenmorris Tiegerman

Advisor: Professor James K. Lang

This experiment was undertaken to determine the efficacy of three play interaction procedures in the manipulation of gaze behavior in autistic children and to determine the relationship between gaze behavior and object manipulation performances.

Subjects were six children with symptomatology of infantile autism who ranged in age from four years to six years.

Three experimental procedures, varying in the amount of manipulative control the child exercised over the experimenter, were presented across seventeen sessions. During each procedure, the child was seated opposite the experimenter

at a table with various objects. Duplicate objects were used by the experimenter.

In procedure I, the subject had complete manipulative control of the experimenter's choice of object, object manipulation, and when she started and stopped manipulating the object. In procedure II, the subject had control over the experimenter's choice of object, and when she started and stopped manipulating the object. In procedure III, the subject had no manipulative control over the experimenter's choice of object, action on an object or when she started and stopped manipulating the object.

Two procedures (each fifteen minutes in length) were presented during a thirty minute session. The order of presentation of the experimental procedures was randomized across sessions and within sessions. All six subjects were involved in each experimental procedure. A two factor analysis of variance for repeated measures was computed separately for frequency and duration of gaze behavior, and for frequency and duration of object manipulated performances.

Results were as follows:

1. There was a significant difference among the play procedures in developing gaze behavior and object manipulated performances.